Toward the discovery of matter creation with neutrinoless math xmlns="http://www.w3.org/1998/Math/MathML" display="inline">mi>β/mi>mi>β/mi>/math> decay

Matteo Agostini, Giovanni Benato, Jason A. Detwiler, Javier Menéndez, and Francesco Vissani

Toward the discovery of matter creation with neutrinoless $\beta\beta$ decay

Matteo Agostini[*]

Department of Physics and Astronomy, University College London, Gower Street, London WC1E 6BT, UK

Giovanni Benato[†]

INFN, Laboratori Nazionali del Gran Sasso, 67100 Assergi, L'Aquila, Italy[‡]

Jason A. Detwiler[§]

*Center for Experimental Nuclear Physics and Astrophysics and Department of Physics,
University of Washington, Seattle, WA 98115, USA*

Javier Menéndez[¶]

*Department of Quantum Physics and Astrophysics and Institute of Cosmos Sciences,
University of Barcelona, 08028 Barcelona, Spain*

Francesco Vissani[**]

INFN, Laboratori Nazionali del Gran Sasso, 67100 Assergi, L'Aquila, Italy

The discovery of neutrinoless $\beta\beta$ decay could soon be within reach. This hypothetical ultra-rare nuclear decay offers a privileged portal to physics beyond the Standard Model of particle physics. Its observation would constitute the discovery of a matter-creating process, corroborating leading theories of why the universe contains more matter than antimatter, and how forces unify at high energy scales. It would also prove that neutrinos and anti-neutrinos are not two distinct particles, but can transform into each other, with their mass described by a unique mechanism conceived by Majorana. The recognition that neutrinos are not massless necessitates an explanation and has boosted interest in neutrinoless $\beta\beta$ decay. The field stands now at a turning point. A new round of experiments is currently being prepared for the next decade to cover an important region of parameter space. In parallel, advances in nuclear theory are laying the groundwork to connect the nuclear decay with the underlying new physics. Meanwhile, the particle theory landscape continues to find new motivations for neutrinos to be their own antiparticle. This review brings together the experimental, nuclear theory, and particle theory aspects connected to neutrinoless $\beta\beta$ decay, to explore the path toward — and beyond — its discovery.

CONTENTS

---

[*] matteo.agostini@ucl.ac.uk
[†] giovanni.benato@lngs.infn.it
[‡] Now at Gran Sasso Science Institute, 67100 L'Aquila, Italy
[§] jasondet@uw.edu
[¶] menendez@fqa.ub.edu
[**] vissani@lngs.infn.it

I. INTRODUCTION

What is "matter"? Ever since the attempts of the ancient philosophers to conceive matter in terms of a few elements, and the even more radical attempts of the early atomists, humankind has been trying to determine what the ultimate building blocks of nature are and whether they are physically indivisible. Lavoisier's idea that "nothing is lost, nothing is created, everything is transformed" is deeply rooted in our modern way of thinking and has taken a very particular form in the context of the Standard Model of particle physics. Nowadays, we assume that energy can transform into balanced quantities of matter and antimatter, and vice versa, that matter and antimatter can annihilate to produce energy, according to immutable rules. Indeed, in all physical processes observed so far, the creation or destruction of matter particles is compensated by the destruction or creation of antimatter particles. More precisely, the differences between the number of baryons and antibaryons, and leptons and antileptons, are immutable quantities, i.e., quantum numbers of our canonical field theory.

We now believe that our universe originated in a Big Bang, and that at the beginning of time it was extremely hot, with energy converting into matter-antimatter and vice versa. Yet, the universe in which we live today contains almost exclusively atoms and not anti-atoms. This observation creates a strong theoretical appeal for hypothetical "matter-creating" or "antimatter-destroying" processes, i.e., phenomena that can break the matter-antimatter balance, and dynamically explain the asymmetry of our universe. At present, the most promising phenomena of this type for observation in the laboratory are the destruction of a proton — which could decay by changing the number of baryons while respecting energy conservation — and the creation of electrons in nuclear decays — which would change the number of leptons.

The quest to observe the creation of electrons is being pursued vigorously in the form of searches for a nuclear decay where the atomic number Z increases by two units while the nucleon number A remains constant: $(A, Z) \to (A, Z + 2) + 2e$. This is commonly known as "neutrinoless $\beta\beta$ decay" ($0\nu\beta\beta$ decay). Here, the creation of electrons can be enabled by the "transmutation" of neutrinos into antineutrinos, which is possible if the neutrino's mass is described by a unique mechanism conceived by Majorana. Thus the matter-antimatter imbalance and neutrino masses could have a common origin.

A symmetry between neutrinos and antineutrinos was postulated by Majorana and further discussed by Racah in 1937. This led Furry to propose the existence of $0\nu\beta\beta$ decay in 1939, building on Goeppert-Mayer's ideas on two-neutrino double-beta ($2\nu\beta\beta$) decay transitions. Pioneering searches for $0\nu\beta\beta$ decay started in the 40s using time-coincidence counting techniques or visual detection of tracks in cloud chambers and photographic emulsions.

Since then, experiments have continued steadily, leading to increasingly stronger constraints which at present reach half-lives exceeding 10^{26} years. This means that a nucleus will take on average more than a million billion times the age of the universe before undergoing $0\nu\beta\beta$ decay. To surpass this sensitivity, experiments must monitor thousands of moles of atoms for years, and have the capability to detect the $0\nu\beta\beta$ decay of a single one of them. The rarity of the sought-after signal sets extremely strict requirements for eliminating other processes that could mimic the decay.

We face a pivotal time for $0\nu\beta\beta$-decay searches. The discovery of neutrino mass at the turn of the century brought to the foreground the question of whether that mass could be of the peculiar type proposed by Majorana. This invigorated the effort in $0\nu\beta\beta$-decay experiments around the world, covering a variety of $\beta\beta$-decay nuclei and detection techniques. These efforts have set the stage for the selection of the most promising methods for further investment. The community is currently proposing next-generation experiments as part of a global enterprise, with the goal for the next decade of extending the half-life sensitivity in multiple nuclei by two orders of magnitude beyond the current limits. This could lead to an observation of the transition.

Meanwhile, the theoretical landscape continues to evolve, and has also been deeply affected by the neutrino mass discovery. Most leading theoretical models suggest that neutrinos have a Majorana mass responsible for lepton number violation, and hence predict $0\nu\beta\beta$ decay. In fact, multiple lepton-number-violating mechanisms that lead to $0\nu\beta\beta$ decay have been identified, so that there is no definitive prediction of its half-life. Nevertheless, running experiments are progressively probing the parameter space available to theoretical scenarios. In particular, if the decay is mediated by the exchange of light neutrinos, all anticipated orderings of the neutrino masses are being tested.

A key role in $0\nu\beta\beta$-decay searches is also played by nuclear theory, which links the experimentally measurable $0\nu\beta\beta$-decay half-life with the underlying particle physics through the modeling of the nuclear behavior. Sophisticated many-body calculations are required to evaluate the impact of the structure of the initial and final nuclei on the decay rate. In addition, the nuclear operators driving the decay need to be consistent with the treatment of the initial and final nuclei. The nuclear theory community is placing significant analytical and computational efforts with the ultimate goal of converting experimental measurements into constraints on the underlying particle physics mechanisms. In the opposite direction, only through nuclear theory can we predict decay half-life values based on selected theoretical scenarios.

In recent years, several review articles have discussed $0\nu\beta\beta$ decay, witnessing the vivid interest of the scientific community in this topic. Each work emphasizes one or more relevant aspects, such as the experimental part (Avignone *et al.*, 2008; Cremonesi and Pavan, 2014; Elliott, 2012; Giuliani and Poves, 2012; Gomez-Cadenas *et al.*, 2012; Schwingenheuer, 2013), the nuclear physics (Ejiri *et al.*, 2019; Engel and Menéndez, 2017; Vergados *et al.*, 2012; Vogel, 2012; Yao *et al.*, 2022b), the connection with neutrino masses (Bilenky and Giunti, 2015; Dell'Oro *et al.*, 2016; Petcov, 2013), other particle physics mechanisms (Deppisch *et al.*, 2012; de Gouvea and Vogel, 2013; Päs and Rodejohann, 2015; Rodejohann, 2011, 2012), or a combination of the above (Dolinski *et al.*, 2019). Elliott and Franz (2015) discusses Majorana fermions in a broader context. In the present work, we mostly focus on the first three aspects, motivated by the intention to follow the theoretical ideas that describe the most plausible expectations for experiments. We bring together theory and experiment to give a comprehensive overview of the field, and explore the path towards a convincing future discovery and elucidation of the mechanism mediating the decay.

We start our journey in Sec. II with an overview of the history and role of $0\nu\beta\beta$ decay. In Sec. III, we revisit the theoretical motivations to search for this matter-creating process, which has a special role in testing the foundations of nature that modern theory formulates in terms of symmetry principles. The reference quantum field theory of particles physics — i.e., the Standard Model — predicts four global symmetries, with corresponding conserved quantities given by the difference between the number of baryons and leptons ($B - L$) and the number of leptons of each flavor ($L_e - L_\mu$, $L_\mu - L_\tau$, $L_e - L_\tau$). The observation of neutrino flavor oscillation violates the last three, forcing us to extend the theory to account for these new phenomena. The only residual global symmetry is that related to $B - L$ conservation, as discussed in Sec. III.A. Testing this symmetry is thus of paramount importance, and $0\nu\beta\beta$ decay is its most sensitive direct probe. Further interest in $0\nu\beta\beta$ decay comes from the fact that the transition is plausibly due to new physics — beyond the Standard Model — at an ultra-high energy scale beyond the reach of current accelerators. In Sec. III.B and III.C, we review the mechanisms that give rise to $0\nu\beta\beta$ decay, how their contributions can be cast in terms of effective field theory operators, and what we can learn about them. The lowest dimension operator — i.e., the dimension 5 Weinberg operator — describes Majorana masses of the light neutrinos and is one of the better-motivated mechanisms for $0\nu\beta\beta$ decay. If this is the dominant contribution to the transition, the half-life of the decay is connected to the neutrino properties and the origin of neutrino masses (Sec. III.D). This creates an exciting interplay between $0\nu\beta\beta$-decay searches, neutrino oscillation experiments, neutrino mass measurements, and cosmology. It also implies that the search for $0\nu\beta\beta$ decay is a well-defined scientific target that can be explored in the next years. Finally, in Sec. III.E, we ex-

plore the connection between $0\nu\beta\beta$ decay and the excess of baryons over antibaryons in the universe.

Section IV reviews recent advances in nuclear theory. First, Sec. IV.A introduces an effective field theory framework based on the symmetries of the fundamental theory governing nuclei, i.e., quantum chromodynamics. Contributions from different $0\nu\beta\beta$-decay mechanisms are organized in terms of effective operators through a master formula that provides a way to estimate the energy scales constrained by $0\nu\beta\beta$-decay searches. Section IV.B describes how each $0\nu\beta\beta$-decay mechanism involves at least one nuclear matrix element (NME), as the decay occurs in a complex many-body nuclear system. We highlight the impact of the recently proposed "short-range operator" — unfortunately with uncertain coupling — that could affect significantly the rate of the decay. In Sec. IV.C, we discuss progress on NME calculations obtained with several many-body approaches, including recent first-principles studies. In addition, we discuss NME uncertainties, and place special importance on recent advances in the understanding of "g_A quenching" (Sec. IV.D), one of the main sources of theoretical uncertainty. In single-β decay the decades-old puzzle seems mostly solved thanks to previously-neglected many-body correlations and two-nucleon currents. However, an extension to higher momentum transfer is needed to estimate the impact on $0\nu\beta\beta$ decay. Finally, Sec. IV.E presents related nuclear properties and reactions, the tests they place on nuclear theory calculations, and the insights they may provide on $0\nu\beta\beta$ decay.

Section V reviews the experimental aspects of $0\nu\beta\beta$-decay searches. This decay can be observed in a variety of nuclei, each of them characterized by specific properties such as Q-value and natural abundance, as discussed in Sec. V.A. Since each isotope enables different detection techniques, the field is very diverse. We review the main detection principles in Sec. V.B. Current sensitivities can only be improved with an increase of the active isotope mass and a concurrent background reduction to unprecedented levels. Section V.C describes the background sources faced by the various experiments, and lists possible new backgrounds arising in future highly sensitive searches. The available techniques to discriminate a possible $0\nu\beta\beta$ decay from background are covered in Sec. V.D. We discuss in Sec. V.E the statistical techniques used to extract the sought-after signal and how two effective parameters — the effective background and effective exposure — can essentially describe the sensitivity of an experiment.

Finally, in Sec. VI, we present a consistent comparison of recent and future experiments, including projects at the research and development phase. We describe each experiment's distinctive features, planned developments, and strategies to reach the desired goal sensitivity.

Several questions are crucial for $0\nu\beta\beta$-decay searches in the upcoming decade. Are we ready for a discovery?

When can we expect it, and what will we be able to learn from an observation? How will advances in other physics areas influence the $0\nu\beta\beta$-decay community? In Sec. VII, we bring together our expectations for particle theory, nuclear theory, and experiments in order to address these questions, and to explore the possible path towards — and beyond — a future discovery of $0\nu\beta\beta$ decay.

We hope for this review to become a useful reference for both $0\nu\beta\beta$-decay experts and nonexperts. With this challenging goal in mind, we alternated introductory and technical sections. We recommend the nonexpert reader to focus on Secs. III.A, III.B, III.D and III.E for an overview of the particle theory context, on Secs. IV.A, IV.C.1 and IV.D for insights on nuclear theory aspects, and on Secs. V and VI.A for an introduction to the experimental techniques and experiments. Experts might also be interested in these sections, as we discuss most topics from a modern point of view, which differs in many aspects from past review works. We also recommend to both experts and nonexperts Sec. II, which gives a historical context for the present-day effort, and Sec. VII, which aims to connect all the dots, bridging theory and experiment, particle and nuclear physics, as well as cosmology and other scientific areas, pointing to a pathway forward toward the discovery of $0\nu\beta\beta$ decay and beyond.

II. HISTORICAL LANDSCAPE

In this section, we summarize the role of $0\nu\beta\beta$ decay in the historical development of particle physics, focusing on its connection with the crucial milestones of neutrino physics, such as: the neutrino postulation (1930-1933); Majorana's hypothesis for the nature of the neutrino (1937); the role of $0\nu\beta\beta$ decay for the neutrino mass (1957-1958); neutrinos in gauge theories (1961-present); and empirical information on the neutrino mass (1967-present). We also cover the connection between $0\nu\beta\beta$ decay and long-standing questions regarding the basic ingredients of matter and fundamental Standard Model symmetries. More details on the history of $0\nu\beta\beta$ decay are discussed in Barabash (2011), Tretyak (2011), De Bianchi (2018), and Vissani (2021).

The terminology α, β and γ rays introduced by Rutherford at the turn of the 20th century marked the recognition of new phenomena beyond atomic physics. The Bohr-Rutherford model of the atom (Bohr, 1913) was a milestone for the field, but could not and did not claim to explain these new phenomena. Soon afterwards, Harkins and Wilson (1915a,b) inferred a model for the nuclei describing them as composed of ^{4}He, ^{3}H and ^{1}H nuclei, and Rutherford (1920a,b) discovered through (α, p) reactions that the hydrogen nucleus was a fundamental component of other nuclei, and named it the *proton* after Prout's *protyle* (Prout, 1816). According to these models, a nucleus with atomic numer Z and mass number A would

have been made of A protons and $(A-Z)$ *nuclear* or *inner* electrons, yielding a nuclear charge Ze. This paradigm could explain the neutrality of atoms, the existence of isotopes and also radioactivity, but was still fundamentally non-relativistic, assuming that particles "are forever", i.e., cannot be created or destroyed. Moreover, it could not predict the nuclear spin for some nuclei — for instance ^{14}N — and predicted a monochromatic β radiation spectrum (Ellis and Wooster, 1927; Meitner and Orthmann, 1930).

To overcome these problems, Pauli (1930) proposed to add a new very light and neutral particle to the nucleus, which was assumed to carry spin and energy. Thus the neutrino was introduced, albeit in a non-relativistic model, similar to the earlier ones. The discovery of the neutron in 1932–33 (Chadwick, 1932, 1933) was an important step forward in the formulation of the modern model of the nucleus (Heisenberg, 1932a,b, 1933; Majorana, 1933). Concurrently, quantum mechanics reached its full maturity, in particular thanks to the relativistic quantum theory of the electron (Dirac, 1928).

All these phenomenological and theoretical aspects were merged in Fermi's theory of β decay (Fermi, 1934), which introduced the possibility of creation and destruction of matter particles. The success of Fermi's theory in describing the observed β-decay rates and spectra convinced the scientific community of the existence of the neutrino and triggered its experimental search.

Shortly thereafter, Wick (1934) exploited Fermi's theory to explain β^+ decay and electron capture, and Wang (1942) proposed to measure the electron-capture nuclear recoil to indirectly detect the neutrino. Between the late thirties and the early fifties, several measurements demonstrated that β decay and electron capture are subject not only to missing energy, but also to an apparent momentum non-conservation, thus pointing to the existence of the neutrino (Allen, 1942; Crane and Halpern, 1938, 1939; Davis, 1952; Leipunski, 1936). The final confirmation arrived in 1956, with the detection of neutrinos in "appearance mode" through inverse β^+ decay $(\bar{\nu}+p \rightarrow n+e^+)$ (Cowan *et al.*, 1956; Reines and Cowan, 1953), another process predicted by Fermi's theory.

Other milestones were achieved in those years. Lee and Yang (1956) questioned the conservation of parity in weak interactions and Wu *et al.* (1957) observed its violation in β decays. Soon after, Landau (1957), Lee and Yang (1957), and Salam (1957) independently came to the conclusion that, *if the neutrino produced by weak interactions was massless,* it would have a fixed and opposite helicity compared to the antineutrino, and parity violation in weak interactions would be maximal. Experimental evidence in favor of the neutrino's fixed helicity (Goldhaber *et al.*, 1958) and the refinements of Fermi's theory in terms of a $(V-A)$ interaction (Feynman and Gell-Mann, 1958; Sudarshan and Marshak, 1958) represented breakthroughs in our understanding of weak inter-

actions. Unfortunately, it implied that the expected rates of $0\nu\beta\beta$ decay were at best much lower than originally predicted (Furry, 1939), and strengthened the idea that neutrinos were massless up to the point that it became regarded as an established fact. However, this paradigm did not block the discussion entirely; in fact, the first discussion of $0\nu\beta\beta$ decay based on the neutrino mass hypothesis appears in 1960 (Greuling and Whitten, 1960). The history is recounted in Vissani (2021).

In the same decades, the understanding of β decay and weak interaction led to further considerations on the possibility of *double-*β decay and its relevance in connection to the neutrino nature. In 1935 Goeppert-Mayer (1935) highlighted the possibility for an isotope to "change into a more stable one by simultaneous emission of two electrons", with a process that would "appear as the simultaneous occurrence of two transitions, each of which does not fulfill the law of conservation of energy separately". She also used Fermi's theory of β decay to predict that such a transition, namely $2\nu\beta\beta$ decay, would have half-life values exceeding 10^{17} yr.

Two fundamental milestones followed. Majorana (1937) introduced an alternative to Dirac's theory where neutral particles can be their own antiparticles, and explicitly mentioned its possible application to neutrinos, saying that "such theory can obviously be modified so that the β emission, both positive and negative, is always accompanied by the emission of a neutrino". Shortly thereafter, Racah (1937) showed that postulating a symmetry between particles and antiparticles in addition to relativistic invariance leads to a new version of Fermi's theory of β decay, and demonstrated that the assumption that neutrinos and antineutrino are the same particle leads directly to Majorana's formalism. Racah also pointed out that Majorana's theory could not apply to neutrons because of their non-zero magnetic moment and because it would imply that a free neutron could undergo both β^+ and β^- decay, contradicting experiment. Racah also highlighted the possibility of neutrinos (antineutrinos) inducing inverse β^+ (β^-) decay if they were Majorana particles.

Furry (1938) pointed out that establishing which formalism applied to the neutrino, Dirac's or Majorana's, would be more difficult than proving the neutrino's existence. He also combined Majorana's theory with the $2\nu\beta\beta$ decay proposed by Goeppert-Mayer, and conceived $0\nu\beta\beta$ decay mediated by the emission and re-absorption of virtual Majorana neutrinos (Furry, 1939). The process does not require the presence of Majorana masses, but simply Majorana neutrinos, which obey Fermi-Racah interactions. Should the interaction be of scalar type, in the theoretical context at the time it could have yielded half-life values as short as 10^{15} years. Furry noted that such a rapid rate would affect the abundance of long-lived isotopes, opening the possibility of geochemical searches for $0\nu\beta\beta$ decay in addition to direct searches.

Furry's hypothesis motivated the first experimental searches for $0\nu\beta\beta$ decay with rates too rapid to be accommodated by Goeppert-Mayer's proposed mechanism. The first limit $T_{1/2} > 3 \cdot 10^{15}$ yr was made with ^{124}Sn in Geiger counters (Fireman, 1948). Follow-on direct experiments (Fireman, 1949; Fireman and Schwarzer, 1952; Fremlin and Walters, 1952; Kalkstein and Libby, 1952; Lawson, 1951; McCarthy, 1953, 1955; Pearce and Darby, 1952) incorporated proportional counters, scintillators, Wilson chambers, and nuclear emulsions using several isotopes, and included some positive claims (Fireman, 1949; Fremlin and Walters, 1952; McCarthy, 1953, 1955) that were disproved in more sensitive experiments — a theme that has repeated itself throughout the history of double-beta decay experiments, see Tretyak (2011). Meanwhile geochemical searches (Inghram and Reynolds, 1949, 1950; Levine *et al.*, 1950), which are sensitive only to the combination of $0\nu\beta\beta$ and $2\nu\beta\beta$ decay and not to each of them separately, yielded very strong limits, as well as the first observation of $\beta\beta$ decay of ^{130}Te with a half-life of $1.4 \cdot 10^{21}$ yr (Inghram and Reynolds, 1950), consistent with the rate of Goeppert-Mayer's $2\nu\beta\beta$ decay.

In the same period, Goeppert-Mayer (1949) also established the foundations of the nuclear shell model — an independent particle model at that time — which was independently also proposed by Jensen and others (Haxel *et al.*, 1949). Together with the interplay between single-particle and collective nuclear motion introduced by Bohr and Mottelson (1953), these works set up the cornerstones for the theoretical understanding of nuclear structure, which eventually — after three decades of theory and computing power advances — led to the first modern calculations of $0\nu\beta\beta$-decay nuclear matrix elements.

Following the lack of observation of rapid $0\nu\beta\beta$ decay, a loss of interest in the process started when Davis (1955) did not observe the reactions predicted by Racah's theory — e.g., ^{37}Cl$(\bar{\nu}, e^-)^{37}$Ar — and the $(V - A)$ theory of weak interactions showed that the $0\nu\beta\beta$-decay rate did not depend on just the nature of the neutrino, but also on its mass, as was elegantly elucidated by Case (1957). For vanishing Majorana mass, the effect would disappear and the transition would become undetectable, a point made particularly clear by Touschek (1957). In addition, the influential paper by Primakoff and Rosen (1959) argued in favor of a Dirac neutrino. As a result, the enthusiasm for $0\nu\beta\beta$ decay declined further, as testified by the reduction of citations over time shown in Fig. 1 of certain fundamental papers on $0\nu\beta\beta$ decay (Case, 1957; Furry, 1939; Goeppert-Mayer, 1935; Majorana, 1937; Racah, 1937).

The neutrino mass hypothesis was revived by ideas on flavor transformations of massive neutrinos (1957-1967) (Maki *et al.*, 1962; Pontecorvo, 1957a,b, 1967), supported by the first observations of solar neutrinos (Cleveland *et al.*, 1998), and eventually experimentally proven by the discovery of neutrino oscillation (Kajita, 2016; McDonald, 2016). Additional interest arrived in the seventies,
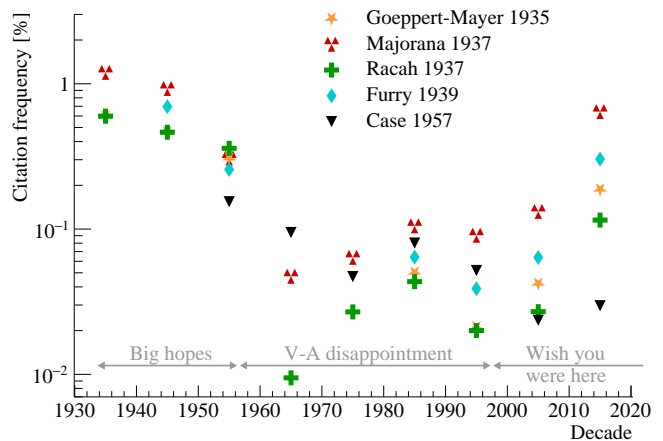
FIG. 1 Citation frequency of some seminal papers on $0\nu\beta\beta$ decay over time, until 2020. The citation frequency is computed as the number of citations per decade divided by the total number of papers with ≥ 10 citations published in the same decade. Data from Inspire. See also Vissani (2021).

the "age of gauge theories", with the conception of the "seesaw mechanism" (Gell-Mann *et al.*, 1979; Minkowski, 1977; Mohapatra and Senjanovic, 1980; Yanagida, 1979), in which a heavy Majorana neutrino generates a tiny mass for the light neutrino emitted in β decay. Furthermore, Weinberg (1979), Wilczek and Zee (1979) showed the usefulness of effective operator analysis to extend the Standard Model of electroweak interactions. In this context, the rates of new phenomena, e.g., $0\nu\beta\beta$ or proton decay, are suppressed by a factor inversely proportional to the scale of "Grand Unification". If new physics exists at an ultra-high scale, the leading mechanism for $0\nu\beta\beta$ decay would be light neutrino exchange. The renewed interest in $0\nu\beta\beta$ decay, boosted by the discovery of neutrino oscillations, was accompanied by an increase in the citation rate of the seminal works, as shown in Fig. 1.

The community has nowadays a common view on $0\nu\beta\beta$ decay, which is a sort of minimal or orthodox vision focused on the supposition that the Standard Model neutrino is a Majorana particle. There are, however, alternative ideas. For instance, Touschek (1948) showed that the observation of $0\nu\beta\beta$ decay does not directly imply the Majorana nature of the neutrino, unless the nature of weak interactions is considered to be known. After the introduction of $(V - A)$ theory, Feinberg and Goldhaber (1959) pointed out the possibility of contributions to $0\nu\beta\beta$ decay unrelated to neutrino mass. The understanding of neutrino oscillation, yielding observable phenomena even with very small neutrino masses, led Pontecorvo (1968) to reiterate the point that $0\nu\beta\beta$ decay could proceed through channels other than the Majorana neutrino mass mechanism. Even today, the possibility of new physics at accelerator or rare process scales, perhaps involving lepton number violation, allows one to imagine a $0\nu\beta\beta$-decay rate significantly greater than that due to

Majorana masses.

The late 1960's to early 1980's also saw a contemporaneous blossoming of experimental techniques in $0\nu\beta\beta$ decay, thanks to inventions such as the Ge(Li) detector (Freck and Wakefield, 1962) and the streamer chamber (Chikovani *et al.*, 1963; Dolgoshein *et al.*, 1964). These led to a leap in half-life sensitivities for direct $0\nu\beta\beta$-decay searches, with efforts by Fiorini and Wu yielding limits on the order of 10^{19-21} yr (Bardin *et al.*, 1967, 1970; Cleveland *et al.*, 1975; Fiorini *et al.*, 1967; Fiorini *et al.*, 1973). This level was also reached with scintillating crystals (der Mateosian and Goldhaber, 1966). During this period, the invention of the high-purity semiconductor Ge (HPGe) detector (Baertsch and Hall, 1970) and time-projection chambers (TPCs) (Nygren, 1974) led to new possibilities for the experimental investigation of $0\nu\beta\beta$ decay.

By the mid-1980s the combination of theoretical motivation and experimental capabilities brought $0\nu\beta\beta$-decay physics into something of a "golden era". Haxton and Stephenson (1984), Doi, Kotani, and Takasugi (Doi *et al.*, 1985) worked out the full theoretical details of the decay, building on earlier work by Primakoff and Rosen (1959, 1969), and subsequently refined by Tomoda (1991). Nuclear matrix element calculations also proceeded in earnest. Studies using the quasiparticle random-phase approximation method showed that they could reproduce extremely long $2\nu\beta\beta$-decay half-lives once proton-neutron pairing is properly taken into account (Vogel and Zirnbauer, 1986). The same physics was found to be relevant for $0\nu\beta\beta$ decay (Engel *et al.*, 1988). Then, in 1987, Moe's group reported the first direct observation of $2\nu\beta\beta$ decay in ^{82}Se using a TPC (Elliott *et al.*, 1987). The process was soon after reported in ^{76}Ge by the ITEP/YePi experiment using HPGe detectors (Vasenko *et al.*, 1990). Ejiri *et al.* (1991) observed the decay in ^{100}Mo using a tracking detector consisting of a planar source sandwiched between drift chambers and scintillator detectors. $2\nu\beta\beta$ decay was also observed in ^{116}Cd in multiple tracking and scintillating crystal experiments (Arnold *et al.*, 1995; Danevich *et al.*, 1995; Ejiri *et al.*, 1995). TPCs and tracking detectors made additional observations in numerous isotopes (Arnold *et al.*, 1996, 1998, 1999; Balysh *et al.*, 1996; Dassie *et al.*, 1995; De Silva *et al.*, 1997; Elliott *et al.*, 1992, 1991), and an assay of a sample of enriched Mo powder using HPGe detectors made the first observation of $2\nu\beta\beta$ decay to an excited state of the final nucleus, in ^{100}Mo (Barabash *et al.*, 1995). The measurement of the half-life of ^{48}Ca (Balysh *et al.*, 1996), the lightest $2\nu\beta\beta$-decay emitter and the one with least complex nuclear structure, was found to be in good agreement with the nuclear shell model prediction (Caurier *et al.*, 1990; Poves *et al.*, 1995), giving confidence to nuclear matrix element calculations.

These experiments achieved exquisite sensitivity also to the $0\nu\beta\beta$-decay mode, culminating in half-life limits at the level of 10^{25} years by the Heidelberg-Moscow

and IGEX experiments in ^{76}Ge (Gonzalez *et al.*, 2000; Klapdor-Kleingrothaus *et al.*, 2001b). A subset of the Heidelberg-Moscow collaboration claimed an observation with half-life on the order of 10^{25} yr initially with 3.1σ significance (Klapdor-Kleingrothaus *et al.*, 2001a), increasing to 4.2σ and then $>6\sigma$ significance in subsequent reanalyses (Klapdor-Kleingrothaus and Krivosheina, 2006; Klapdor-Kleingrothaus *et al.*, 2004). This claim was strongly questioned by Feruglio *et al.* (2002), Aalseth *et al.* (2002), Schwingenheuer (2013), and ultimately ruled out by more sensitive experiments, with the first definitive exclusion at $>99\%$ CL coming from the GERDA experiment (Agostini *et al.*, 2013).

GERDA (Agostini *et al.*, 2020b) along with KamLAND-Zen (Abe *et al.*, 2022) and other experiments from the modern era (Adams *et al.*, 2022; Anton *et al.*, 2019; Arnquist *et al.*, 2022) (see Sec. VI) have now explored half-lives in the range 10^{25} yr to a few times 10^{26} yr. At present, major investments are being made in the USA (Aprahamian *et al.*, 2015), Europe (Giuliani *et al.*, 2019), and elsewhere (see Sec. VI) to mount experiments capable of reaching 10^{28} yr and beyond. A broad class of models predicts high discovery potential for this next-generation of searches. If nature so chooses, the most exciting chapter in the history of neutrinoless double-beta decay could be about to unfold.

III. PARTICLE PHYSICS THEORY AND MOTIVATIONS

Neutrinoless double-beta decay is of fundamental importance for particle physics, and over time became central also to several other fields, including nuclear physics and cosmology. In this section, we highlight the key aspects of this connection from a modern perspective.

We first discuss in Sec. III.A the role of global symmetries in particle physics and their associated conserved quantities, and in particular lepton number L and the difference between baryon and lepton number $B - L$, which are both tested by $0\nu\beta\beta$-decay experiments. In Sec. III.B, we consider the role and meaning of the neutrino's Majorana mass, and of other effective operators which parameterise possible violations of the global symmetries. Sec. III.C focuses on specific theoretical models that predict lepton number violation phenomena. Then, in Sec. III.D, we discuss observational neutrino physics, introducing the parameter describing the contribution of known neutrinos to $0\nu\beta\beta$ decay: the effective Majorana neutrino mass $m_{\beta\beta}$. Finally, the link between the excess of baryons in the observable universe and the violation of the global symmetries of the Standard Model (SM) is examined in Sec. III.E.

Secs. III.A, III.B, III.D and III.E are all introductory and contain basic material needed to develop an overview of the field. These parts are intended for nonexpert readers. Section III.C covers a wide range of theoretical mod-

els connected to $0\nu\beta\beta$ decay and, because of its technical nature, it is intended for a more expert audience.

A. Global symmetries

In this section we first examine the role played by global symmetries — those associated with the conservation of baryon and lepton number — for the understanding of particle physics (Sec. III.A.1). Then, we review their meaning in the Standard Model, emphasising the exact (non-anomalous) symmetries, and in particular the combination $B - L$ (Sec. III.A.2). Finally, we discuss $0\nu\beta\beta$ decay in relation to these symmetries (Sec. III.A.3), arguing that it qualifies as a process in which a net amount of matter particles is created.

1. Baryon and lepton number conservation

Nuclear theory was directly based on the idea that the total number of nucleons remains the same in any transformation. This was soon generalized into a "conservation law for the number of heavy particles" (*baryon conservation*) by Wigner (1949), who noted that the proton could decay into $p \to e^+ + \pi^0$ unless some law forbids it. For light matter particles, namely electrons and neutrinos (leptons), the situation was less clear, especially in view of the elusive nature of neutrinos (Marx, 1953; Zeldovich *et al.*, 1993). The four-fermion theory of the weak interaction is formulated in a manner that allows the assignment of a conserved number to the sum of charged and neutral leptons, where antimatter particles are assigned a negative sign. However, after Majorana proposed his theory of massive neutrinos, it became clear that it was not even possible to tell *a priori* whether a neutrino and an antineutrino are two distinct particles, or two states of the same particle differing only by helicity. Tests of the hypothetical decay $(A, Z) \to (A, Z+2) + 2e$, carried out since the 1940's, have not yet revealed any hint that the number of leptons could vary. Early direct searches for neutrino masses — such as those conducted by Hanna and Pontecorvo (1949) — and studies of their helicity suggested that neutrinos are practically massless (Landau, 1957; Lee and Yang, 1957; Salam, 1957), and contributed to a reduced interest in Majorana's proposal. Moreover, subsequent investigations showed that the beam of muon neutrinos from π^+ decay produces leptons and not antileptons. In short, it was hypothesized that also the *number of leptons does not change* in any interaction. A beautiful summary of the situation can be found in Feinberg and Goldhaber (1959).

The discussion deepened with the emergence of the various families of particles. For instance, the question of why $\mu \to e + \gamma$ is forbidden became as important as that of whether proton decay exists, and motivated the introduction of separate *muon and electron number conservation laws*. At this point, however, an apparent difference between baryons and leptons emerged: the conservation of the hadronic families was violated by weak interactions in transformations between neutrons and protons, while that of leptonic families was not.

Nonetheless, the perception of a correspondence between hadrons and leptons remained. The strengths of their weak interactions were found to be the same (Pontecorvo, 1947; Puppi, 1948), and mixing among leptons and among quarks was introduced in the early sixties on theoretical bases (Cabibbo, 1963; Katayama *et al.*, 1962; Maki *et al.*, 1962). Inspired by the work of Gell-Mann and Pais (1955), Pontecorvo (1957b) introduced the idea of neutrino transmutation, noting its connection to neutron-antineutron and hydrogen-antihydrogen transmutations, i.e., violations of baryon number. Finally, the seminal work of Sakharov (1967) on baryogenesis suggested a specific $B - L$ conservation law, and discussed explicitly the possibility of proton decay associated with the Planck mass scale $M_P = \sqrt{\hbar c / G_N}$, defined in terms of the speed of light and Planck and Newton's constants. The decay rate is thus strongly suppressed.

2. The Standard Model and $B - L$

Let us come to the age of the Standard Model of particle physics and its $\mathrm{SU}(3)_c \times \mathrm{SU}(2)_L \times \mathrm{U}(1)_Y$ gauge group. The renormalizable quantum field theory follows from the conventional choice of 15 quarks (u, d) and leptons (e, ν) per family,

$$
\begin{array}{llllllll}
u_{r,L} & u_{g,L} & u_{b,L} & \nu_L & u_{r,R} & u_{g,R} & u_{b,R} & \\
d_{r,L} & d_{g,L} & d_{b,L} & e_L & d_{r,R} & d_{g,R} & d_{b,R} & e_R,
\end{array}
$$

with an important feature: baryon number B, the three lepton numbers L_e, L_μ, L_τ, and the total lepton number $L = L_e + L_\mu + L_\tau$, are accidentally conserved, i.e., their associated symmetries emerge accidentally without being *a priori* required. This is in agreement with experiments.

Not all of these global symmetries are expected to be exactly obeyed. They are all symmetries of the classical Lagrangian density, but some of them are not symmetries of the full quantum theory, and can hence be violated by quantum fluctuations. In jargon, these are called anomalous symmetries (Adler, 1969; Bardeen, 1969; Steinberger, 1949). Indeed, the divergence of the leptonic and the baryonic currents are not zero ('t Hooft, 1976), but rather $\partial^\mu J_\mu^{(B)} = \partial^\mu J_\mu^{(L)} = 3g^2/(32\pi^2)\mathrm{Tr}[F_{\mu\nu}\widetilde{F}^{\mu\nu}]$ where g is the $\mathrm{SU}(2)_L$ gauge coupling and $F_{\mu\nu}$ the field strengths, so these currents are not conserved. The exact (non-anomalous) SM global symmetries are

$$B - L , \quad L_e - L_\mu , \quad L_\mu - L_\tau , \tag{1}$$

along with their linear combinations, e.g., $L_e - L_\tau$. In fact, the SM predicts the existence of non-perturbative

transitions that violate other combinations, e.g., $B+L$, as is well-known in "baryogenesis" and "leptogenesis" theories that attempt to explain the cosmic excess of baryons. Suffice it here to remark the existence of an effective operator formed by the left doublets $q_{\mathrm{L}} = (u_{\mathrm{L}}, d_{\mathrm{L}})^t$ and $\ell_{\mathrm{L}} = (\nu_{\mathrm{L}}, e_{\mathrm{L}})^t$, that respects all the anomaly-free symmetries and violates the other ones.

It should be noted that the observation of neutrinos other than those initially produced in "neutrino appearance" experiments, even before invoking an interpretation in terms of massive neutrino oscillation, demonstrated the violation of the anomaly-free symmetries $L_{\mathrm{e}} - L_\mu$ and $L_\mu - L_\tau$ (Dell'Oro et al., 2018a,b). For example, SNO observed the appearance of muon and tau neutrinos in the solar electron neutrino flux (Ahmad et al., 2001), and various experiments have seen the appearance of new neutrinos from muon neutrino beams: electron neutrinos in T2K (Abe et al., 2014) and tau neutrinos in the case of OPERA (Agafonova et al., 2018). A straightforward implication is that *the only residual symmetry of the Standard Model is $B - L$.* If this symmetry is respected, we can distinguish perfectly matter particles from antimatter particles, as described in the Standard Model. However, if $B - L$ is violated, we should expect transitions between matter and antimatter particles, for example, the transformations between neutrinos and antineutrinos discussed in Sec. III.B.1. Thus experimentally investigating $B - L$ is of paramount importance, and the process $(A, Z) \to (A, Z + 2) + 2e$ provides a direct test of it. Note, incidentally, that the observation of the otherwise extremely interesting decay of the proton via $p \to e^+ + \pi^0$ or any other mode induced by dimension-6 operators would not.

3. What is a proper name for $(A, Z) \to (A, Z + 2) + 2e$?

So far, in this section, we have avoided referring to the process $(A, Z) \to (A, Z+2)+2e$, as "neutrinoless double-beta decay". We did it intentionally, with the aim of examining first the meaning and the importance of the process at hand. Not only is it possible to characterize this decay quite directly as a "creation of two electrons", using a terminology accessible even to laypersons, it is also possible to call it the "creation of leptons without antileptons", using jargonic parlance highlighting specifically the violation of L. Most importantly, considering the SM structure, this term should be associated with the violation of $B - L$, the only residual global symmetry allowing the distinction of matter from antimatter particles. This process can thus be described as the "creation of matter without antimatter", or more precisely the creation of particles of matter, in this case electrons. This is different from usual weak decays, such as normal β decays, which produce electrons (matter particles) accompanied by the same number of antineutrinos (antimatter

particles), and thus do not change L.

The traditional name for the process, "neutrinoless double-beta decay", is formally correct but rather obscure as it defines the process in terms of particles that are *not* produced — something akin to calling a hippopotamus a "trunkless elephant". Moreover, it uses "beta-rays" for electrons, a term that dates back to Rutherford's time when it was surmised that electrons live in the atomic nucleus. The standard terminology was introduced to contrast this process with the "ordinary" $\beta\beta$ decay of Göppert-Mayer, and reminds us the theoretical belief that the transition is dominantly triggered by the exchange of virtual Majorana neutrinos, which are valuable points. However, we think that these are not good reasons to understate the importance of this process for the current understanding of matter and its interactions (Dell'Oro et al., 2018a,b).

B. Majorana neutrinos and other sources of lepton number violation

In this section we present the main mechanisms that can lead to lepton number violating effects and $0\nu\beta\beta$ decay. We first introduce the simplest case, in which ordinary neutrinos are endowed with a Majorana mass and the fermionic spectrum of the Standard Model is not modified. As we argue in Sec. III.B.1, this assumption means that neutrinos, unlike all other fermions, are at the same time particles of matter and antimatter. In Sec. III.B.2, we then take full advantage of the structure of the Standard Model, and discuss the numerous effective operators that parameterize all possible lepton-number-violating effects. Finally, in Sec. III.B.3, we examine the simplest renormalizable extension of the Standard Model leading to Majorana neutrino masses, namely, the inclusion of right-handed neutrinos.

1. Majorana neutrinos: a bridge between matter and antimatter

Majorana's neutrinos are both particles and antiparticles. This often-heard statement is far from being trivial. To clarify its meaning, it is useful to remember that neutrinos are particles with spin $1/2$, i.e. fermions. Fermions constitute matter (and antimatter), whereas bosons constitute forces. In the context of the Standard Model of Glashow, Weinberg and Salam, neutrinos along with all other particles are distinct from their antiparticles. Such a difference is evident for charged fermions, but what about for neutral ones?

In fact, Standard-Model neutrinos are neutral. They have hypercharge but this is broken spontaneously, leaving only two ways to distinguish neutrinos from antineutrinos. The first way concerns the helicity of the particle: it is negative for the neutrino and positive for the
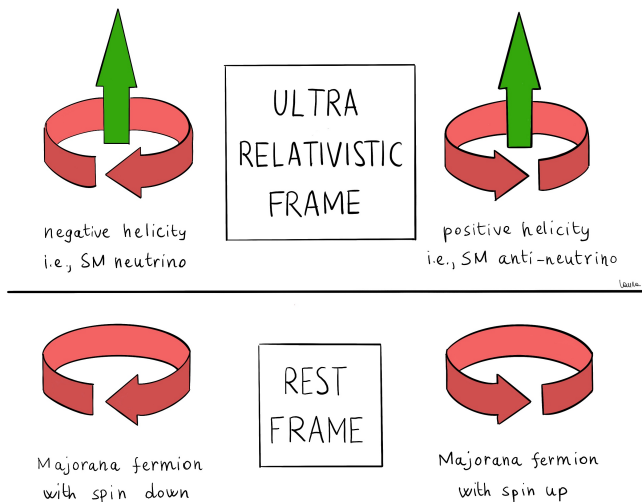
FIG. 2 Artistic illustration of the relation between the neutrino and antineutrino helicity, which is given by the projection of the spin (red arrow) onto the momentum (green arrow). The helicity distinguishes neutrinos from antineutrinos in the ultra-relativistic limit (top panel). However, in the rest frame the neutrino and antineutrino are two spin states of the same particle (lower panel). Image courtesy of L. Manenti.

antineutrino. The second way is based on the charged lepton that accompanies charged lepton interactions: for example, in all observed $\beta^{\mp}$-decays, the (anti)neutrino is co-produced with a particle of (negative) positive charge.

The neutrino's helicity is a consequence of the chiral structure of the weak interactions — formally corresponding to the presence of the P_L projector in the charged interactions — but only provided that the neutrino mass is exactly zero. If neutrinos are massive, helicity coincides with chirality only in the ultra-relativistic limit. All experimental observations related to weak interactions have been made, and can be made, only on ultra-relativistic neutrinos. However, as a thought experiment, we can consider observing a neutrino and an antineutrino in their rest frame, whose existence is guaranteed by their tiny masses measured through oscillation experiments. In this frame, the momentum and helicity of the neutrino and antineutrino are both zero and, in the absence of additional quantum numbers, the two particles can differ only by the orientation of their spin. Therefore, symmetry under rotations implies that the two states must be the same particle. In conclusion, the structure of the Standard Model, together with the hypothesis that neutrinos have mass, suggests that the neutrino and the antineutrino are the very same particle in the rest frame. The point is summarised graphically in Fig. 2 and discussed also by Dell'Oro *et al.* (2016).

A different conclusion can be drawn assuming the existence of some property discriminating the two particles even in the rest frame, for instance lepton number. In this case, two additional neutral particle states must exist in the rest frame, and they must be "sterile", i.e., unable to couple to the Standard Model gauge fields. This possibility is what people refer to when they speak about Dirac neutrinos. It should be stressed that Dirac neutrinos require *invoking* an ad-hoc property, such as lepton number, as opposed to *inferring* such a property from the model structure. Invoking an ad-hoc property can be perceived as unnatural, in which case one might favor Majorana's neutrinos.

Majorana neutrinos would be unique among fermions and provide a bridge between matter and antimatter. Majorana's hypothesis evidently confronts us with a blatant violation of the L symmetry. Since baryon number is not affected by neutrinos, the $B - L$ symmetry would also be broken.

The previous considerations obviously do not constitute a formal proof that neutrinos are Majorana particles. There is currently no experimental evidence of $B - L$ violation, except for the indirect cosmological observation that there are more atoms than anti-atoms. However, cosmological observations are unable to test potential lepton asymmetries created by neutrinos, which could compensate the baryon asymmetry. These considerations highlight the crucial importance of experimentally testing the conservation of $B - L$, in particular, through the study of $0\nu\beta\beta$ decay.

2. Effective operators and energy scale

A general theorem from Helset and Kobach (2020) states that the variations of lepton number ΔL and baryon number ΔB obey

$$\frac{\Delta L - \Delta B}{2} = d \bmod 2, \tag{2}$$

where d is the canonical dimension of the operator causing the transition, $\mathcal{O}_d$. This operator is a polynomial of SM fields and possibly also right handed neutrinos, i.e., sterile neutrinos under the SM interactions. As usual, fermionic fields contribute $+3/2$ to d and bosonic fields (or derivatives) contribute $+1$. In the case of $0\nu\beta\beta$ decay, where baryon number is conserved and $\Delta L = \pm 2$, the canonical dimension must be odd, and the new physics scale Λ that parameterizes the operators $\mathcal{O}_d$ appears as $1/\Lambda^{d-4}$. After spontaneous symmetry breaking (SSB), the electroweak scale $v = (\sqrt{2}G_{\mathrm{F}})^{-1/2} = 246$ GeV, which is plausibly smaller than Λ, is brought into play in the numerator of the operator, where G_{F} is Fermi's constant.

A useful introduction to the role of effective operators can be found in the original works of Weinberg (1979, 1980), Wilczek and Zee (1979), Babu and Leung (2001), and Choi *et al.* (2002). The full classification of all operators of dimension 7 and 9 has been recently completed by Lehman (2014), Li *et al.* (2021b) and Liao and Ma (2020).

Omitting right handed neutrinos, there is no renormalizable operator that breaks L (or B); at dimension 5 there is only one operator, the well known Weinberg operator (Weinberg, 1979, 1980); at dimension 7 there are 13 operators that obey $\Delta L = 2$; at dimension 9 there are several hundreds of them; we still do not have a systematic study of the number of operators at dimension 11.

The dimension-5 operator leads to a Majorana mass for ordinary neutrinos and can be constructed starting from the following gauge invariant combination of a leptonic doublet ℓ and a Higgs doublet H:

$$\ell_{\mathrm{L}}^t \varepsilon H = \frac{1}{\sqrt{2}} \left(\nu_{\mathrm{L}}, e_{\mathrm{L}} \right) \begin{pmatrix} 0 & 1 \\ -1 & 0 \end{pmatrix} \begin{pmatrix} 0 \\ v+h \end{pmatrix} \quad (3)$$

$$= \frac{1}{\sqrt{2}} v\, \nu_{\mathrm{L}} + \text{interactions}, \quad (4)$$

where H is given in the physical gauge, and $\varepsilon = i\sigma_2$ is the invariant matrix of $\mathrm{SU(2)_L}$. This term behaves just like a spinor field under Lorentz transformations, so we can use it to form the Minkowski-Weinberg operator, namely the following Lorentz invariant term of the Lagrangian density

$$\delta \mathcal{L} = -\frac{1}{2M} (\ell_{\mathrm{L}a}^t \varepsilon H) C_{ab}^{-1} (\ell_{\mathrm{L}b}^t \varepsilon H) + \text{h.c.} \quad (5)$$

where C is the charge conjugation matrix and $a, b = 1, 2, 3, 4$ are four-spinorial indices. After SSB, this yields a bilinear term in ν_{L}, i.e., a Majorana mass term. Thus we identify

$$m = \frac{v^2}{2M} \approx 50\,\mathrm{meV} \times \frac{6 \cdot 10^{14}\,\mathrm{GeV}}{M}, \quad (6)$$

a relation showing that the neutrino mass values m, which have been discovered by means of neutrino oscillation, correspond to very large masses M. We note that this mass scale strongly differs from $v = 246\,\mathrm{GeV}$, the electroweak mass scale, and is smaller than the Planck mass: a valuable indication of new physics.

The $d = 7$ operators that after SSB have a structure $\mathcal{O} = \bar{e}\nu\bar{u}d v^2/\Lambda^3$ need SM "dressing" to specify the $0\nu\beta\beta$-decay transition; this implies the exchange of virtual neutrinos (the inclusion of a neutrino propagator) but without the need for further lepton number violation. Moreover, there are dimension-7 operators (Lehman, 2014) involving the W boson that after spontaneous symmetry breaking produce effective operators with structures $gW\,\bar{e}^2\,\bar{u}d\,/\Lambda^3$ and $(gW\,\bar{e})^2\,v^2/\Lambda^3$. Together with the usual SM interactions between the W and the quarks, these lead to contact operators of the type $(\bar{e}\bar{u}d)^2/(\Lambda^3 v^2)$ (Cirigliano et al., 2017).

The dimension ≥ 9 operators considered above are contact terms and by construction produce $\mathcal{O} \propto ee(u\bar{d})^2$ after SSB; they are multiplied by $1/\Lambda^5$ or v^2/Λ^7 when the dimension is 9 or 11, respectively. Therefore it is quite common to restrict attention to the cases with dimension ≤ 9, which are expected to provide larger contributions to $0\nu\beta\beta$ decay (see, e.g., Bonnet et al. (2013) for dimension-9 operators).

The naïve scaling of transition amplitudes for operators of various dimensions are

$$\dim 5:\ G_{\mathrm{F}}^2 \frac{v^2}{\Lambda} \frac{1}{p^2}, \quad \dim 7:\ G_{\mathrm{F}} \frac{v}{\Lambda^3} \frac{1}{p}, \quad \dim 9:\ \frac{1}{\Lambda^5}, \quad (7)$$

where $p \sim 200\,\mathrm{MeV}$ is the virtual momentum of the neutrino, estimated as the inverse of the typical distance between nucleons in nuclei. This suggests a suppression by powers of $\epsilon = p/v\Lambda^2 < 10^{-4}$ if $\Lambda \geq 1\,\mathrm{TeV}$. This would indicate that the amplitude decreases with dimension. These naïve expectations are supported by the cursory bounds illustrated in Choi et al. (2002), assuming $0\nu\beta\beta$-decay half-life values longer than $10^{25}\,\mathrm{yr}$. On the other hand, the above approach neglects the possible presence of small coefficients — e.g. Yukawa couplings — that could in principle suppress the lower dimension terms more than the other ones. If for instance we consider the reasonable value $m_\nu \sim 10\,\mathrm{meV}$ suggested by experiments for the Majorana neutrino mass, rather than estimating the theoretical mass as $m_\nu \sim v^2/\Lambda$, we would write the dimension-5 amplitude as $G_{\mathrm{F}}^2 m_\nu/p^2$, which is of the same order as the dimension-7 (dimension-9) term if $\Lambda \sim 10^3\,\mathrm{TeV}$ ($\Lambda \sim 10\,\mathrm{TeV}$). In any case, these estimations are useful for a first orientation at best. Moreover, considerations of hadronization and nuclear matrix elements can have an impact of orders of magnitude, see the discussion after Eq. (20) in Sec. IV.

3. Majorana and right-handed neutrinos

We know that at least two of the three known neutrinos are not massless, and it is usually assumed that no other light neutrinos mix with them (Dentler et al., 2018). This simple remark poses a macroscopic theoretical question: why are the masses of the three ordinary neutrinos so different from — so much smaller than — those of the other SM fermions? The answer could be related to the Weinberg operator described in the previous section. This operator was originally introduced by Minkowski (1977) in the context of specific models including new ultra-heavy neutrinos that are neutral under the SM interactions. In this case, the operator is multiplied by a coefficient inversely proportional to the heavy neutrino masses and directly proportional to the square of Yukawa interactions Y between neutrinos. In fact, Yukawa interactions guarantee the mixing of ordinary (left-handed) and new (right-handed) neutrinos, as recalled in Sec. III.C.2. The general expression of the corresponding Majorana mass, in terms of mass matri-

ces, is

$$M_\nu = -M_{\mathrm D}\ M_{\mathrm R}^{-1}\ M_{\mathrm D}^t \quad \text{with} \quad M_{\mathrm D} = \frac{1}{\sqrt{2}}Yv, \quad (8)$$

where $M_{\mathrm D}$ is the Dirac mass matrix, and $M_{\mathrm R}$ is that of the heavy neutrinos. This mechanism for the generation of ordinary neutrino masses is called the *seesaw mechanism*: in analogy to the children's game in which a heavier child lifts a lighter one, the mass of the light neutrino is inversely proportional to the scale of the heavy neutrino's mass.

The model with ultra-heavy (right-handed) neutrinos illustrates an important and rather general feature: the smallness of the ordinary neutrino masses can be attributed partly or mainly to the occurrence of small (adimensional) coefficients, the Yukawa couplings. In other words, by simply measuring small neutrino masses, it is not possible to deduce that the scale of new physics is large. This is evident for Dirac neutrino masses — where $M_{\mathrm R} = 0$ and Eq. 8 does not apply, having $M_\nu = M_{\mathrm D}$ — but it also applies to Majorana neutrino masses. This kind of difficulty was clear since the beginning. The very first paper on the topic (Minkowski, 1977) has the eloquent title $\mu \to e\gamma$ *at a rate of one out of* 10^9 *muon decays?* and intentionally assumes $50\,\mathrm{GeV}$ for the heavy neutrino mass, which shows the awareness of the importance of testing the seesaw hypothesis for ordinary neutrino masses.

If the right handed neutrino masses are not too large, a few direct or indirect laboratory tests are possible — see Alekhin *et al.* (2016) for a fully worked out example. It is worth mentioning that a "hierarchy problem" occurs with new right handed neutrinos heavier than $\sim 10^4\,\mathrm{TeV}$ (Vissani, 1998a), which could serve as a motivation for supersymmetric models (Barbieri and Giudice, 1988) discussed in Sec. III.C.3. Finally, as mentioned in Sec. III.E, the scenario with ultra-heavy neutrinos can be somewhat subject to valuable constraints requiring the validity of specific models for baryogenesis.

To conclude, the only BSM phenomenon observed so far is neutrino oscillation, which requires that the masses of at least two ordinary neutrinos are not zero. This situation resembles that of weak interactions long before the SM, before Fermi's theory. All we can say is that we have theoretical reasons to suspect that the neutrino masses are due to the dimension-5 operator. Despite the simplicity of these statements, the essential objectives for real progress are to demonstrate that the neutrino masses have a Majorana character and that the total number of leptons and $B - L$ are violated.

C. Models for lepton number violation

In this section, we review some proposals on how to extend the Standard Model, highlighting their connec-

tions to neutrino masses and $0\nu\beta\beta$ decay. We start from unified models, based on the gauge principle, just like the Standard Model (Sec. III.C.1). We then discuss the reasons for extending the fermion spectrum and include right-handed neutrinos (Sec. III.C.2). Finally, we consider supersymmetric extensions in Sec. III.C.3 and close with a wide range of models compatible with observable signals in the laboratory in Sec. III.C.4.

1. Gauge theories and lepton violation at very high energy scales

There are various gauge groups that extend the SM and have been regarded with interest for some of their features and new predicted phenomena. Among the features are the possibility of gauge coupling unification (Grand Unification); this can be complete or partial, in the sense that it might require the existence of intermediate scales.

The new phenomenon predicted by these models and which received the greatest emphasis in the 1970s is the occurrence of proton decay, but later it was realized that also the existence of non-zero neutrino masses was a generic consequence of several models (Gell-Mann *et al.*, 1979; Mohapatra and Senjanovic, 1980). The experimental evidence for non-zero neutrino masses add motivation for SO(10) (Fritzsch and Minkowski, 1975), which can break into SU(5) (Georgi and Glashow, 1974) or into $\mathrm{SU}(4)_{\mathrm c} \times \mathrm{SU}(2)_{\mathrm L} \times \mathrm{SU}(2)_{\mathrm R}$ (Pati and Salam, 1974). These models are characterized by dimensionless Yukawa couplings y, and the scale Λ of the new, heavy particles, e.g., heavy right-handed neutrino masses. In the simplest case, called type I seesaw, Eq. 6 is recovered with scale $1/M$ given by $y^2/\Lambda \sim 1/M$. Other cases besides the type I seesaw are possible and are realised in actual models such as those based on SO(10), as discussed below. Notice that the same value of M can be obtained with y of order one and $\Lambda \sim M$, but also with correspondingly smaller y and Λ.

It is worth mentioning here the fact that proton decay has still not been found, and that its search continues to be strongly motivated from the theory side. Proton decay, together with neutrino masses, keep drawing attention to SO(10), a well-defined model for which it is important to keep deriving quantitative predictions and related uncertainties. Recall that this is a gauge group with only one coupling constant, which includes a right-handed neutrino in each fermion family together with the known leptons and quarks of the Standard Model. Put differently, this is the unification group that overcomes the asymmetry of particle content highlighted in Eq. III.A.2, necessarily including — within its 16-dimensional spinors — right-handed neutrinos.

2. Right-handed neutrinos and the νSM

There are many good reasons to postulate the existence of three right-handed neutrinos. First, they are a plausible mechanism to provide mass to light neutrinos (Minkowski, 1977; Yanagida, 1979). In addition, as previously discussed, they imply a full symmetry between left and right spinors of the SM (Mohapatra and Senjanovic, 1980). They also allow the promotion of the $B - L$ symmetry to a non-anomalous gauge symmetry; indeed they are required in SO(10) and other unification groups (Gell-Mann *et al.*, 1979). Further, they could explain baryogenesis via leptogenesis, as first argued in (Fukugita and Yanagida, 1986), see Sec. III.E.

Right-handed neutrinos can be incorporated in the SM as gauge singlet Weyl fermions N_i, with Lagrangian terms connecting them to the leptonic weak doublets ℓ_α:

$$\mathcal{L}_{\nu\mathrm{SM}} = N_i i\partial_\mu\gamma^\mu N_i - Y_{\alpha,i}\ell_\alpha H N_i - \frac{M_i}{2}N_i N_i + h.c., \quad (9)$$

where H is the Higgs weak doublet, the $Y_{\alpha,i}$ are Yukawa couplings, and M_i are Majorana masses for the N_i. This comprises a minimal, renormalizeable Standard Model extension that accounts for neutrino masses while remaining consistent with gauge invariance, and is referred to as the "νSM" (Asaka *et al.*, 2005; de Gouvea, 2005, 2007). The case $M_i = 0$ corresponds to Dirac neutrinos, but when $M_i \neq 0$, the mass term has the L- and $B - L$-violating structure of Eq. 5, and after SSB gives rise to Majorana mass terms for the light neutrinos.

In most models the new neutrinos are heavy and do not have direct implications at low energy scales except for SM neutrino masses. In other models right handed neutrinos are lighter, about 1-10 keV, and can explain dark matter and possibly also the cosmic baryon excess (Asaka *et al.*, 2005); interestingly, these models make no new contributions, other than the Majorana masses of light neutrinos, to $0\nu\beta\beta$ decay (Bezrukov, 2005).

3. Supersymmetry at accelerator energies

Supersymmetry is a symmetry between fermions and bosons. The SM extension to a supersymmetric theory is possible but requires the introduction of several new particles, heavy enough to not have been observed yet. The hypothesis that the masses of supersymmetric particles are not too far from the electroweak scale has been regarded with interest because an approximate supersymmetry can decouple the high mass scales from the electroweak scale, but to date these particles have not been found in direct searches.

If the gauge principle — i.e., all terms allowed by the postulated symmetries are present in the Lagrangian density — is applied to the supersymmetric SM, lepton number and/or baryon number are not automatically conserved. Usually, this situation is felt as a shortcoming

of generic supersymmetric models to be emended, as it triggers the instability of neutral fermions, which would otherwise make useful dark matter candidates. The usual solution is to postulate a new discrete symmetry, called R-parity, that amounts to the imposition of lepton and baryon number conservation and allows one to recover the dark matter candidate. In fact, in the usual parlance, the "supersymmetric SM" implicitly assumes R-parity. At accelerator energies, these types of models have no significant implications for neutrino masses.

4. Other new physics near the Standard Model scale

To provide a more complete case study, we would like to conclude this overview of models by highlighting some of the theoretical scenarios that are compatible with new contributions to $0\nu\beta\beta$ decay in addition to that due to the masses of light neutrinos. Without any claim to completeness, and with the aim of illustrating some interesting possibilities, we will focus on R-parity breaking supersymmetry, on low-scale seesaw, and on left-right gauge theories see e.g. (Agrawal *et al.*, 2021; Alekhin *et al.*, 2016; Deppisch *et al.*, 2015a; Golling *et al.*, 2016) for a wider discussion. A common feature of these models is the appearance of very small couplings, which ensure consistency with available observations and, in particular, allow the smallness of neutrino masses to be explained, replacing the role of the GUT energy scales in the standard theoretical reference frame (seesaw).

Supersymmetry with broken R-parity. Let us begin by returning to consider certain supersymmetric extensions of the Standard Model. As we have already argued, the supersymmetric extension of the Standard Model does not rule out the existence of violations of lepton number L at the mass scale of the supersymmetry itself. This consideration is evident, noting that the "superfield" containing the Higgs doublet (H^0, H^-) has the same quantum numbers as that containing the leptonic doublet (ν_e, e), and each contains both fermions and bosons. L-violating couplings between these superfields that are sufficiently small can explain the neutrino mass and give rise to new contributions to $0\nu\beta\beta$ decay. They also lead to additional interesting phenomenology for lepton number violation, see for instance (Bolton *et al.*, 2022; Faessler *et al.*, 2008; Hall and Suzuki, 1984; Hirsch *et al.*, 2000a,b; Nilles and Polonsky, 1997; Ross and Valle, 1985). Furthermore, these models include leptoquarks and dileptons, with masses in a region potentially accessible to direct (accelerator) investigation, and can lead to several interesting manifestations.

TeV scale seesaw. The possibility of neutrinos with masses M_R around the TeV scale or even lower has been widely discussed, see (Drewes, 2013) for a review. Electroweak fits are affected and, in some cases, improved by the inclusion of the new heavy neutrino states (Akhmedov *et al.*, 2013). Moreover, these states can have a significant impact on $0\nu\beta\beta$ decay and can even constitute the main contribution to the transition rate (Atre *et al.*, 2009; Bhupal Dev *et al.*, 2013; Mitra *et al.*, 2012). In this case, it is a contact contribution whose dimensional fit scales as $G_F^2 \ M_{LR}^2/M_R^3$, where M_{LR} denotes the Dirac mass. However, the natural neutrino mass contribution from the seesaw, M_{LR}^2/M_R, must be suppressed by means of a particular matrix structure; this can be achieved without excessive fine-tuning if the right-handed neutrino mass respects an upper limit ~ 10 GeV (Mitra *et al.*, 2012).

Left-right models near the electroweak scale. In the last decade, an elegant, minimal extension of the gauge principle which underlies the "Standard Model" has been explored in order to realise a predictive theoretical scheme[1] at a relatively low mass scale (Maiezza *et al.*, 2010), in which neutrinos are naturally endowed with mass (see in particular (Nemevsek *et al.*, 2013; Senjanovic and Tello, 2019)), a situation that could lead to a rich phenomenology. In fact, the presence of new and relatively large gauge couplings would be compatible with the actual production of new particle states at accelerators (in contrast with the previous class of models, where the production is due to the Yukawa couplings, that are not expected to be large). Furthermore, it has been observed that $0\nu\beta\beta$ decay would be a natural manifestation of this type of pattern (Tello *et al.*, 2011). This research programme has stimulated wide interest and subsequent discussions; we refer to the literature for the progress and insights that have followed (Awasthi *et al.*, 2013; Chakrabortty *et al.*, 2012; Li *et al.*, 2021a; Lindner *et al.*, 2016).

5. Discussion

In the earliest theoretical proposals, the physics giving rise to neutrino masses was assumed to be confined to very large energies: this leads one to expect that the (small) Majorana masses of ordinary neutrinos controls the rate of $0\nu\beta\beta$ decay. Although we believe it is prudent to consider this case the reference one, as illustrated in the previous section, we cannot exclude the possibility of significant additional contributions, which could justify even more optimistic expectations.

———

[1] However, neutrinos are treated very differently to other particles, complicating further steps toward unifying gauge interactions.

Moreover, we note that the reference expectation concerning the leading contribution to $0\nu\beta\beta$ decay is based on a number of assumptions. In particular, it assumes that the Standard Model is a good approximation of physics at the scales accessible today, and that there are no new light particles that play an important role in lepton number violation. However, there are indications (albeit indirect and not yet of unambiguous interpretation) of possible experimental anomalies, which depart from the expectations of the Standard Model, and whose interpretation might ultimately require new relatively light particles: e.g., those related to the $g-2$ muon (Abi *et al.*, 2021), the mass of the W boson (Aaltonen *et al.*, 2022) (see also (Cacciapaglia and Sannino, 2022)) or flavour physics, see e.g. (D'Alise *et al.*, 2022).

In addition, there are rather general questions that the Standard Model is unable to address, such as providing a candidate for non-baryonic dark matter, or giving reasons for the origin of the baryonic asymmetry. It cannot be ruled out that also these issues point to the existence of new light particles, which might also play some role for $0\nu\beta\beta$ decay.

D. Majorana masses and neutrino phenomenology

In this section we analyze the earliest proposed and most straightforward mechanism driving a non-zero rate for $0\nu\beta\beta$ decay, i.e., Majorana neutrino masses. First we recall the experimental evidence for neutrino masses, provided by neutrino oscillation experiments. Then, we introduce the essential formalism and the relevant parameter $m_{\beta\beta}$, often called the *effective Majorana neutrino mass*. Next, the general aspects of the connection between $m_{\beta\beta}$ and $0\nu\beta\beta$ decay are introduced. Finally, we discuss the experimental constraints on $m_{\beta\beta}$, as well as indications (empirical and theoretical) on its value. The quantitative implications for future experiments will be worked out in Sec. VII.

1. Neutrino oscillation

The definitive evidence of neutrino oscillation implies that neutrinos are massive. However it does not provide information on either the absolute mass scale (Gribov and Pontecorvo, 1969) or the Majorana phases (Bilenky *et al.*, 1980). In addition, the observed oscillation phenomena do not probe the Dirac or Majorana nature of neutrino masses, as the neutrinos and antineutrinos are observed (observable) only in the ultra-relativistic regime (Bilenky *et al.*, 1980). Nevertheless, considering our discussion in Sec. III.B on the importance of testing $B-L$ in addition to the theoretical arguments in favor of Majorana neutrino masses based on the SM structure, the recognition that neutrinos have mass strongly motivates

searches for $0\nu\beta\beta$ decay.

The parameters of massive neutrinos have been quantified by oscillation experiments assuming three-flavor oscillation (Zyla *et al.*, 2020). The squared mass differences are known with 1%–2% precision and the squared sines of the mixing angles relevant for $0\nu\beta\beta$ decay are known at the 3%–4% level. One less clear aspect for which progress is expected in the coming years concerns the arrangement of the neutrino masses, i.e., the neutrino mass ordering, sometimes also referred to as the neutrino mass hierarchy. The question concerns the discrimination between the *normal* ordering (NO), when the three neutrinos have a mass spectrum that resembles the charged fermion spectra, and the *inverted* ordering (IO), when they do not. At present, global fits indicate a preference for the NO at the $\sim 3\sigma$ level (Capozzi *et al.*, 2021; Esteban *et al.*, 2020). However, this preference should be taken with a heavy grain of salt. Indeed, our current best probes for the mass ordering — i.e., accelerator-based experiments that are directly sensitive to it — favor the inverted ordering. The overall preference for normal ordering is driven by the comparison between the neutrino mass squared difference measured in ν_μ disappearance at accelerators and ν_e disappearance at reactors, and is strengthened by the multivariate analysis of Super-Kamiokande atmospheric neutrino data not fully integrated in the global fits.

Finally, various experiments hint at the existence of a new light neutrino with mass of $O(1\,\mathrm{eV})$ (Dentler *et al.*, 2018; Giunti and Lasserre, 2019). Such a neutrino must be sterile, i.e., non-interacting, in view of the measurements done at the Large Electron-Positron (LEP) collider that limit the number of active light neutrinos to three (Decamp *et al.*, 1990; Giunti and Lasserre, 2019). Updated limits on sterile neutrinos from $0\nu\beta\beta$ decay, compared with those from other observational probes, are discussed in Bolton *et al.* (2020). However, as repeatedly argued in the literature, see, e.g., Dentler *et al.* (2018), different experiments hint at sterile neutrinos with different parameters, and global fits show tensions among datasets. Given the absence of strong theoretical arguments favoring such sterile neutrinos, and the lack of phenomenological support, we focus here on the scenario with three massive neutrinos.

2. Formalism for the $m_{\beta\beta}$ parameter

Due to the absence of electric charge, neutrinos admit a more general type of mass than Dirac's one. As described generically in Sections III.B.2 and III.B.3, a general bilinear term $-\bar\Psi M_\nu \Psi^{\mathrm{C}}/2 + h.c.$ can be added to the SM Lagrangian density, where the charge conjugate spinor is $\lambda^{\mathrm{C}} = C\bar\lambda^t$, and the vector Ψ, which includes only left spinors, can be written as $\Psi^t = (\nu_{\mathrm{Le}}, \nu_{\mathrm{L}\mu}, \nu_{\mathrm{L}\tau})$ in the SM, or $\Psi^t = (\nu_{\mathrm{Le}}, \nu_{\mathrm{L}\mu}, \nu_{\mathrm{L}\tau}, \nu_{\mathrm{Re}}^{\mathrm{C}}, \nu_{\mathrm{R}\mu}^{\mathrm{C}}, \nu_{\mathrm{R}\tau}^{\mathrm{C}})$ when three right handed neutrinos are assumed. This Lagrangian

density is called a Majorana mass term, and includes Dirac's term as a particular case. The mass matrix M_ν is complex and symmetric, and can be decomposed as

$$M_\nu = U \, \mathrm{diag}(m_1, m_2, \ldots, m_{\mathrm{n}}) \, U^t, \qquad (10)$$

where $U^\dagger U = \mathbb{I}_{\mathrm{n}\times\mathrm{n}}$ and $m_{\mathrm{i}} \geq 0$ are the masses of the neutrinos. The minimal case includes just the SM neutrinos, with $\mathrm{n} = 3$ and U the Pontecorvo–Maki–Nakagawa–Sakata (PMNS) mixing matrix. It is common practice to define

$$m_{\beta\beta} = \left| \sum_{i=1}^{3} |U_{\mathrm{ei}}^2| \, e^{i\varphi_{\mathrm{i}}} \, m_{\mathrm{i}} \right|, \qquad (11)$$

where the φ_{i} are called Majorana phases and cannot be probed by oscillation experiments. $m_{\beta\beta}$ is the ee-element of the mass matrix $|(M_\nu)_{\mathrm{ee}}|$, and thus is also referred to as "the effective Majorana mass" of the electron neutrino. This Majorana mass term changes the electronic lepton number by two units, and contributes linearly to the $0\nu\beta\beta$-decay amplitude.

The free Lagrangian density for a single neutrino is

$$\mathcal{L} = i\,\bar\nu_{\mathrm{L}} \, \partial_\mu \gamma^\mu \, \nu_{\mathrm{L}} + \frac{m}{2}\nu_{\mathrm{L}}^t C^\dagger \nu_{\mathrm{L}} - \frac{m}{2}\bar\nu_{\mathrm{L}} C \bar\nu_{\mathrm{L}}^t, \qquad (12)$$

where $\partial_\mu = \partial/\partial x^\mu$, γ^μ are the 4×4 Dirac matrices and m is a mass parameter that can be chosen to be real and positive by changing the phase of ν. Adding the total derivative term $-i/2\partial_\mu(\bar\nu_{\mathrm{L}}\gamma^\mu\nu_{\mathrm{L}})$ does not change the action, and introducing the Majorana spinor $\chi = \nu_{\mathrm{L}} + C\bar\nu_{\mathrm{L}}^t$, the Lagrangian density reads the same as the usual free case, apart from the factor of 2 because the field is self-conjugate[2]:

$$\mathcal{L} = \frac{i}{2}\bar\chi \, \partial_\mu \gamma^\mu \, \chi - \frac{m}{2}\bar\chi\chi. \qquad (13)$$

Introducing the left chirality projector $P_{\mathrm{L}} = (1 - \gamma_5)/2$, and noting that $\nu_{\mathrm{L}} = P_{\mathrm{L}}\chi$, we find the lepton number violating propagator that describes the exchange of virtual Majorana neutrinos:

$$P_{\mathrm{L}}\langle 0|T[\chi(x)\bar\chi(y)]|0\rangle P_{\mathrm{L}} =$$
$$= m \times \int \mathrm{d}^4 q \, \frac{i\,P_L\,e^{-iq(x-y)}}{q^2 - m^2 + i0^+}$$
$$= -\langle 0|T[\nu_{\mathrm{L}}(x)\nu_{\mathrm{L}}(y)]|0\rangle C^\dagger, \quad (14)$$

where $|0\rangle$ is the vacuum state and T indicates that the product of the quantised neutrino fields is time-ordered.

Considering the SM electron neutrino, $\nu_{\mathrm{e}} = \sum_i U_{\mathrm{ei}}\nu_{\mathrm{i}}$, the only modifications required to describe the propagator that appears in $0\nu\beta\beta$ decay are i) including the factor

---

[2] $C\bar\chi^t = \chi$. In a sense, particle and antiparticle nature coexist.
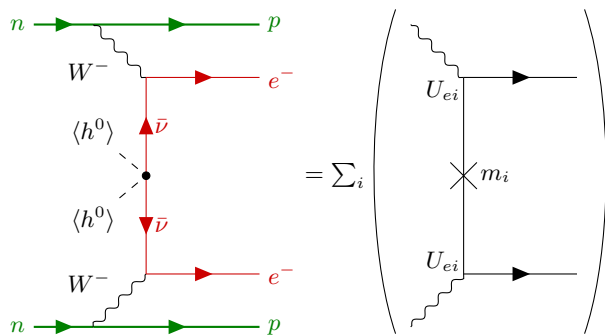
FIG. 3 Diagram of $0\nu\beta\beta$ decay with light neutrino exchange. On the right, we show the corresponding scheme in terms of neutrino mass eigenstates and the PMNS mixing matrix U.

U_{ei}^2 and ii) using also m_{i} for each massive neutrino state. Using this propagator to compute the decay rate, only the absolute value of the parameter matters. Thus the practical recipe is to replace $m \rightarrow |\sum_i U_{\mathrm{ei}}^2 \, m_{\mathrm{i}}| \equiv m_{\beta\beta}$. Figure 3 shows the Feynman diagram for $0\nu\beta\beta$ decay with light neutrino exchange.

Note finally that Majorana mass terms violate the SM hypercharge symmetry. However, this violation can be attributed to the Higgs field vacuum expectation value, i.e., to SSB of the electroweak group.

3. Implications for $0\nu\beta\beta$ decay

As previously discussed, several operators can contribute to $0\nu\beta\beta$ decay. Regardless of which are the responsible BSM mechanisms, the decay rate can be divided into four pieces. The first is the phase-space factor G that indicates the feasibility of the decay according to its kinematics. Its value depends mainly on the energy difference between the initial and final states, or $Q_{\beta\beta}$. The second piece is a hadronic matrix element g that encodes the coupling of the weak interaction to nucleons. In Fermi and Gamow-Teller (GT) transitions this is given by g_V and g_A, respectively, while for $0\nu\beta\beta$ decay a genuine two-nucleon coupling g^{NN} needs to be considered as well. The third piece is a nuclear matrix element (NME) M that represents the amplitude for the nuclear transition from the initial to the final state nucleus. NMEs depend on the nuclear structure of the initial and final nuclei, and also on the nuclear transition operator, and are covered extensively in Sec. IV. Finally, the decay rate also depends on the responsible BSM mechanism, introducing the scale Λ associated with lepton-number violation. Considering all possible decay channels i, the schematic expression for the $0\nu\beta\beta$-decay rate Γ can be written in terms of the half-life $T_{1/2}$ as:

$$\frac{\Gamma_{0\nu}}{\ln 2} = \frac{1}{T_{1/2}^{0\nu}} = \sum_i G_i \, g_i^4 \, |M_i|^2 \, f_i(\Lambda) + \text{interferences},$$
(15)

where f_i is a dimensionless function encompassing BSM physics. In the case of light neutrino exchange, f_i is conventionally written as the square of $m_{\beta\beta}$ normalized by the square of the electron mass.

The evidence of neutrino masses and the fact that the Weinberg operator has the lowest dimension suggests that the leading contribution to $0\nu\beta\beta$ decay is likely due to Majorana neutrino masses. From this point of view, the discussion of a full model might be considered premature, as was the W-boson hypothesis right after the discovery of Fermi interactions. On the other hand, it is not possible to exclude *a priori* the possibility that the scale of lepton number violation is not far from the one probed with accelerators or rare decays.

In this case a new question arises: how do we avoid an exceedingly large value of neutrino masses and in particular of $m_{\beta\beta}$? A more detailed discussion on this topic is given in de Gouvea and Jenkins (2008) and Mitra *et al.* (2012). Solving this type of situation is possible if the light neutrino masses are connected to small Yukawa couplings, see, e.g., Maiezza *et al.* (2010) for a model based on left-right symmetry.

A very well known consideration is the so-called black box or Schechter-Valle theorem — even though the term theorem can be disputed and is not used by the authors. The original work (Schechter and Valle, 1982) states that *the observation of $0\nu\beta\beta$ decay implies the existence of a Majorana mass term for the neutrino for a "natural" gauge theory,* and further specifies that *one postulates a "strong-naturality" in which no global conservation laws are assumed "a priori".* Thus obtaining a quantitative statement on $m_{\beta\beta} = 0$ is possible only within a model. In a minimal setup, the value of $m_{\beta\beta}$ induced by the black box diagram is so small that it lacks any practical interest (Duerr *et al.*, 2011). Moreover and most simply, it seems possible to arrange for $m_{\beta\beta} = 0$ without contradicting the current knowledge of neutrino masses. In fact, considering that $m_{\beta\beta}$ is the m_{ee} component of M_ν, it is easy to imagine the elements of M_ν falling into a hierarchy resembling those of the other SM fermions, in which case m_{ee} could be exceedingly small (de Gouvea, 2022).

Considering only the light neutrino exchange contribution to $0\nu\beta\beta$ decay, Eq. (15) simplifies to

$$\frac{1}{T_{1/2}^{0\nu}} = G_{01} \, g_A^4 \, \left(M_{\mathrm{light}}^{0\nu}\right)^2 \, \frac{m_{\beta\beta}^2}{m_e^2},$$
(16)

where G_{01} and $M_{\mathrm{light}}^{0\nu} = M_{\mathrm{long}}^{0\nu} + M_{\mathrm{short}}^{0\nu}$ are the phase space and NME specific to light neutrino exchange, re-

spectively. Eq. (16) already reflects a long- and short-range contribution to the NME. For simplicity the dominant coupling of the long-range part, g_A, is factored out, but the short-range part is proportional to another two-nucleon coupling g^{NN}. See Sec. IV.A for more details.

4. Predictions on $m_{\beta\beta}$

The definition of $m_{\beta\beta}$ given in Eq. 11 shows how this quantity depends on a total of seven parameters, as only θ_{12} and θ_{13} enter U_{ei}, and only two Majorana phases are non degenerate. Neutrino oscillation experiments are sensitive only to the two mixing angles, two neutrino mass squared differences, and the mass ordering. Thus experimental data can currently bound only four out of seven degrees of freedom, leaving the other three fully unconstrained. Two of these unconstrained degrees of freedom are naturally associated to the Majorana phases. The third one is related to the three neutrino masses m_i, which are constrained by the measurements of only two mass squared differences. This freedom raises the question of how to predict the value of $m_{\beta\beta}$, an issue discussed since Vissani (1999).

One option is to constrain the remaining parameters using theoretical considerations of neutrino masses, but despite the wide literature on the subject we cannot make any definitive statement yet. Some models have been considered more appealing, for instance those based on the gauge principle, or those trying to connect neutrino masses to the masses of other fermions, or perhaps, to a lesser extent, those predicting a more easily explorable parameter space. The challenge is not the shortage but rather the overabundance of proposals, and the lack of criteria to identify the correct one, if any. The history of the theoretical investigation of neutrinos has produced wrong predictions at almost every turn: parity was supposed to be respected but is maximally violated in neutrino interactions; θ_{12} was supposed to be small, but it is about $30°$; θ_{13} was thought to be very small until recently, when it was found to be as large as the Cabibbo angle; neutrinos were supposed to give a large (or significant) contribution to the cosmological energy density, but apparently they do not; etc. In short, history calls for caution toward a purely theoretical approach to making useful predictions on $m_{\beta\beta}$.

In early investigations, predictions for $m_{\beta\beta}$ were often obtained by assuming special values for its three unconstrained degrees of freedom. In particular, the Majorana phases were frequently set to zero, or such as to provide special values of $e^{i\varphi_i}$, e.g., real values. In recent times, the focus has shifted on the maximally allowed range of $m_{\beta\beta}$ values. This is derived by leaving the Majorana phases free to minimize and maximixe $m_{\beta\beta}$ for any choice of the last degree of freedom associated to neutrino masses. Analytic expressions defining the ex-

treme $m_{\beta\beta}$ values are compact (Vissani, 1999): $m_{\beta\beta}^{\max} = \sum_{i=1}^{3} |U_{ei}^2| m_i$ and $m_{\beta\beta}^{\min} = \max\left\{ 2|U_{ei}^2| m_i - m_{\beta\beta}^{\max}, 0 \right\}$. The third degree of freedom is often parameterized using the lightest neutrino mass m_{light} (Vissani, 1999). Other conventional options are the observables measured by experiments studying β spectra end-points — i.e., the effective kinematic electron neutrino mass $m_\beta = \sqrt{\sum_i |U_{ei}^2| m_i^2}$ — or by cosmological surveys — i.e., the sum of the neutrino masses $\Sigma = \sum_i m_i$ (Fogli et al., 2004). Figure 4 shows the maximally allowed range for $m_{\beta\beta}$ as a function of these three parameterizations. The ambiguity in the neutrino mass ordering (NO vs. IO) results in two distinct regions, which overlap at high (degenerate) neutrino mass scales, but separate at lower values. It is within these regions that experiments can test $0\nu\beta\beta$ decay via light neutrino exchange. In view of recent analyses showing some preference for NO, one of the two regions might be favored, but these are still mild indications at the moment as discussed in Sec. III.D.1.

Next-generation $0\nu\beta\beta$-decay experiments will fully probe the parameter space allowed for inverted ordered neutrinos, for which the smallest allowed $m_{\beta\beta}$ value is 18.4 ± 1.3 meV (Agostini et al., 2021b). At the same time, these experiments will also test a significant fraction of the parameter space allowed for the normal ordering. However, for the normal ordering there is no lower bound on $m_{\beta\beta}$, which could be extremely small or even null, far out of the reach of conceivable future searches. If neutrinos are Majorana particles, data on $m_{\beta\beta}$ will indirectly constrain also m_β and Σ, and vice versa, creating an exciting interplay among future experiments.

The most stringent constraints on m_β come from the KATRIN experiment, which is designed to kinematically measure the mass of the electron antineutrino with sub-eV precision, by reconstructing the energy distribution of the electrons emitted in tritium β decays close to the end-point. In the next few years, KATRIN will push the exploration of m_β values from the current limit of 0.8 eV (Aker et al., 2022) down to 0.2 eV (Aker et al., 2019). Any measurement of m_β in this range would be incompatible with the existing limits on $0\nu\beta\beta$-decay unless neutrinos are Dirac particles. In the Majorana neutrino scenario, it would hint towards non-standard neutrino models (and cosmological models), and/or alternative $0\nu\beta\beta$-decay mechanisms.

Cosmological data are strongly sensitive to the neutrino radiation density and the neutrino masses, which affect both Big Bang nucleosynthesis and the large scale structure of the universe, inducing characteristic signatures in the relative abundance of elements and the cosmic microwave background (CMB) / baryon acoustic oscillation (BAO) power spectra. These effects are covered in several reviews, for instance Dolgov (2002), Patterson (2015), Archidiacono et al. (2017), and Lattanzi and Gerbino (2018). Neutrino constraints coming from cos-
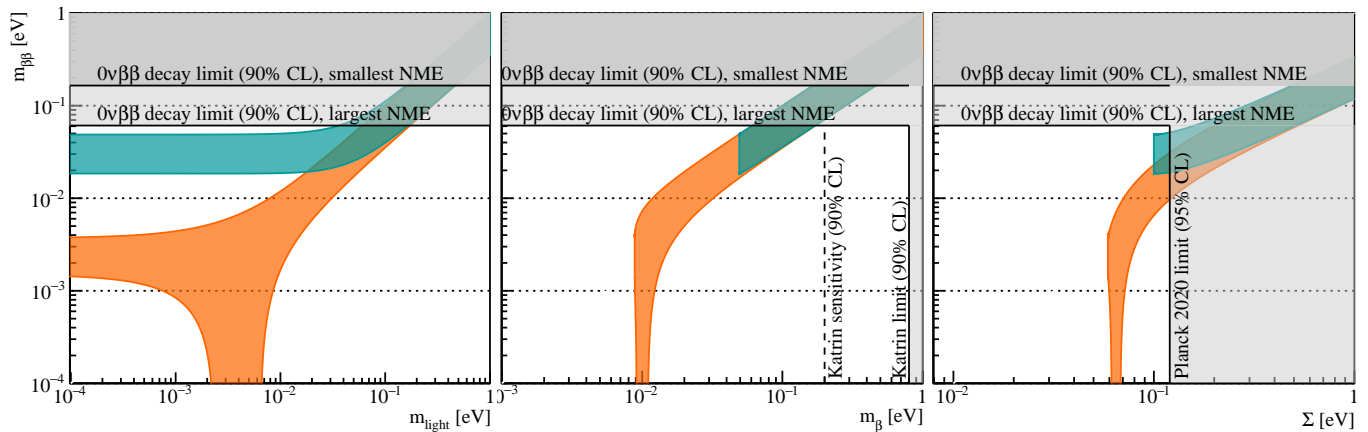
FIG. 4 Maximally allowed parameter space for $m_{\beta\beta}$ as a function of m_{light}, m_β, and Σ, assuming the central value of the neutrino oscillation parameters (Zyla *et al.*, 2020). The orange and green areas show the parameter space allowed assuming normal and inverted ordering, respectively. The shaded areas indicate the regions already excluded by $0\nu\beta\beta$-decay experiments (Gando *et al.*, 2016) and cosmological observations (Aghanim *et al.*, 2020); the vertical lines in the middle panel correspond to the KATRIN limit (Aker *et al.*, 2022) and sensitivity (Aker *et al.*, 2019).

mology are relatively robust, even though they are not as direct as those from laboratory experiments, and need to rely on the Standard Model for cosmology, called ΛCDM. The current bound on the sum of the neutrino masses is $\Sigma < 120\,\text{meV}$ (Aghanim *et al.*, 2020). It stems from the combination of large-scale structure measurements due to Planck with other measurements at small scales, including lensing and BAO data. There exist other sensitive data, such as measurements of the Lyman-alpha forest. Their inclusion helps to break some degeneracies, typically yielding stronger constraints on Σ (Di Valentino *et al.*, 2021; Palanque-Delabrouille *et al.*, 2020). The analysis is also relatively robust against standard modifications of ΛCDM.

The next surveys, for instance DESI and EUCLID, aim at measuring Σ with an accuracy of $20\,\text{meV}$ (Font-Ribera *et al.*, 2014; Kitching *et al.*, 2015). Such a measurement will have important implications for $0\nu\beta\beta$ decay. First, the lowest value of Σ is bounded by the measurement of the neutrino mass squared differences. This minimum value is $\Sigma > 59\,\text{meV}$ for the normal ordering, and $\Sigma > 100\,\text{meV}$ for the inverted one, assuming the central values of the neutrino oscillation parameters (Zyla *et al.*, 2020). This means that the next surveys are guaranteed to resolve a value for Σ consistent with these limits if the ΛCDM paradigm is valid and consistent with Standard-Model physics. Further, measurement of Σ below $100\,\text{meV}$ would disfavor the inverted ordering hypothesis, as pointed out in Dell'Oro *et al.* (2015). Moreover, any measurement of Σ would naturally set a lower bound on $m_{\beta\beta}$, even in the case of the normal ordering. This is already qualitatively visible in Fig. 4, but a proper estimation needs to take into account all uncertainties on the oscillation parameters and the anticipated $20\,\text{meV}$ accuracy of the measurement on

Σ. Figure 5 shows the dependence of the lower bound on $m_{\beta\beta}$ on the true unknown value of Σ, obtained by propagating all uncertainties via random sampling. Should the value of the neutrino mass sum be just below the current limits, $m_{\beta\beta}$ would be bounded to be larger than $10\,\text{meV}$, a value testable by the coming $0\nu\beta\beta$-decay experiments assuming favorable NME calculations.

We close this section with a remark concerning the normal mass ordering parameter space. Although vanishing $m_{\beta\beta}$ values are possible from a mathematical and empirical point of view, the question of whether this is plausible or not is much more subtle. Figure 4 shows the maximum allowed parameter space on bilogarithmic scales. This choice under-emphasizes the value of the observational progress and stresses somewhat artificially the role of the lowest values of the masses. In the future, a linear or even bilinear scale might be appropriate; indeed some experiments have begun to plot their results in this way (Abe *et al.*, 2022; Arnquist *et al.*, 2022).

Recent Bayesian analyses have tried to build a probability distribution for $m_{\beta\beta}$, at the price of making assumptions on the (prior) probability distribution for the Majorana phases and the additional free mass scale parameter, be it m_{light}, m_β or Σ. If one invokes "naturalness" arguments and parameterize the ignorance on the Majorana phases with a flat prior, vanishing $m_{\beta\beta}$ values get strongly disfavored as first pointed out by Benato (2015), Agostini *et al.* (2017), and Caldwell *et al.* (2017). One could also try to consider the less favorable value of the Majorana phases and quantify the minimal discovery probabilities (Agostini *et al.*, 2021a). Finally, flavor symmetry can also be invoked to constrain at the same time the phases and, e.g, m_{light}, bringing a large part of the parameter space for normal ordering within the reach of the forthcoming experiments (Agostini *et al.*, 2016).
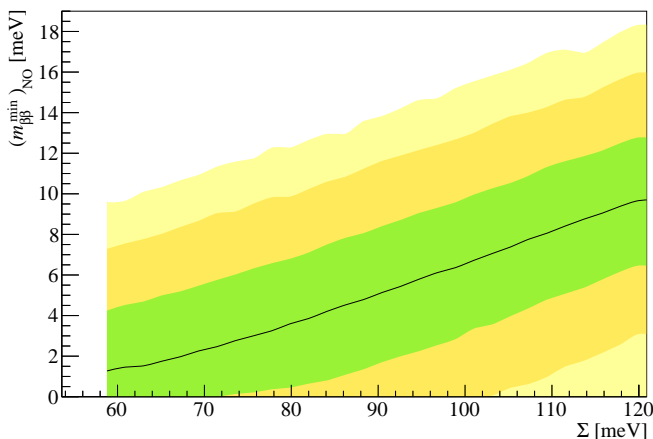
FIG. 5 Posterior probability distribution of the lower bound on $m_{\beta\beta}$ as a function of the true value of Σ, assuming normal ordering. The distribution is constructed by random sampling of the oscillation parameters within their Gaussian uncertainties (Zyla *et al.*, 2020) assuming that Σ will be measured with 20 meV accuracy. The solid black line shows the median lower bound, while green, orange and yellow color bands show the distribution 68%, 95% and 99% probability central intervals. Note that the median limit does not go to zero, not even when $m_{\beta\beta}$ can vanish, as the limit is averaged over an extended Σ range accounting for the measurement uncertainty.

These analyses identified several scenarios in which the discovery power for future experiments is significant, even considering normal-ordered neutrino masses. The more the priors disfavor vanishing values for the lightest neutrino mass and cancelling Majorana phases, the higher the discovery power. The dependence on the prior on the lightest neutrino mass will significantly weaken in the future should the value of Σ be measured by cosmological surveys (Ettengruber *et al.*, 2022).

Although we have already warned the reader against making predictions on $m_{\beta\beta}$ using purely theoretical arguments, we want to draw the attention to the broad class of models examined in a number of articles (Dell'Oro *et al.*, 2018a,b; Vissani, 1998b, 2001), which merely focus on the coarse structure of the neutrino mass matrix without claiming an understanding of the coefficients of order 1. This class of mass matrices correctly anticipated the large mixing angle solution and the fact that θ_{13} is of the order of the Cabibbo angle $\theta_C \sim 0.2$, and they also predict the normal ordering scenario currently favored by available data. They were proposed after the first evidence appeared that the atmospheric neutrino mixing is large, which showed that the neutrino mass matrix deviates from the hierarchical and quasi-diagonal structure typical of the Yukawa couplings of charged fermions. This consideration leads to the reasonable assumption that the elements of the $\mu - \tau$ block are larger than the others (Vissani, 1998b). According to these models, one

would expect

$$m_{\beta\beta} = \mathcal{O}(1) \times \sqrt{\Delta m_{\mathrm{atm}}^2} \times \theta_C^n \text{ with } n = 1 \text{ or } 2 \quad (17)$$

where $\Delta m_{\mathrm{atm}}^2$ is the parameter probed by atmospheric neutrino oscillation, i.e., the mass squared difference $|m_3^3 - m_1^2|$ or $|m_3^3 - m_2^2|$ depending on the mass ordering. This leads to $m_{\beta\beta} \approx 10\,\mathrm{meV}$ or $2\,\mathrm{meV}$. This cannot be considered as a replacement for a complete theory. But it is interesting and gratifying that the explorations that have been conducted on motivated models, particularly those based on SO(10) (Altarelli and Meloni, 2013; Bajc *et al.*, 2006; Bertolini *et al.*, 2012; Buccella *et al.*, 2012; Dueck and Rodejohann, 2013; Joshipura and Patel, 2011; Matsuda *et al.*, 2002; Ohlsson and Pernow, 2021), are consistent with these generic expectations.

Another mass scale of interest for $m_{\beta\beta}$ is given by the solar neutrino mass squared difference:

$$m_{\beta\beta} \sim \sqrt{\Delta m_{\mathrm{sol}}^2} = 8.6 \pm 0.1\,\mathrm{meV}, \quad (18)$$

with $\Delta m_{\mathrm{sol}}^2 = m_2^2 - m_1^2$. This mass scale has been precisely measured by neutrino oscillation measurements, and typical models with NO neutrino masses favor $m_{\beta\beta}$ values around this magnitude. Its numerical value is similar to what is obtained by Eq. 17 assuming $n = 1$, i.e., $m_{\beta\beta} \approx 10\,\mathrm{meV}$.

Thus there is an accumulation of theoretical motivation for exploring $m_{\beta\beta}$ values around 8–10 meV. This scale is interesting also from the experimental point of view: it is almost in the middle of the parameter space remaining after reaching the bottom of the inverted ordering, and can constitute a challenging, and yet conceivable goal for the experimental community. Future experiments able to explore this parameter space would have exciting discovery opportunities as it does not seem very plausible that $m_{\beta\beta}$ is exactly zero. However, it is clear that we need more precise indications from theory to guide the experimental program. In particular, it seems more important than ever to bring to full maturity the design of a predictive and motivated model of neutrino and charged fermion masses based on reliable theoretical principles, for example, SO(10).

E. The cosmic baryon excess and models of its origin

While particles and antiparticles are basically equivalent at the level of fundamental physics, on a cosmic scale, the universe contains only baryons. As discussed in Sec. III.E.1, the Standard Model is unable to account for this observational fact, and this suggests that there may have been some unknown physics at work in the early universe. A large and very interesting class of extensions of the Standard Model succeeds in this task by using the same ingredients that explain the masses of light neutrinos and/or give rise to leptonic number violation phenomena: these are the leptogenesis models, described in

Sec. III.E.2. We discuss the connection between these models and $0\nu\beta\beta$ decay in Sec. III.E.3, attempting an assessment on the most promising models.

1. Observations and theoretical challenges

Cosmology has collected evidence that the universe contains only baryons. Their amount has been measured in several ways: in the present universe, with direct astronomical observations (de Graaff *et al.*, 2019; Tanimura *et al.*, 2019); at recombination time, with the study of the cosmic microwave background (Aghanim *et al.*, 2018); and at much earlier times, with big-bang nucleosynthesis (Pisanti, 2020). These determinations, especially the last two, are rather precise and compatible with each other. The amount of anti-baryons is insignificant and consistent with secondary production mechanisms. The lepton asymmetry, stored in the neutrinos produced in the big-bang, is only loosely bounded by observations of primordial nucleosynthesis (Mangano *et al.*, 2012). If it is similar in size to the baryonic one, it is practically impossible to measure.

The meaning of the observed baryon excess has been widely discussed in the context of theoretical cosmology. Following (Sakharov, 1967), it was discussed which models were able to provide sufficient violations of global symmetries and CP, to dynamically generate cosmic baryon asymmetry. Recall, the SM predicts non-perturbative processes that violate $B + L$ (Harvey and Turner, 1990; 't Hooft, 1976; Kuzmin *et al.*, 1985). However, when their effect is quantified in the context of cosmological evolution, they prove insufficient to account for the observed asymmetry (Bochkarev and Shaposhnikov, 1987; Kajantie *et al.*, 1996). Thus a dynamical explanation of the origin of the baryon excess is possible only in a suitable SM extension; such a theoretical program goes under the name *baryogenesis*. A new source of violation of global symmetries (B and L) from physics beyond the SM is necessary for any successful explanation of the cosmic baryon excess. The hypothetical observation of lepton number violation in the laboratory would give strong support to this interpretation, even before reaching quantitative predictions.

2. Leptogenesis models

A specific class of SM extensions, called baryogenesis through leptogenesis or in short *leptogenesis* models, explain the cosmic baryon density though lepton number violating effects. Most typically, these rely on the same ingredients that also explain neutrino masses (see Sec. III.C.2).

The first proposal of Fukugita and Yanagida (1986) is based only on the existence of right-handed neutrinos with very large (GUT scale) Majorana masses. Their decays out of equilibrium lead to a leptonic asymmetry ΔL, due to interference effects in the decay of the heavy neutrinos beyond lowest perturbation order and due to complex (CP-violating) Yukawa couplings. Subsequently, the non-perturbative SM processes mentioned above that violate $B + L$ convert this leptonic asymmetry into the cosmic baryon excess. The same process also leaves a comparable asymmetry between neutrinos and antineutrinos, a determination of which is beyond experimental reach.

The issue of model dependence cannot be ignored. For example, the Grand Unified SO(10) models discussed in Sec. III.C.1 contain heavy right-handed neutrinos and can thus be considered to be in the class of models required by the original leptogenesis proposal, but they also contain other sources of lepton number violation, such as SU(2) triplets, which makes it less easy to study the consequences and draw unambiguous conclusions from the theory. In fact, the number of variants of leptogenesis models that are formally allowed is very large (Shaposhnikov, 2009), and some of them correspond to very different scenarios.

Interestingly, it is possible to build models that involve relatively light new particles, potentially within the reach of laboratory experiments. One such model is the mechanism of (Akhmedov *et al.*, 1998), which is compatible with the νSM (Asaka *et al.*, 2005), but does not change the rate of $0\nu\beta\beta$ (Bezrukov, 2005). Furthermore, there is a broad class of low-scale leptogenesis models (mentioned in Sec. III.C.4) that can be verified in the laboratory, especially through the search for $0\nu\beta\beta$, as evidenced in a number of papers (Drewes and Eijima, 2016; Drewes *et al.*, 2017, 2022a,b; Hernández *et al.*, 2016).

3. Provisional assessments

The generic scenario described above for the origin of cosmic baryons is not precise enough to be verifiable, but it can be qualitatively corroborated by laboratory measurements on, e.g., the Majorana character of neutrino masses and CP violation in neutrino oscillation. It has at least been observed that baryogenesis at a high energy scale is hardly compatible with any mechanism causing $0\nu\beta\beta$ decay other than the exchange of Majorana neutrinos (Deppisch *et al.*, 2015b). It is also noteworthy that the long baseline searches for CP violation have recently received strong support (Gonokami, 2018; Ritz *et al.*, 2014). Thus although leptogenesis cannot be tested directly by laboratory measurements, the experimental community is at least poised to deeply probe its key testable predictions.

The fact that to date we can only observe the cosmic baryon excess, but we have very few other possibilities to test our ideas about it, sometimes induces a certain dis-

couragement. Perhaps, in view of the provisional character of present knowledge, baryogenesis should be regarded not as a theoretical need, but just as a point in favor for SM extensions that can model it.

However, the original models, in which baryon/leptogenesis occurs at very high energy scales, seem much more promising in the perspective of a unified theory. For example, in unified theories such as SO(10), one can explain small neutrino masses by the seesaw mechanism, one can incorporate a correspondence between quarks and leptons (which has been a good theoretical guide in the past), and there is no need to invoke strong differences in their Yukawa couplings. In this spirit, and for the purposes of experimental investigations, it seems reasonable to us to consider this hypothesis as the reference one.

IV. NUCLEAR PHYSICS THEORY AND IMPLICATIONS

Most atomic nuclei are unstable because of the weak interaction. Nuclei decay by emitting or capturing electrons — known as β decay or electron capture (EC), respectively — resulting in a final nuclide more bound than the initial one and with the same number of nucleons. In β decay a neutron turns into a proton, while the opposite occurs in EC, so that electric charge is conserved. In addition, either neutrinos (in EC) or antineutrinos (in β decay) are emitted to conserve energy, momentum and lepton number. In a nucleus, β decay can also turn a proton into a neutron, but this is disfavored with respect to EC because a positron needs to be produced, reducing the available energy: $Q_{\beta+} = Q_{\text{EC}} - 2m_e$.

When dominant first-order weak processes occur, second-order $\beta\beta$ decay or double EC (ECEC) are in practice impossible to observe, due to the small coupling associated with the *weak* interaction. For some selected nuclei, however, $2\nu\beta\beta$ decay and ECEC dominate, for instance when first-order decays are energetically forbidden while second-order channels are not. The attractive nuclear pairing interaction brings additional binding to nuclei with even numbers of protons and neutrons, so that some even-even nuclei are more bound than their odd-odd neighbors, but less bound than their even-even second-neighbors. Figure 6 illustrates this by showing the mass excess for isobars with $A = 76$ nucleons. Alternatively, β decays can be very suppressed because of a large mismatch in total angular momentum between the initial and final nuclei, so that β- and $2\nu\beta\beta$-decay rates are comparable (Alanssari *et al.*, 2016). In these special cases, $\beta\beta$ decay or ECEC can be measured. The nucleus decays into a more bound system with two more protons and two fewer neutrons, or the other way around, emitting or capturing at the same time two electrons and the corresponding (anti)neutrinos. Such measurements demand experiments sensitive to half-life values as long as
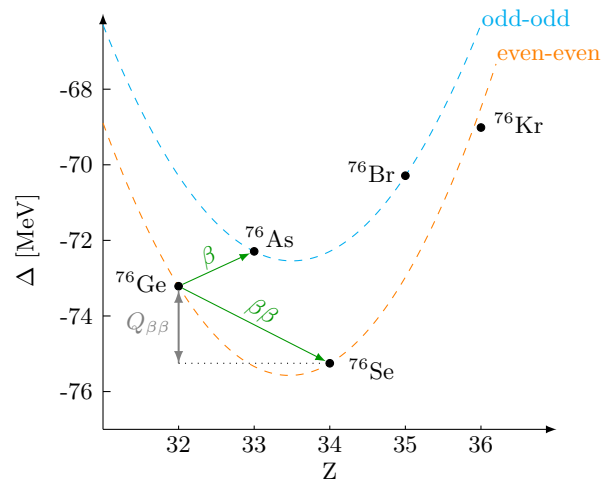

FIG. 6 Mass excess $\Delta = (m_A - A) \cdot u$ for isobars with mass m_A and mass number $A = 76$, where u is the atomic mass unit. Even-even (odd-odd) nuclei lie on the bottom (top) curve.

$T_{1/2}^{2\nu\beta\beta} > 10^{18}$ yr (Barabash, 2020).

The nuclear transition underlying $2\nu\beta\beta$ decay and ECEC can be thought of as proceeding via virtual transitions to excited states of the intermediate odd-odd nucleus, and many body methods can be used to compute the corresponding nuclear matrix elements (NMEs), albeit with some uncertainty. The case of $0\nu\beta\beta$ decay is fundamentally different in two essential ways. First, the mediating mechanism results in significant momentum transfer between the two nucleons involved in the decay. While $2\nu\beta\beta$ decay and ECEC are restricted to a subset of the intermediate nuclear states with angular momentum-parity 1^+, the high momentum transfer in $0\nu\beta\beta$ makes all intermediate states accessible. Second, although it is the case for light neutrino exchange, the mediating mechanism is not required to couple to the nucleons via weak interaction vertices, and thus in general the process is not always a second-order weak process. A more generic framework is thus required to compute $0\nu\beta\beta$ decay rates.

In this section, we first summarize in Sec. IV.A the $0\nu\beta\beta$-decay rate as given by an effective field theory (EFT) that exploits the separation of scales between particle (BSM), hadron, and nuclear structure scales. Section IV.B presents expressions for the NMEs for $0\nu\beta\beta$ decay mediated by the exchange of "light" and "heavy" particles with respect to the typical momentum transfer $p = |\boldsymbol{p}| \sim 200\,\text{MeV}$, including the recently recognized short-range contribution to light-neutrino-exchange. Section IV.C discusses current NME calculations, while Sec. IV.D is devoted to the so-called "g_A quenching" puzzle that could affect NME predictions. Additional nuclear observables that test calculations and can provide information about the values of the NMEs are outlined in Sec. IV.E.

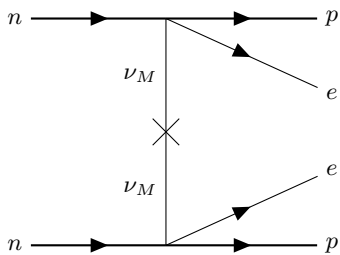The content of Secs. IV.A, IV.C.1, IV.C.2 and IV.D is

FIG. 7 Diagram representing long-range light-neutrino exchange contribution to $0\nu\beta\beta$ decay.

targeted to both nonexperts and experts, while Sec. IV.B, the remaining of Sec. IV.C and the final Sec. IV.E cover somewhat more technical aspects.

A. $0\nu\beta\beta$-decay rate in effective field theory

$0\nu\beta\beta$ decay is necessarily triggered by BSM physics. As discussed in Sec. III, the experimentally best motivated and most studied mechanism is the exchange of the known light neutrinos — if they are Majorana particles — corresponding to the diagram in Fig. 7. This scenario predicts a $0\nu\beta\beta$-decay rate that only depends on the mass of the lightest neutrino and the neutrino mass ordering, in addition to a NME. Nonetheless, in general any BSM extension that violates lepton number leads to $0\nu\beta\beta$ decay. Because BSM models are typically defined at higher energy-momentum scales than the electroweak scale ($\sim 250\,\mathrm{GeV}$), or the relevant scales for hadrons ($\sim 1\,\mathrm{GeV}$) and nuclei ($\sim m_\pi \sim 200\,\mathrm{MeV}$), an EFT approach is best suited to organize different $0\nu\beta\beta$-decay contributions (Cirigliano *et al.*, 2017, 2018c; Prezeau *et al.*, 2003). Including information from all these energy scales provides an advantage for assigning the importance of each decay channel, but valuable alternative EFTs usually neglecting chiral (m_π/GeV) aspects have also been proposed (Deppisch *et al.*, 2018, 2020a; Graf *et al.*, 2018; Horoi and Neacsu, 2016a; Pas *et al.*, 1999, 2001).

1. Decay amplitudes

Above the electroweak scale, lepton number violation and therefore $0\nu\beta\beta$ decay are usually considered to be generated by dimension-5 (light-neutrino exchange), dimension-7, or dimension-9 effective operators (Cirigliano *et al.*, 2017, 2018c; Graesser, 2017), see Sec. III.B.2. The operators are suppressed by the typical scale Λ at which the BSM physics enters: $1/\Lambda$, $1/\Lambda^3$, and $1/\Lambda^5$, for dimension-5, dimension-7, and dimension-9, respectively. In the standard scenario the scale is set by the light-neutrino masses where $m_{\beta\beta} \propto 1/\Lambda$.

Below the electroweak symmetry breaking SSB scale,

heavy fields such as the W_L, Z, and Higgs bosons are integrated out. This leads to operators with different powers of the Higgs vacuum expectation value v, expressed in terms of the Fermi constant as $v = (\sqrt{2}\,G_F)^{-1/2} \approx 246\,\mathrm{GeV}$. In terms of Standard Model fields, dimension-3 (light-neutrino exchange), dimension-6, dimension-7, and dimension-9 operators are generated. The dimension-3 operator is unique, whereas in general multiple operators of a given dimension violate lepton number. After evolving to the hadronic and nuclear scales, the different contributions to the $0\nu\beta\beta$-decay amplitude can be organized as follows (Cirigliano *et al.*, 2018c)

$$
\begin{aligned}
T_{1/2}^{-1} =\,& g_A^4 \{ G_{01}(|\mathcal{A}_\nu|^2 + |\mathcal{A}_R|^2) \\
&+ 2G_{04}|\mathcal{A}_{m_e}|^2 + 4G_{02}|\mathcal{A}_E|^2 + G_{09}|\mathcal{A}_M|^2 \\
&- 2(G_{01} - G_{04})Re[\mathcal{A}_\nu^* \mathcal{A}_R] + 2G_{04}Re[\mathcal{A}_{m_e}^*(\mathcal{A}_\nu + \mathcal{A}_R)] \\
&- G_{03}Re[(\mathcal{A}_\nu + \mathcal{A}_R)\mathcal{A}_E^* + 2\mathcal{A}_{m_e}\mathcal{A}_E^*] \\
&+ G_{06}Re[(\mathcal{A}_\nu - \mathcal{A}_R)\mathcal{A}_M^*] \},
\end{aligned}
\tag{19}
$$

where the $\mathcal{A}_i$ are transition amplitudes labeled by the lepton structure to which they correspond: $\mathcal{A}_\nu$ corresponds to light-neutrino exchange (besides other operators), $\mathcal{A}_R$ involves lepton right-handed currents, the $\mathcal{A}_{m_e}$ and $\mathcal{A}_E$ amplitudes are multiplied by the electron mass and energies, respectively, and $\mathcal{A}_M$ by the nucleon mass. The phase-space factors G_{0i} depend on the electron wavefunctions, and have been calculated accurately (Horoi and Neacsu, 2018; Kotila and Iachello, 2012; Stefanik *et al.*, 2015).

In general, each amplitude $\mathcal{A}_i$ receives contributions from operators of different dimension (here we refer to the dimension of operators below the electroweak scale). The amplitude that receives the most contributions is $\mathcal{A}_\nu$. In particular, this is the relevant amplitude for dimension-3, dimension-7, and the majority of dimension-6 operators. In turn, $\mathcal{A}_M$ is dominant for one type of dimension-6 operator and four dimension-9 operators, and $\mathcal{A}_R$ gets the dominant contribution from four other dimension-9 operators. The amplitudes $\mathcal{A}_E$ and $\mathcal{A}_{m_e}$ are kinematically suppressed by a factor m_e/m_N. Because of this, their importance is relatively minor: $\mathcal{A}_E$ is only dominant for one type of dimension-6 operator, and $\mathcal{A}_{m_e}$ is always subleading.

In principle, the angular and energy distributions of the electrons emitted in $0\nu\beta\beta$-decay can be used to discriminate the leptonic structure responsible for the decay (Ali *et al.*, 2007; Arnold *et al.*, 2010; Cirigliano *et al.*, 2017; Horoi and Neacsu, 2016a). However, most BSM operators have leading contributions that enter into $\mathcal{A}_\nu$, the amplitude related to light-neutrino exchange. Therefore in general it will not always be possible to disentangle the BSM extension responsible for $0\nu\beta\beta$ decay by measuring angular and energy distributions.
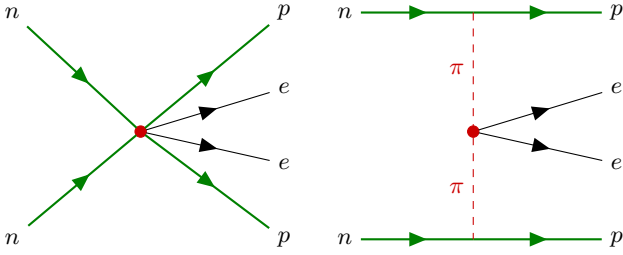
FIG. 8 Diagrams for contact (left) and two-pion exchange (right) contributions to $0\nu\beta\beta$ decay.

2. The master formula

The transition amplitudes $\mathcal{A}_i$ include a combination of hadronic and nuclear matrix elements. They also depend on the Wilson coefficients that couple BSM and Standard Model fields, which depend on the BSM scale Λ. In the case of light neutrino exchange, Eq. (19) simplifies to Eq. (16). The combination of light neutrino masses $m_{\beta\beta}$ sets the scale for lepton number violation.

In a more general scenario, additional contributions emerge, modifying Eq. (16) as

$$
T_{1/2}^{-1} = G_{01}\, g_A^4\, \left(M_{\text{light}}^{0\nu}\right)^2 \frac{m_{\beta\beta}^2}{m_e^2}
$$
$$
+ \frac{m_N^2}{m_e^2} \tilde{G}\, \tilde{g}^4\, \tilde{M}^2 \left(\frac{v}{\tilde{\Lambda}}\right)^6 + \frac{m_N^4}{m_e^2\, v^2} \tilde{G}'\, \tilde{g}'^4\, \tilde{M}'^2 \left(\frac{v}{\tilde{\Lambda}'}\right)^{10} + \cdots ,
$$
(20)

where the second and third terms are typical contributions from dimension-7 and dimension-9 operators, respectively. For any given BSM extension, several of these contributions are expected. They can interfere with each other, and also with the light-neutrino exchange channel, as indicated by Eq. (19). However, interference terms are not expected to dominate (Ahmed and Horoi, 2020; Ahmed et al., 2017).

The factors in front of the dimension-7 and -9 terms are given by EFT (Cirigliano et al., 2017, 2018c). They capture chiral enhancement factors of the nucleon over the pion mass, m_N/m_π, with respect to the naive analysis in Eq. (7). These nuclear effects appear because, when mediated by the exchange of a heavy particle (Fig. 8, left), the $0\nu\beta\beta$-decay amplitude is dominated by the virtual exchange of pions (Fig. 8, right). Each pion exchanged enhances the amplitude by m_N/m_π.

All phase-space factors in Eq. (20), G_{01}, $\tilde{G}$, and $\tilde{G}'$, are known, and have typical values $G \sim 10^{-14}\,\text{yr}^{-1}$. The hadronic matrix elements g_A, $\tilde{g}$, and $\tilde{g}'$ can be calculated by lattice QCD or measured. The present knowledge on $\tilde{g}$, $\tilde{g}'$ values is collected in Ref. (Cirigliano et al., 2018c), and agrees with the EFT expectation that they all are of the same of order. The NMEs $M_{\text{light}}^{0\nu}$, $\tilde{M}$, and $\tilde{M}'$ can be calculated by nuclear theory, and they are sometimes suppressed or enhanced due to nuclear structure

effects, see Sec. IV.B.4. In addition to the terms explicitly included in Eq. (20), Yukawa couplings can suppress some contributions. These small couplings are the reason that in some models the $0\nu\beta\beta$ rate stemming from dimension-9 operators can dominate over light-neutrino-exchange and dimension-7 channels when $\tilde{\Lambda} \sim \tilde{\Lambda}'$.

Therefore a $0\nu\beta\beta$-decay measurement will constrain, in addition to $m_{\beta\beta}$, the scales of any given BSM extension, $\tilde{\Lambda}$ and $\tilde{\Lambda}'$. These new-physics scales are determined by the values of the BSM parameters, typically in terms of small dimensionless Wilson coefficients $C \sim v/\Lambda$, and Yukawa couplings. For instance, in the left-right symmetric models discussed in Sec. III.C.4, the Wilson coefficients can be related to the heavy mass of the right-handed W_R boson, $C \sim M_{W_L}/M_{W_R}$, or to the small mixing between the right- and left-handed sectors, $C \sim \xi_{LR}$. Most studies interpret the constraints of $0\nu\beta\beta$-decay limits on left-right symmetric models in terms of M_R and ξ_{LR} (Horoi and Neacsu, 2016a; Li et al., 2021a; Sarkar et al., 2020; Stefanik et al., 2015).

3. Experimental constraints on new physics scales

Typical constraints by present $0\nu\beta\beta$-decay experiments, $T_{1/2}^{-1} \gtrsim 10^{26}\,\text{yr}$, can be estimated from Eq. (20), see also the comparison with the naive expectation in Eq. (7). In the light-neutrino exchange mechanism, phase-space factors and typical NMEs lead to $m_{\beta\beta} \lesssim 100\,\text{meV}$. Likewise, for dimension-7 and dimension-9 operators, $\tilde{\Lambda} \gtrsim 200\,\text{TeV}$ and $\tilde{\Lambda}' \gtrsim 5\,\text{TeV}$, respectively (Cirigliano et al., 2017, 2018c). In contrast, a direct substitution in Eq. (20) assuming the EFT expected values for hadronic and nuclear matrix elements anticipates $\tilde{\Lambda} \gtrsim 500\,\text{TeV}$ and $\tilde{\Lambda}' \gtrsim 8\,\text{TeV}$. The actual constraints are not as tight because nuclear structure effects suppress $\tilde{M}$ and $\tilde{M}'$ NMEs, as discussed in Sec. IV.B.4. For dimension-9 operators the impact of the NME cancellation is smaller because $\tilde{\Lambda}'$ enters to a higher power.

Future improvements in $0\nu\beta\beta$-decay half-life limits of one order of magnitude will tighten the constraints on $m_{\beta\beta}$ by about a factor of about 3. BSM scales for dimension-7 operators $\tilde{\Lambda}$ would improve by an additional 50%, because of their $1/\tilde{\Lambda}^3$ dependence. Constraints for dimension-9 operators would improve $\tilde{\Lambda}'$ by 25%, since they enter as $(1/\tilde{\Lambda}')^5$.

B. Nuclear matrix elements

In general, each $0\nu\beta\beta$-decay mechanism needs a particular NME. However, in practice only few different NMEs are required in the dominant channels for each operator leading to $0\nu\beta\beta$ decay. NMEs encode how the decay occurs within a highly correlated many-body system. These nuclear structure aspects can enhance or suppress the

values of the NMEs.

1. Light and heavy neutrino exchange

The starting point of most derivations of the $0\nu\beta\beta$-decay NME for neutrino exchange is the leading weak current for one nucleon (Park *et al.*, 2003; Tomoda, 1991):

$$
\begin{aligned}
\mathcal{J}^0 &= \tau \left[g_V(p^2) \right], \\
\boldsymbol{J} &= \tau \left[g_A(p^2)\boldsymbol{\sigma} - g_P(p^2)\frac{\boldsymbol{p}\,(\boldsymbol{p}\cdot\boldsymbol{\sigma})}{p^2 + m_\pi^2} + i g_M \frac{\boldsymbol{\sigma}\times\boldsymbol{p}}{2m_N} \right],
\end{aligned}
\tag{21}
$$

in terms of the so-called vector (V), axial (A), pseudoscalar (P) and magnetic (M) terms, labeled after the corresponding hadronic couplings g_V, g_A, g_P and g_M. The vector and axial terms are responsible for Fermi and Gamow-Teller β decays, respectively, while g_P and g_M only contribute to processes with finite momentum transfer ($\boldsymbol{p}$) such as $0\nu\beta\beta$ decay. The currents also depend on the nucleon isospin τ and spin $\boldsymbol{\sigma}$.

The $0\nu\beta\beta$-decay rate is then given by the product of two one-body hadronic currents, following second-order perturbation theory in the weak interaction:

$$
\sqrt{\Gamma_{0\nu\beta\beta}} = m_{\beta\beta}\cdot\frac{g_A^2}{R}\cdot\int d\boldsymbol{x}\int d\boldsymbol{y}\; L^{\mu\rho}(\boldsymbol{x},\boldsymbol{y})\int d\boldsymbol{p}\,e^{i\boldsymbol{p}(\boldsymbol{x}-\boldsymbol{y})}.
$$
$$
\frac{R}{g_A^2}\sum_{n,m,a}\langle 0_f^+|\frac{\mathcal{J}_n^{\mu\dagger}(\boldsymbol{x})\,|J_a^P\rangle\langle J_a^P|\,\mathcal{J}_m^{\rho\dagger}(\boldsymbol{y})}{\sqrt{m_\nu^2+\boldsymbol{p}^2}\left[\sqrt{m_\nu^2+\boldsymbol{p}^2}+E_a^{\text{rel}}\right]}|0_i^+\rangle,
\tag{22}
$$

where $L^{\mu\rho}$ includes the electrons and γ matrices evaluated at positions $\boldsymbol{x}$ and $\boldsymbol{y}$. This term generates the phase space factor, divided by the approximate nuclear radius $R = 1.2A^{1/3}$ fm introduced to make the NME dimensionless. m_ν is the mass of the exchanged particle, and the hadronic coupling g_A^2 is explicitly factored out to follow the usual convention leading to Eq. (16). The remaining terms in Eq. (22) correspond to the NME, which includes a sum over nucleons n, m. The ground states of the initial (i) and final (f) nuclei have angular momentum and parity $J^P = 0^+$, and the sum is over all states of the intermediate nucleus (a) with odd number of protons and neutrons. $E_a^{\text{rel}} = E_a - (E_i + E_f)/2$, where E denotes the energy of the states.

The momentum transfer in $0\nu\beta\beta$ decay is $p \sim 100 - 200$ MeV for the exchange of light neutrinos, and larger for heavy-particle exchange. Therefore it is common to regard Eq. (22) as practically independent of the intermediate states, because $E_a^{\text{rel}} \sim 10$ MeV$\ll p$, and replace E_a^{rel} with an average $\langle E\rangle$. This is called the closure approximation. Explicit QRPA and shell model calculations estimate that the closure approximation is good to 10% (Muto, 1994; Sen'kov and Horoi, 2013, 2016). Evaluating Eq. (22) for $m_\nu \ll p$ and $m_\nu \gg p$ allows one to define a long-range NME for light-neutrino exchange and a heavy-neutrino exchange NME, respectively:

$$
M_{\text{long}}^{0\nu} = \frac{1.2A^{1/3}\,\text{fm}}{g_A^2}\cdot
$$
$$
\langle 0_f^+|\sum_{n,m}\tau_m^-\tau_n^-\left[H_F^\nu(r)\mathbb{1}+H_{GT}^\nu(r)\boldsymbol{\sigma}_n\cdot\boldsymbol{\sigma}_m+H_T^\nu(r)\,S_{nm}\right]|0_i^+\rangle,
\tag{23}
$$

and $M_{\text{heavy}}^{0\nu}$ has the same form, but it is divided by m_π^2 and depends on potentials H^N instead of H^ν. Here $r = |\boldsymbol{r}_n - \boldsymbol{r}_m|$ is the distance between nucleons. The three spin structures are denoted as Fermi (F), Gamow-Teller (GT) and tensor (T), with the latter operator defined as $S_{nm} = 3(\hat{r}\cdot\boldsymbol{\sigma}_n)(\hat{r}\cdot\boldsymbol{\sigma}_m) - \boldsymbol{\sigma}_n\cdot\boldsymbol{\sigma}_n$. Compared to Eq. (22), $M_{\text{heavy}}^{0\nu}$ is multiplied by a factor m_ν^2/m_π^2, which allows a better comparison because then $M_{\text{long}}^{0\nu} \sim M_{\text{heavy}}^{0\nu} \sim 1$ (Cirigliano *et al.*, 2017, 2018c). This definition differs by a factor $m_\pi^2/(m_N m_e)$ from the standard one in the literature.

Since in $0\nu\beta\beta$ decay the exchanged particles are not emitted, they become part of the transition operator, and thus the NME. The so-called neutrino potential $H^\nu(r)$ for the exchange of light particles is given by

$$
H_{\text{spin}}^\nu(r) = \frac{2}{\pi}\int j_{\text{spin}}(pr)\frac{h_{\text{spin}}(p)}{p(p+\langle E\rangle)}p^2 dp,
\tag{24}
$$

and the heavy-neutrino potential $H^N(r)$ is defined likewise without the denominator $p(p+\langle E\rangle)$. The subindex distinguishes spin structures. The spherical Bessel function j_0 applies to Fermi and GT potentials, while the tensor goes with j_2. The functions $h_{\text{spin}}(p)$ are given by

$$
\begin{aligned}
h_F &= h_F^{VV}, \\
h_{GT} &= h_{GT}^{AA} + h_{GT}^{AP} + h_{GT}^{PP} + h_{GT}^{MM}, \\
h_T &= h_T^{AP} + h_T^{PP} + h_T^{MM},
\end{aligned}
\tag{25}
$$

with

$$
\begin{aligned}
h_F^{VV} &= g_V^2\; f^2(p/\Lambda_V), \\
h_{GT}^{AA} &= g_A^2\; f^2(p/\Lambda_A), \\
h_{GT}^{AP} &= -h_T^{AP} = -g_A^2\frac{2}{3}\frac{p^2}{p^2+m_\pi^2}\; f^2(p/\Lambda_A), \\
h_{GT}^{PP} &= -h_T^{PP} = g_A^2\frac{1}{3}\frac{p^4}{(p^2+m_\pi^2)^2}\; f^2(p/\Lambda_A), \\
h_{GT}^{MM} &= 2\,h_T^{MM} = \frac{g_M^2}{6}\frac{p^2}{m_N^2}\; f^2(p/\Lambda_V),
\end{aligned}
\tag{26}
$$

where the superscripts correspond to the terms in the one-body current in Eq. (21) leading to each neutrino potential. The magnetic coupling, $g_M = 1 + \kappa_1 = 4.71$, depends on the anomalous isovector nucleon magnetic moment κ_1. The standard phenomenological derivation includes a momentum-dependent dipole form factor

$f(x) = 1/(1 + x^2)^2$ for all terms, with axial and vector regulators $\Lambda_{A,V} \sim 1\,\text{GeV}$.

Organizing by spin structure, the NME for light-neutrino exchange can thus be written as

$$M_{\text{long}}^{0\nu} = M_{GT}^{AA} + M_F^{VV} + M_{GT}^{AP} + M_{GT}^{PP} + M_{GT}^{MM}$$
$$+ M_T^{AP} + M_T^{PP} + M_T^{MM} \quad , \quad (27)$$

and for heavy-neutrino exchange $M_{\text{heavy}}^{0\nu}$ is defined likewise, but with components $M_{GT,\text{h}}^{AA}, M_{F,\text{h}}^{VV}, \cdots$ given by $H_{\text{spin}}^N(r)$ instead of $H_{\text{spin}}^\nu(r)$. The superscripts have the same meaning as in Eq. (26). NMEs are also available for $m_\nu \sim p$ (Barea *et al.*, 2015b; Blennow *et al.*, 2010; Faessler *et al.*, 2014).

2. Short-range operator for light neutrino exchange

A more systematic derivation can be obtained within the EFT for $0\nu\beta\beta$ decay (Cirigliano *et al.*, 2018a,b,c). The EFT replicates all terms given in Sec. IV.B.1, with small differences only. In addition, the EFT provides an expansion, or counting, of the different contributions that determines which of them should be considered at a given EFT order. For instance, in the EFT, including the closure energy $\langle E \rangle$ in Eq. (24) is a higher-order effect. Likewise, the momentum dependence of the axial and vector form factors in $h_{\text{spin}}(p)$, besides quadratic terms, appear also at higher order in the EFT. However, the numerical impact of the differences introduced by the EFT with respect to the expressions used by most NME calculations is about few percent (Menéndez *et al.*, 2011; Rodin *et al.*, 2006). In addition, the EFT also predicts additional contributions not considered in practical calculations yet. Preliminary estimations suggest that the additional terms are numerically small corrections to the light-neutrino exchange $M^{0\nu}$ (Cirigliano *et al.*, 2018b), with one exception.

A novel, potentially relevant term was introduced by Cirigliano *et al.* (2018a), and described in detail in Cirigliano *et al.* (2019). The main idea is that the exchange of high-energy light neutrinos, which is naively expected to be a high-order correction, may be in fact a leading-order contribution. The NME associated with this new contact diagram can be defined as

$$M_{\text{short}}^{0\nu} = \frac{1.2 A^{1/3}\,\text{fm}}{g_A^2}$$
$$\langle 0_f^+ | \sum_{n.m} \tau_m^- \tau_n^- \mathbb{1} \left[\frac{2}{\pi} \int j_0(qr) h_S\, q^2 dq \right] | 0_i^+ \rangle, \quad (28)$$

which follows the structure of Eqs. (23)–(24). The neutrino potential $h_S = 2g_\nu^{\text{NN}} f_S(p/\Lambda_S)$ depends on a two-nucleon coupling expected to scale as $g_\nu^{\text{NN}} \sim 1/m_\pi^2$, with regulator f_S and scale Λ_S. The momentum dependence

of f_S can be more general than the momentum transfer p. The new matrix element depends on the nuclear structure of the initial and final nuclei, and on the contact coupling g_ν^{NN}, satisfying $M_{\text{short}}^{0\nu}/(g_\nu^{\text{NN}} m_\pi^2) \sim M_{\text{heavy}}^{0\nu} \sim M_{\text{long}}^{0\nu}$. In fact, $M_{\text{short}}^{0\nu}$ is related to the short-range NME for heavy-neutrino exchange, sharing the same spin structure as $M_{F,\text{h}}^{VV}$. The short-range term cannot be derived by the product of two one-nucleon weak currents as in Eq. (22), which explains why g_ν^{NN} appears linearly in h_S, in contrast to g_A which is always squared.

The contact coupling g_ν^{NN} is not known experimentally. Because both the value and sign of g_ν^{NN} are unknown, the new short-range term could either enhance or reduce expected $0\nu\beta\beta$-decay rates, but it could also have a small impact if $g_\nu^{\text{NN}} \ll 1/m_\pi^2$. Lattice QCD calculations of the neutrinoless two-nucleon decay can determine g_ν^{NN} and efforts in this direction are ongoing (Davoudi and Kadam, 2021; Davoudi *et al.*, 2021; Davoudi and Kadam, 2022). Alternatively, g_ν^{NN} can be inferred from an approximated calculation of the same process using perturbative QCD methods (Cirigliano *et al.*, 2021a,b) that describe well the related charge-independence-breaking in the electromagnetic sector. This avenue has been used to obtain $M_{\text{short}}^{0\nu}$ in ^{48}Ca, suggesting a positive contribution that enhances the long-range NME by about 40% (Wirth *et al.*, 2021). A similar enhancement around $30\% - 50\%$ has been found for transitions in nuclei from ^{48}Ca to ^{136}Xe (Jokiniemi *et al.*, 2021b), assuming g_ν^{NN} values taken from the charge-independence-breaking term of different nuclear Hamiltonians, an assumption supported by (Cirigliano *et al.*, 2021a) and (Richardson *et al.*, 2021). Given the potential impact of this contribution, a more robust determination of g_ν^{NN} should be pursued.

Including the short-range term, the light-neutrino exchange rate in Eq. (16) is modified as

$$T_{1/2}^{-1} = G_{01}\, g_A^4 \left(M_{\text{long}}^{0\nu} + M_{\text{short}}^{0\nu} \right)^2 \frac{m_{\beta\beta}^2}{m_e^2}, \quad (29)$$

leading to the light-neutrino exchange NME $M_{\text{light}}^{0\nu} = M_{\text{long}}^{0\nu} + M_{\text{short}}^{0\nu}$. Likewise, a short-range contribution is expected for the exchange of heavy neutrinos discussed in Sec. IV.B.1 (Dekens *et al.*, 2020). In this case the contact coupling g_ν^{NN} depends on the neutrino mass in a non trivial way. Analyses of BSM scenarios with heavy sterile neutrinos thus need to complement the NME dependence on the neutrino mass with this additional dependence.

3. Two-body currents

Nucleons are composite particles. Nuclear structure calculations, however, ignore that nucleons are formed by quarks and gluons and thus exhibit possible nucleon excitations. To compensate for the missing degrees of freedom and other high-energy effects, the one-body current in Eq. (21) needs to be complemented with two-body

or meson-exchange currents (2BC). In the EFT, 2BC are associated with hadronic couplings, denoted by c_i, that also appear in the nucleon-nucleon forces that describe the same physics (Baroni *et al.*, 2016; Krebs *et al.*, 2017; Park *et al.*, 2003).

The importance of 2BC has been appreciated for decades (Brown and Wildenthal, 1987; Towner, 1997). However only EFT identifies the leading 2BC diagrams and predicts the value of the couplings. While 2BC appear at higher EFT order than the terms introduced in Sec. IV.B.1, long-range 2BC are enhanced because they encode $\sim 300\,\text{MeV}$ nucleon excitations to the Δ-isobar (Bernard *et al.*, 1997; van Kolck, 1994). In fact, an EFT with explicit Δ's places 2BC at next-to-next to leading order, which is the same order as other contributions in Eq. (27) (Epelbaum *et al.*, 2008). EFT weak 2BC play a limited ($\lesssim 5\%$) but key role to reproduce experimental β-decays half-lives (Gazit *et al.*, 2009; Pastore *et al.*, 2018a) and neutrino scattering cross-sections(Butler *et al.*, 2001; Nakamura *et al.*, 2001) in light $A \leq 14$ nuclei. In heavier $20 \lesssim A \leq 100$ systems, 2BC reduce β decay matrix elements by $\sim 10\% - 20\%$ (Ekström *et al.*, 2014; Gysbers *et al.*, 2019), as discussed in detail in Sec. IV.D.

$\beta\beta$ decay involves the product of two weak currents, like in Eq. (22), so that 2BC generate three- and four-body transition operators. Approximating 2BC as effective one-body currents via normal-ordering with respect to a symmetric nuclear matter reference state gives the estimate (Menéndez *et al.*, 2011)

$$
\begin{aligned}
\boldsymbol{\mathcal{J}}^{1b} + \boldsymbol{\mathcal{J}}^{2b}_{\text{eff}} = \tau \Bigg[& g_A \boldsymbol{\sigma} - \boldsymbol{\sigma} \frac{2k_F^3 \, g_A}{3\pi^2 F_\pi^2} \bigg(-\frac{c_D}{4 g_A \Lambda_\chi} \\
& + \frac{2c_4 - c_3}{3} \left[1 - \frac{3m_\pi^2}{k_F^2} + \frac{3m_\pi^3}{k_F^3} \text{atan}\!\left(\frac{k_F}{m_\pi}\right) \right] \bigg) \Bigg], \quad (30)
\end{aligned}
$$

which modifies the GT term in Eq. (21). The c_i couplings and Fermi momentum $k_F \sim 200\,\text{MeV}$ reduce the GT operator by $\sim 20\%$ (Gysbers *et al.*, 2019), suggesting that 2BC contribute to "g_A quenching", see Sec. IV.D. An improved expression is given by Ney *et al.* (2022), which shows that the impact is reduced on neutron-rich nuclei. Similar expressions modify the pseudoscalar and magnetic terms in Eq. (21) (Hoferichter *et al.*, 2020).

The EFT 2BC in Eq. (30), when extended to finite momentum transfer, reduce $0\nu\beta\beta$-decay NMEs by $\sim 30\%$ (Engel *et al.*, 2014; Menéndez *et al.*, 2011). This is less than doubling the reduction in βdecay matrix elements, because 2BC predict a milder reduction of the GT operator at $p \sim 200\,\text{MeV}$. An improved treatment including three-body operators found only a $\sim 10\%$ NME reduction for ^{76}Ge (Wang *et al.*, 2018), but a short-range term similar in nature to the one discussed in Sec. IV.B.2 could not be evaluated because of the unknown coupling. In sum, 2BC could moderately modify $0\nu\beta\beta$-decay NMEs, perhaps similarly to or less than GT β decays. Calculations with exact 2BC will provide an answer.

4. Other exchange mechanisms

BSM physics is typically mediated by a heavy particle. Nevertheless, whenever permitted by symmetries of the operator, the EFT predicts (Prezeau *et al.*, 2003) that the dominant contribution to the $0\nu\beta\beta$-decay rate will be through the pion-exchange diagrams shown in Fig. 8, enhanced by a factor $(m_N/m_\pi)^2$ as discussed in Sec. IV.A.2. On the other hand, for dimension-7 operators, contact and pion-exchange diagrams compete with the short-range coupling to the nucleon magnetic moment, proportional to g_M in Eq. (21). The latter is enhanced with respect to the naive estimate because of the large coupling $g_M = 4.71$.

In general, many nuclear matrix elements contribute to $0\nu\beta\beta$ decay mediated by BSM physics (Cirigliano *et al.*, 2018c). The relevant combinations additional to $M^{0\nu}_{\text{long}}$ and $M^{0\nu}_{\text{short}}$ are

$$
\begin{aligned}
M^{PS} &= \frac{1}{2} M^{AP}_{GT} + M^{PP}_{GT} + \frac{1}{2} M^{AP}_T + M^{PP}_T, \\
M^M &= M^{MM}_{GT} + M^{MM}_T, \\
M^{PS}_{\text{heavy}} &= \frac{1}{2} M^{AP}_{GT,\text{h}} + M^{PP}_{GT,\text{h}} + \frac{1}{2} M^{AP}_{T,\text{h}} + M^{PP}_{T,\text{h}}, \\
M^{AP}_{\text{heavy}} &= M^{AP}_{GT,\text{h}} + M^{AP}_{T,\text{h}}, \qquad\qquad (31)
\end{aligned}
$$

where the superscripts on the left-hand side NMEs indicate pseudoscalar (PS), magnetic (M) and axial-pseudoscalar (AP) in reference to the one-nucleon terms in Eq. (21). Tensor contributions are usually much smaller than GT ones, according to NME calculations in $\beta\beta$ emitters (Barea *et al.*, 2015a; Hyvarinen and Suhonen, 2015; Menéndez *et al.*, 2009b). All six NMEs are combinations of the contributions to the light- and heavy-neutrino exchange matrix elements introduced in and below Eq. (27).

The NMEs M^{PS} and M^{MM} are dominant for dimension-7 operators, while M^{PS}_{heavy}, M^{AP}_{heavy}, and $M^{0\nu}_{\text{short}}$ are the most relevant for dimension-9 operators. The naive EFT counting that neglects nuclear structure effects predicts $M^{PS} \sim M^{PS}_{\text{heavy}} \sim M^{AP}_{\text{heavy}} \sim M^{0\nu}_{\text{long}}$. However, calculations (Barea *et al.*, 2015a; Hyvarinen and Suhonen, 2015; Menéndez *et al.*, 2009b) show that the two terms in M^{PS} have opposite sign and mostly cancel, in both GT and tensor parts, so that $M^{PS} \sim M^{PS}_{\text{heavy}} \sim M^{0\nu}_{\text{long}}/10$. This nuclear-structure-based suppression is responsible for the reduced sensitivity of $0\nu\beta\beta$-decay experiments to the physics scale of typical dimension-7 and dimension-9 operators compared to naive EFT expectations, discussed in Sec. IV.A.3. On the other hand, EFT indicates that $M^M \sim (m_\pi^2/m_N^2) M^{0\nu}_{\text{long}}$. In contrast, the magnetic term is enhanced by the large hadronic coupling g_M, leading to $M^M \sim M^{0\nu}_{\text{long}}/10$, so that it competes with M^{PS} as the dominant NME for dimension-7 operators. For a discussion on how these cancellations impact the BSM physics sensitivities of $0\nu\beta\beta$-decay ex-

periments compared to LHC searches, see Graesser *et al.* (2022).

Different NMEs for BSM $0\nu\beta\beta$-decay mechanisms have also been proposed and calculated in Doi *et al.* (1985); Kotila *et al.* (2021); Tomoda (1991); and Vergados *et al.* (2012).

C. Many-body methods

In the absence of a $0\nu\beta\beta$-decay observation, and as long as the light-neutrino masses, their ordering, or the BSM parameters responsible for the decay are not known, NMEs need to be obtained from theoretical nuclear structure calculations. Here we present updated NME results and describe briefly the nuclear many-body methods used to obtain them. A more thorough discussion of NMEs and nuclear many-body methods can be found in Engel and Menéndez (2017).

1. Current status for long-range nuclear matrix elements

Comparisons of NMEs obtained with different many-body approaches are common in the $0\nu\beta\beta$-decay literature (Bahcall *et al.*, 2004; Engel and Menéndez, 2017; Feruglio *et al.*, 2002; Gomez-Cadenas *et al.*, 2012; Vogel, 2012). Figure 9 shows updated results for $0\nu\beta\beta$-decay NMEs of eight $\beta\beta$ emitters, covering calculations from the nuclear shell model (NSM), the quasiparticle random-phase approximation (QRPA) method, the interacting boson model (IBM) and energy-density functional (EDF) theory. Also included are recent ab initio ^{48}Ca NMEs obtained with the in-medium generator coordinate method (IM-GCM), a multi-reference version of the similarity renormalization group (IMSRG), and coupled-cluster (CC) theory, and ^{48}Ca ^{76}Ge and ^{82}Se NMEs from the valence-space (VS) IMSRG method. Table I collects the NMEs for the five nuclei most relevant for next-generation experiments, and indicates the range of NMEs for each nuclear structure method, obtained by combining the results of different calculations for each approach.

The variation in $M^{0\nu}$ in Fig. 9, about a factor three, highlights the uncertainties introduced by the approximate solutions of the nuclear many-body problem. With few exceptions among the $\beta\beta$ emitters considered, the NMEs follow a similar trend: shell model NMEs tend to be smallest, and EDF theory ones largest, with the IBM and QRPA somewhere in between. Recent QRPA calculations by Fang *et al.* (2018) including deformation (violet bars), however, modify this picture as they find smaller NMEs than spherical QRPA calculations, close to the shell model NMEs. These results follow a tendency of smaller QRPA NMEs hinted by the sophisticated QRPA of Mustonen and Engel (2013) — magenta
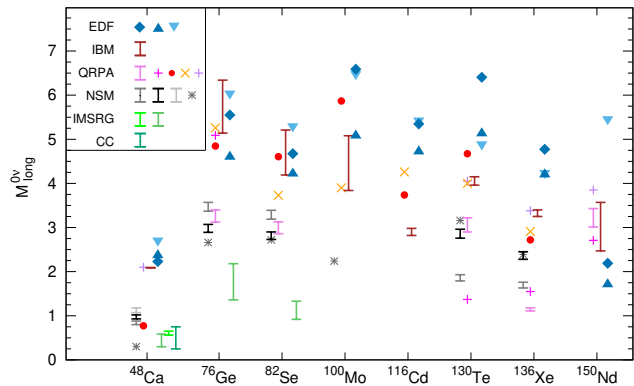

FIG. 9 Nuclear matrix elements $M_{\text{long}}^{0\nu}$ for light-neutrino exchange from different many-body methods. NSM: black (Menéndez, 2018), grey (Horoi and Neacsu, 2016b), light-grey (Iwata *et al.*, 2016) bars, grey stars (Coraggio *et al.*, 2020, 2022); QRPA: deformed in violet bars (Fang *et al.*, 2018)), and spherical in magenta (Mustonen and Engel, 2013) and purple (Terasaki, 2015, 2020; Terasaki and Iwata, 2019) crosses, red circles (Šimkovic *et al.*, 2018b), orange multiplication signs (Hyvarinen and Suhonen, 2015); IBM: brown bars (Barea *et al.*, 2015a; Deppisch *et al.*, 2020a); EDF theory: nonrelativistic in blue diamonds (Rodriguez and Martinez-Pinedo, 2010), blue up-triangles (López Vaquero *et al.*, 2013)), and relativistic in light-blue down-triangles (Song *et al.*, 2017); IMSRG: IM-GCM in the light green ^{48}Ca bar (Yao *et al.*, 2020), and valence space in green bars (Belley *et al.*, 2021); and CC theory: dark green ^{48}Ca bar (Novario *et al.*, 2021).

crosses. Nevertheless, the deformed QRPA likely underestimates NMEs because the current calculation misses the effect of configuration mixing that enhances their value (Rodriguez and Martinez-Pinedo, 2010). Finally, the ^{48}Ca NMEs from the IM-GCM (Yao *et al.*, 2020), VS-IMSRG (Belley *et al.*, 2021), and CC (Novario *et al.*, 2021) theory are consistent with each other and smaller than the shell model ones. The VS-IMSRG ^{76}Ge and ^{82}Se NMEs are also smaller than in other calculations, but currently the ab initio description of these nuclei is of lower quality than for ^{48}Ca, see Sec. IV.E.

Overall, the smaller ab initio NMEs suggest that phenomenological NMEs might be overestimated. This is consistent with the fact that, as discussed in the following sections, the many-body methods predicting larger NMEs, energy-density functional theory and the IBM, do not include explicitly proton-neutron pairing correlations which are known to reduce the value of the NMEs. Further, especially for ^{48}Ca and ^{76}Ge ab initio results are not far from shell-model and some of the QRPA ones, the only two-body methods which so far have predicted $2\nu\beta\beta$ or 2νECEC half-lives before their measurement (see Sec. IV.D.3). Nonetheless, especially compared to concerns related to a dramatic reduction of NMEs due to "g_A quenching" (see Sec. IV.D), the overestimation of the more phenomenological NMEs appears relatively moder-

TABLE I NMEs $M^{0\nu}$ for light neutrino exchange calculated with the shell model, QRPA, EDF theory and IBM methods, for the $0\nu\beta\beta$ decay of nuclei considered for next-generation experiments. The combined NME range for each many-body method is also shown. All NMEs were obtained with the bare value of g_A and do not include the short-range term proportional to g_ν^{NN}.

		^{76}Ge	^{82}Se	^{100}Mo	^{130}Te	^{136}Xe
Shell model	Menéndez (2018)	$2.89, 3.07$	$2.73, 2.90$	$-$	$2.76, 2.96$	$2.28, 2.45$
	Horoi and Neacsu (2016b)	$3.37, 3.57$	$3.19, 3.39$	$-$	$1.79, 1.93$	$1.63, 1.76$
	Coraggio *et al.* (2020, 2022)	2.66	2.72	2.24	3.16	2.39
	min–max	$2.66 - 3.57$	$2.72 - 3.39$	2.24	$1.79 - 3.16$	$1.63 - 2.45$
QRPA	Mustonen and Engel (2013)	5.09	$-$	$-$	1.37	1.55
	Hyvarinen and Suhonen (2015)	5.26	3.73	3.90	4.00	2.91
	Šimkovic *et al.* (2018b)	4.85	4.61	5.87	4.67	2.72
	Fang *et al.* (2018)	$3.12, 3.40$	$2.86, 3.13$	$-$	$2.90, 3.22$	$1.11, 1.18$
	Terasaki (2020)	$-$	$-$	$-$	4.05	3.38
	min–max	$3.12 - 5.26$	$2.86 - 4.61$	$3.90 - 5.87$	$1.37 - 4.67$	$1.11 - 3.38$
EDF theory	Rodriguez and Martinez-Pinedo (2010)	4.60	4.22	5.08	5.13	4.20
	López Vaquero *et al.* (2013)	5.55	4.67	6.59	6.41	4.77
	Song *et al.* (2017)	6.04	5.30	6.48	4.89	4.24
	min–max	$4.60 - 6.04$	$4.22 - 5.30$	$5.08 - 6.59$	$4.89 - 6.41$	$4.20 - 4.77$
IBM	Barea *et al.* (2015a) [a]	5.14	4.19	3.84	3.96	3.25
	Deppisch *et al.* (2020a)	6.34	5.21	5.08	4.15	3.40
	min–max	$5.14 - 6.34$	$4.19 - 5.21$	$3.84 - 5.08$	$3.96 - 4.15$	$3.25 - 3.40$

[a] With the sign change in the tensor part indicated in Deppisch *et al.* (2020a).

ate, taking into account that the ab initio methods used for ^{48}Ca reproduce well β-decay matrix elements without any adjustments.

2. Uncertainties and other nuclear matrix elements

Beyond these main features, Fig. 9 highlights that more calculations are available for some $0\nu\beta\beta$ decays than others. On the one hand, ^{48}Ca has been studied by all many-body methods, including three ab-initio ones. This is because ^{48}Ca is doubly-magic, and therefore can be described with relatively simple nuclear correlations. Indeed, most of the latest calculations roughly converge to rather small NME values. On the other hand, neither ab initio nor shell model NMEs are available for ^{116}Cd, or ^{150}Nd, and the only ^{100}Mo shell-model NMEs are very recent (Coraggio *et al.*, 2022). The difficulty is that these nuclei have a very complex nuclear structure with several neutrons and protons away from closed shells. In fact, for ^{150}Nd EDF results, which typically agree with each other, disagree by a factor of three, indicating the challenge of the calculations. The remaining decays lie in between, even though for instance the $A = 76$ nuclear structure might include subtleties due to deformation, see Sec. IV.E.

Unfortunately, the phenomenological character of most NME calculations prevents a reliable estimation of theoretical uncertainties. For instance, the impact of enlarging the configuration space in the shell model, or the effect of including explicit proton-neutron pairing correlations in EDF theory, are hard to quantify. Part of the

theoretical uncertainties, however, are easier to evaluate. For instance, the difference in the shell model results in Fig. 9 (black and grey bars and stars), or the EDF theory calculations (diamonds and up and down triangles) give an estimate of the uncertainty of each approach when the parameters of the model, typically the nuclear Hamiltonian, are varied. Likewise, the difference between spherical QRPA NMEs (red circles, magenta and purple crosses, orange multiplication symbols) and the IBM uncertainty (brown error bar) estimate this kind of theoretical uncertainty. On the other hand, smaller uncertainties shown as error bars in Fig. 9 explore a very small part of this uncertainty, because only a very limited subset of the parameters of the model — typically those associated with short-range correlations (SRC), see below — is varied. Symbols without error bars in Fig. 9 indicate that no parameter variation was explored. These kind of uncertainties have been recently evaluated more systematically in the shell model for energy levels (Yoshida *et al.*, 2018a) and electroweak matrix elements in light nuclei (Fox and Johnson, 2019), and in heavier systems with EDF theory (Neufcourt *et al.*, 2019). First efforts based on systematic calculations to assign these kind of theoretical uncertainties to $0\nu\beta\beta$-decay NMEs are available for ^{48}Ca in the shell model (Horoi *et al.*, 2022) and for all $0\nu\beta\beta$-decay candidates in the shell model and QRPA (Jokiniemi *et al.*, 2022). The latter give uncertainties for these methods comparable to the min-max ones in Table I.

Ab initio calculations in principle allow for a quantification of the theoretical uncertainties (Cirigliano *et al.*, 2022). The error bars in the ab initio results in Fig. 9 are
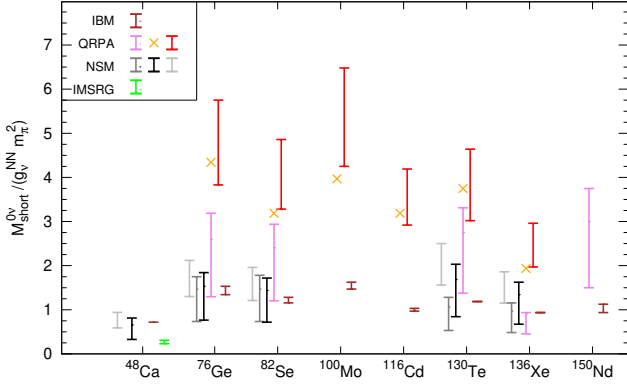
FIG. 10 Short-range light-neutrino exchange NMEs $M_{\text{short}}^{0\nu}$ without the coupling g_ν^{NN}. Results from the NSM: black (Menéndez, 2018), grey (Neacsu and Horoi, 2015; Sen'kov and Horoi, 2016; Sen'kov et al., 2014), light grey (Jokiniemi et al., 2021b) bars; the QRPA: deformed in violet bars (Fang et al., 2018), spherical in orange mulitplication signs (Hyvarinen and Suhonen, 2015) and red bars (Jokiniemi et al., 2021b)); the IBM: brown bars (Barea et al., 2015a; Deppisch et al., 2020a); and the IM-GCM: light green bars (Wirth et al., 2021).
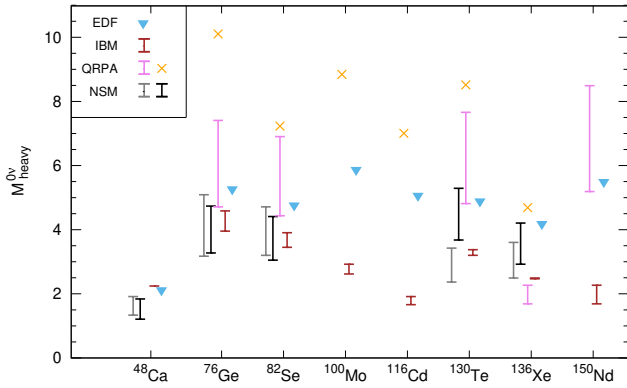

FIG. 11 Nuclear matrix elements $M_{\text{heavy}}^{0\nu}$ for the heavy-neutrino exchange $0\nu\beta\beta$ decay. Results from the NSM: black (Menéndez, 2018) and grey (Horoi and Neacsu, 2016b) bars; the QRPA: deformed in violet bars (Fang et al., 2018) and spherical in orange multiplication signs (Hyvarinen and Suhonen, 2015); the IBM: brown bars (Barea et al., 2015a; Deppisch et al., 2020a); and relativistic EDF theory: light-blue down-triangles (Song et al., 2017). Note that $M_{\text{heavy}}^{0\nu}$ differs by $(m_N\, m_e)^2/m_\pi^2$ with respect to the standard definition.

dominated by the uncertainty from the nuclear Hamiltonians used, except for CC theory, where the dominant error stems from the many-body method, which had to be extended to deal with $0\nu\beta\beta$ decay, see Sec. IV.C.7. Nonetheless, even the ab initio NME uncertainties in Fig. 9 are underestimated, because a relevant ingredient, two-body currents at finite momentum transfers, is not yet included in the calculations.

An additional uncertainty not immediately apparent in Fig. 9 concerns the possible reduction of the NMEs, usually known as "g_A quenching". This effect was proposed to compensate the finding that calculated GT β matrix elements tend to overpredict measured values by a roughly uniform factor. This introduces a potentially large uncertainty, because a naive direct quenching of the axial coupling constant $g_A^{\text{eff}} = 0.7 g_A$, as has been suggested often in the literature, would reduce the $0\nu\beta\beta$-decay NMEs by $(0.7)^2 \sim 1/2$, and decay rates by $(0.7)^4 \sim 1/4$. The "g_A quenching" highlights deficiencies in the nuclear theory calculations, but it is not clear how to scale them from β to $0\nu\beta\beta$ decays. For this reason, Fig. 9 assumes the unquenched $g_A = 1.27$. Recent ab initio calculations that reproduce β decays without any "g_A quenching" pave the way to solve this puzzle (Gysbers et al., 2019). We address this issue in detail in Sec. IV.D.

In addition to the nuclear structure of the initial and final nuclei, the range of the $0\nu\beta\beta$-decay operator has a strong impact on the NMEs. Figures 10 and 11 compare $M_{\text{short}}^{0\nu}/(g_\nu^{\text{NN}} m_\pi^2)$ and $M_{\text{heavy}}^{0\nu}$, corresponding to the short-range light-neutrino exchange term (without coupling) and the exchange of heavy neutrinos, discussed in Secs. IV.B.2 and IV.B.1, respectively. Except for the QRPA, short-range and heavy-neutrino NMEs are close. This suggests that differences in $M_{\text{long}}^{0\nu}$ are due to how longer-range nuclear correlations are treated differently in the various many-body methods (Menéndez, 2018).

As for the contact term, combining the short-range NMEs in Fig. 10 with g_ν^{NN} values from charge-independent-breaking Hamiltonians leads to sizable contributions with respect to $M_{\text{long}}^{0\nu}$ (Jokiniemi et al., 2021b), both for the shell model (light grey bars, $\sim 30\%$ impact) and for the QRPA (red bars, $\sim 50\%$ effect). These NMEs are consistent with other shell model and QRPA estimations in Fig. 10; the main difference is that the latter use a dipole f_S instead of a gaussian. The value of g_ν^{NN} is found to be positive in ^{48}Ca and other lighter nuclei in (Wirth et al., 2021). Therefore, Fig. 10 suggests that the difference between NMEs in Fig. 9 will persist, with QRPA continuing to prefer larger $M_{\text{light}}^{0\nu}$ values.

The large error bars in Figs. 10 and 11 are due to SRCs, typically ignored because doing so simplifies computations and does not affect much most nuclear structure properties. However, for $0\nu\beta\beta$-decay NME SRCs are extracted from calculations which include SRCs explicitly (Cruz-Torres et al., 2018; Kortelainen et al., 2007; Šimkovic et al., 2009) typically via prescriptions used in other many-body calculations. The error bars in Fig. 9, 10, and 11 indicate a higher sensitivity to SRCs in $M_{\text{heavy}}^{0\nu}$ and $M_{\text{short}}^{0\nu}$ than in $M_{\text{long}}^{0\nu}$, where the impact is relatively small as also indicated by Engel and Hagen (2009). Nonetheless, very recently, the SRCs captured by an ab initio method have been combined with the shell model using an effective theory for SRCs validated in comparisons to SRC measurements (Cruz-Torres et al., 2021). The results suggest a larger $\sim 30\%$ reduction in $M_{\text{long}}^{0\nu}$

due to SRCs (Weiss *et al.*, 2021), which is similar to the effect found by Benhar *et al.* (2014).

Finally, M_{heavy}^{PS} and M_{heavy}^{AP} matrix elements defined in Sec. IV.B.4 calculated with the shell model (Horoi and Neacsu, 2016b; Menéndez, 2018) and the QRPA (Hyvarinen and Suhonen, 2015) show agreement similar to that in Fig. 11. Likewise, shell model and QRPA M^M and M^{PS} matrix elements compare similarly to $M_{\text{long}}^{0\nu}$ in Fig. 9. Therefore, the nuclear matrix elements needed for light neutrino exchange and any other mechanism appear to have similar uncertainties.

3. The nuclear shell model

The nuclear shell model is the primary method used to describe nuclear structure (Brown, 2001; Caurier *et al.*, 2005; Otsuka *et al.*, 2020; Poves, 2017). Modern shell-model calculations are based on mixing nuclear configurations within a given space. Usually the configuration space comprises one major harmonic oscillator shell for protons and neutrons, but due to advances in computing power two-shell calculations are increasingly more common. Within the configuration space, the shell model includes the most general nuclear correlations. This is sufficient to describe well the spectroscopy of nuclei from oxygen to lead.

Most calculations of $0\nu\beta\beta$-decay NMEs are currently limited to one shell (Coraggio *et al.*, 2020, 2022; Menéndez, 2018; Menéndez *et al.*, 2009b; Neacsu and Horoi, 2015; Sen'kov and Horoi, 2013, 2016; Sen'kov *et al.*, 2014). So far the only two-shell calculation is for ^{48}Ca (Iwata *et al.*, 2016), which results in a moderate $\sim 20\%$ NME enhancement over the one-shell NME — light-grey bars in Fig. 9. It also reveals a subtle competition: pairing-like excitations enhance NMEs (Caurier *et al.*, 2008), while particle-hole-like ones reduce NME values (Horoi and Brown, 2013). The overall effect of larger configuration spaces is thus expected to be limited. Two-shell calculations in heavy nuclei demand approximate solutions, for instance using the GCM with collective degrees of freedom — deformation, isoscalar and isovector pairing — as coordinates (Hinohara and Engel, 2014; Jiao and Johnson, 2019; Jiao *et al.*, 2018; López Vaquero *et al.*, 2013; Menéndez *et al.*, 2016). For ^{76}Ge a GCM two-shell calculation (Jiao *et al.*, 2017) finds a slight NME reduction. Likewise, studies that explore the impact of larger configuration spaces with perturbation theory — grey stars in Fig. 9 — also suggest a $20\% - 30\%$ change on NMEs at most (Coraggio *et al.*, 2020; Holt and Engel, 2013). The only exception is ^{48}Ca, which as a doubly-magic nucleus probably needs additional refinement in this framework.

The Monte Carlo shell model is a novel approach that aims to capture the most relevant correlations when handling multi-shell configuration spaces (Otsuka and Tsunoda, 2016; Shimizu *et al.*, 2017). A relatively small number of angular-momentum-projected deformed basis states is sufficient to explore the most relevant configurations, tackling spaces with $\gg 10^{20}$ Slater determinants (Ichikawa *et al.*, 2019; Marsh *et al.*, 2018) — the standard shell model is limited to $\sim 10^{11}$ explicit configurations. A related strategy based on the superposition of quasiparticle states is more suited to $0\nu\beta\beta$-decay NMEs, and may enable calculations for e.g. ^{150}Nd (Shimizu *et al.*, 2021).

The success of the shell model is based on effective nuclear Hamiltonians adapted to each configuration space (Caurier *et al.*, 2005). High quality Hamiltonians are important for $0\nu\beta\beta$-decay studies, because schematic interactions can lead to NMEs outside the shell-model range discussed in Sec. IV.C.1 (Higashiyama *et al.*, 2020; Yoshinaga *et al.*, 2018). Nonetheless, even effective Hamiltonians derived from nucleon-nucleon potentials demand phenomenological adjustments, mainly in the part that describes single-particle degrees of freedom, i.e. the monopole component. Due to this, shell model NMEs have a phenomenological component. This limitation is lifted by effective Hamiltonians built by ab initio methods. They are derived without phenomenological adjustments from chiral EFT nucleon-nucleon and three-nucleon interactions (Bogner *et al.*, 2014; Dikmen *et al.*, 2015; Jansen *et al.*, 2014; Stroberg *et al.*, 2017) connected to the underlying theory of the nuclear force, QCD. Ab initio methods are described in Sec. IV.C.7.

4. The QRPA and its variants

The QRPA was the first many-body method to reliably address $\beta\beta$ decay (Engel *et al.*, 1988; Vogel and Zirnbauer, 1986). Contrary to the nuclear shell model, the QRPA uses large configuration spaces encompassing several harmonic oscillator shells. On the other hand, the nuclear correlations included in the QRPA are more limited than the ones the shell model captures. The QRPA relies on small amplitude nuclear correlations, and has been reviewed for instance in Suhonen and Civitarese (1998), Avignone *et al.* (2008), and Engel and Menéndez (2017).

One aspect particularly relevant for QRPA $0\nu\beta\beta$-decay studies is the strength of the proton-neutron pairing interaction. Several prescriptions have been proposed to fix its value, for instance, using β decay data involving the intermediate, initial or final $\beta\beta$-decay nuclei (Engel *et al.*, 1988), or using $2\nu\beta\beta$ decay (Rodin *et al.*, 2003) — the latter strategy is used in the orange multiplication signs in Fig. 9. These approaches share the disadvantage that the proton-neutron pairing interaction is difficult to disentangle from a possible "g_A quenching" needed by the QRPA, see Sec. IV.D. Recently, two alternatives have been proposed. The first imposes SU(4) symme-

try and therefore a vanishing double GT matrix element (Šimkovic *et al.*, 2018b) — red circles in Fig. 9. The second demands the equivalence, in the closure approximation explained above Eq. (23), of the NMEs through intermediate $(N-1, Z+1)$ and $(N-2, Z)$ nuclei, with respect to the (N, Z) initial one (Terasaki, 2015) — purple crosses in Fig. 9. These choices lead to mildly different NMEs. On the other hand, the QRPA fixes the isovector part of the proton-neutron interaction by demanding that $2\nu\beta\beta$-decay Fermi matrix elements vanish (Hyvarinen and Suhonen, 2015; Šimkovic *et al.*, 2013). This condition effectively restores isospin symmetry, which is a robust symmetry in nuclei.

Most QRPA calculations assume spherical initial and final nuclei. This simplification may not be justified in some cases, leading to overestimated $0\nu\beta\beta$-decay NMEs, as suggested by EDF theory, shell model and IMSRG studies (Menéndez *et al.*, 2009a, 2011; Rodriguez and Martinez-Pinedo, 2010; Yao *et al.*, 2020). Recently, Fang *et al.* (2018) calculated QRPA NMEs including deformation — violet bars in Fig. 9. The deformed QRPA NMEs are much smaller than in most spherical QRPA calculations, in fact they are comparable to shell model NMEs. The main reason is the suppression due to the small overlap between the initial and final nuclei, which is reduced for states with different deformation. This overlap, usually neglected in QRPA calculations, has been shown to lead to very small NMEs (Mustonen and Engel, 2013) — magenta crosses in Fig. 9. However, Fang *et al.* (2018) and Mustonen and Engel (2013) probably underestimate NMEs because they assume only one deformation for each nuclear state. A more realistic description should consider the mixing between different configurations, for instance via the GCM (Hinohara and Engel, 2014; Rodriguez and Martinez-Pinedo, 2010), which enhances NME values.

5. Energy-density functional theory

The largest NMEs in Figs. 9 and 11 derive from EDF theory. This approach is used extensively, and describes very well the ground state properties and spectroscopy of medium-mass and heavy nuclei (Bender *et al.*, 2003). Based on a mean-field description, EDF theory calculations incorporate additional correlations beyond the mean field via restoration of symmetries — notably particle number and angular momentum — and configuration mixing in terms of the GCM (Egido, 2016; Robledo *et al.*, 2019). The variational solution of the Schrödinger equation is obtained self-consistently in configuration spaces of about a dozen harmonic oscillator shells. Unlike other many-body methods, EDF theory can calculate any nucleus with a common nuclear functional (or interaction).

EDF $0\nu\beta\beta$-decay NMEs are computed in the closure approximation. The same level of sophistication in odd nuclei can only be achieved at a much larger computational cost, and is only feasible in lighter nuclei (Bally *et al.*, 2014). This also prevents tests of β and $2\nu\beta\beta$-decay EDF matrix elements. Two EDF versions have been applied to $0\nu\beta\beta$ decay: using nonrelativistic (López Vaquero *et al.*, 2013; Rodriguez and Martinez-Pinedo, 2010) and relativistic (Song *et al.*, 2017; Yao *et al.*, 2015) functionals, both including the GCM (Yao *et al.*, 2022b). The two sets of NMEs are quite similar except in ^{150}Nd, see Fig. 9. The significantly larger NMEs of EDF with respect to the shell model can be traced back to nuclear correlations: a comparison of NMEs for calcium isotopes calculated with uncorrelated nuclear states found NME agreement as good as $\sim 30\%$ (Menéndez *et al.*, 2014) instead of the factor of ~ 3 difference in Fig. 9. Actual $\beta\beta$ emitters are strongly correlated nuclei.

Possible explanations for the large EDF theory NMEs are high-seniority components of the nuclear states beyond the reach of EDF theory, and proton-neutron pairing correlations (Menéndez *et al.*, 2016) not explicitly taken into account. Shell model and GCM studies suggest that both effects reduce NME values (Hinohara and Engel, 2014). The precise impact, however, needs to be checked in actual EDF theory calculations. An extension to handle nuclear Hamiltonians instead of functionals, so that proton-neutron pairing can be accommodated explicitly, has been proposed recently (Bally *et al.*, 2021).

6. The interacting boson model

The IBM (Arima and Iachello, 1976, 1978) exploits symmetry arguments to model nuclei as a collection of bosons, called s-, p-, d-bosons... according to their angular momentum. Bosonic operators are then mapped to nucleon degrees of freedom (Otsuka *et al.*, 1978), typically using the shell model as a reference.

IBM calculations of $0\nu\beta\beta$ decay use the closure approximation. Typical IBM configuration spaces encompass one harmonic oscillator shell for neutrons and protons — like the shell model. On the other hand, like EDF theory, calculated IBM NMEs for $\beta\beta$ emitters (Barea and Iachello, 2009; Barea *et al.*, 2015a) do not explicitly include proton-neutron pairing correlations, which could lead to an overestimation of the NMEs, as discussed in Sec. IV.C.5. Recently, p-bosons that capture explicitly proton-neutron pairing correlations have been introduced in NME calculations for isotopes around ^{48}Ca (Van Isacker *et al.*, 2017). For light-neutrino exchange, IBM NMEs take intermediate values with respect to other NME results, see Fig. 9, while IBM NMEs are similar to most other NMEs for $0\nu\beta\beta$ decay mediated by the exchange of a heavy particle, see Figs. 10 and 11.

7. Ab initio methods

Ab initio or first principles nuclear structure calculations solve the many-body problem by treating explicitly all nucleons in the nucleus, interacting though realistic nuclear forces. Ab initio methods handle nucleon-nucleon and three-nucleon forces and, likewise, they can accommodate one-body operators as well as 2BC. They yield in general excellent agreement for the nuclear properties of light and medium-mass nuclei (Barrett *et al.*, 2013; Carlson *et al.*, 2015; Freer *et al.*, 2018; Hagen *et al.*, 2014; Hebeler *et al.*, 2015; Hergert *et al.*, 2016; Navrátil *et al.*, 2016). Here we briefly review the most common ab initio approaches applied to β and $\beta\beta$ decays.

Quantum Monte Carlo (QMC) techniques are one of the most accurate ab initio methods in very light $A \lesssim 12$ nuclei (Carlson *et al.*, 2015), with promising extensions proposed for medium-mass systems (Lonardoni *et al.*, 2018). The QMC approach is based on the time evolution of a trial nuclear state, according to the nuclear Hamiltonian, towards the lowest-energy configuration. With sufficiently long evolution, the exact properties of the ground state can be obtained. QMC β decay calculations are discussed in Sec. IV.D.1. More interestingly, Pastore *et al.* (2018b) and Weiss *et al.* (2021) have studied $0\nu\beta\beta$-decay NMEs in $A \leq 12$ nuclei. While these isotopes are not of experimental interest, QMC NMEs provide benchmarks for other approaches that can also cover heavier nuclei. Compared to shell model NMEs for ^{10,12}Be, QMC ones are $\sim 20\%$ smaller (Wang *et al.*, 2019), but the ratio between QMC $M_{\text{short}}^{0\nu}$ and $M_{\text{long}}^{0\nu}$ NMEs is consistent with Figs. 9 and 10 (Cirigliano *et al.*, 2019). QMC nuclear states include reliable SRCs, which can be combined with the shell model via the generalized contact formalism (Weiss *et al.*, 2021). This results in NMEs for heavy $\beta\beta$ emitters reduced by about 30% with respect to the shell model ones in Fig. 9.

The no-core shell model (NCSM) is the ab initio extension of the nuclear shell model to very large configuration spaces (Barrett *et al.*, 2013; Navrátil *et al.*, 2016). Unlike the nuclear shell model, the lowest-energy nucleons are treated explicitly, which implies the absence of a core. On the other hand, high-energy orbitals are added to the configuration space until reaching convergence. Because of the combinatorial scaling of the shell model framework, the NCSM is limited to very light nuclei $A \lesssim 22$, and reaching these nuclei actually requires strategies to select the most relevant configurations (Abe *et al.*, 2012b; Roth, 2009). Section IV.D.1 presents NCSM β decay results in light systems, and Basili *et al.* (2019) and Yao *et al.* (2021) gives benchmark NCSM $0\nu\beta\beta$-decay NMEs from ^{6}He to ^{22}O that include full nuclear correlations.

The IMSRG introduced in Sec. IV.C.1 is based on unitary transformations that simplify the solution of the many-body problem (Hergert *et al.*, 2016). Transition operators, including $\beta\beta$-decay ones, are transformed con-

sistently. The IMSRG relies on adding correlations on top of a reference state, which needs to be a reasonable approximation, sufficiently close to the exact solution. The advantage of the IMSRG over NCSM or QMC is the polynomial, rather than exponential, scaling with the number of nucleons, making extensions to $\beta\beta$ decay feasible. Two versions of the IMSRG have been applied to $\beta\beta$ decay: the IM-GCM described here and the VS-IMSRG discussed in the last paragraph of this section. Since the initial and final $\beta\beta$ nuclei typically involve substantial nuclear correlations, the IM-GCM uses a combination of various reference states (Yao *et al.*, 2018) and then exploits the GCM to explore additional nuclear correlations such as deformation and proton-neutron pairing. The IM-GCM NMEs agree well with NCSM benchmarks in light systems (Basili *et al.*, 2019; Yao *et al.*, 2021). Yao *et al.* (2020) have obtained a ^{48}Ca $M_{\text{long}}^{0\nu}$ smaller than other calculations — see Fig. 9 — complemented by a $M_{\text{short}}^{0\nu}$ NME which enhances $M_{\text{light}}^{0\nu}$ by about 40% (Wirth *et al.*, 2021). Strategies to study heavier $\beta\beta$ emitters are in progress (Romero *et al.*, 2021).

The CC method is also based on adding nuclear correlations to a reference state (Hagen *et al.*, 2014). Such correlations can be singles, doubles, triples, etc., according to the number of creation-annihilation operators allowed. Similar to the IMSRG, CC calculations scale polynomially. At present, however, CC studies are mostly limited to spherical nuclei in the vicinity of magic or semimagic isotopes — those nuclei for which nuclear correlations are especially small (Hagen *et al.*, 2016; Morris *et al.*, 2018). CC β decays in heavy nuclei are discussed in Sec. IV.D.1. Very recently, Novario *et al.* (2021) have calculated the ^{48}Ca $0\nu\beta\beta$-decay NME, see Fig. 9. An extension of the CC framework breaking rotational invariance was necessary to take into account the deformation of ^{48}Ti (Novario *et al.*, 2021). The NME is consistent with the IM-GCM one, but with larger uncertainty. More recent CC nuclear structure calculations restore rotational symmetry through angular momentum projection (Hagen *et al.*, 2022).

The NCSM (Dikmen *et al.*, 2015), CC (Jansen *et al.*, 2014) and IMSRG (Bogner *et al.*, 2014; Stroberg *et al.*, 2017) can be formulated to yield an effective Hamiltonian in a shell model space. At the same time, they solve the energy of the shell model core. Therefore the ab initio calculation can be separated in two steps: first, the energy of the shell model core and an effective shell model interaction are obtained. Second, the shell model techniques described in Sec. IV.C.3 are used to calculate observables such as nuclear energies or NMEs. In particular, the valence-space version of the IMSRG method (VS-IMSRG) has been used extensively, with good agreement on nuclear properties up to tin (Stroberg *et al.*, 2019; Taniuchi *et al.*, 2019). The VS-IMSRG ^{48}Ca $0\nu\beta\beta$-decay NME is in good agreement with the IM-GCM and CC ones (Belley *et al.*, 2021), see Fig. 9. Furthermore,

first VS-IMSRG NMEs have been obtained for the heavier ^{76}Ge and ^{82}Se see Sec. IV.E.

D. "g_A quenching"

The so-called "g_A quenching" is a potential source of uncertainty in $0\nu\beta\beta$-decay NMEs. Most calculations of GT β decay matrix elements overpredict experiment, indicating the need of a correction, sometimes attempted by quenching the value of the axial coupling g_A. Very recently β decay has been studied with the ab initio methods introduced in Sec. IV.C.7. These calculations suggest that the overprediction of matrix elements is more likely related to the GT β decay operator than to g_A. Ab initio $0\nu\beta\beta$-decay studies including 2BC are needed to assess whether the NMEs discussed in Sec. IV.C require a compensation similar to GT β decay ones, less compensation, or none at all.

1. β decay half-life values

Theoretical nuclear structure typically does not reproduce well β-decay half-life values in GT transitions of nuclei with masses similar to those of $\beta\beta$ emitters. Calculated GT decay half-lives tend to underestimate data, which means that theoretical matrix elements are overestimated. As a pragmatic fix to this deficiency, a quenching factor is usually introduced to reduce the strength of the GT operator, and consequently the calculated GT matrix elements. Remarkably, in the nuclear shell model a common quenching factor $\boldsymbol{\sigma}\tau \to q\boldsymbol{\sigma}\tau$ with $q \sim 0.7 - 0.8$ is sufficient to bring agreement with experiments for GT matrix elements across and entire mass range (Chou et al., 1993; Martínez-Pinedo et al., 1996; Wildenthal et al., 1983). Nevertheless, to the extent that the need of quenching reflects the deficiency of a given nuclear many-body method to describe GT transitions, each nuclear structure model can be expected to need its own quenching factor (Ejiri et al., 2019). In general, more sophisticated approaches require less severe quenching.

An alternative view expresses the phenomenological modification required in GT transitions as a "quenching" of the axial coupling constant, g_A (Suhonen, 2017). The corresponding label "g_A quenching" is used widely in the literature. However, similar phenomenological adjustments have been advocated in nuclear electromagnetic transitions — in particular, magnetic dipole transitions — which do not depend on g_A (von Neumann-Cosel et al., 1998). Therefore it may be more appropriate to associate the quenching factor to the transition operator instead of the hadronic coupling g_A.

The origin of the quenching has been debated extensively, with two primary explanations. One possibility is missing nuclear correlations, because calculations are performed in limited configuration spaces (Arima et al., 1987; Bertsch and Hamamoto, 1982). Another possibility is corrections to the transition operator, such as 2BC — meson-exchange currents — presented in Sec. IV.B.3. They reflect neglected degrees of freedom, such as nucleon excitations to the Δ isobar (Menéndez et al., 2011). Even though both effects were investigated for decades (Brown and Wildenthal, 1987; Towner, 1997), the outcome was not conclusive.

Nuclear theory is finally in a position to address β decays in not only light but also medium-mass and even heavy nuclei with ab initio methods that correct for both of the aforementioned deficiencies. For $A \lesssim 12$ systems that undergo β decay the experimental rate can be confronted with ab initio QMC and NCSM calculations. The theoretical predictions of GT matrix elements are in excellent agreement — within a few percent — with experiment, without the need of any adjustment (Gysbers et al., 2019; Pastore et al., 2018a). Gysbers et al. (2019) also studied GT transitions of nuclei with mass number $A \sim 30$ and $A \sim 50$ with the VS-IMSRG. In contrast to standard shell model calculations that need sizable quenching, the VS-IMSRG reproduces measured GT transitions to better than 10%. Gysbers et al. (2019) also presented a detailed ab initio CC study of the GT decay of the doubly-magic ^{100}Sn — the largest GT transition observed in the nuclear chart. The CC result agrees very well with the measured GT matrix element, without any adjustment. The VS-IMSRG and CC analyses both conclude that nuclear correlations not included in previous calculations and 2BC contribute in a similar amount to the GT matrix element. Further, the relative importance of 2BC and correlations depends on the nuclear interaction used: two body effects are larger for interactions with a less pronounced short-range character. That is, these two effects are intertwined. For instance, in QMC GT matrix elements obtained with "hard" potentials with marked short-range repulsion, the effect of 2BC is very small. In contrast, in "softer" potentials with less rich short-range correlations, the impact of 2BC is more relevant. In general, there may not be a dominant contribution to quenching, but two entangled ones with relative impact dependent on the nuclear interaction used.

The same considerations apply when comparing calculations to GT transitions extracted from charge-exchange reactions (Frekers and Alanssari, 2018; Fujita et al., 2011; Ichimura et al., 2006). The shell model reproduces data well once the same quenching as in β decay is included (Caurier et al., 2012; Iwata et al., 2015), perhaps because the normalization of GT transitions extracted from experimental cross-sections involves β-decay half-lives. Using perturbation theory to obtain a GT operator that captures correlations beyond the configuration space also leads to good agreement with experiment (Coraggio et al., 2019).

The findings of Gysbers et al. (2019) bring immediate

implications. Since 2BC are partially responsible for GT quenching, the expectation that 2BC are less important in $0\nu\beta\beta$ than in GT decay, as discussed in Sec. IV.B.3, suggests that assuming a quenching q^2 in $0\nu\beta\beta$ decay relative to q for β decay is not justified. The first ab initio calculations have also explored the impact of missing nuclear correlations in $0\nu\beta\beta$ decay. In ^{48}Ca they suggest that the value of the $0\nu\beta\beta$-decay NME is only moderately reduced (Belley *et al.*, 2021; Novario *et al.*, 2021; Yao *et al.*, 2020). Perturbation theory studies also find a milder impact of additional correlations in $0\nu\beta\beta$ decay than in GT transitions (Coraggio *et al.*, 2020).

2. β decay spectra

The energy spectrum of the emitted electron is fixed by kinematics because a single nuclear matrix element dominates GT transitions. By contrast, several matrix elements contribute to non-unique forbidden β decays, and the electron spectrum is related to their relative impact (Behrens and Bühring, 1971).

This idea has been exploited to show that the shape of the β spectrum of for example ^{113}Cd depends on the relative value of nuclear matrix elements divided in two groups: those proportional to the vector and axial couplings g_V and g_A (Haaranen *et al.*, 2017, 2016) — the groups stem from the leading terms in Eq. (21). Assuming that all axial and all vector matrix elements need to be corrected by the same quenching, a fit to the β spectrum leads to a preferred value of the ratio g_A/g_V. Higher sensitivities appear if competing contributions from different matrix elements partially cancel, a feature identified in other non-unique β decays as well (Kostensalo *et al.*, 2017; Kostensalo and Suhonen, 2017; Kumar *et al.*, 2020).

A comparison to measurements of the ^{113}Cd β spectrum suggests a ratio of about $g_A/g_V \sim 0.9$, valid for the shell model and other many-body methods (Bodenstein-Dresler *et al.*, 2020). The ratio $g_A/g_V \sim 0.9$ is roughly consistent with the "g_A quenching" observed in β decay but does not reproduce the ^{113}Cd half-life. This inconsistency, also found in other β decays (Kumar *et al.*, 2021), could be explained if each axial or vector matrix element is affected by a different deficiency, and therefore needs its own quenching factor. Even though at least some of the matrix elements may require a similar quenching (Al Kharusi *et al.*, 2020), a different behavior has been indeed observed in shell model studies of non-unique β decays (Warburton *et al.*, 1988; Yoshida *et al.*, 2018b; Zhi *et al.*, 2013). In summary, β-decay spectra of non-unique forbidden decays provide complementary tests of the quality of nuclear theory calculations, and are will help to determine whether "g_A quenching" can be resolved by simple scaling of the axial coupling.

3. $2\nu\beta\beta$ decay and 2νECEC

$\beta\beta$ decay and ECEC with the emission of two (anti)neutrinos have been measured in a dozen nuclei (Aprile *et al.*, 2019; Barabash, 2020). Since the initial and final nuclei are common to two-neutrino and neutrinoless decays, a good description of $\beta\beta$ and ECEC decay is a key test of $0\nu\beta\beta$-decay predictions. The calculation of the corresponding nuclear matrix elements is, however, more challenging than for the neutrinoless mode. This is because the emission of neutrinos reduces the momentum transfer below typical nuclear energy differences, and the closure approximation leading to Eq. (23) is not always justified (closure is, nonetheless, typically used by the IBM (Barea *et al.*, 2015a)). Thus the intermediate nucleus with an odd number of neutrons and protons needs to be calculated explicitly.

The remarkable nuclear shell model prediction of the ^{48}Ca decay rate (Caurier *et al.*, 1990; Poves *et al.*, 1995) before its measurement (Balysh *et al.*, 1996) highlighted the power of the use of this many-body method to predict $\beta\beta$ decay rates. These works assumed that the same deficiency present in GT matrix elements in the vicinity of ^{48}Ca was also present in $\beta\beta$ decay, so that the quenching needed for β decay was used in $\beta\beta$ decay. Following the same strategy, the ^{124}Xe two-neutrino ECEC was predicted (Coello Pérez *et al.*, 2019) in very good agreement with the subsequent, recent observation (Aprile *et al.*, 2019). Likewise, shell model $\beta\beta$-decay matrix elements in other nuclei reproduce measured decay rates when corrected by quenching factors which are in reasonable agreement with those needed for GT transitions (Caurier *et al.*, 2012; Kostensalo and Suhonen, 2020; Neacsu and Horoi, 2015; Sen'kov and Horoi, 2016). Only in ^{136}Xe the quenching needed in $\beta\beta$ decay may be more pronounced (Caurier *et al.*, 2012). Matrix elements obtained with perturbation theory on top of the shell model also reproduce the measured half-life well (Coraggio *et al.*, 2019, 2022).

Other many-body methods can also access $\beta\beta$ decays. The QRPA often uses $2\nu\beta\beta$ decay to fix the strength of the proton-neutron pairing interaction (Rodin *et al.*, 2003), but when alternative schemes are adopted predicted $\beta\beta$-decay rates are qualitatively good, both when the QRPA is used with phenomenological Hamiltonians (Šimkovic *et al.*, 2018b) and with energy-density functionals (Hinohara and Engel, 2022; Mustonen and Engel, 2013). In fact, the QRPA half-life for ^{124}Xe (Pirinen and Suhonen, 2015; Suhonen, 2013) well-predicted its subsequent measurement, albeit with a larger uncertainty than the shell model. The larger error arises from the difficulty of disentangling quenching from the strength of the proton-neutron pairing in the QRPA, see Sec. IV.C.4. An effective theory for $\beta\beta$ and ECEC decay, based on β and EC data (Coello Pérez *et al.*, 2018), also predicted well the ^{124}Xe $2\nu\beta\beta$-decay half-life, including a quanti-

fied theoretical uncertainty (Coello Pérez *et al.*, 2019). The same method very recently has given predictions for $0\nu\beta\beta$ NMEs (Brase *et al.*, 2021) with quantified uncertainties, favoring smaller values than all methods in Table I. Very recently, IBM $2\nu\beta\beta$-decay calculations have been performed beyond the closure approximation (Nomura, 2022).

Ab initio methods can calculate $\beta\beta$-decay matrix elements as well, but this is more challenging because of the relevance of the intermediate states. For ^{48}Ca, CC theory mildly overestimates the experimental matrix element even when including the effect of 2BC, as it does in β decay (Novario *et al.*, 2021). In turn, the VS-IMSRG ^{48}Ca matrix element is too small even without 2BC (Belley *et al.*, 2021).

Similarly to β decay, measured $\beta\beta$-decay spectra further test nuclear theory. Even if only one nuclear matrix element dominates the decay rate, precisely measured spectra can be sensitive to small deviations caused by subleading matrix elements (Šimkovic *et al.*, 2018a). A precision analysis of the ^{136}Xe summed electron energy spectrum provides limits which confront shell model and QRPA predictions (Gando *et al.*, 2019). The results constrain both the quenching needed to reproduce the half-life — different for each calculation — and the ratio of the leading and subleading matrix elements. The analysis is consistent with most of the theoretical predictions, but excludes part of the QRPA results.

In addition, a precise $\beta\beta$-decay spectrum measurement can inform the distribution of the leading $\beta\beta$-decay matrix element as a function of the virtual states in the intermediate odd-odd nucleus through which the decay proceeds (Šimkovic *et al.*, 2001), see Eq. (22). Recent analyses in ^{100}Mo (Armengaud *et al.*, 2020a; Arnold *et al.*, 2019) and ^{82}Se (Azzolini *et al.*, 2019b) suggest that only the lowest $J^P = 1^+$ state contributes, the so-called single-state dominance. Charge-exchange reactions also hint at single-state dominance in the $2\nu\beta\beta$ decay of ^{96}Zr (Thies *et al.*, 2012). This behavior should be reproduced by all theoretical calculations.

E. Connections to nuclear structure measurements

Besides β and $\beta\beta$ decays, a good description of the main properties of the nuclear states is a necessary requirement for trustworthy $0\nu\beta\beta$-decay NME calculations. On the other hand, processes with similar momentum transfer — muon capture and neutrino-nucleus scattering — can give additional insights. Double Gamow-Teller (DGT) and second-order electromagnetic transitions may offer a unique opportunity due to their relation to $0\nu\beta\beta$-decay NMEs.

1. Spectroscopy and charge exchange

Nuclei involved in $\beta\beta$ decay have even numbers of protons and neutrons. Due to the attractive nuclear pairing interaction, they have $J^P = 0^+$ ground states, with vanishing quadrupole and magnetic moments. Theoretical calculations, therefore, need to be confronted with other ground state properties. A valuable source of information comes from orbital occupation probabilities deduced from analyses of low-energy nucleon adding and removing reactions (Entwisle *et al.*, 2016; Freeman and Schiffer, 2012; Freeman *et al.*, 2017; Szwec *et al.*, 2016). In fact, various studies have used the experimental results to improve the description of the initial and final $\beta\beta$-decay nuclei (Deppisch *et al.*, 2020a; Kotila and Barea, 2016; Menéndez *et al.*, 2009; Suhonen and Civitarese, 2008, 2010). The impact on the NMEs is illustrated by the IBM error bar in Fig. 9. This moderate effect proved beneficial to bring QRPA and shell model NME predictions in better agreement to each other.

In addition, the quality of nuclear structure calculations is assessed by comparing excitation energies of low-lying states (ENSDF, 2021) and their electromagnetic transitions (XUNDL, 2021). In particular, the shell model and EDF theory agree with data very well (Coraggio *et al.*, 2019; Hoferichter *et al.*, 2019; Horoi and Neacsu, 2016b; Neacsu and Horoi, 2015; Rodriguez and Martinez-Pinedo, 2010; Song *et al.*, 2014; Vietze *et al.*, 2015), even though more subtle aspects such as pairing correlations (Roberts *et al.*, 2013; Sharp *et al.*, 2019) or the triaxial character of $A = 76$ (Ayangeakaa *et al.*, 2019; Henderson *et al.*, 2019; Toh *et al.*, 2013) and $A = 130$ (Hicks *et al.*, 2022; Morrison *et al.*, 2020) nuclei have also been explored experimentally and challenge all theoretical studies. Further, the shape of GT strength distributions as a function of energy is also sensitive to the nuclear structure of the nuclei involved, and has been used to test and improve nuclear interactions (Alanssari *et al.*, 2016). Thus, the comparison to the experimental GT strength at low energies is another stringent test for calculations (Caurier *et al.*, 2012; Coraggio *et al.*, 2019; Iwata *et al.*, 2015) and for instance shows that ^{100}Mo is currently more difficult to describe than other $\beta\beta$ nuclei (Coraggio *et al.*, 2022). While nuclear structure data for otherwise-stable $\beta\beta$ nuclei has been collected over decades, modern experiments keep illuminating new aspects that test theoretical predictions, for instance recent work on heavy $A = 136$ (Nzobadila Ondze *et al.*, 2021; Rebeiro *et al.*, 2021) and $A = 150$ (Basak *et al.*, 2021) nuclei. It is very important to pursue further studies of this kind, as they may indicate physics missing in the calculations but relevant for $0\nu\beta\beta$ decay. For instance, recent measurements on magnetic dipole transitions in $A \sim 150$ nuclei have been used to fix IBM parameters, giving significant changes in NMEs to excited states (Beller *et al.*, 2013; Kleemann *et al.*, 2021).

Similar benchmarks are demanded for ab initio calculations. In fact, the CC theory framework had to be extended by breaking rotational invariance to describe ^{48}Ca decay (Novario *et al.*, 2021) due to the deformation of ^{48}Ti. The IM-GCM and VS-IMSRG calculations of Yao *et al.* (2020) and Belley *et al.* (2021) describe ^{48}Ca and ^{48}Ti in good agreement with experiment. In contrast, the VS-IMSRG excitation spectra for the heavier nuclei ^{76}Ge, ^{76}Se, ^{82}Se, and ^{82}Kr are too stretched in energy (Belley *et al.*, 2021).

Unfortunately, two methods that describe well the nuclear structure properties of $\beta\beta$-decay nuclei can differ significantly in their $0\nu\beta\beta$-decay NME predictions. For example, both relativistic (Song *et al.*, 2014) and non-relativistic EDF theory (Rodriguez and Martinez-Pinedo, 2010) describe the nuclear structure of ^{150}Nd and ^{150}Sm well, but predict NMEs a factor three apart. In fact, a recent statistical shell-model analysis in the decay of ^{48}Ca to ^{48}Ti finds that the nuclear structure properties of these nuclei are in general modestly correlated with the $0\nu\beta\beta$-decay NME (Horoi *et al.*, 2022). Nonetheless, nuclear structure is relevant: the energy of the lowest 2^+ state in ^{48}Ti, which is a measure of the deformation of that nucleus, is a property with a higher correlation. In the same fashion, a demand for the IM-GCM ab initio calculation was to describe well the low-lying electric quadrupole transition in ^{48}Ti (Yao *et al.*, 2018). The consistent ^{48}Ca NMEs obtained with three ab initio approaches brings hope for more confident $0\nu\beta\beta$-decay NME results in the future.

2. Muon capture and neutrino scattering

Nuclear structure or β decay measurements do not probe, however, momentum transfers $p \sim 100\,\text{MeV}$ similar to $0\nu\beta\beta$ decay. Two other processes offer the opportunity to do so. The first is muon capture, mostly explored with the QRPA (Jokiniemi and Suhonen, 2019; Jokiniemi *et al.*, 2019; Zinner *et al.*, 2006). An ideal comparison would involve capture branching ratios to low-energy excited states, which can also be computed with the shell model and VS-IMSRG (Jokiniemi *et al.*, 2021a). The second process is inelastic neutrino-nucleus scattering. In the very few nuclei, such as ^{12}C, for which data are available (Formaggio and Zeller, 2012), different shell model studies disagree on whether matrix elements at finite momentum transfer are overpredicted, like in β decay, or not (Hayes *et al.*, 2003; Hayes and Towner, 2000; Suzuki *et al.*, 2006; Volpe *et al.*, 2000). Given the relevance of large momentum transfer observables to test calculations of $0\nu\beta\beta$-decay NMEs, it would be important to get more data on both muon capture and neutrino-nucleus scattering.

3. Two-nucleon processes: $\beta\beta$ decay, pair transfers, double Gamow-Teller, and $\gamma\gamma$ transitions

$0\nu\beta\beta$ decay is also special from the nuclear structure point of view. None of the observables discussed in Sec. IV.E.1 or IV.E.2 have been found to be well correlated to $0\nu\beta\beta$ decay. Nuclear processes involving two nucleons are more promising.

Until very recently, no clear correlation had been observed between $2\nu\beta\beta$- and $0\nu\beta\beta$-decay NMEs, other than an analytical relation between the corresponding transition densities (Simkovic *et al.*, 2011). However, Horoi *et al.* (2022) find that the ^{48}Ca $2\nu\beta\beta$-decay NME is the quantity best correlated with this nucleus' $0\nu\beta\beta$-decay NMEs from a set of 24 nuclear structure properties of ^{48}Ca and ^{48}Ti. This result is supported by subsequent work by Jokiniemi *et al.* (2022), which finds a good linear correlation between the two $\beta\beta$-decay NMEs across the nuclear chart for shell model and QRPA calculations. Using the correlation, $0\nu\beta\beta$-decay data can be used to predict $0\nu\beta\beta$-decay NMEs.

Two-nucleon transfer amplitudes have also been related to $0\nu\beta\beta$ decay (Brown *et al.*, 2014). A recent experiment involving a two-neutron transfer from ^{138}Ba to ^{136}Ba found a larger contribution of pairs of neutrons coupled to angular momentum $J = 0$ than predicted by the shell model (Rebeiro *et al.*, 2020). The size of the missing contributions is about 50%. This result suggests that the $J = 0$ contribution to $0\nu\beta\beta$-decay NMEs could also be underestimated. This experimental finding is consistent with theoretical work finding a $\sim 25\%$ enhancement when increasing the shell model configuration space (Iwata *et al.*, 2016), but which also predicts more contributions from $J > 0$ neutron pairs which suppress the NME. The latter cancellation is still to be confirmed by experiments.

Double charge-exchange reactions can also provide insights on NMEs, in a similar connection to the one between β decay and (single) charge-exchange reactions. This is in spite of the fact that charge-exchange experiments probe the strong instead of the weak interaction. An experimental program pursues this approach (Cappuzzello *et al.*, 2018), which demands developments in reaction theory (Bellone *et al.*, 2019; Lenske *et al.*, 2019).

Connections between DGT transitions and $\beta\beta$ decay have been indicated for decades (Auerbach *et al.*, 1989; Vogel *et al.*, 1988). DGT transitions can be explored with double charge-exchange reactions (Takahisa *et al.*, 2017; Takaki *et al.*, 2015; Uesaka *et al.*, 2015). Most works, however, focus on sum rules or the DGT giant resonance (Auerbach and Minh Loc, 2018; Roca-Maza *et al.*, 2019; Sagawa and Uesaka, 2016). Shimizu *et al.* (2018) studied DGT transitions to the ground-state of the final nucleus, i.e., between the initial and final $\beta\beta$-decay nuclei. Remarkably, a comparison of shell model DGT and $0\nu\beta\beta$-decay NMEs shows a very good linear correlation, valid

from calcium to xenon (Brase *et al.*, 2021). The same correlation is fulfilled for EDF theory (Rodriguez and Martinez-Pinedo, 2013), even though for any $\beta\beta$ emitter EDF NMEs are much larger than shell model ones, see Fig. 9. Further, the IBM also finds a linear correlation (Barea *et al.*, 2015a; Santopinto *et al.*, 2018). The QRPA in general does not observe a correlation (Šimkovic *et al.*, 2018b), but it does so when exploring different values of the proton-neutron pairing (Jokiniemi *et al.*, 2022). The origin of the linear correlation could be explained by the relatively short-range character of both DGT and $0\nu\beta\beta$-decay NMEs (Anderson *et al.*, 2010; Bogner and Roscher, 2012) in the shell model — neutrons more than ~ 3 fm apart almost do not contribute to these processes — in contrast to the QRPA where DGT transitions receive contributions from nucleons separated by long distances. Further work is needed to establish the robustness of the correlation between DGT and $0\nu\beta\beta$ decay, and to connect experimental cross-sections with DGT matrix elements. A very recent *ab initio* study also finds a linear correlation between DGT and $0\nu\beta\beta$-decay NMEs, albeit somewhat weaker than in the shell model (Yao *et al.*, 2022a). The likely reason are the additional nuclear correlations included in the *ab initio* calculations.

Second order electromagnetic transitions have been measured recently in competition with the much faster single γ decays (Söderström *et al.*, 2020; Walz *et al.*, 2015). Electromagnetic decays connect states in the same nucleus, so that a relation with $0\nu\beta\beta$ decay can only be expected in the final $\beta\beta$-decay system, when the initial state is the double isobaric analogue — the state with the same nuclear structure but rotated in isospin space — of the initial $\beta\beta$-decay state. A recent study finds a linear correlation between $\gamma\gamma$ magnetic dipole and $0\nu\beta\beta$-decay NMEs in the shell model framework (Romeo *et al.*, 2021), opening the door to exploring $0\nu\beta\beta$ decay with nuclear spectroscopy.

V. EXPERIMENTAL ASPECTS AND METHODS

Neutrinoless double-beta decay can be observed in a variety of isotopes, each of them characterized by specific features, such as the Q-value, the natural abundance, or material properties. Because of this, each isotope enables different detection techniques, with their own strengths and technical challenges. This makes the experimental field extremely diverse and always in evolution.

This section presents the modern experimental methods used to search for $0\nu\beta\beta$ decay. We summarize the $0\nu\beta\beta$-decaying candidate isotopes in Sec. V.A and their related detection concepts and event reconstruction techniques in Sec. V.B. Section V.C describes the background interfering processes which can mimic $0\nu\beta\beta$-decay events in recent and future experiments, while the techniques to discriminate them are reviewed in Sec. V.D. Finally,

the statistical techniques used to extract the sought-after signal are covered in Sec. V.E, where we find that the sensitivity of these experiments is driven not only by the amount of deployed isotope, but critically also by the background rate, with a distinct advantage for those experiments that are at or near the "background-free" regime.

While all of these sections are written to be accessible for both expert and nonexpert readers, Sec. V.A, Sec. V.B, and Sec. V.D are more general in nature, while Sec. V.C and Sec. V.E are more technical. The detailed aspects of specific experiments that might be of higher interest for experts in the field are the subject of Sec. VI, which makes extensive use of Sec. V.E to present each project on an equal footing.

A. Isotopes

$0\nu\beta\beta$ decay is observable in isotopes for which the single β decay is energetically forbidden and the only allowed decay channel is $\beta\beta$ decay. Nature provides 35 such isotopes that can undergo $\beta^-\beta^-$, and 34 that can undergo $\beta^+\beta^+$, $\varepsilon\beta^+$, or $\varepsilon\varepsilon$ (Tretyak and Zdesenko, 2002) — for a review of $\beta^+\beta^+$, $\varepsilon\beta^+$, and $\varepsilon\varepsilon$ processes, see (Maalampi and Suhonen, 2013). The candidate isotopes for experimental searches are those readily available at the level of thousands of moles (i.e., hundreds of kg) or more, with a high Q-value and thus a large decay rate, and compatible with existing detection technologies. A number of the key isotopes meeting these criteria is listed in Tab. II.

Acquiring isotope is feasible if the market can supply it in large amounts at an affordable cost on the timescale of years or less. Isotopic enrichment drives the total cost for the material but allows a minimization of the $\beta\beta$-inactive material, which is mandatory for most detector technologies. Isotopes with a high natural abundance and with low-abundant neighboring isotopes are easier, and thus cheaper, to enrich. The cost also depends on the viable enrichment technologies (gas ultracentrifuge is a cost-effective, high-throughput technique used for nearly all $\beta\beta$ isotopes), on the chemical processes involved, on the level of enrichment, and on the required purity of the final material. Finally, isotopes of elements used in commercial applications are typically cheaper due to their mature supply chains. On the other hand, when an experiment requires a quantity of material that is of the order of the yearly global supply, competing commercial demands lead to higher costs, and if significant quantities of depleted material enter the commercial supply chains, independent supply chains must anyway be pursued.

The $0\nu\beta\beta$-decay rate scales as $Q_{\beta\beta}^5$ for light neutrino exchange, and $Q_{\beta\beta}^7$ for other exchange mechanisms (Haxton and Stephenson, 1984). Higher Q-values thus lead to a more rapid decay, yielding higher sensitivity. Moreover,

TABLE II Target isotopes currently being pursued by leading $0\nu\beta\beta$-decay experiments. The reported $2\nu\beta\beta$-decay half-life values are the most precise available in literature. The $0\nu\beta\beta$-decay half-life values are the most stringent 90% C.L. limits.

Isotope	Daughter	$Q_{\beta\beta}$[a] [keV]	f_{nat}[b] [%]	f_{enr}[c] [%]	$T_{1/2}^{2\nu\beta\beta}$[d] [yr]	$T_{1/2}^{0\nu\beta\beta}$[e] [yr]
^{48}Ca	^{48}Ti	$4\,267.98(32)$	$0.187(21)$	16	$\left(6.4^{+0.7}_{-0.6}(\mathrm{stat})^{+1.2}_{-0.9}(\mathrm{syst})\right)\cdot 10^{19}$	$> 5.8\cdot 10^{22}$
^{76}Ge	^{76}Se	$2\,039.061(7)$	$7.75(12)$	92	$(1.926\pm 94)\cdot 10^{21}$	$> 1.8\cdot 10^{26}$
^{82}Se	^{82}Kr	$2\,997.9(3)$	$8.82(15)$	96.3	$\left(8.60\pm 0.03(\mathrm{stat})^{+0.19}_{-0.13}(\mathrm{syst})\right)\cdot 10^{19}$	$> 3.5\cdot 10^{24}$
^{96}Zr	^{96}Mo	$3\,356.097(86)$	$2.80(2)$	86	$(2.35\pm 0.14(\mathrm{stat})\pm 0.16(\mathrm{syst}))\cdot 10^{19}$	$> 9.2\cdot 10^{21}$
^{100}Mo	^{100}Ru	$3\,034.40(17)$	$9.744(65)$	99.5	$\left(7.12^{+0.18}_{-0.14}(\mathrm{stat})\pm 0.10(\mathrm{syst})\right)\cdot 10^{18}$	$> 1.5\cdot 10^{24}$
^{116}Cd	^{116}Sn	$2\,813.50(13)$	$7.512(54)$	82	$\left(2.63^{+0.11}_{-0.12}\right)\cdot 10^{19}$	$> 2.2\cdot 10^{23}$
^{130}Te	^{130}Xe	$2\,527.518(13)$	$34.08(62)$	92	$\left(7.71^{+0.08}_{-0.06}(\mathrm{stat})^{+0.12}_{0.15}(\mathrm{syst})\right)\cdot 10^{20}$	$> 2.2\cdot 10^{25}$
^{136}Xe	^{136}Ba	$2\,457.83(37)$	$8.857(72)$	90	$(2.165\pm 0.016(\mathrm{stat})\pm 0.059(\mathrm{syst}))\cdot 10^{21}$	$> 1.1\cdot 10^{26}$
^{150}Nd	^{150}Sm	$3\,371.38(20)$	$5.638(28)$	91	$\left(9.34\pm 0.22(\mathrm{stat})^{+0.62}_{-0.60}(\mathrm{syst})\right)\cdot 10^{18}$	$> 2.0\cdot 10^{22}$

[a] Values from (Alanssari *et al.*, 2016; Fink *et al.*, 2012; Kolhinen *et al.*, 2010; Kwiatkowski *et al.*, 2014; Lincoln *et al.*, 2013; Mount *et al.*, 2010; Rahaman *et al.*, 2008; Rahaman, S. and Elomaa, V. V. and Eronen, T. and Hakala, J. and Jokinen, A. and Kankainen, A. and Rissanen, J. and Suhonen, J. and Weber, C. and Äystö, J., 2011; Redshaw *et al.*, 2009, 2007).

[b] Values from (Meija *et al.*, 2016).

[c] Values from (Abgrall *et al.*, 2021; Artusa *et al.*, 2017; Barabash *et al.*, 2014, 2011; Dafinei *et al.*, 2017; Gando *et al.*, 2012; JSC Isotope, last accessed: Sep. 2020a,l,l; Kishimoto, 2018). Enrichment is performed via gas centrifuge for all isotopes except for ^{48}Ca, for which the unpublished report in (Kishimoto, 2018) used electrophoresis (Kishimoto *et al.*, 2015). For ^{96}Zr, 86% is commercially available (JSC Isotope, last accessed: Sep. 2020a), however a 91% enrichment was achieved at smaller scale (Finch, 2015). For ^{116}Cd, 82% is the highest value used in a $0\nu\beta\beta$-decay experiment(Barabash *et al.*, 2011), however enrichment up to 99.5% is possible(JSC Isotope, last accessed: Sep. 2020d). For ^{150}Nd, 91% is the highest value used in a $0\nu\beta\beta$-decay experiment(Barabash *et al.*, 2018), however enrichment up to 98% is possible(JSC Isotope, last accessed: Sep. 2020c).

[d] Values from (Agostini *et al.*, 2015; Albert *et al.*, 2014; Alduino *et al.*, 2017b; Argyriades *et al.*, 2010; Armengaud *et al.*, 2020a; Arnold *et al.*, 2016a,b; Azzolini *et al.*, 2019b; Barabash *et al.*, 2018).

[e] 90% C.L. limits from (Adams *et al.*, 2021b, 2022; Agostini *et al.*, 2020b; Argyriades *et al.*, 2010; Armengaud *et al.*, 2021; Arnold *et al.*, 2016a; Azzolini *et al.*, 2019c; Barabash *et al.*, 2018; Gando *et al.*, 2016; Umehara *et al.*, 2008).

higher Q-values (greater than $\sim 2\,\mathrm{MeV}$) are advantageous because fewer processes can mimic the $0\nu\beta\beta$-decay signal.

The candidate isotope must be suitable for use with a detection technology capable of identifying a single $0\nu\beta\beta$-decay signal in thousands of moles of material. Thus the detector must be able to distinguish the signal from mimicking processes. Consolidated detector technologies have been available for decades for some isotopes, or have lately become available for others. Recent promising developments might allow exploiting further isotopes in the future. Finally, some isotopes lend themselves to advantageous detection techniques. For example, some sources can be made directly into detectors, such as ^{76}Ge and ^{136}Xe, minimizing the amount of inactive, background-generating material near or within the detector.

B. Signal detection

$0\nu\beta\beta$ decay is a nuclear decay, and thus is a random process obeying Poisson statistics. Given that $0\nu\beta\beta$-decay half-life values are much longer than the age of the universe, the expected signal rate is homogeneous in time for the entire duration of an experiment. $0\nu\beta\beta$ decay is a three body process with the final state composed of the nuclear recoil plus the two emitted electrons. Since the electron mass is orders of magnitudes smaller than that of the daughter nucleus, the nuclear recoil energy is neg-

ligible ($<0.1\,\mathrm{keV}$), and the sum of the electron energies is practically equivalent to the available energy, i.e., to $Q_{\beta\beta}$. The daughter nucleus can be produced either in its ground state or in some excited state, and then relax down to its ground state emitting γ rays.

In principle, the measurable quantities in $0\nu\beta\beta$ decay are the kinetic energies and momenta of the emitted electrons, as well as the position and time of the decay. Additionally, any γ ray emitted in $0\nu\beta\beta$ decay to excited states can be measured, and the daughter nucleus can be tagged via atomic or molecular means as well.

For all isotopes, $0\nu\beta\beta$ decay competes with its $2\nu\beta\beta$-decay mode, a five body decay with two electrons and two anti-neutrinos emitted. The anti-neutrinos escape undetected, hence the sum energy of the two electrons is $\leq Q_{\beta\beta}$. The electron momenta in both modes vary statistically, and the daughter nucleus and any γ ray emitted by the daughter de-excitation are common between the $0\nu\beta\beta$- and $2\nu\beta\beta$-decay modes. Thus measurement of the sum electron energy is a necessary condition for discovery: the $0\nu\beta\beta$ decay will feature a peak at $Q_{\beta\beta}$, the $2\nu\beta\beta$-decay mode a continuum from zero to $Q_{\beta\beta}$ (Fig. 12). In a high-resolution experiment free of other background sources, an energy measurement is also a sufficient condition for discovery.

The measurement of energy is optimal if the candidate isotope is part of the detector itself. This condition simultaneously maximizes the detection efficiency (by op-
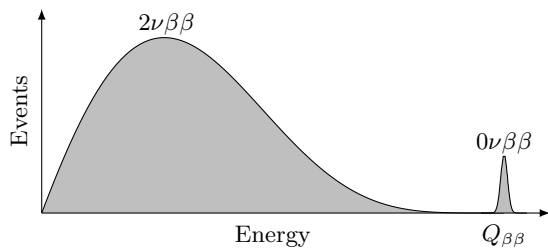
FIG. 12 Theoretical spectra of $2\nu\beta\beta$ and $0\nu\beta\beta$ decays with 1.5% energy resolution (FWHM) and arbitrary normalization.

timizing containment) while minimizing any energy loss, providing a clear signature for the signal as a $0\nu\beta\beta$-decay peak over the background, with shape governed by the energy resolution function of the detector. The resolution function is characterized by its full width at half-maximum (FWHM), which is given by $2\sqrt{2\ln 2}\,\sigma$ for a Gaussian resolution function of width σ, but can also be used to characterize and compare less ideal detector responses. A $0\nu\beta\beta$-decay event reconstructs at $Q_{\beta\beta}$ for those nuclei within the active volume of the detector with a fully calibrated non-zero energy response, and for those events whose ejecta are fully contained within the active volume.

In many detectors, the measurement of energy is accompanied by identification of the time and sometimes also the position of the energy deposition within the detector. These observables further improve the $0\nu\beta\beta$-decay signal identification by discriminating correlated or time-varying backgrounds as well as background contributions with spatial distributions distinct from that of the parent isotope. For large monlithic detectors with strong self-shielding, the discrimination of external backgrounds can be captured with a fiducial volume cut that removes high-background regions near the detector edges that do not contribute to the sensitivity.

Particle tracking allows to independently measure the single electron momenta and directions and consequently their angular correlation. Precise tracking of electrons with MeV-scale energies, including the measurement of the decay location, is only achievable in low-pressure gaseous detectors or highly pixelated solid detectors at present — here we refer to pressures $\sim 1\,\mathrm{bar}$ as low, and $\sim 10-20\,\mathrm{bar}$ as high. For the former, the quest to maximize the isotope mass motivates the use of composite detectors with solid sources sandwiched between gaseous tracking detectors. Pixelated detectors on the other hand require small surface to volume ratios. In either case, the passage of the decay electrons through passive material near the detection medium induces an unavoidable energy loss and distorts the expected $Q_{\beta\beta}$ peak in the sum energy spectrum. In monolithic solid or liquid detectors the electrons emitted in $0\nu\beta\beta$ decay scatter multiple times within a few mm^3 before being

absorbed, making precise tracking of the decay electrons and identification of the decay vertex impractical. In high-pressure gas detectors a $0\nu\beta\beta$-decay event will feature two electron tracks of several cm length originating from the same unknown location. The single electron momenta and angular correlation cannot be measured unambiguously, but the single electron energies can be estimated.

The presence of the final state nucleus at the event vertex is a nearly unique feature of $\beta\beta$ decays. The first experimental discovery of $2\nu\beta\beta$ decay was made using geochemical methods in which trace levels of $\beta\beta$ decay daughters were detected in materials containing the parent isotope (Inghram and Reynolds, 1950). The tagging of de-excitation gammas in the final state can provide such identification in real-time but requires the phase-space-suppressed decay to an excited state of the daughter nucleus. Nevertheless, such excited state decays have been observed in a number of $\beta\beta$ nuclei (Belli et al., 2020), and for some nuclei, $2\nu\beta\beta$ decay has been probed unambiguously only via excited state decays, e.g., ^{110}Pd and ^{102}Pd (Lehnert et al., 2016). Modern efforts to perform real-time tagging of the daughter nucleus in its ground state are based on its atomic features, as first proposed by Moe (1991), and are advantageous if the background reduction outweighs the $0\nu\beta\beta$-decay signal loss due to the tagging inefficiency. If methods can be developed to perform such tagging with high efficiency, with sufficient resolution such a search would be effectively background-free.

1. Detector concepts

Fig. 13 shows the three detector concepts used to search for $0\nu\beta\beta$-decay: solid state detectors with an embedded source, monolithic liquid or gas detectors with an embedded or dissolved source, and composite detectors with external sources.

Solid state detectors consist of crystals grown from material containing the $\beta\beta$ isotope. The crystal mass typically ranges from a few hundred grams to few kilograms, depending on the material. The crystal volumes are up to hundreds of cubic centimetres: they can fully contain electrons of a few MeV emitted at their center, but can miss a fraction of the energy for those emitted near the borders. Typical containment efficiencies for solid detectors are in the 70–95% range, depending on the material and detector dimensions. The energy released by the two electrons cannot be distinguished, thus crystal-based experiments mainly perform calorimetric measurements. The primary readout channels are ionization and phonons, yielding energy resolutions up to the per-mill level. Scintillating detectors are also pursued. A main feature of these experiments is granularity, allowing a staged approach where the total detector mass can be
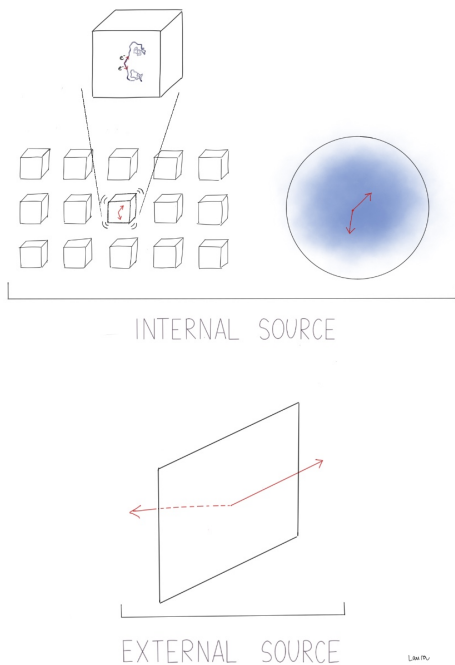
FIG. 13 Artistic rendition of the concepts used to search for $0\nu\beta\beta$ decay: internal-source experiments using solid state (top left) or monolithic liquid or gas detectors (top right), and composite experiments for which the source is external to the detection apparatus (bottom). Image courtesy of L. Manenti.

increased in steps using the same infrastructure. On the other hand, the production and operation of a large number of detectors can be challenging.

Monolithic liquid and gas based experiments are single detector systems where the $\beta\beta$ isotope either coincides with or is dissolved in the active material. Typical linear dimensions range from 1 to 10 meters. Liquid detectors of this size are larger than both the range of electrons and the attenuation length of γ rays with few MeV of energy. This guarantees a containment efficiency close to 100%, and yields an increasing sensitivity to a $0\nu\beta\beta$-decay signal towards the detector core, where the presence of background events is suppressed (see Sec. V.C). Gas detectors can have linear dimensions up to a few meters, yielding a $\gtrsim 75\%$ containment efficiency. The possible readout channels are scintillation light and ionization (see Sec. V.B.2), so the active material is surrounded (fully or partly) by light or charge detectors. Liquid and gas detectors are primarily used for calorimetry, but with sufficient spacial resolution they can provide some event topology and electron tracking reconstruction capability, particularly in gas detectors. Given that the $\beta\beta$ isotope is homogeneously distributed in the active material, in these detectors it is not possible to unambiguously identify the starting point of the electron tracks. Thus measurements of single electron energies and emission angle distributions can be estimated only with significant uncertainties. Due to self-shielding, in monolithic exper-

iments the background from external γ rays decreases exponentially as the linear dimension increases. Meanwhile, backgrounds from the readout scales with the instrument area, and isotope mass scales with the volume. These qualities make them among the most easily scalable technology in terms of signal-to-background ratio. If the $\beta\beta$-decaying isotope is dissolved in the active material, a staged approach is possible by increasing the isotope concentration in phases. On the other hand, if the source coincides with the active material, an increase in mass will require the deployment, and thus the construction, of a new, larger infrastructure.

In composite experiments, the $\beta\beta$-decaying isotope is embedded in a sub-millimetre thin foil to allow the electrons to escape with minimal energy losses. The source is surrounded by low-pressure gas detectors that measure the single electron momenta. The full reconstruction of the decay kinematics allows efficient discrimination of $0\nu\beta\beta$-decay events from other processes. Composite experiments also present several challenges. The energy reconstruction is biased by the energy losses, and the composite detector system yields a low detection efficiency. Both the isotope mass and number of readout detectors are proportional to the foil area, thus mass scaling is less advantageous than for other technologies. On the other hand, composite systems are not bound to the measurement of a single isotope, and offer uniquely precise measurement of the decay vertex and angular correlation, providing the possibility to distinguish between different $0\nu\beta\beta$-decay mechanisms through the measurement of the electron angular correlation.

2. Event reconstruction

The event reconstruction in $0\nu\beta\beta$-decay experiments can exploit four primary detection channels: ionization, phonons, scintillation light, and Cherenkov light. These channels are summarized in Fig. 14 and discussed in this section. We also address briefly methods being pursued for real-time daughter nucleus tagging.

Energetic charged particles traversing a material lose energy due to ionization processes in which charge carriers (e.g., ions, electrons, holes) are produced. The charge carriers can be collected via an electric field, and read out as an electrical signal. The number of produced charge carriers is inversely proportional to the ionization energy for gas and liquids, or to the mean energy necessary for the creation of an electron-hole pair in semiconductor crystals. The best achievable energy resolution is determined by the variance in the number of charge carriers, which exhibit sub-Poisson fluctuations characterized by the Fano factor (F) (Fano, 1947). The optimal resolution for measuring energy deposition E is thus FWHM $= 2.355\sqrt{F\,w\,E}$, where w is the mean energy required to produce a charge carrier, and we have used the
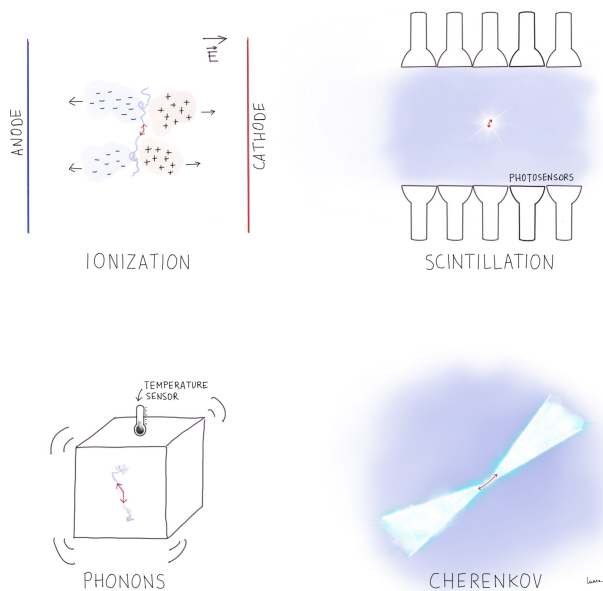
FIG. 14 Artistic rendition of the channels exploited by experiments to detect the electrons emitted in $0\nu\beta\beta$ decay. Image courtesy of L. Manenti.

Gaussian approximation with $2\sqrt{2\ln 2} \approx 2.355$. Typical Fano factors for ionization detectors are ∼0.1-0.2. The value of w ranges from a few eV in semiconductor detectors to tens of eV in noble elements. In practice, the energy resolution is further limited by the charge collection efficiency, which strongly depends on the detector technology. For instance, energy resolution in a xenon time projection chamber (TPC) can be optimal in the gas phase, but is degraded in the liquid phase due to charge recombination (Bolotnikov and Ramsey, 1997). An important aspect of the ionization channel is that the charge collection is typically slower than the electronic readout. Hence, the charge arrival time allows reconstruction of the spatial distribution of the ionization, and thus provides a handle in the identification of different event topologies.

Energy released in a crystal results also in the production of phonons, collective excitations of the crystal lattice. Phonons can be detected by sensors capable of collecting and transforming them into an electrical signal proportional to the deposited energy. Since phonons do not leave the crystal, they eventually thermalize, and can thus be detected from the difference in temperature they induce in crystals cooled to cryogenic temperatures (∼10 mK), for example using neutron transmutation doped germanium (NTD) sensors (Haller *et al.*, 1984; Palaio *et al.*, 1983), superconducting transition-edge sensors (TES) (Irwin, 1995; Irwin and Hilton, 2005), Metallic Magnetic Calorimeters (MMC) (Fleischmann *et al.*, 2005), or Kinetic Inductance Detectors (KID) (Day *et al.*, 2003; Moore *et al.*, 2012; Swenson *et al.*, 2010). NTDs have a volume of $O(10)\,\text{mm}^3$

and resistances in the 1-100 MΩ range, provide signals of few seconds length and feature a large dynamic range, which makes them suitable for measuring energies up to ∼ 10 MeV. TESs, MMCs and KIDs have lower noise and thresholds than NTDs but a narrower dynamic range, thus they are typically employed for detecting smaller signals where a low threshold is crucial. To a rough approximation, the energy resolution for phonon detection from the deposition of energy E in a crystal at temperature T is: FWHM $= 2.355\sqrt{\varepsilon_a[F\,E + C(T)\cdot T] + \sigma_n^2}$, where $\varepsilon_a = k_B T$ is the average phonon activation energy, the second term involving the heat capacity $C(T) \propto T^3$ accounts for fluctuations from phonon exchange with the thermal bath, and σ_n is the contribution from noise. The massive devices required for $0\nu\beta\beta$-decay searches typically have long thermalization time scales that make the readout sensitive to noise in the vibrational frequency range, so in practice the contribution from σ_n has dominated. In general, crystals employed in $0\nu\beta\beta$-decay searches feature an energy resolution which can be as good as 5 keV. As the name suggests, cryogenic calorimeters excel at measuring energy. Nevertheless, for some crystals different particles induce slightly different signal shapes, thus allowing — to some extent — particle identification techniques.

Following the incidence of ionizing radiation, certain organic materials, inorganic crystals, and noble elements de-excite by scintillation light emission. The light yield depends on the material, and exhibits nonlinearities due to effects such as scintillation quenching (ionization density dependence), which must be characterized and calibrated in-situ. Typical light yield values for organic materials and noble elements are ∼10 photons per keV of deposited energy, but can be as high as ∼70 photons/keV. The emission spectrum is continuous, material-dependent, and goes from the ultraviolet to the visible range. The light is detected via the photo-electric effect using optical sensors, such as photo-multiplier tubes (PMT), silicon photo-multipliers (SiPM), or avalanche photo-diodes (APD). Each light sensor is characterized by a quantum efficiency, defined as the detection probability for an incoming photon. The quantum efficiency is also a function of photon frequency, and typically has a maximum of 30–40% for PMTs, but approaches ∼100% for the other technologies. If the scintillation spectrum does not match well with the quantum efficiency profile, a wavelength shifter is placed between the main scintillator and the detector. Wavelength shifters are scintillator materials that absorb higher frequency (e.g., ultraviolet) photons and emit lower frequency ones. In the end, the detected number of photons thus depends on the scintillation spectrum, the quantum efficiency profile, the wavelength shifter transmission spectrum (if present), and the probability for a photon to travel from the scintillator to the detector, during which a photon can be reflected, refracted, scattered, or ab-

sorbed. In many liquid organic scintillators the emission and absorption spectra overlap, and so a photon can also be re-emitted multiple times before being detected. The light yield can be tuned by adding as a solute a second scintillator that shifts the photons to higher wavelength, where the primary scintillator is transparent. The energy resolution is given by FWHM $= 2.355\sqrt{E\,Y\,\langle P_t\rangle\,f_\Omega\epsilon_q}$, where Y is the light yield, $\langle P_t\rangle$ is the average transmission probability, f_Ω is the fractional solid angle instrumented with photosensitive surfaces, and ϵ_q is the quantum efficiency of the light detector. The product of these four factors yields the number of photoelectrons collected per unit energy deposition, and has typical values on the order of one photon per keV or less. The relatively small number of detected quanta, combined with a Fano factor of $\sim$1 due to the small fraction of E that ends up as detected scintillation light, results in a FWHM that is an order of magnitude larger than the one obtained in the ionization channel. A crucial aspect of scintillators is the time profile of their light emission. The de-excitation typically follows a double-exponential profile with decay times differing by over an order of magnitude. The fast component provides a precise measurement of the event time. In large scintillator experiments, the measurement of the fast component for the same event at opposite sides of the detector also provides the location of the energy deposit, via time-of-flight measurement. Moreover, in many scintillators the ratio between the amount of light in the fast and the slow component depends on the interacting particle, thus allowing particle identification.

Cherenkov radiation is emitted when a charged particle travels in a medium at a speed higher than the phase velocity of light in the same medium. The Cherenkov spectrum is a continuum that is more intense at short wavelengths (ultraviolet) but ranges up into the red. A 1 MeV electron produces hundreds of photons, depending on the refractive index of the medium (Aberle *et al.*, 2014). Thus Cherenkov radiation effectively cannot be used for calorimetry in $0\nu\beta\beta$-decay experiments, but can provide some information on the identity and the initial directions of the emitted electrons. Its mere presence identifies the particles as electrons as opposed to alphas or nuclear recoils. Cherenkov light is also emitted on a cone pointed along the particle direction. The electrons do not follow a straight trajectory in a solid or liquid, but a large fraction of the Cherenkov photons are produced at the beginning of the track, when the electron direction is still aligned with its emission direction. The Cherenkov cone is hence smeared by the electron scattering, but can be used to some extent for event topology reconstruction.

Multiple channel readouts are beneficial to improve the reconstruction of event topology or to discriminate electrons from other ionizing particles. For example, the ionization or phonon channels can be used for calorimetry, while scintillation can be exploited for distinguish-

ing between β/γ and α particles, and to provide a more accurate event timing, improving the spatial reconstruction performed with the ionization signal. In liquid noble TPCs, the collection of scintillation light along with ionization can also improve the energy reconstruction (Anton *et al.*, 2020), as fluctuations in charge recombination that quench ionization also result in increased scintillation. The simultaneous readout of scintillation and Cherenkov light is possible even if more complicated, as their emission spectra and time profiles partly overlap. Cherenkov and scintillation light can be distinguished by timing (Caravaca *et al.*, 2017, 2020; Gruszko *et al.*, 2019; Land *et al.*, 2021) provided that the light detector has a sub-ns response time. The scintillation light emission can be slowed down and/or wavelength-shifted (Graham *et al.*, 2019), or suppressed with optical filters (Kaptanoglu *et al.*, 2019), albeit at the cost of reduced light yield, leading to sub-optimal energy resolution. This technique was recently demonstrated in neutrino detectors (Agostini *et al.*, 2022a) and is proposed for use in future $0\nu\beta\beta$ experiments (Askins *et al.*, 2020).

Finally, we briefly mention attempts to reconstruct the identity of the final-state nucleus after the decay. Real-time tagging of the daughter nucleus is being pursued in liquid and gas Xe TPC experiments, in which the final state nucleus is the alkaline earth metal Ba. Tagging of single atoms of Ba can be achieved using, e.g., fluorescence imaging (Chambers *et al.*, 2019; McDonald *et al.*, 2018; Rivilla *et al.*, 2020). The Ba ion following a decay can either be probed in-situ or transported to an imaging stage via drifting in static or dynamic electric fields, or by the physical motion of a collection probe (Brunner *et al.*, 2015; Twelker *et al.*, 2014). Efforts are underway to realize these techniques.

C. Mimicking processes

$0\nu\beta\beta$-decay events can be mimicked by a plethora of other physics processes, which can be induced by cosmic rays, elements in the actinide decay chains, anthropogenic radioactive isotopes, neutrinos, and $2\nu\beta\beta$ decay. While few of these create a peak at or near $Q_{\beta\beta}$, continuum backgrounds also pose a problem since more signal counts are then required to observe a peak exceeding the level of fluctuations. Hence these background sources must also be either eliminated or mitigated and minimized.

1. Cosmic-ray induced processes

$0\nu\beta\beta$-decay experiments are conducted in deep underground laboratories where they are shielded from the otherwise overwhelming background due to cosmic rays generated in the Earth's atmosphere. While most of the
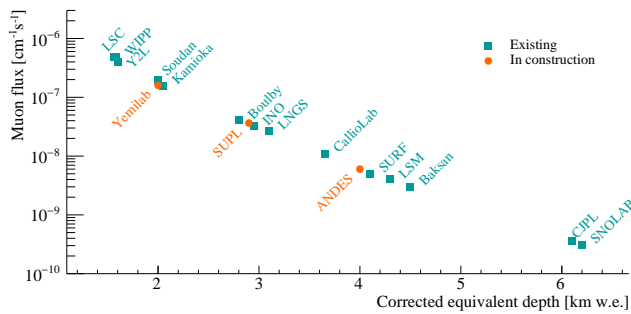
FIG. 15 Muon flux as a function of kilometers of water-equivalent depth (km w.e.) for a selection of deep underground laboratories worldwide. The actual depth is corrected for the overburden shape, if it is not flat. Thus laboratories located under a mountain have a slightly lower equivalent depth than the actual one. Figure adapted from Ianni (2020).
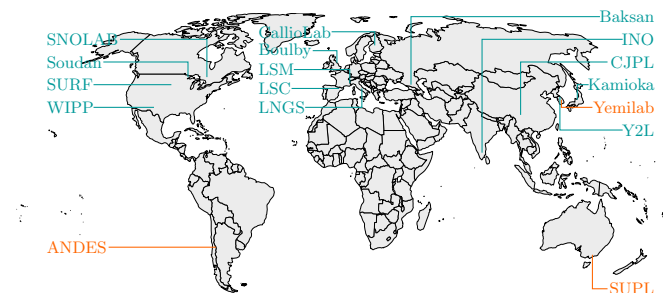

FIG. 16 Worldwide map of deep underground laboratories. The existing laboratories are marked in teal, while the laboratories that are planned or under construction are in orange. The labels are linked to the laboratory webpages.

generated particles are absorbed by a small amount of material, muons can penetrate kilometers of rock and create background either directly, by interacting within the detector, or indirectly, by producing protons and neutrons or showers of particles in the material surrounding the experimental setup. The muon flux decreases by roughly an order-of magnitude for every ~1.5 km of water or ~0.5 km or rock. The muon flux attenuation for a selection of deep underground laboratories around the world is shown in Fig. 15. The corresponding laboratory location is shown in Fig. 16. We refer the reader to Ianni (2020) for a recent review of operating and planned undeground laboratories.

The muons reaching a deep underground laboratory have energies up to several TeV and an angular distribution that depends on depth, density and profile of the rock surrounding the laboratory (Ambrosio et al., 1995). While large monolithic experiments can directly reconstruct muons crossing the detector active volume, TPCs and granular experiments are typically immersed in water tanks equipped with PMTs to detect the muon-induced Cherenkov light, or surrounded by plastic scintillator panels. Without these precautions, cosmic rays would be a major background for most of the experiments

(Freund et al., 2016).

Cosmic rays can also induce spallation as they traverse material. The nucleons emitted by spallation[3] have energies up to the GeV scale and can cause a variety of secondary nuclear processes, including further spallation and fission. The relevance of these processes is three-fold. First, they can activate unstable "cosmogenic" nuclei in the experiment materials prior to their deployment underground (Avignone et al., 1986; Brodzinski et al., 1990). Cosmogenic nuclei are worrisome when their decay can mimic $0\nu\beta\beta$-decay events, e.g., if they undergo β decay with a high end-point and have a half-life comparable to run-time of the experiment. Thus it is common practice to minimize the above-ground exposure of all materials that constitute or are near the detector, and store them underground before the construction of the experiment to reduce the contamination due to short-lived isotopes (Abgrall et al., 2015). In some cases, selected materials are directly fabricated underground (Aalseth, 2005; Bandac et al., 2017; Hoppe et al., 2014). Secondly, spallation from residual underground muons can induce the same activation in-situ. Its occurrence is obviously much more rare than on the surface, but it can be relevant for liquid scintillator experiments, where the amount of active material is much larger than that of the isotope only. If the isotopes activated in situ have a half-life of up to some minutes, the corresponding events can be identified through a delayed time-coincidence with the original muon event. Isotopes with a longer half-life can be more problematic. Finally, muon spallation in the nearby rock can generate a penetrating, energetic neutron background that must be mitigated (see Sec. V.C.4).

2. Elements in the actinide decay chains

$0\nu\beta\beta$-decay mimicking events can be induced by naturally occurring radiation from the decays of primordial elements in the actinide decay chains. Such elements are found ubiquitously in all materials. In particular, ^{238}U and ^{232}Th are the progenitors of long decay chains made of 10 and 14 isotopes, respectively. The actinides produce α, β, and γ radiation across a wide energy range: α particles between 4 and 9 MeV; β radiation mostly concentrated below 2 MeV, with the exception of ^{214}Bi that β decays with an end-point of 3.3 MeV; and γ rays of various energies up to the ^{208}Tl line at 2.6 MeV (rare branches yield some higher energy γ rays). An experiment is essentially vulnerable to mimicking events coming from any α, β, and γ particles or their coincidences with energies above the Q value of the $\beta\beta$ isotope used

------

[3] With loose terminology, by spallation we mean spallation, evaporation, as well as any associated/subsequent hadronic showering.
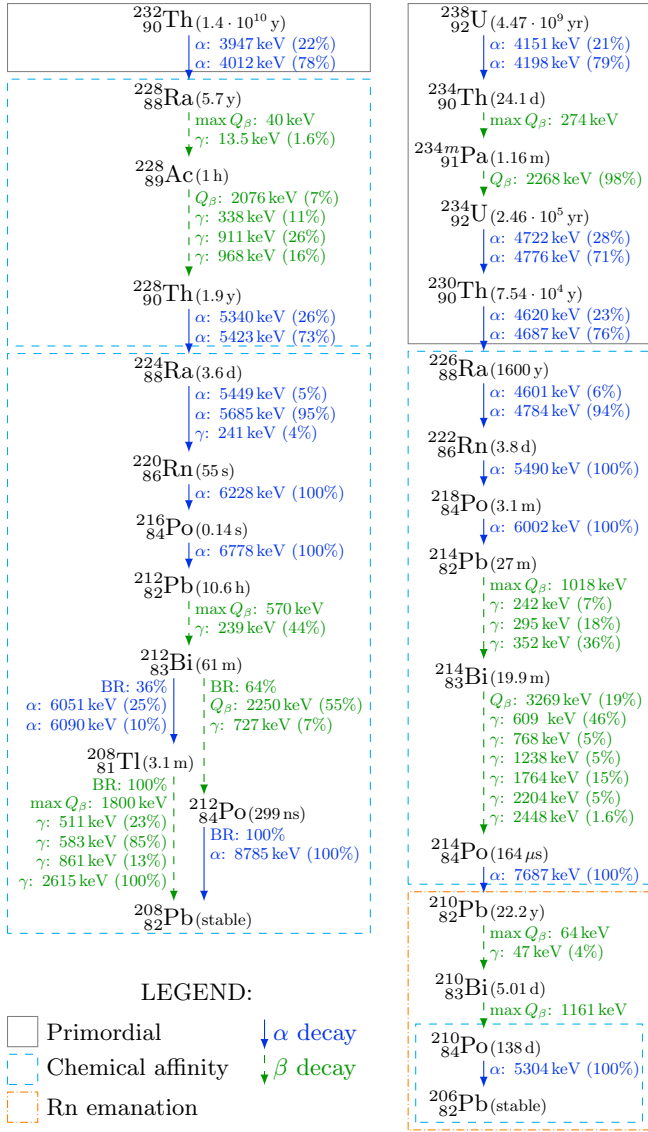
$^{232}_{90}$Th$_{(1.4 \cdot 10^{10}\,\mathrm{y})}$
 ↓ α: 3947 keV (22%)
 ↓ α: 4012 keV (78%)
$^{228}_{88}$Ra$_{(5.7\,\mathrm{y})}$
 ¦ max Q_β: 40 keV
 ↓ γ: 13.5 keV (1.6%)
$^{228}_{89}$Ac$_{(1\,\mathrm{h})}$
 ¦ Q_β: 2076 keV (7%)
 ¦ γ: 338 keV (11%)
 ¦ γ: 911 keV (26%)
 ↓ γ: 968 keV (16%)
$^{228}_{90}$Th$_{(1.9\,\mathrm{y})}$
 ↓ α: 5340 keV (26%)
 ↓ α: 5423 keV (73%)
$^{224}_{88}$Ra$_{(3.6\,\mathrm{d})}$
 ↓ α: 5449 keV (5%)
 ↓ α: 5685 keV (95%)
 ↓ γ: 241 keV (4%)
$^{220}_{86}$Rn$_{(55\,\mathrm{s})}$
 ↓ α: 6228 keV (100%)
$^{216}_{84}$Po$_{(0.14\,\mathrm{s})}$
 ↓ α: 6778 keV (100%)
$^{212}_{82}$Pb$_{(10.6\,\mathrm{h})}$
 ¦ max Q_β: 570 keV
 ↓ γ: 239 keV (44%)
$^{212}_{83}$Bi$_{(61\,\mathrm{m})}$
 BR: 36% | BR: 64%
 α: 6051 keV (25%) | Q_β: 2250 keV (55%)
 α: 6090 keV (10%) | γ: 727 keV (7%)
$^{208}_{81}$Tl$_{(3.1\,\mathrm{m})}$
 BR: 100%
 max Q_β: 1800 keV
 γ: 511 keV (23%)
 γ: 583 keV (85%)
 γ: 861 keV (13%)
 γ: 2615 keV (100%)
$^{212}_{84}$Po$_{(299\,\mathrm{ns})}$
 BR: 100%
 α: 8785 keV (100%)
$^{208}_{82}$Pb$_{(\mathrm{stable})}$

$^{238}_{92}$U$_{(4.47 \cdot 10^{9}\,\mathrm{yr})}$
 ↓ α: 4151 keV (21%)
 ↓ α: 4198 keV (79%)
$^{234}_{90}$Th$_{(24.1\,\mathrm{d})}$
 ↓ max Q_β: 274 keV
$^{234m}_{91}$Pa$_{(1.16\,\mathrm{m})}$
 ↓ Q_β: 2268 keV (98%)
$^{234}_{92}$U$_{(2.46 \cdot 10^{5}\,\mathrm{yr})}$
 ↓ α: 4722 keV (28%)
 ↓ α: 4776 keV (71%)
$^{230}_{90}$Th$_{(7.54 \cdot 10^{4}\,\mathrm{y})}$
 ↓ α: 4620 keV (23%)
 ↓ α: 4687 keV (76%)
$^{226}_{88}$Ra$_{(1600\,\mathrm{y})}$
 ↓ α: 4601 keV (6%)
 ↓ α: 4784 keV (94%)
$^{222}_{86}$Rn$_{(3.8\,\mathrm{d})}$
 ↓ α: 5490 keV (100%)
$^{218}_{84}$Po$_{(3.1\,\mathrm{m})}$
 ↓ α: 6002 keV (100%)
$^{214}_{82}$Pb$_{(27\,\mathrm{m})}$
 ¦ max Q_β: 1018 keV
 ¦ γ: 242 keV (7%)
 ¦ γ: 295 keV (18%)
 ↓ γ: 352 keV (36%)
$^{214}_{83}$Bi$_{(19.9\,\mathrm{m})}$
 ¦ Q_β: 3269 keV (19%)
 ¦ γ: 609 keV (46%)
 ¦ γ: 768 keV (5%)
 ¦ γ: 1238 keV (5%)
 ¦ γ: 1764 keV (15%)
 ¦ γ: 2204 keV (5%)
 ↓ γ: 2448 keV (1.6%)
$^{214}_{84}$Po$_{(164\,\mu\mathrm{s})}$
 ↓ α: 7687 keV (100%)
$^{210}_{82}$Pb$_{(22.2\,\mathrm{y})}$
 ¦ max Q_β: 64 keV
 ↓ γ: 47 keV (4%)
$^{210}_{83}$Bi$_{(5.01\,\mathrm{d})}$
 ↓ max Q_β: 1161 keV
$^{210}_{84}$Po$_{(138\,\mathrm{d})}$
 ↓ α: 5304 keV (100%)
$^{206}_{82}$Pb$_{(\mathrm{stable})}$

LEGEND:
☐ Primordial   ↓ α decay
▢ Chemical affinity ↓ β decay
▢ Rn emanation

FIG. 17 ^{238}U and ^{232}Th decay chains. For each isotope we report α's with intensity $I > 1\%$, γ's with $I > 5\%$ or energy close to the Q-value of a $\beta\beta$ isotope, and β's with a Q-value above 2 MeV. The boxes highlight chain parts typically found in equilibrium: in black are isotopes due to the primordial material radioactivity; in dashed blue are isotopes in equilibrium with its predecessor Ra isotopes, and ^{210}Po; in dash-dotted orange are isotopes in equilibrium with ^{210}Pb, caused by ^{222}Rn emanation and the subsequent ^{210}Pb accumulation.

(Tab. II). The α particles can also undergo (α,n) reactions and thus produce a neutron background, discussed in Sec. V.C.4. Figure 17 summarizes the ^{238}U and ^{232}Th decay chains, listing all α particles with intensity $> 1\%$ and all γ with intensity $> 5\%$ or energy close to the Q-value of some $\beta\beta$ isotope. We also report all β particles with an end-point > 2 MeV, otherwise we just report the highest possible end-point.

Most experiments have the capability of identifying

and suppressing background from actinides via the study of event topology or particle identification techniques, which are covered in detail in Sec. V.D. However the base levels of actinide backgrounds are set by the purity of the employed materials, especially those closest to the detector. The purity in turn depends on the material origin and fabrication history. The ^{238}U and ^{232}Th chains feature isotopes with very different decay times and chemical properties. In particular, Ra has a very different chemical behavior than U and Th, hence it is common to find different concentrations of Ra and U/Th. As a result, decay chains are often not in secular equilibrium, but are split in correspondence to the Ra isotopes, as highlighted by the dashed blue boxes in Fig. 17. Additionally, both chains include isotopes of Rn, an inert gas with high mobility and permeability that is emanated by natural radioactivity in the surrounding environment. When Rn decays near a component during handling and fabrication, its decay progeny can become embedded in and contaminate the component surfaces. Rn can also diffuse in from the experiment infrastructure and contaminate the detector *in situ*, as is the case, e.g., for Rn emanated from the surface of large vessels containing liquid scintillators or cryogenic liquids (Wojcik *et al.*, 2017). ^{222}Rn from the ^{238}U chain is particularly relevant because it leads to the accumulation of the long-lived ^{210}Pb ($T_{1/2} = 22.3$ y). Thus the last part of the ^{238}U chain is often out-of equilibrium (orange dash-dotted box in Fig. 17). Moreover, while the Pb and Bi species can be cleaned off the surfaces relatively easily, ^{210}Po ($T_{1/2} = 138$ d) is difficult to remove without aggressive, surface-specific techniques (Guiseppe *et al.*, 2018), and is thus often found to generate background on its own, unsupported by ^{210}Pb.

In order to reduce the backgrounds from natural radioactivity, special care must be put into the selection, fabrication or purification of pure materials for use in or near the detector. Material selection and actinide material purity demonstration is performed using several primary assay methods: mass spectrometry, γ spectroscopy, neutron activation analysis, and α spectroscopy.

Mass spectrometry (MS) involves atomizing and ionizing the sample material followed by electromagnetic separation of chemical species by their mass-to-charge ratio. Inductively Coupled Plasma Mass Spectrometry (ICP-MS) is a common technique that can reach sensitivities of $\leq 10^{-14}$ g/g for ^{238}U and ^{232}Th using less than a gram of material (LaFerriere *et al.*, 2015; Nisi *et al.*, 2017). Atomization is performed by nebulizing liquid or dissolved samples, or by laser ablation from surfaces of solid samples, followed by ionization by the ICP. ICP-MS is advantageous for its short measurement time (hours) and the small amount of material required, but is limited by isomeric interference and is usually only sensitive to long-lived decay chain progenitors, which are present in the sample in much larger quantities than their short-

lived descendants. Thus ICP-MS cannot detect whether a chain is out of equilibrium. Other MS techniques include glow discharge mass spectrometry, thermal ionization mass spectrometry, and accelerator mass spectrometry.

γ spectroscopy is performed with low-background high-purity germanium (HPGe) detectors operated underground (Baudis *et al.*, 2011; Theodórsson, 2004). It is a non-destructive technique applicable to a variety of isotopes and can reach sensitivities down to the μBq/kg level (Laubenstein, 2017). The sensitivity, though, depends on the sample mass and measurement time: typical measurements last for a few weeks with samples of 0.1–1 kg. The advantages of γ spectroscopy include the possibility to identify any γ-emitting isotope, independently of its mass, and the capability — to some extent — to independently measure the activity of separate parts of a decay chain out of the secular equilibrium.

Neutron activation analysis (NAA) is a technique that combines the activation of an isotope via the exposure to a high intensity neutron flux and the subsequent measurement of the activated nuclei with γ spectroscopy (Fernandes, 2011). Of particular relevance for actinide analysis are the production of ^{239}Np (T$_{1/2}$ = 2.4 d) from ^{238}U, and ^{233}Pa (T$_{1/2}$ = 27 d) from ^{232}Th. Knowing the neutron flux and cross section for the neutron activation cross section — or measuring their product with a reference sample — it is possible to reconstruct the original concentration of the target from the decay rates of the activated nuclei. NAA sensitivity can be superior to that of γ spectroscopy (Clemenza, 2018) but like MS is only sensitive to long-lived decay chain progenitors. Moreover, it can require a non-trivial sample preparation and is subject to possible backgrounds from the neutron activation of stable nuclei present in the sample itself. The latter consideration makes NAA inappropriate for assay of most metals.

Finally, α spectroscopy is useful exclusively for measuring superficial concentrations at depths shallower than the α range in the measured material, i.e., $O(10)\,\mu$m. It can be performed with surface barrier detectors or large ionization chambers, whose main limitations are the sensitive surface size and energy resolution, respectively. The best sensitivity achieved by an α counter is at the level of 30 nBq/cm^2 (Warburton *et al.*, 2004), which is an order of magnitude worse than the values required by, e.g., calorimetric $0\nu\beta\beta$-decay experiments (Armstrong *et al.*, 2019).

Strict procedures are also followed to avoid contaminating the materials through exposure to Rn. Sensitive parts are typically stored or even assembled in radon-free environments. Small volumes such as storage vessels or glove boxes are flushed with boil-off nitrogen from large liquid nitrogen dewars (Wojcik *et al.*, 2017), while larger environments such as clean rooms can be flushed with Rn-free air obtained from dedicated radon abatement systems (Benato *et al.*, 2018). Rn emanation from material within the detector is especially problematic for Xe-based experiments, due to a γ line from ^{214}Bi at 2448 keV, very close to the ^{136}Xe $Q_{\beta\beta}$. Continuous Xe purification has been demonstrated via adsorption on activated charcoals (Abe *et al.*, 2012a) or cryogenic distillation (Aprile *et al.*, 2017). Similarly, Rn suppression by ≥ 3 orders of magnitude was also demonstrated via distillation on n-dodecane, a common admixture in liquid scintillator (Keefer *et al.*, 2015).

In addition to the maximization of the detector radio-purity, the actinide purity of the surrounding components and laboratory environment must be kept under control as well. In this case, high-energy γ rays are the most worrisome component due to their long attenuation lengths. $\beta\beta$-decay detectors must therefore be completely enveloped by a material capable of efficiently absorbing γ radiation without inducing further background. This can be achieved in several ways, including: a set of concentric passive (non-instrumented) layers of shielding material with increasing radio-purity, typically Pb and Cu (Abgrall *et al.*, 2014; Alduino *et al.*, 2017c); a high-purity cryogenic liquid such as Ar possibly instrumented to detect the scintillation light produced by incoming radiation (Agostini *et al.*, 2018b); for liquid scintillator experiments, the division of the detector medium into an inner region loaded with the $\beta\beta$ isotope and an outer region with no isotope working as an active shield (Andringa *et al.*, 2016; Gando *et al.*, 2012). These shielding layers are designed to be thick enough to eliminate external radiation as a concern.

3. Anthropogenic radioactivity

Background can be induced by anthropogenic radioactivity, in particular as a result of nuclear accidents or nuclear weapon tests. The great majority of these isotopes are β emitters, and in some case are the progenitor of a decay chain. In order to represent a potential background source for $0\nu\beta\beta$-decay experiments, the decay chains must include an isotope with a Q-value greater than $Q_{\beta\beta}$, and a dominant half-life on the same order as an experiment's lifetime. Table III lists some examples of potentially worrisome isotopes with $Q_\beta > 2$ MeV reported by IAEA (2015). Of these, only ^{108m}Ag has been detected so far (Gando *et al.*, 2012). The actual relevance of these isotopes as potential backgrounds must be assessed for each experiment separately. While a pure β emitter such as ^{144}Pr could be worrisome for most experiments, an isotope that also emits γ rays (e.g., ^{108m}Ag) could be tagged with event topology reconstruction capabilities.

TABLE III Anthropogenic isotopes. Isotopes belonging to the same chain are grouped between horizontal lines.

Isotope	Half-life	Q_β [keV]	Detected	Notes
^{88}Y	107 d	3008	No	Several γ lines
^{90}Sr	28.8 y	546	No	
^{90}Y	64 h	2279	No	Pure β emitter
^{110m}Ag	250 d	3008	Yes	Several γ lines
^{134}Cs	2 y	2059	No	Several γ lines
^{144}Ce	285 d	319	No	
^{144}Pr	17.3 m	2997	No	Pure β emitter

4. Neutrons

In the previous sections we have mentioned several processes producing neutrons. The actual background induced in a $0\nu\beta\beta$-decay experiment depends on the neutron flux and energy spectrum, on the location of neutron emission, and on the employed materials. In the present context, neutrons can be divided in two groups: above surface neutrons originating from cosmic rays in the atmosphere, and underground neutrons produced by muon spallation, (α, n) reactions on light nuclei, and spontaneous fission reactions, mainly from ^{238}U. Above ground neutrons represent the dominant cause of cosmogenic activation in detector materials prior to their installation underground, previously discussed in Sec. V.C.1. Underground neutrons can be further divided between external neutrons generated in the rock or in the concrete walls, and internal neutrons generated inside or next to the detector. Neutrons from (α, n) and fission reactions have energies $\lesssim 10$ MeV (Wulandari *et al.*, 2004), while those from spallation can reach several GeV (Mei and Hime, 2006). The activity of underground neutrons from (α, n) and fission reactions is only of order ~ 1 n/yr/g, but the high mass of rock within a scattering length of the neutrons yields a flux 2–3 orders of magnitude higher than that of neutrons from spallation (Wulandari *et al.*, 2004).

The flux of neutrons from (α, n) and fission reactions is efficiently suppressed by neutron shielding of moderate thickness, located outside the γ shielding. One possible strategy is to enclose the experiment in a thick layer (a few tens of cm) of neutron moderator such as polyethylene, with the innermost layer (a few cm) comprised of a material with high neutron absorption cross section (e.g., boric acid or borated polyethylene (Abgrall *et al.*, 2014; Alduino *et al.*, 2018)). The outer layer slows down the neutrons to thermal energies, while the inner one captures them. Alternatively, a ≥ 1 m layer of water can be used both for moderation and absorption: in this way, a water tank can simultaneously act as a neutron shield and a muon veto detector (Ackermann *et al.*, 2013). In the case of liquid scintillator detectors, the outermost scintillator region serves as a very effective neutron moderator, providing active tagging in addition to high neutron capture capability.

While external neutrons with energies $\lesssim 10$ MeV are efficiently suppressed with a neutron shield, high energy neutrons can still reach the detector. Additional neutrons can also be produced within the neutron shield by muons or, again, (α, n) and fission reactions taking place in the γ shield, the active material, or in calibration sources (Baudis *et al.*, 2015). These neutrons can undergo elastic and inelastic scattering, or be captured to produce stable or unstable nuclei and possibly yield prompt γ de-excitations. The interactions induce a variety of signatures that strongly depend on the detector technology and employed materials. The most worrisome for $0\nu\beta\beta$-decay experiments are the in-situ activation of long-lived isotopes in or next to the detector, and inelastic scatterings yielding penetrating γ rays with energies comparable to $Q_{\beta\beta}$.

Finally, one possible technique to minimize the neutron induced background consists in embedding in the γ shielding or in the detector medium a material with high-cross section for neutron capture, and possibly that produces events with a signature that does not mimic a $0\nu\beta\beta$-decay event. An example could be ^{6}Li, which undergoes the $^6\text{Li} + n \rightarrow \alpha +^3\text{H}$ reaction with a Q-value of 4.8 MeV(Poda and Giuliani, 2017).

5. Neutrinos

Neutrinos represent a potential source of irreducible background for $0\nu\beta\beta$-decay experiments. Sources with appreciable neutrino fluxes include solar neutrinos, atmospheric neutrinos, geoneutrinos, reactor neutrinos and the diffuse supernova neutrino background (DSNB). Due to their higher flux at energies below 20 MeV, solar neutrinos are the most worrisome background source. Their spectrum is composed of several contributions corresponding to the primary nuclear reactions in the sun (Fig. 18). Solar neutrinos can undergo two types of interactions in a $0\nu\beta\beta$-decay experiment, elastic scattering (ES) and charged current (CC) interactions (Elliott and Engel, 2004):

$$\text{ES:} \quad \nu + \text{e}^- \rightarrow \nu + \text{e}^- \tag{32}$$

$$\text{CC:} \quad ^{Z}\text{A} + \nu \rightarrow \, ^{Z+1}\text{A} + e^- \, [+\gamma(\text{s})] + Q_\nu \tag{33}$$

$$^{Z+1}\text{A} \rightarrow \, ^{Z+2}\text{A} + \beta^- + \nu \, [+\gamma(\text{s})] + Q_\beta \tag{34}$$

In ES, a neutrino scatters off an electron in the detector. The electron is scattered non-isotropically, and its energy spectrum is a continuum up to the end-point of the solar neutrino spectrum, ~ 19 MeV. Only neutrinos with energy $E_\nu > Q_{\beta\beta}$ contribute, and given the low flux of hep neutrinos, in practice only ^{8}B neutrinos are relevant (Fig. 18). The expected background per unit
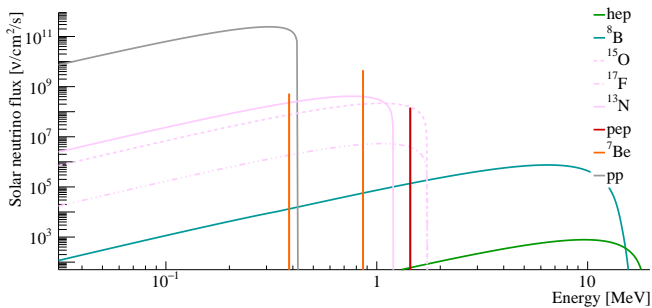
FIG. 18 Solar neutrino spectra. Data from (Agostini *et al.*, 2018a; Bahcall, 1994; Bahcall *et al.*, 1996; Bahcall and Ulrich, 1988; Bergstrom *et al.*, 2016). The curves labeled hep, pep, and pp correspond to neutrinos emitted in helium-proton, proton–electron–proton, and proton-proton fusion, respectively.

sensitive mass is $\sim 2 \cdot 10^{-7}$ counts/keV/kg/yr (de Barros and Zuber, 2011; Elliott and Engel, 2004). For current and next-generation experiments this is negligible for experiments in which the active material is mostly made of the $\beta\beta$ isotope, but becomes significant for liquid scintillator experiments with dissolved sources (Andringa *et al.*, 2016; de Barros and Zuber, 2011; Elliott and Engel, 2004). A partial suppression of the ES background might be achievable exploiting the signal directionality (Askins *et al.*, 2020), at a non-negligible cost in terms of signal efficiency.

In CC interactions, the $\beta\beta$ isotope (A, Z) undergoes inverse β decay to the ground state or an excited state of the $(A, Z+1)$ isotope (Eq. 33), the intermediate isotope of the $\beta\beta$ decay to $(A, Z+2)$. Since $(A, Z+1)$ is heavier than (A, Z), the reaction has a threshold of $E_t = m_{A,Z+1} - m_{A,Z}$, so neutrinos with energy $E_\nu \simeq E_t + Q_{\beta\beta}$ pose a possible background in this prompt event. In some cases the intermediate nucleus can then capture an electron and decay back to the original $\beta\beta$ parent isotope, but it more often undergoes β^- decay to the same final state of the $\beta\beta$ decay, $(A, Z + 2)$ (Eq. 34), releasing an energy $Q_\beta > Q_{\beta\beta}$ that can pose a delayed background. The actual relevance of CC interactions as a background depends on the $\beta\beta$ isotope and the corresponding value of E_t, the emission of de-excitation γ rays in the two involved reactions that could modify the event topology, and the half-life of the intermediate state, which could allow a time correlation analysis. Without applying any of these event identifications, the intermediate nucleus β decay yields a background of 10^{-3}–10^{-1} events/keV/ton$_\text{iso}$/yr (Ejiri and Elliott, 2014, 2017).

Other neutrino sources do not represent a significant background source primarily due to their low flux. However the presence of antineutrinos in these sources requires consideration of additional inverse β interactions that could give a background, particularly at sites with appreciable reactor neutrino fluxes. In the case of atmo-

spheric and DSNB neutrinos, the CC interaction energies are also so high that the nucleus is often left in a highly excited state, leading to background signatures similar to in-situ cosmogenic activation but with much lower production rate.

6. $2\nu\beta\beta$ decay

The only intrinsic and irreducible background for $0\nu\beta\beta$ decay is the concurrent $2\nu\beta\beta$-decay channel. The two processes induce a similar event topology, with the exception of the energy signature: a peak at $Q_{\beta\beta}$ for $0\nu\beta\beta$ decay, and a continuum from zero to $Q_{\beta\beta}$ for $2\nu\beta\beta$ decay (Fig. 12). The detector resolution results in some of the highest energy $2\nu\beta\beta$-decay events reconstructing with energies at $Q_{\beta\beta}$. Although the event topologies differ in detail — in the energy distributions and angular correlations between the emitted electrons (Kotila and Iachello, 2012) — those differences can only be leveraged at high statistics with tracking detectors capable of making those measurements. Thus the relevance of the $2\nu\beta\beta$-decay background depends primarily on the energy resolution and the $2\nu\beta\beta$-decay half-life. In practice, $2\nu\beta\beta$-decay contributes significantly to the background only for experiments with a resolution of some percent. Additionally, if the $2\nu\beta\beta$-decay rate is high compared to the desired $0\nu\beta\beta$-decay sensitivity, $2\nu\beta\beta$-decay events can pile-up and contribute to the background at $Q_{\beta\beta}$. In practice, this is relevant only for cryogenic calorimeters using ^{100}Mo as candidate isotope (Armatol *et al.*, 2020).

D. Signal and background discrimination techniques

In the previous sections we highlighted some of the features that distinguish each possible background component from the $0\nu\beta\beta$-decay signal. In this section we collect and summarize the experimental techniques available to discriminate the two. Although many of these techniqes have been mentioned in the previous sections, our aim is to achieve a concise listing. We organize the discussion according to the key features of the signal. The primary signature is a peak at $Q_{\beta\beta}$ in the sum energy spectrum. $0\nu\beta\beta$-decay events must also be homogeneously distributed in time and space, with a rate proportional to the fraction of target isotope in the active material. The electrons are subject to a localized energy deposition, whose dimension depends on the electron attenuation length: $O(1-10)$ mm for solids and liquids, and $O(10)$ cm for high-pressure gases. The events are uncorrelated with any other physical processes, and the final state includes the presence a particular daughter nucleus.

As described above, energy is the only necessary and sufficient observable for a discovery, hence energy reso-

lution is crucial to minimize the background level in the vicinity of $Q_{\beta\beta}$. Of particular concern are the irreducible $2\nu\beta\beta$-decay contribution that extends up to $Q_{\beta\beta}$, and emissions of the ^{238}U and ^{232}Th decay chains (α, β, or γ particles) with energies greater than $Q_{\beta\beta}$. Often the background at $Q_{\beta\beta}$ can be approximated as flat. If not, a spectral fit over a larger energy region is required to properly constrain the background at $Q_{\beta\beta}$ using the information obtained from the rest of the spectrum. Since the lifetime of an experiment spans several years, calibrating the energy scale and monitoring its stability over time is fundamental for avoiding any degradation of energy resolution in the physics spectrum, and for a precise characterization of the detector response.

The expected $0\nu\beta\beta$-decay signal is uniform in the volume containing the isotope. The same is true for some background processes — e.g., $2\nu\beta\beta$ decay, neutrino, and often neutron reactions — but does not hold for others, especially those induced by natural or anthropogenic radioactive contaminants located outside the detector. Thus the detector medium can act as a self-shield, with the inner part subject to a lower background than the outer one. This is a natural feature of monolithic experiments, while for granular experiments it can be approximated by dividing the detectors into concentric layers.

The electrons emitted by $0\nu\beta\beta$ decay carry a directional correlation due to the angular momentum exchanged by the mediating mechanism. However the direction of any one electron emitted in sequential decays are uncorrelated. On the other hand, some backgrounds, for example the elastic scattering of solar neutrinos with electrons, are not isotropic. Directional reconstruction, e.g., with the detection of Cherenkov light, is therefore useful for suppressing these backgrounds.

The event topology of a $0\nu\beta\beta$ decay is clearly defined for each detector technology: an energy deposition contained in $O(1 - 1000)\,\mathrm{mm}^3$ in a solid or liquid detector; a track of $O(10 - 30)\,\mathrm{cm}$ length with two blobs at its extremes in a high-pressure gas TPC; a pair of distinguished electron tracks with a common origin in a low-pressure tracking detector. Depending on the detector spatial resolution, several particles might be distinguishable: muons induce long tracks that cross the detector medium, or hit multiple detectors of a granular experiment, and generate a signal in muon veto detectors; γ rays have a longer range and can undergo Compton scattering, inducing multiple energy depositions at different locations independently of the detector technology; α particles have a shorter range easily identifiable in gas detectors; β particles produce a track with a single blob in a high-pressure TPC, or a single track in a tracking detector. These signatures can also be combined and thus facilitate their identification, e.g., in the case of a radioactive isotope decaying via α or β decay with the subsequent emission of de-excitation γ rays.

For some readout channels such as scintillation and Cherenkov light, different particles induce a different detector response. Therefore an additional means of background suppression is particle identification via signal shape analysis. A common strategy is having multiple read-out channels: one optimized for energy reconstruction, the other for particle discrimination. Examples are scintillation experiments with Cherenkov readout for α and single β identification, or cryogenic calorimeters with scintillation light readout for α vs β/γ discrimination.

$0\nu\beta\beta$ decays are homogeneous in time and uncorrelated with anything else. Conversely, some backgrounds are identifiable due to their specific time correlations. This is the case for delayed coincidences between the decays of several isotopes in the ^{238}U and ^{232}Th chain (e.g., the Bi-Po sequences, see Fig. 17), between the decay of a cosmogenically activated isotope (e.g., ^{68}Ga in Ge) and the detection of its parent muon in the muon veto, or between inverse β decay and the subsequent β decay in solar neutrino CC reactions.

Finally, daughter nucleus tagging is an additional tool for background suppression, which distinguishes $\beta\beta$ decays (but not exclusively $0\nu\beta\beta$ decays) from anything else except solar neutrino CC reactions. Another background characterization method is abundance scaling, where different measurements with enriched vs non-enriched materials or loaded vs non-loaded active material allow an experiment to isolate backgrounds that are not related to the presence of the $\beta\beta$ decay isotope.

E. Statistical analysis and sensitivity

1. Signal extraction

As discussed in the previous sections, all $0\nu\beta\beta$-decay experiments measure multiple observables for each event. Some observables are related to the amount and spatial distribution of the energy deposited within the detector. Others are related to the timing and type of particles involved in the event. The value of several of these observables is well-defined for $0\nu\beta\beta$-decay events. For instance, each event should have energy equal to the decay Q-value, and be contained within a small region of the detector. Background events will also have specific features, resulting in characteristic observable values.

All experiments in the field use a multivariate analysis to extract the sought-after $0\nu\beta\beta$-decay signal. The observables define the basis of a multi-dimensional parameter space, in which signal and background events are distributed according to multivariate probability distributions. Since $0\nu\beta\beta$-decay events have well-defined features, the bulk of their probability distribution will be restricted to a small volume of the parameter space. On the other hand, most of the background events will be outside of this small volume, populating other regions. Thus the signature of a possible $0\nu\beta\beta$-decay signal is an

excess of events compared to the background expectation in a narrow region of the multi-dimensional parameter space. We will refer to this volume with a maximum signal-to-background ratio as the *sensitive volume*. The rest of the parameter space is effectively used to constrain the background contribution to the sensitive volume.

The signal and background probability distributions are often well separated for one or more observables. In such cases, it is advantageous to apply a cut on such observables, discarding background data without a significant reduction of the signal-detection efficiency, while decreasing the dimensionality of the parameter space, and also reducing systematic uncertainty due to imperfect knowledge of the distributions in the observables. These considerations make applying cuts often advantageous even when there is some overlap, between signal and background, although in such cases the reduced dimensionality and systematic uncertainty must be weighed against any loss of statistical precision. For observables where signal and background strongly overlap, a full multivariate fit is unavoidable. However in many experiments, the signal-background separation is good for most of the observables, and the multivariate analysis can be simplified into a 1-dimensional fit of the energy spectrum with negligible degradation of sensitivity.

The analysis techniques of the field at present are rather established and uniform. Most experiments report frequentist maximum likelihood fits based on likelihood ratio tests (Zyla *et al.*, 2020). Monte-Carlo parametric-boostrapping methods are often used to compute the test statistic probability distributions or to confirm their behavior when asymptotic formulae are assumed (Cowan *et al.*, 2011). Given the low counting rate and the fact that the parameter of interest is constrained to non-negative values, the test statistic distribution can significantly differ from a chi-square function (Algeri *et al.*, 2019). While frequentist methods have historically been dominant (Cousins, 1995), recently most experiments also report results based on Bayesian methods, with inference deriving from the marginalized posterior distribution. Given the lack of a strong signal to date, the choice of prior distribution continues to significantly affect posterior probabilities.

2. Discovery and exclusion sensitivity

The reach of $0\nu\beta\beta$-decay experiments is traditionally quoted in terms of discovery and exclusion sensitivity, two statistical concepts belonging to frequentist inference. The discovery sensitivity corresponds to the expected number of signal events for which an experiment has 50% chance to observe an excess of events over the background at 99.73% confidence level (CL). The exclusion sensitivity corresponds to the expected number of signal events that an experiment has 50% chance of excluding at 90% CL.

The discovery and exclusion sensitivity confidence levels are less stringent compared to other fields — e.g., the particle accelerator community — due to the lack of a "look elsewhere" effect (the $0\nu\beta\beta$ peak must occur at $Q_{\beta\beta}$) and simpler-to-control systematic uncertainties (NSAC NLDBD Subcommittee, 2014, 2015). In particular, the CL required for a discovery is equivalent to excluding 3σ two-sided fluctuation of a Gaussian random variable, and not one-sided 5σ fluctuation as for accelerator experiments. Other sensitivity definitions have been used (Alduino *et al.*, 2017a; Caldwell and Kroninger, 2006), including Bayesian concepts based on Bayes factors and posterior distributions, but these are not common in the field at present.

A precise evaluation of the expected number of signal events (λ_s) fulfilling the sensitivity definitions above requires calculations considering probability distributions in the multivariate space and experiment-specific information. However, it can be approximated by considering a counting analysis in the sensitive volume, with known background expectation λ_b. Uncertainties on λ_b can usually be neglected, as experiments are able to constrain its value using large background-dominated regions of the multivariate parameter space. As both the signal and background events are generated by Poisson random processes, the discovery sensitivity can be calculated by solving this system of equations:

$$\begin{cases} P(X \leq x|\lambda_b) \geq 99.73\% \\ P(X \geq x|\lambda_b + \lambda_s) \geq 50\%\,, \end{cases} \tag{35}$$

where $P(X \leq x|\lambda)$ is the Poisson probability of observing a number of events X smaller or equal to x given an expectation λ. For a given λ_b value, the system has a unique solution that can be found by calculating the minimum x satisfying the first equation, substituting it in the second equation, and then finding the minimum λ_s that satisfies the resulting inequality. The exclusion sensitivity can be similarly computed by solving:

$$\begin{cases} P(X \leq x|\lambda_b) \geq 50\% \\ P(X \geq x|\lambda_b + \lambda_s) \geq 90\%\,. \end{cases} \tag{36}$$

Although the Poisson mass function is discrete, an actual multivariate fit operates with non-integer number of events in the form of the probability distribution weights for each event. We can reproduce this behavior by interpolating the Poisson mass function with a normalized upper incomplete gamma function, and re-define the probability in the systems above as:

$$P(X > x|\lambda) \doteq \frac{\Gamma(x+1, \lambda)}{\Gamma(x+1)}\,. \tag{37}$$

This definition leads to the discovery and exclusion sensitivity shown in Fig. 19. Also shown in Fig. 19 is an

approximation of Eqs. 35 from Cowan *et al.* (2011) using elementary functions.

The discovery sensitivity degrades rapidly as the expected number of background events increases: the greater λ_b, the greater λ_s must be to create an excess incompatible with background fluctuations. For large enough values, the background fluctuations become Gaussian and the sensitivity scales only as $\sqrt{\lambda_b}$. For instance, when $\lambda_b = 100$, a 3σ discovery sensitivity requires $\lambda_s \geq 3\sqrt{100} = 30$. Conversely, the lower the background, the lower the signal expectation needs to be for a discovery. For any $\lambda_b \leq -\ln(99.73\%) \sim 0.0027$, the experiment has more than 99.73% probability of observing no background events, and the observation of a single event becomes a discovery [4]. In this "background-free" regime, the discovery sensitivity saturates: the first of Eqs. (35) is always solved for $x = 0$, and so the second one is solved for $\lambda_s \lesssim -\ln(50\%) \sim 0.69$. In between these two regimes, for $\lambda_b < 1$, the sensitivity is not independent of λ_b but only degrades weakly with increasing λ_b. Experiments in this "quasi-background-free" regime reap most of the benefits of a background-free experiment, but still require a few signal counts to claim an observation.

The exclusion sensitivity behaves similarly to the discovery sensitivity, but it saturates for larger background expectations, at $\lambda_b = -\ln(50\%)$. Below this threshold, the experiment always has $\geq 50\%$ probability to observe no background events, and a further reduction of the background expectation cannot improve the median upper limit on the signal strength. The first of Eqs. 36 is thus always solved for $x = 0$, and the second one yields $\lambda_s = \ln(1 - 90\%) \sim 2.3$ events.

The saturation of both sensitivities is connected to the properties of the Poisson probability, and is thus an intrinsic feature of the frequentist median sensitivity. This behavior can be problematic when the sensitivity is used as a figure of merit to optimize or compare experiments, and alternative sensitivity definitions have been recently proposed (Bhattiprolu *et al.*, 2021).

The expected number of signal and background events in an experiment can be computed starting from two effective parameters, the *sensitive background* ($\mathcal{B}$) and *sensitive exposure* ($\mathcal{E}$). As they are connected to the sensitivity, these parameters capture well the performance of an experiment. The sensitive exposure is the product of: the number of moles of isotope in the active fiducial detector volume, the live time, and the signal detection efficiency, i.e., the probability for a $0\nu\beta\beta$-decay event to occur in the sensitive volume. The sensitive background is the number of background events in the sensitive volume after all

---

[4] For a truly zero background experiment, one event is enough to claim a discovery. In a similar fashion, encountering a unicorn is enough to claim its existence, provided that we have a template of a unicorn to which to compare the observed candidate.
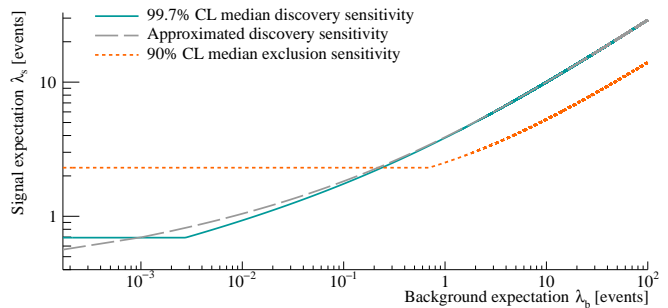
FIG. 19 Median 99.7% CL discovery sensitivity and median 90% exclusion sensitivity as a function of the expected number of background events. The discovery sensitivity shows the signal event expectation at which an experiment has 50% chance to observe a 99.7% CL excess of events over the background. The exclusion sensitivity is instead the signal event expectation that can be excluded at 90% CL with 50% probability, assuming that there is no signal. The plot shows also the approximated discovery sensitivity extracted using the asymptotic formulae from Cowan *et al.* (2011).

analysis cuts, divided by $\mathcal{E}$. Using these definitions, the expected number of signal and background counts in the sensitive volume is given by:

$$\lambda_s(T_{1/2}) = \frac{\ln 2 \cdot N_A \cdot \mathcal{E}}{T_{1/2}} \qquad \text{and} \qquad \lambda_b = \mathcal{B} \cdot \mathcal{E} \quad (38)$$

where N_A is Avogadro's number and $T_{1/2}$ is the half-life of the decay. Given that λ_s depends on $T_{1/2}$, the discovery and exclusion sensitivities on the expected number of events can be directly translated into sensitivities on the $0\nu\beta\beta$-decay half-life. $T_{1/2}$ sensitivities are the most common parameter reported by the experiments.

Next-generation searches aim to monitor tons of material for a decade, reaching sensitive exposures at the level of $\mathcal{E} \sim 10^5 - 10^6$ mol·yr. Such an exposure gives the possibility to observe a handful of signal events even for $0\nu\beta\beta$-decay half-life values of $10^{27} - 10^{28}$ years. As illustrated by Fig. 19, a requirement for discovery is that the number of background events is similar to the number of expected signal events. Thus experiments aim at reaching backgrounds at the level of $\mathcal{B} < 10^{-4} - 10^{-5}$ events per mole of material per year. The concepts proposed to achieve this incredibly challenging performance are described in the next section.

VI. RECENT AND FUTURE EXPERIMENTS

A broad experimental program has been mounted in the last two decades to search for $0\nu\beta\beta$ decay. Very diverse technologies have been developed and tested, leading to experiments with half-life sensitivities up to 10^{26} years. Thanks to these achievements, a number of new projects are being prepared with the goal of increasing

the sensitivity by up to two orders of magnitude, opening the window to new energy frontiers and conclusively testing the scenario in which $0\nu\beta\beta$ decay is mediated by inverted-ordered neutrinos (Agostini *et al.*, 2021b).

In this section, we discuss recent and future phases of existing experiments. In Sec. VI.A, we review the experimental landscape and use the experiments' key performance parameters to evaluate their strength, strategy, and sensitivity. We then focus on the detection concept and technical aspects of each project. Experiments based on high-purity germanium detectors are reviewed in Sec. VI.B, time-projection chambers in Sec. VI.C, large liquid scintillator detectors in Sec. VI.D, cryogenic calorimeters in Sec. VI.E, and tracking calorimeters in Sec. VI.F. New technologies that are currently being tested and newly proposed experimental designs are summarized in Sec. VI.G. Sec. VI.A should be accessible to all readers, while the other sections listed above are intended for more expert readers.

A. Experimental landscape

Each experiment is characterized by a set of key performance parameters that are captured by the concepts of sensitive exposure ($\mathcal{E}$) and sensitive background ($\mathcal{B}$) defined in Sec. V.E.2. The sensitive exposure and background are directly connected to the half-life sensitivity, and carry valuable information on the strategy pursued by each project. Indeed, different combinations of $\mathcal{E}$ and $\mathcal{B}$ can give the same sensitivity, and exposure increase can be traded for background reduction or vice versa.

The sensitive exposure and background are effective parameters whose values are often not intuitive: they refer to the detector performance in the sensitive volume, where the signal-to-background ratio is maximal and drives the experimental sensitivity. We calculate the value of $\mathcal{E}$ starting from the product of isotope mass m_{iso} and data taking time, and correct it for a number of efficiencies: the active (or fiducial) fraction of the target mass $\varepsilon_{\mathrm{act}}$, the probability that the energy deposited by the decay is fully contained within the detector $\varepsilon_{\mathrm{cont}}$, and the multivariate analysis efficiency to tag events in the sensitive volume $\varepsilon_{\mathrm{mva}}$. Although $\varepsilon_{\mathrm{mva}}$ would conceptually include the efficiency for a signal to fall in the energy region of interest (ROI) dominating the sensitivity, we separate this contribution and also quote the energy resolution (σ) as well as the width of the effective ROI in units of σ, assuming a Gaussian approximation. To calculate $\mathcal{B}$, we extract the rate of background events in the sensitive volume from the experiments' specifications. The values of these parameters and efficiencies are listed in Tab. IV and shown graphically in Fig. 20. When the value of a parameter cannot be computed from published specifications, we report effective values reproducing the nominal sensitivity of the experiment. Details of

these approximations are discussed in the following subsections.

Figure 20 illustrates how each detection concept is characterized by specific parameter combinations. Liquid and gas detectors have large isotope masses and a relatively low signal detection efficiency due to the non-uniform background rate, with a small detector region driving the sensitivity. Solid state detectors operate a smaller isotope mass, but with higher efficiency and energy resolution. As a result, an isotope mass lower by a factor of 10 can be balanced by higher resolution and efficiency, yielding a similar sensitive exposure and sensitivity.

Figure 21 shows a scatter plot of the sensitive exposure and background for the listed projects. Recent experiments populate the top left part of the plot, corresponding to exposures of thousands of mole-years — i.e., tens or hundreds of kilograms of target mass operated for a few years — and background rates between 10^{-3} and 10^{-1} events per mole-year. To improve the sensitivity, future experiments need to either increase $\mathcal{E}$ or reduce $\mathcal{B}$. Often a sequence of experimental upgrades with progressive incremental improvements is planned, ultimately leading to a combined factor of ~ 100 improvement.

These figures highlight the strengths and limitations of each detection concept, indicating the natural strategies to maximize the sensitivity, which are most evident in the $\mathcal{E}/\mathcal{B}$ ratios. For example, ^{130}Te experiments have large $\mathcal{E}/\mathcal{B}$ values (the blue markers are systematically above the other points in Fig. 21). Given the high natural abundance of ^{130}Te, for them it is more efficient to increase the exposure rather than reducing the background. Conversely, ^{76}Ge-based experiments have small $\mathcal{E}/\mathcal{B}$ values. For them, reducing the background is easier than increasing the target mass, as their strengths are good energy resolution and advanced event reconstruction capabilities. Experiments based on other isotopes have intermediate $\mathcal{E}/\mathcal{B}$ values, suggesting some flexibility in finding a trade off between the two quantities.

Although the sensitive exposure and background are valuable parameters to characterize an experiment, the reach of an experiment is not fully captured by the $T_{1/2}$ sensitivity. The phase space factor also plays a strong role, and the nuclear structure of the isotopes deeply affects the connection between $T_{1/2}$ and the underlying decay mechanism. For instance, assuming the decay is mediated by the exchange of light Majorana neutrinos, the discovery power of an experiment is better quantified by the effective Majorana mass sensitivity. We hence include in the table and figures values for the $m_{\beta\beta}$ sensitivities, whose ratios provide a good figure of merit also assuming several other decay mechanisms. We will discuss in detail the discovery power of the experiments in Sec. VII.

TABLE IV Fundamental parameters driving the sensitive background and exposure of recent and future phases of existing experiments. The last two columns report the discovery sensitivity on the $0\nu\beta\beta$-decay half-life for 10 years of livetime, and the corresponding sensitivity on $m_{\beta\beta}$ for the range of NMEs specified in Tab. I. For completed experiments, sensitivities are computed using the reported final exposure. MJD, KLZ, and SuperNEMO-D refer to the MAJORANA DEMONSTRATOR, KamLAND-Zen, and the SuperNEMO Demonstrator, respectively.

| Experiment	Isotope	Status	Lab	m_{iso} [mol]	$\varepsilon_{\mathrm{act}}$ [%]	$\varepsilon_{\mathrm{cont}}$ [%]	$\varepsilon_{\mathrm{mva}}$ [%]	σ [keV]	ROI $[\sigma]$	$\varepsilon_{\mathrm{ROI}}$ [%]	$\mathcal{E}$ $\left[\frac{\mathrm{mol\cdot yr}}{yr}\right]$	$\mathcal{B}$ $\left[\frac{\mathrm{events}}{\mathrm{mol\cdot yr}}\right]$	λ_b $\left[\frac{\mathrm{events}}{\mathrm{yr}}\right]$	$T_{1/2}$ [yr]	$m_{\beta\beta}$ [meV]
High-purity Ge detectors (Sec. VI.B)															
GERDA-II	^{76}Ge	completed	LNGS	$4.5\cdot10^2$	88	91	79	1.4	-2,2	95	273	$4.2\cdot10^{-4}$	$1.1\cdot10^{-1}$	$1.2\cdot10^{26}$	93-222
MJD	^{76}Ge	completed	SURF	$3.1\cdot10^2$	91	91	86	1.1	-2,2	95	212	$3.3\cdot10^{-3}$	$7.1\cdot10^{-1}$	$4.7\cdot10^{25}$	149-355
LEGEND-200	^{76}Ge	construction	LNGS	$2.4\cdot10^3$	91	91	90	1.1	-2,2	95	1684	$1.0\cdot10^{-4}$	$1.7\cdot10^{-1}$	$1.5\cdot10^{27}$	27-63
LEGEND-1000	^{76}Ge	proposed		$1.2\cdot10^4$	92	92	90	1.1	-2,2	95	8736	$4.9\cdot10^{-6}$	$4.3\cdot10^{-2}$	$1.3\cdot10^{28}$	9.0-21
Xe time projection chambers (Sec. VI.C)															
EXO-200	^{136}Xe	completed	WIPP	$1.2\cdot10^3$	46	100	84	31	-2,2	95	438	$4.7\cdot10^{-2}$	$2.1\cdot10^{+1}$	$2.4\cdot10^{25}$	111-477
nEXO	^{136}Xe	proposed	SNOLAB	$3.4\cdot10^4$	64	100	66	20	-2,2	95	13700	$4.0\cdot10^{-5}$	$5.5\cdot10^{-1}$	$7.4\cdot10^{27}$	6.1-27
NEXT-100	^{136}Xe	construction	LSC	$6.4\cdot10^2$	88	76	49	10	-1.0,1.8	80	167	$5.9\cdot10^{-3}$	$9.9\cdot10^{-1}$	$7.0\cdot10^{25}$	66-281
NEXT-HD	^{136}Xe	proposed		$7.4\cdot10^3$	95	89	44	7.7	-0.5,1.7	65	1809	$4.0\cdot10^{-5}$	$7.2\cdot10^{-2}$	$2.2\cdot10^{27}$	12-50
PandaX-III-200	^{136}Xe	construction	CJPL	$1.3\cdot10^3$	77	74	65	31	-1.2,1.2	76	374	$3.0\cdot10^{-3}$	$1.1\cdot10^{+0}$	$1.5\cdot10^{26}$	45-194
LZ-nat	^{136}Xe	construction	SURF	$4.7\cdot10^3$	14	100	80	25	-1.4,1.4	84	440	$1.7\cdot10^{-2}$	$7.5\cdot10^{+0}$	$7.2\cdot10^{25}$	64-277
LZ-enr	^{136}Xe	proposed	SURF	$4.6\cdot10^4$	14	100	80	25	-1.4,1.4	84	4302	$1.7\cdot10^{-3}$	$7.3\cdot10^{+0}$	$7.1\cdot10^{26}$	20-87
Darwin	^{136}Xe	proposed		$2.7\cdot10^4$	13	100	90	20	-1.2,1.2	76	2312	$3.5\cdot10^{-4}$	$8.0\cdot10^{-1}$	$1.1\cdot10^{27}$	17-72
Large liquid scintillators (Sec. VI.D)															
KLZ-400	^{136}Xe	completed	Kamioka	$2.5\cdot10^3$	44	100	97	114	0,1.4	42	450	$9.8\cdot10^{-3}$	$4.4\cdot10^{+0}$	$3.3\cdot10^{25}$	95-408
KLZ-800	^{136}Xe	taking data	Kamioka	$5.0\cdot10^3$	55	100	100	105	0,1.4	42	1143	$5.5\cdot10^{-3}$	$6.2\cdot10^{+0}$	$2.0\cdot10^{26}$	38-164
KL2Z	^{136}Xe	proposed	Kamioka	$6.7\cdot10^3$	80	100	97	60	0,1.4	42	2176	$3.0\cdot10^{-4}$	$6.5\cdot10^{-1}$	$1.1\cdot10^{27}$	17-71
SNO+I	^{130}Te	construction	SNOLAB	$1.0\cdot10^4$	20	100	97	74	-0.5,1.5	62	1232	$7.8\cdot10^{-3}$	$9.7\cdot10^{+0}$	$1.8\cdot10^{26}$	31-144
SNO+II	^{130}Te	proposed	SNOLAB	$5.1\cdot10^4$	27	100	97	57	-0.5,1.5	62	8521	$5.7\cdot10^{-3}$	$4.8\cdot10^{+1}$	$5.7\cdot10^{26}$	17-81
Cryogenic calorimeters (Sec. VI.E)															
CUORE	^{130}Te	taking data	LNGS	$1.6\cdot10^3$	100	88	92	3.2	-1.4,1.4	84	1088	$9.1\cdot10^{-2}$	$9.9\cdot10^{+1}$	$5.1\cdot10^{25}$	58-270
CUPID-0	^{82}Se	completed	LNGS	$6.2\cdot10^1$	100	81	86	8.5	-2,2	95	41	$2.8\cdot10^{-2}$	$1.2\cdot10^{+0}$	$4.4\cdot10^{24}$	283-551
CUPID-Mo	^{100}Mo	completed	LSM	$2.3\cdot10^1$	100	76	91	3.2	-2,2	95	15	$1.7\cdot10^{-2}$	$2.5\cdot10^{-1}$	$1.7\cdot10^{24}$	293-858
CROSS	^{100}Mo	construction	LSC	$4.8\cdot10^1$	100	75	90	2.1	-2,2	95	31	$2.5\cdot10^{-4}$	$7.6\cdot10^{-3}$	$4.9\cdot10^{25}$	54-160
CUPID	^{100}Mo	proposed	LNGS	$2.5\cdot10^3$	100	79	90	2.1	-2,2	95	1717	$2.3\cdot10^{-4}$	$4.0\cdot10^{-1}$	$1.1\cdot10^{27}$	12-34
AMoRE-II	^{100}Mo	proposed	Yemilab	$1.1\cdot10^3$	100	82	91	2.1	-2,2	95	760	$2.2\cdot10^{-4}$	$1.7\cdot10^{-1}$	$6.7\cdot10^{26}$	15-43
Tracking calorimeters (Sec. VI.F)															
NEMO-3	^{100}Mo	completed	LSM	$6.9\cdot10^1$	100	100	11	148	-1.6,1.1	42	3	$9.4\cdot10^{-1}$	$3.0\cdot10^{+0}$	$5.6\cdot10^{23}$	505-1485
SuperNEMO-D	^{82}Se	construction	LSM	$8.5\cdot10^1$	100	100	28	83	-4.2,2.4	64	15	$3.3\cdot10^{-2}$	$5.0\cdot10^{-1}$	$8.6\cdot10^{24}$	201-391
SuperNEMO	^{82}Se	proposed	LSM	$1.2\cdot10^3$	100	100	28	72	-4.1,2.8	54	185	$5.3\cdot10^{-3}$	$9.8\cdot10^{-1}$	$7.8\cdot10^{25}$	67-131
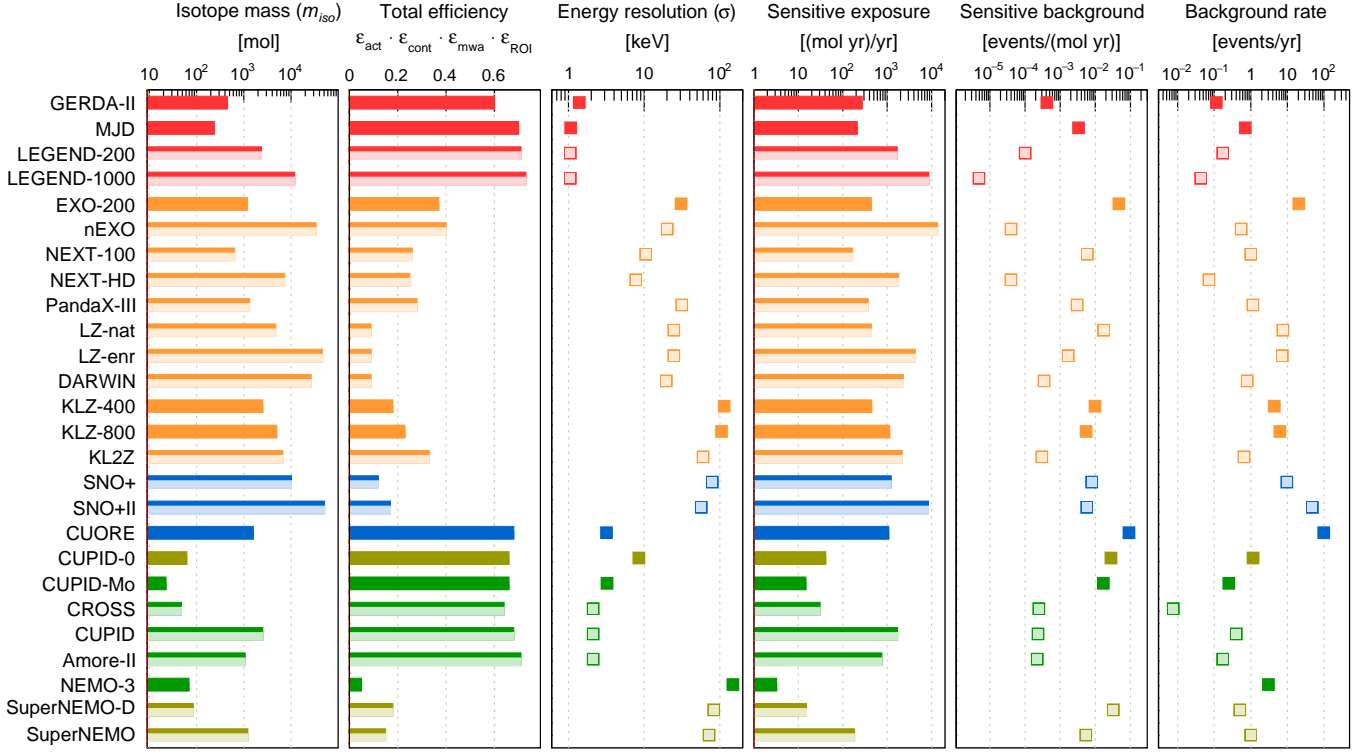
FIG. 20 Fundamental parameters driving the sensitive background and exposure, and hence the sensitivity, of recent and future phases of existing experiments (see Eq. 38). Red bars are used for ^{76}Ge experiments, orange for ^{136}Xe, blue for ^{130}Te, green for ^{100}Mo, and sepia for ^{82}Se. Similar exposures are achieved with high mass but poorer energy resolution and efficiency by gas and liquid detectors, or with small mass but high resolution and efficiency by solid state detectors. The sensitive exposure is computed for one year of livetime. Ligher shades indicate experiments which are under construction or proposed.
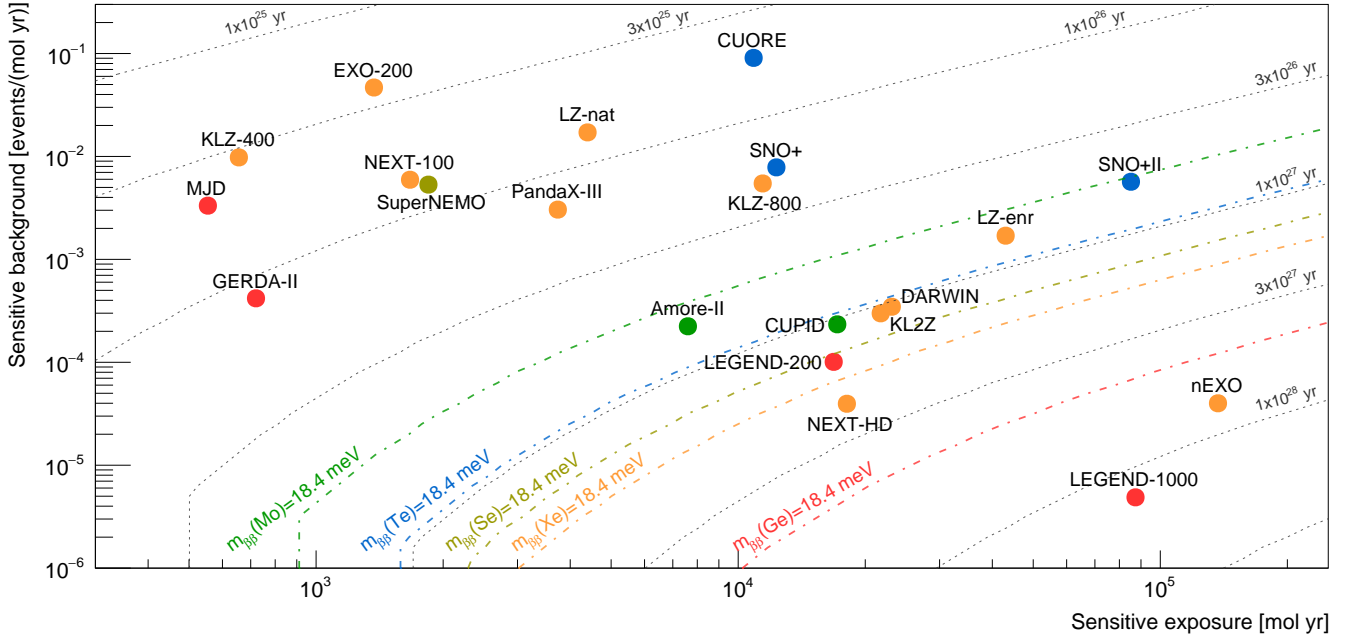
FIG. 21 Sensitive background and exposure for recent and future experiments. Grey dashed lines show specific discovery sensitivity values on $0\nu\beta\beta$-decay half-lives, and colored dashed lines indicate the half-life sensitivities required to test the bottom of the inverted ordering scenario for ^{76}Ge, ^{136}Xe, ^{130}Te ^{100}Mo, and ^{82}Se, assuming for each isotope the largest QRPA NME value listed in Tab. I. For completed experiments the final reported exposure is used, otherwise a 10 yr lifetime is assumed.
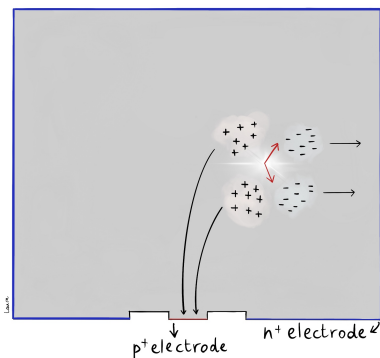
FIG. 22 Artistic illustration of a high-purity Ge (HPGe) detector and its $0\nu\beta\beta$-decay detection concept. Electron and hole clusters created by ionization are collected to the electrodes by an electric field. Image courtesy of L. Manenti.

B. High-purity Ge semiconductor detectors

High Purity Germanium (HPGe) detectors represent the longest-standing technology used for $0\nu\beta\beta$-decay searches (Avignone and Elliott, 2019). The first $0\nu\beta\beta$-decay experiment based on Ge detectors was in 1967 (Fiorini *et al.*, 1967) and, since then, Ge-based experiments have stayed at the forefront of the field. Fig. 22 shows an example of the state-of-the-art model.

HPGe detectors are semiconductor devices. A detector consists of a single crystal grown by the Czochralski method (Depuydt *et al.*, 2006) from Ge-material enriched up to 92% in ^{76}Ge. The detectors used by recent and future experiments are all p-type crystals, with two conductive electrodes obtained through B implantation (p+ electrode) and Li diffusion (n+ electrode). The semiconductor junction forms between the n+ electrode and the p-type crystal, and is extended throughout the whole detector volume by applying a reverse bias of a few thousands volts. Electrons and holes produced within the crystal by ionization drift along the electric field, inducing a current. The current integral is proportional to the energy deposited within the detector, and its time-structure carries information on the event topology. The detector size is currently limited to 1-3 kg, and multiple detectors need to be operated simultaneously to reach a competitive amount of isotope mass. These detectors are operated in ultra-low background environments, surrounded by shielding material and active veto systems.

HPGe detectors feature high $0\nu\beta\beta$-decay detection efficiencies. The presence of conductive electrodes on the detector surface reduces the active volume fraction to $\varepsilon_{\rm act} \sim 90\%$ and leads to energy loss for a fraction of the $0\nu\beta\beta$-decay events ($\varepsilon_{\rm cont} \sim 90\%$). The $0\nu\beta\beta$-decay event tagging efficiency, $\varepsilon_{\rm mva} \sim 80-90\%$, is typically limited by signal-background discrimination methods based on the analysis of the current time-structure. Given the low background level and high resolution, the optimal en-

TABLE V Specific parameters of experiments using Ge detectors: total detector mass, fractional isotopic abundance, shielding strategy, and background index normalized over the entire detector mass. The background index is what is historically quoted by these experiments but, differently from our sensitive background, is not normalized over the signal detection efficiencies and detector resolution. The values are taken from (Abgrall *et al.*, 2021; Agostini *et al.*, 2020b; Alvis *et al.*, 2019a), averaging over multiple datasets for GERDA-II and the MAJORANA DEMONSTRATOR.

Experiment	m_{tot} [kg]	f_{iso} [%]	Shield	Background $\left[\frac{\text{events}}{\text{keV}\cdot\text{kg}\cdot\text{yr}}\right]$
GERDA-II	39	87	liquid Ar	$5.2\cdot10^{-4}$
MJD	20	88	Cu & Pb	$6.0\cdot10^{-3}$
LEGEND-200	200	90	liquid Ar	$2\cdot10^{-4}$
LEGEND-1000	1000	91	liquid Ar	$1\cdot10^{-5}$

ergy region of interest (ROI) for $0\nu\beta\beta$-decay searches is $Q_{\beta\beta}\pm2\sigma$, containing 95% of the signal. Specific parameter values of ^{76}Ge experiments are listed in Tab. V.

The GERDA experiment operated a compact array of about 40 detectors in a cryostat containing $64\,\text{m}^3$ of liquid argon (LAr) (Agostini *et al.*, 2018b). Several detector geometries were used during the experiment, giving an average ^{76}Ge mass of $\sim$34 kg. The LAr acted as a passive shielding against natural radioactivity from any contamination outside the cryostat, and also attenuated background produced by radioactive isotopes in the materials near the detectors, such as the holders or cables. The LAr was also used as an active veto system by detecting its scintillation light produced when a background event deposits energy in the argon volume. The average energy resolution achieved during the second phase of the experiment (GERDA-II) was $\sigma = 1.4\,\text{keV}$, and the average background index was $5.2^{+1.6}_{-1.3}\cdot10^{-4}$ events/(keV·kg·yr), corresponding to $\mathcal{B} = 4.2\cdot10^{-4}$ events/(mol·yr)(Agostini *et al.*, 2020b). With these parameters, at present, GERDA has achieved the lowest sensitive background in the field. The remnant background composition was traced to U and Th in the material surrounding the detectors, and α- and β-decaying isotopes on the detector surfaces (Agostini *et al.*, 2020c). The final result of GERDA is a constraint of $T_{1/2} > 1.8\cdot10^{26}$ yr at 90% C.L., consistent with the median upper limit expected for no signal, derived including also the data from Phase I of the experiment.

The MAJORANA DEMONSTRATOR (MJD) (Abgrall *et al.*, 2014) employed a compact array of up to 58 detectors comprised of both enriched and natural Ge. 27 kg of isotope were operated in enriched detectors (Arnquist *et al.*, 2022). The HPGe crystals are deployed in two vacuum cryostats shielded from the environmental background by a layer of underground-electroformed copper, commercially obtained copper, and high-purity lead. The detectors incorporate a point-like p+ electrode provid-

ing very low-energy threshold and an excellent energy resolution of $\sigma = 1.1\,\text{keV}$ at $Q_{\beta\beta}$, which is currently the best in the field. With a sensitive background of $\mathcal{B} = 3.3 \cdot 10^{-3}$ events/(mol· yr), the experiment reported a limit of $T_{1/2} > 8.3 \cdot 10^{25}$ yr at 90% C.L. with a limit setting sensitivity of $T_{1/2} = 8.1 \cdot 10^{25}$ yr. The background is dominated by a distant source of thorium (Arnquist et al., 2022).

The next-generation Ge-based experiments will be realized in the framework of the LEGEND project (Abgrall et al., 2021), with two stages planned: LEGEND-200 and LEGEND-1000. In the first, ∼200 kg of Ge detectors will be operated in the GERDA setup after upgrading part of the infrastructure. Compared to GERDA, a further reduction of the background is anticipated thanks to the use of larger-mass detectors (resulting in fewer cables and electronic components), improved light readout, and materials with improved radiopurity, such as the electro-formed copper developed for the MAJORANA DEMON-STRATOR. An energy resolution equal to or better than the one achieved in the MAJORANA DEMONSTRA-TOR is expected. These improvements would bring the LEGEND-200 background to $2 \cdot 10^{-4}$ events/(keV· kg· yr), less than a factor of 3 lower than what was achieved by GERDA. With a sensitive background of $\mathcal{B} = 1.0 \cdot 10^{-4}$ events/(mol· yr), LEGEND-200 will achieve a discovery sensitivity of 10^{27} yr in 5 years of live time. For LEGEND-1000, a new infrastructure able to host 1 ton of target mass will be realized. A further twenty-fold background reduction is expected with the usage of underground argon, and lower radioactivity levels in cables and electronics. LEGEND-1000 expects a sensitive background of $\mathcal{B} = 4.9 \cdot 10^{-6}$ events/(mol· yr), leading to a discovery sensitivity of $T_{1/2} = 1.3 \cdot 10^{28}$ yr after 10 years of operation.

We note that during preparation of this manuscript plans were announced (Yue, 2021) for a $0\nu\beta\beta$-decay-focused branch of the CDEX effort (Wang et al., 2017), culminating in a ton-scale ^{76}Ge experiment. At present public details for this project are insufficient for estimating its sensitivity.

C. Xe time projection chambers

Time projection chambers (TPCs) were the first technology used to observe $2\nu\beta\beta$ decay in real time (Elliott et al., 1987) and have remained at the forefront of $0\nu\beta\beta$-decay searches ever since. In these detectors, a static electric field is applied in a region containing a liquid or gaseous medium. As shown in Fig. 23, the electrons and ions liberated by ionizing radiation drift to analyzing planes which reconstruct their number and position in the plane normal to the field. The position along the field is derived from the drift durations. The event reconstruction allows to discriminate spatially-localized $0\nu\beta\beta$-
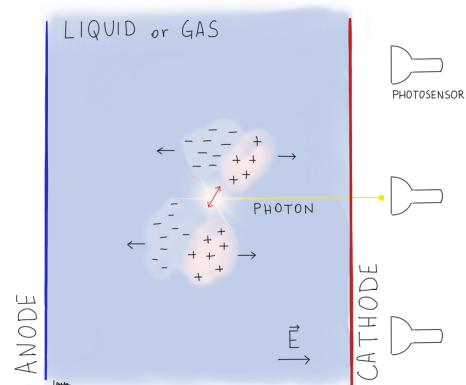
FIG. 23 Artistic illustration of a Xe TPC and its $0\nu\beta\beta$-decay detection concept. Electron and hole clusters created by ionization are collected to the electrodes by an electric field. In addition, scintillation light is detected by light sensors, providing the timing of the event. Image courtesy of L. Manenti.

decay events from spatially extended ones, such as those produced by multiple Compton scattering. Depending on the spatial resolution, even the full 3D tracks of the two electrons emitted in $0\nu\beta\beta$ decay can in principle be reconstructed, making it possible to discriminate them from from single β-decays, γ-ray scattering and absorption, or nuclear recoils from neutron scattering.

TPCs are particularly well-suited to searches for the $0\nu\beta\beta$ decay of ^{136}Xe. The source itself is an inert noble element and can be used directly in TPCs in its purified form as a liquid, gas, or both. In either phase, Xe exhibits VUV scintillation emitted promptly with an energy deposition. Experiments able to detect the scintillation light signal can reconstruct the full 3D topology of the event using a single analyzing plane. The intensity of the scintillation light also provides a complementary measurement of energy, whose anti-correlation with the ionization signal can significantly enhance the energy resolution (Conti et al., 2003).

If the electric field is strong enough, the collision between drifting electrons and gas molecules results in the emission of secondary scintillation light, called electroluminescence (EL). Single-phase high-pressure gas TPCs (recently reviewed in (Gomez-Cadenas et al., 2019)) shape the field near the electrode to create a region where the incoming electrons produce EL. Dual-phase TPCs obtain the same result using a short gaseous EL layer at the top of the liquid volume. The EL signal gives a precise measure of the number of ionization electrons, improving the energy resolution. With a fine enough spatial resolution of the light collection, the EL signal can also be used for track reconstruction. The energy resolution of experiments reading out the electroluminescence light is limited by fluctuations in the number of primary ionization electrons. These fluctuations are small and independent of fluid density up to about 0.6 g/cm^3 (∼100 bar),

but above that pressure grow rapidly (Bolotnikov and Ramsey, 1997).

Xe TPCs also potentially lend themselves to techniques for observation of the $\beta\beta$ daughter Ba ion, as first suggested by Moe (1991). Single-atom trapping and imaging was first achieved with Ba (Neuhauser et al., 1980). Xe is a transparent fluid, offering multiple options for tagging based on fluorescence imaging techniques. The nEXO Collaboration is pursuing a strategy using a cryogenic probe (Twelker et al., 2014) to electrostatically attract the Ba ion in the vicinity of a signal event and freeze it in a volume of Xe, then transport it to a fluorescence imaging stage capable of single-atom detection (Chambers et al., 2019). The NEXT collaboration aims to transport Ba^{++} ions to single-molecule fluorescence imaging (SMFI) sensors for example using RF carpets (Brunner et al., 2015; Jones et al., 2021). Single-Ba-atom sensitivity with SMFI (McDonald et al., 2018) and an implementation applicable to high-pressure gas Xe TPCs (Rivilla et al., 2020) have been demonstrated. Both collaborations are still working to demonstrate that their tagging schemes can be achieved with sizeable efficiency and in an actual $0\nu\beta\beta$-decay experiment. We do not discuss these techniques further in this review.

Liquid Xe volumes operated in TPCs provide self-shielding from external radiation, whose contribution to the background drops exponentially with the distance from the outer Xe surface. Of particular worry is the ^{214}Bi gamma line at 2447.7 keV, just below the ^{136}Xe $Q_{\beta\beta}$ at 2457.8 keV, and often not resolved. Xe TPC experiments use a multi-variate analysis to handle the varying background rate throughout the detector volume. However, the sensitivity of the experiment is essentially driven by the innermost region of the detector, while the outer region is used primarily to constrain the background extrapolation to the detector center. A fiducial volume may be defined or tuned to demark these regions, leading to ε_{act} = 10–60% depending on the enrichment level and the radioactivity of the structural materials. The background in that fiducial volume is then treated as an effective parameter, tuned to reproduce the half-life sensitivities reported by the experiments. The most sensitive energy region of interest varies, depending on the background level and whether the ^{214}Bi gamma line is resolved. Containment efficiencies are $\varepsilon_{act} \sim 100\%$ for liquid Xe TPCs after the effective fiducial volume cut, while they are typically 70–80% for gaseous detectors.

The most sensitive Xe TPC experiment to date was EXO-200 (Auger et al., 2012), which used liquid-phase enriched Xe, with 161 kg of ^{136}Xe. The TPC employed two drift regions with a common cathode at the detector center. The ionization was read out via crossed wire planes at the anodes. The prompt scintillation light was read out by large-area avalanche photodiodes. The combined signal achieved an energy resolution of $\sigma = 28$ keV at $Q_{\beta\beta}$ (Anton et al., 2019), or 31 keV when averaged over

the full dataset. Backgrounds and field non-uniformity near the detector edges required fiducialization, restricting the analysis to the innermost 75 kg of Xe. An extensive screening campaign (Leonard et al., 2008, 2017) and a sophisticated analysis incorporating topological background discrimination (Delaquis et al., 2018) led to an averaged background level within the fiducial volume of $1.8 \cdot 10^{-3}$ events/(keV·kg·yr), corresponding to $\mathcal{B}$ =4.7·10^{-2} events/(mol·yr), dominated by the ^{214}Bi gamma line originating from ^{238}U chain decays outside of the Xe volume. The experiment reported an ultimate limit for $0\nu\beta\beta$ decay of $T_{1/2} > 3.5 \cdot 10^{25}$ yr at 90% C.L. with a sensitivity for limit setting of $T_{1/2} = 5.0 \cdot 10^{25}$ yr (Anton et al., 2019). Our counting analysis described in Sec. V.E.2 reproduces the EXO-200 limit sensitivity with no tuning required.

nEXO (Adhikari et al., 2022; Al Kharusi et al., 2018) builds on EXO-200's technology and aims at using 5 tons of Xe enriched to 90% in ^{136}Xe. The TPC design features one monolithic drift volume with ionization read out by silica tiles patterned with metallic electrode strips, and scintillation detection by an array of VUV-sensitive silicon photomultipliers on the TPC walls behind the field-shaping grid, yielding an energy resolution of $\sigma = 20$ keV. The effective background index that reproduces nEXO's published discovery sensitivity is $2.1 \cdot 10^{-6}$ events/(keV·kg·yr), corresponding to $\mathcal{B} = 4.0 \cdot 10^{-5}$ events/(mol·yr), a factor of $\sim$1000 improvement over EXO-200. nEXO is expected to achieve a discovery sensitivity of $T_{1/2} = 7.4 \cdot 10^{27}$ yr after 10 years of live time.

NEXT (Granena et al., 2009; Nygren, 2009) implements a high-pressure gaseous Xe TPC equipped with an EL region. Tracking information is obtained from a SiPM array at the anode, while PMTs at the cathode provide optimal energy resolution. NEXT-White (Monrabal et al., 2018), a proof-of-principle detector with 5 kg of Xe at 10 bar, demonstrated an energy resolution of $\sigma = 10$ keV at $Q_{\beta\beta}$ (Renner et al., 2019), and tracking performance capable of discriminating single and double electron track events, retaining 57% of signal events while rejecting background by a factor of 27 (Simón et al., 2020). A second stage, NEXT-100 (Alvarez et al., 2012; Martín-Albo et al., 2016), with a pressure of 15 bar and containing 87 kg of ^{136}Xe, is currently under construction. The NEXT-100 projected background is dominated by remnant events from U/Th in the PMTs and other detector components, giving a background index of $4 \cdot 10^{-4}$ events/(keV·kg·yr), or $\mathcal{B} = 5.9 \cdot 10^{-3}$ events/(mol·yr). NEXT-HD (Adams et al., 2021a), a concept for a future ton-scale phase of NEXT, is a symmetric TPC with a common central cathode, large enough to accommodate a full ton of ^{136}Xe in the form of enriched Xe gas at 15 bar. The design of NEXT-HD substitutes PMTs with an all-SiPM light readout at both TPC ends, using wavelength-shifting fibers to enhance

TABLE VI Specific parameters of Xe-TPC experiments: total mass, fractional isotopic abundance, phase, signal readout, effective background index in units of events per kg of mass in the fiducial volume, and the ratio R between the effective background index used for our sensitivity calculation and the mean background quoted by the experiments, when available. Values taken from Refs. (Adams *et al.*, 2021a; Adhikari *et al.*, 2022; Agostini *et al.*, 2020a; Akerib *et al.*, 2020; Al Kharusi *et al.*, 2018; Alvarez *et al.*, 2012; Anton *et al.*, 2019; Chen *et al.*, 2017; Martín-Albo *et al.*, 2016).

Experiment	m_{tot}	f_{iso}	Phase	Readout	Effective Background	R
	[kg]	[%]			$\left[\dfrac{\text{events}}{\text{keV}\cdot\text{kg}\cdot\text{yr}}\right]$	
EXO-200	161	81	liquid	LAPPDs + wires	$1.8 \cdot 10^{-3}$	1
nEXO	5109	90	liquid	electrode tiles + SiPM s	$2.1 \cdot 10^{-6}$	N/A
NEXT-100	97	90	gas	SiPMs + PMTs	$4.0 \cdot 10^{-4}$	1
NEXT-HD	1100	90	gas	SiPMs + PMTs	$4.0 \cdot 10^{-6}$	1
PandaX-III-200	200	90	gas	Micromegas	$1.0 \cdot 10^{-4}$	1
LZ-nat	7 000	9	dual-phase	PMTs	$1.1 \cdot 10^{-4}$	0.4
LZ-enr	7 000	90	dual-phase	PMTs	$1.1 \cdot 10^{-4}$	0.4
DARWIN	39 300	9	dual-phase	PMTs	$3.4 \cdot 10^{-6}$	0.85

light collection further. Gas additives to reduce diffusion are expected to enhance both the energy resolution and tracking resolution relative to NEXT-100. The expected reduction in background index by a factor of 100 thus leads to an even large reduction in sensitive background, predicted to be $\mathcal{B} = 4.0 \cdot 10^{-5}$ events/(mol· yr). NEXT-BOLD aims to take this concept one step further by instrumenting the NEXT-HD TPC with Ba tagging capability (Rivilla *et al.*, 2020), potentially achieving half-life sensitivity on the order of 10^{28} years.

Another experiment based on the high-pressure gas Xe TPC technique is PandaX-III-200 (Chen *et al.*, 2017). The initial phase uses 180 kg ^{136}Xe in a volume of enriched Xe gas at 10 bar, deployed in a symmetric TPC with a common cathode. In contrast to the all-photon-based readout pursued by NEXT, PandaX-III-200 exclusively relies on an ionization-only readout of just the drift electrons using the Micromegas detector technology, where a high-field region near the anode provides avalanche amplification. The expected energy resolution is $\sigma = 31\,$keV at $Q_{\beta\beta}$, while simulated topological discrimination based on track reconstruction predicts up to two orders-of-magnitude background reduction with 42% signal efficiency (Galan *et al.*, 2020). Backgrounds are dominated by U/Th contamination of the Micromegas readout plane. The total background index goal is 10^{-4} events/(keV·kg· yr), giving $\mathcal{B} = 3 \cdot 10^{-3}$ events/(mol· yr).

LZ (Akerib *et al.*, 2015) and DARWIN (Aalbers *et al.*, 2016) both employ dual-phase natural-Xe TPCs with EL readout to perform direct searches for WIMP Dark Matter. These detectors also have sensitivity to $0\nu\beta\beta$ decay even with natural Xe targets (Agostini *et al.*, 2020a; Akerib *et al.*, 2020). The instrumentation required for detection of the faint nuclear recoils from WIMPs naturally leads to higher external backgrounds than for a detector optimized for $0\nu\beta\beta$ decay. With 7 tons of Xe (640 kg ^{136}Xe) in the LZ inner

vessel and and 40 tons (3.6 tons ^{136}Xe) total in DARWIN, self-shielding reduces these background dramatically, but external ^{214}Bi still dominates in both experiments. Reproducing the LZ sensitivity requires an effective background index of $1.2 \cdot 10^{-4}$ events/(keV· kg· yr), giving $\mathcal{B}=1.7 \cdot 10^{-2}$ events/(mol· yr). A subsequent run with enriched Xe (90% ^{136}Xe) would have enhanced sensitivity. DARWIN's larger mass affords it a lower effective background index of $3.4 \cdot 10^{-6}$ events/(keV· kg· yr), or $\mathcal{B}=3.5 \cdot 10^{-4}$ events/(mol· yr), with ^{137}Xe β decays representing an important background contribution.

A summary of all TPCs significant experimental parameters is given in Tab. VI.

D. Large liquid scintillators

In what is perhaps the most successful departure from the "source = detector" paradigm followed by most $0\nu\beta\beta$-decay experiments, large liquid scintillators offer the advantage of dissolving or loading vast amounts of isotope into the most sensitive regions of some of the lowest-radioactivity experiments ever constructed. With typical mass-loading fractions on the few percent level, a kton-scale scintillator detector can reach ton-year exposures with relative ease. Energy depositions within the detector generate scintillation photons, which are detected by PMTs viewing the target volume as shown in Fig. 24. Event energy, position, and topology reconstruction is performed using the number, pattern, and timing of the detected photons. The position reconstruction is particularly important for these self-shielding detectors, whose inner volume has the lowest background and drives the sensitivity. The effective fiducial volume fractions range between $\varepsilon_{act} = 20\%$–80%, due to a combination of self-sheilding and whether the target isotope is spread through the whole scintillator volume or confined to its central part. Containment efficiencies are maximal in the
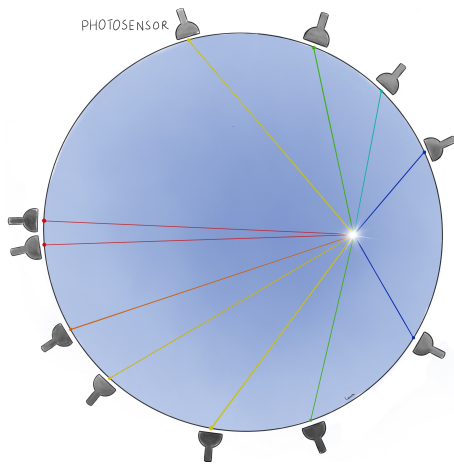
FIG. 24 Artistic illustration of a large liquid scintillator detector and its $0\nu\beta\beta$-decay detection concept. The position of an event can be reconstructed through the time of flight of the scintillation photons. Image courtesy of L. Manenti.

fiducial volume ($\varepsilon_{cont} = 100\%$).

The challenge for these detectors lies in their limited energy resolution due to the relatively low number of scintillation photons produced by energy depositions at $Q_{\beta\beta}$. Events due to $2\nu\beta\beta$ decay pose a problematic background in the energy region of interest, and the extraction of a $0\nu\beta\beta$-decay signal relies on an energy spectral analysis sensitive to distortion at the end-point of the $2\nu\beta\beta$-decay energy distribution. Such an analysis requires a precise understanding of the detector response and energy reconstruction systematic effects. The $0\nu\beta\beta$-decay background reduces the optimal energy region of interest to values above $Q_{\beta\beta}$, with an effective 40–60% loss in detection efficiency. Like for the case of Xe TPCs, an effective background index for the fiducial volume was tuned to reproduce published experimental sensitivities.

The presence of the large mass of liquid scintillator also increases the prevalence of solar neutrino backgrounds and cosmogenic activation products. The latter includes in particular ^{10}C which is readily generated in organic liquid scintillators. Vetoing schemes based on proximity to muon tracks and the detection of neutron capture gammas in delayed time coincidence can reduce these background contributions by roughly an order of magnitude at the cost of some exposure loss ($\varepsilon_{mva} = 97\%$, see, e.g., Gando et al. (2016)).

KamLAND-Zen (KLZ) is an upgrade of the Kam-LAND apparatus (Eguchi et al., 2003) tailored to the search of $0\nu\beta\beta$ decay: a nylon balloon is deployed in the active detector volume and filled with liquid scintillator in which enriched Xe has been dissolved. A successful first phase deployment, KamLAND-Zen 400 (KLZ-400) with up to 340 kg of ^{136}Xe, led to the strongest half-life limits for its time despite an unexpected background likely originating from fallout from the Fukushima nu-

clear disaster (Gando et al., 2013, 2016). The second phase, KamLAND-Zen 800 (KLZ-800), is currently running with $\sim$680 kg of ^{136}Xe redeployed in a larger, cleaner balloon. With just 1.6 years of data KLZ-800 produced a world-leading half-life limit $T_{1/2} > 2.3 \cdot 10^{26}$ yr at 90% C.L. with a limit setting sensitivity of $T_{1/2} = 1.3 \cdot 10^{26}$ yr (Abe et al., 2022). The background measured in the KLZ-800 fiducial volume corresponds to $\mathcal{B} = 5.5 \cdot 10^{-3}$ events/(mol· yr). The KLZ-800 sensitivity is well-reproduced by the background-dominated approximation. The KamLAND-Zen collaboration is already preparing a follow-on phase, KamLAND2-Zen (KL2Z) (Shirai, 2017), in which $\sim$1 ton of ^{136}Xe will be deployed. A major upgrade of the experiment is conceived for KL2Z to improve the energy resolution at $Q_{\beta\beta}$ from $\sigma =$114 keV to 60 keV. The upgrade includes the installation of new light concentrators and PMTs with higher quantum efficiency as well as purer liquid scintillator. A sensitive background reduction by a factor 20 over KLZ-800 is expected for KL2Z, afforded primarily by the envisioned improvement in the detector resolution. An effective background that is a factor of 0.45 times the predicted background reproduces the expected KL2Z sensitivity.

SNO+ (Albanese et al., 2021; Andringa et al., 2016) is a follow up of the SNO experiment building on the SNO infrastructure (Boger et al., 2000). It is a multi-purpose neutrino experiment, with a ^{130}Te-based $0\nu\beta\beta$-decay search as one of its main physics goals. SNO's acrylic sphere will be filled with $\sim$780 tons of liquid scintillator, loaded with tellurium, with the surrounding SNO cavern instrumented as a water Cherenkov active veto. As of the time of writing, SNO+ is filled with liquid scintillator and taking data, with Te loading scheduled to commence soon. A multi-staged approach is foreseen (Grant, 2020). Initially $\sim$1.3 tons of ^{130}Te (0.5% ^{nat}Te loading) will be used and an energy resolution of $\sigma =$80 keV is expected. The predicted background corresponds to $\mathcal{B} = 7.8 \cdot 10^{-3}$ events/(mol· yr), and is dominated by ^{8}B solar neutrino elastic scatters. The goal of a subsequent phase is to increase the ^{130}Te mass to 6.6 tons (2.5% ^{nat}Te loading) and improve the energy resolution to 57 keV. This is achievable thanks to an improvement of the light yield to 800 pe/MeV (Klein, 2017). The predicted background corresponds to $\mathcal{B} = 5.7 \cdot 10^{-3}$ events/(mol· yr).

A summary of the relevant parameters for KamLAND-Zen and SNO+ is given in Tab. VII.

E. Cryogenic calorimeters

Cryogenic calorimeters, often referred to as bolometers, are one of the most versatile types of detectors for rare events searches. Their first development dates back to the 1980s and, since then, they have been successfully employed for $0\nu\beta\beta$-decay and dark-matter searches (Brofferio and Dell'Oro, 2018). Bolometers con-

TABLE VII Specific parameters for liquid scintillator experiments: isotope, total mass, fractional isotopic abundance, fractional mass of the loaded material, effective background per kg (of isotope) in the fiducial volume, and the ratio R of that to the mean background in the fiducial volume. Values taken from Refs. (Albanese *et al.*, 2021; Andringa *et al.*, 2016; Gando *et al.*, 2016; Gando, 2020; Shirai, 2017).

Experiment	Isotope	m_{tot} [kg]	f_{iso}	Loading [%wt.]	Effective Background $\left[\frac{\text{events}}{\text{keV}\cdot\text{kg}\cdot\text{yr}}\right]$	R
KLZ-400	^{136}Xe	378	0.91	2.9	$1.8 \cdot 10^{-4}$	1
KLZ-800	^{136}Xe	745	0.91	3.0	$1.1 \cdot 10^{-4}$	1
KL2Z	^{136}Xe	1000	0.91	2.7	$1.1 \cdot 10^{-5}$	0.45
SNO+I	^{130}Te	3825	0.91	0.5	$2.5 \cdot 10^{-4}$	1
SNO+II	^{130}Te	19125	0.91	2.5	$2.3 \cdot 10^{-4}$	1
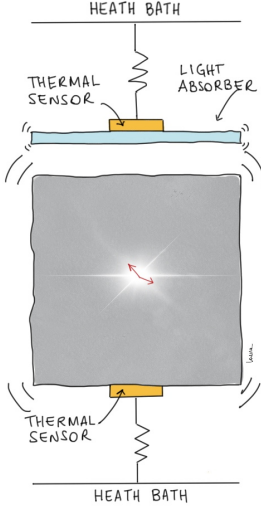
FIG. 25 Artistic illustration of a cryogenic calorimeter and its $0\nu\beta\beta$-decay detection concept. Phonon and scintillation light signals are read-out through superconductive thermal sensors. Image courtesy of L. Manenti.

sist of crystals coupled to thermal sensors measuring the phonons induced by particles impinging on the crystal lattice, or the heat induced by phonon recombination (see Fig. 25). Typically the crystals used in $0\nu\beta\beta$-decay experiments have masses between 0.2 and 0.8 kg and are operated at 10–20 mK. Their energy resolutions are typically in the range $\sigma = 2$–10 keV, and the containment efficiency varies between 70–90%, depending on the crystal type and size.

Bolometers have an active volume fraction of 100%, which makes them sensitive to background due to α-decaying isotopes on their surfaces, or on the surfaces of nearby materials. In scintillating crystals, e.g., ZnSe or Li$_2$MoO$_4$, it is possible to discriminate α from β/γ particles by their different light yields. The scintillation light is detected by a second bolometer placed in front of the crystal and consisting of a Ge or Si wafer instrumented with the NTD, TES or KID sensors discussed in Sec. V.B.2. Alternatively, surface events can be discrim-

TABLE VIII Specific parameters for cryogenic calorimeter experiments: crystal molecule, total mass, fractional isotopic abundance, and background per kg of total mass. All experiments except CUORE use a combined readout of heat and scintillation light and have an NTD readout, except for AMoRE-II, which uses MMCs. Values taken from Refs. (Adams *et al.*, 2022; Armengaud *et al.*, 2021; Armstrong *et al.*, 2019; Azzolini *et al.*, 2019c; Bandac *et al.*, 2020; Lee, 2020).

Experiment	Crystal	m_{tot} [kg]	f_{iso} [%]	Background $\left[\frac{\text{events}}{\text{keV}\cdot\text{kg}\cdot\text{yr}}\right]$
CUORE	$^{\text{nat}}$TeO$_2$	742	34[a]	$1.5 \cdot 10^{-2}$
CUPID-0	Zn$^{\text{enr}}$Se	9.65	96	$3.5 \cdot 10^{-3}$
CUPID-Mo	Li$_2$$^{\text{enr}}MoO_4$	4.16	97	$4.7 \cdot 10^{-3}$
CROSS	Li$_2$$^{\text{enr}}MoO_4$	8.96	98	$1.0 \cdot 10^{-4}$
CUPID	Li$_2$$^{\text{enr}}MoO_4$	472	$\geq$95	$1.0 \cdot 10^{-4}$
AMoRE-II	Li$_2$$^{\text{enr}}MoO_4$	200	96	$1.0 \cdot 10^{-4}$

[a] CUORE is using natural tellurium.

inated from bulk events via pulse-shape analysis using crystals with an Al-film coating, as is being pursued by CROSS (Bandac *et al.*, 2020). In such devices, a ionizing particle interacting close enough to the coated surface will create quasi-particles that can be trapped in the superconductive Al layer for $O(1)$ ms (Bandac *et al.*, 2020). In all cases, the $0\nu\beta\beta$-decay tagging efficiency is $\varepsilon_{\text{mva}} \sim 90\%$.

Bolometric experiments feature high granularity, providing good suppression of the external γ backgrounds via the rejection of events releasing energy in multiple crystals. The full absorption of phonons yields response times that can be as long as 0.1 s with NTD sensors. Hence, the probability of having two $2\nu\beta\beta$ decays piling up is not negligible, especially when considering large crystals and isotopes with relatively short $2\nu\beta\beta$-decay half-life. Techniques to mitigate this potential background are currently being developed.

At present, the largest bolometric experiment is CUORE, operating $\sim$750 kg of TeO$_2$ crystals with natural isotopic composition (giving 206 kg ^{130}Te) in a custom cryogen-free dilution refrigerator (Alduino *et al.*,

2019). The TeO_2 crystal detector technology is reviewed in (Brofferio *et al.*, 2019). CUORE has demonstrated the feasibility of a ton-scale bolometric experiment, achieving an energy resolution of $\sigma = 3.2\,keV$. With a background of $1.5 \cdot 10^{-2}$ events/(keV· kg· yr), corresponding to a sensitive background $\mathcal{B} = 9.1 \cdot 10^{-2}$ events/(mol· yr), CUORE has set the most stringent constraints on $0\nu\beta\beta$ decay of ^{130}Te: $T_{1/2} > 2.2 \cdot 10^{25}$ yr at 90% C.L., with an exclusion sensitivity of $T_{1/2} = 2.8 \cdot 10^{25}$ yr (Adams *et al.*, 2022).

In the coming years, a strong boost in sensitivity is expected with CUPID (Armstrong *et al.*, 2019), which will deploy enriched crystals with particle identification capabilities in the CUORE cryostat. Several projects have been realized to identify the optimal crystal and light detector technology. Among these, CUPID-0 operated abut 5 kg of ^{82}Se in form of enriched ZnSe scintillating crystals, demonstrating a background of $3.5^{+1.0}_{-0.9} \cdot 10^{-3}$ events/(keV· kg· yr) (Azzolini *et al.*, 2019a,c), a factor 3.3 times lower than that of CUORE. A limitation of ZnSe crystals is their relatively poor energy resolution ($\sigma = 8.5\,keV$) due to sub-optimal crystal purity. In parallel, CUPID-Mo (Armengaud *et al.*, 2020b) has collected data with 20 enriched Li_2MoO_4 crystals for a total isotope mass of 2.3 kg. CUPID-Mo has demonstrated a resolution of $\sigma = 3.2\,keV$, and >99.9% α rejection with >99.9% acceptance of β/γ events (Armengaud *et al.*, 2020b, 2021; Welliver, 2021). Finally, the CROSS collaboration is using Al-coated Li_2MoO_4 crystals to extensively investigate their surface/bulk discrimination capabilities, and is planning to deploy 32 enriched Li_2MoO_4 crystals for a total isotope mass of 4.7 kg. The goal of the CROSS demonstrator is to reach a background $< 10^{-4}$ events/(keV· kg· yr) (Bandac *et al.*, 2020), which could boost the sensitiviy of bolometric experiments beyond the IO region.

CUPID's baseline design is based on 250 kg of $Li_2^{enr}MoO_4$ instrumented with light readout in the CUORE cryostat. Assuming achieved crystal quality and background levels, and the readout of scintillation light for particle discrimination, CUPID projects a background of 10^{-4} events/(keV· kg· yr), more than a factor 100 lower than CUORE. With a sensitive background $\mathcal{B} = 2.3 \cdot 10^{-4}$ events/(mol· yr),CUPID will reach a $1.1 \cdot 10^{27}$ yr discovery sensitivity with 10 yr of live time. With additional purification of the crystal material, the use of light detectors instrumented with lower threshold and higher bandwidth sensors (e.g., TES), and the development of pulse shape discrimination techniques, CUPID can achieve a background of $2 \cdot 10^{-5}$ events/(keV· kg· yr). Ultimately, a background level of $5 \cdot 10^{-6}$ events/(keV· kg· yr) is conceivable with the deployment of 1 ton of isotope in a new cryostat featuring an active cryogenic shield (Nones, 2021).

In parallel, the AMoRE collaboration has demonstrated the feasibility of using scintillating crystals with an MMC readout both on the phonon and photon chan-

nels for large experiments (Lee, 2020). The first phase of the experiment, AMoRE-I, is currently collecting data with a mix of ^{100}Mo-enriched Li_2MoO_4 and $CaMoO_4$ crystals for a total mass of $\sim$6 kg, and is characterized by a background $< 10^{-3}$ events/(keV· kg· yr). The next phase, AMoRE-II, will make use of 200 kg of $Li_2^{enr}MoO_4$ crystals, for an isotope mass of 110 kg. With a target background index of $< 10^{-4}$ events/(keV· kg· yr), corresponding to a sensitive background $\mathcal{B} = 2.2 \cdot 10^{-4}$ events/(mol· yr), AMoRE-II will reach a discovery sensitivity of $6.7 \cdot 10^{25}$ yr with 10 yr of data.

F. Tracking calorimeters

Tracking calorimeters are the only actively-pursued detection concept in which the $0\nu\beta\beta$-decay isotope material is decoupled from the detector. The source is in the form of a foil sandwiched by drift chambers with an applied magnetic field for discriminating electrons and positrons, beyond which lies calorimeters for measuring energy (see Fig. 26. Due to the requirement that the foils be very thin to minimize energy losses prior to the electrons exiting the source, scaling up the isotope mass is particularly challenging for this technology. However, tracking calorimetry has the unique capability of precisely measuring properties of the decay kinematics such as single-β energy spectra and opening angle distributions, which are connected to the Lorentz structure of the mechanism mediating the decay (Ali *et al.*, 2007; Arnold *et al.*, 2010).

The most sensitive tracking calorimeter to date was NEMO-3, which set competitive constraints on a variety of target isotopes, particularly ^{100}Mo (Arnold *et al.*, 2015). Its successor, SuperNEMO (Piquemal, 2006), builds on the same design principles and is currently in preparation. The SuperNEMO project is divided in two phases: a SuperNEMO Demonstrator (SuperNEMO-D) consisting of one module with 7 kg of ^{82}Se, and a full-scale experiment consisting of multiple modules for a total ^{82}Se mass of 100 kg. Future phases with different isotopes are still open.

The energy resolution of a single calorimeter was $\sigma \sim 100\,keV$ for NEMO-3, and is expected to be $\sim$50 keV for SuperNEMO thanks to improved light collection and the use of PMTs with higher quantum efficiency. Some fraction of the energy emitted in a $\beta\beta$ decay event is inevitably released in the passive source foil: as a result, the $0\nu\beta\beta$-decay signature is peaked below $Q_{\beta\beta}$, and features a low-energy tail, significantly overlapping with the $2\nu\beta\beta$-decay continuum spectrum. The optimal ROI strongly depends on the expected number of background events at the end of the data taking: it corresponds to $[-1.6,1.1]\,\sigma$ for NEMO-3, and to a $\sim$4 σ range around the degraded peak below $Q_{\beta\beta}$ for SuperNEMO and SuperNEMO Demonstrator.

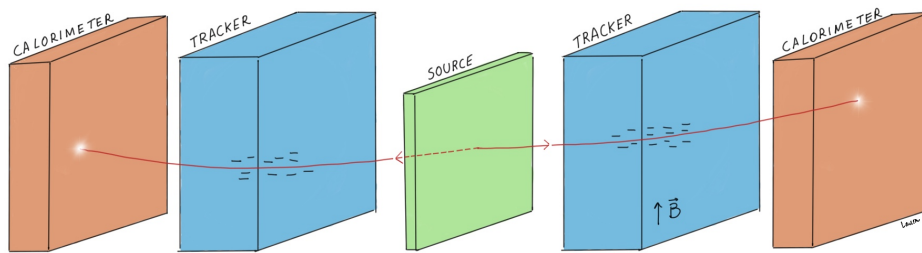In tracking calorimeters, the reconstructed event kine-

FIG. 26 Artistic illustration of a tracking-calorimeter detector and its $0\nu\beta\beta$-decay detection concept. The charge, momentum, and energy of the particles ejected by the source is measured through a combination of magnetic-field trackers and calorimeters. Image courtesy of L. Manenti.

matics can be used to suppress most backgrounds, at the price of a lower signal efficiency. This was 11% in NEMO-3, and is expected to reach 28% in SuperNEMO thanks to the improved spacial resolution of the tracker. The most significant residual backgrounds come from ^{222}Rn in the tracker, and the β decays of ^{208}Tl and ^{214}Bi on the source foil. SuperNEMO aims to suppress the last two by a factor 50 and 30, respectively, and has partially achieved it so far (Calvez, 2017; Povinec, 2017). In our calculation, we use the design value for SuperNEMO of $9.8 \cdot 10^{-5}$ events/(keV$\cdot$kg$\cdot$yr), and the experimentally measured contaminations for the Demonstrator (Calvez, 2017), giving $\mathcal{B} = 5.3 \cdot 10^{-3}$ events/(mol$\cdot$yr). Given the particular shape of the $0\nu\beta\beta$- and $2\nu\beta\beta$-energy distributions, a spectral fit has higher sensitivity compared to a simple counting analysis. By reducing the background to 20%, we match the sensitivity quoted by the collaboration, which corresponds to a 10-yr discovery sensitivity of $9 \cdot 10^{24}$ and $8 \cdot 10^{25}$ yr for SuperNEMO-D and SuperNEMO, respectively.

G. Other detector concepts

Several additional projects exist that use technologies other than the ones discussed so far. Some technologies have already lead to proof-of-principle experiments, which however are not yet competitive in terms of sensitivity. In most cases, the projects are still at an early R&D phase, and a significant effort is required to demonstrate that the underlying technology can be scaled to a $0\nu\beta\beta$-decay experiment capable of covering the inverted ordering region or beyond. In Tab. IX we list a selection of such projects appearing in the literature, highlighting their isotope of choice (where defined) and key features.

VII. PROSPECTS AND EXPECTATIONS

In this section we bring together our expectations from the theory and experimental landscape, and address some of the key questions related to $0\nu\beta\beta$ decay. Section VII.A

summarizes near-term prospects and how ongoing efforts are going to shape the field. In Sec. VII.B, we discuss what we would learn from a discovery under different assumptions on the underlying theory framework. Section VII.C addresses the question of how likely a discovery is in the next round of experiments, also in terms of nuclear and particle theory inputs. Sec. VII.D reviews other discovery opportunities of $0\nu\beta\beta$-decay experiments not related to the lepton-number violating $0\nu\beta\beta$ decay. Finally, Sec. VII.E speculates on the neutrino's role as a possible catalyst for the next paradigm shift in fundamental physics, which may lead us to a new theory beyond the Standard Model of particle physics.

This section aims at addressing in a comprehensive way the most important questions of experts and nonexperts alike. Its content is largely covered by the previous sections, but it is here presented stressing the connections between theory and experiment, as well as between particle and nuclear theory. We refer the reader to the previous sections for more information and detailed lists of references.

A. Where are we heading?

1. Experiment

In the next decade, several experiments will be constructed to search for $0\nu\beta\beta$ decay at new uncharted half-life scales using multiple nuclei and different technologies. Three scenarios can unfold, depending on the half-life of the process, and whether the decay exists at all.

The signal half-life could be just beyond current constraints, at a scale of 10^{25}–10^{26} years, depending on the isotope. In this first scenario, hundreds of $0\nu\beta\beta$-decay events will be observed in each next-generation experiment. The half-life will be measured with statistical uncertainty at the level of $\sim$10%. Systematic uncertainties in $0\nu\beta\beta$-decay experiments are typically $\lesssim$10%, and will not limit the accuracy of the measurement in this strong signal scenario. These first measurements will likely be followed by a second round of experiments, not devel-

TABLE IX Other detector concepts. Existing experiments are marked with a dagger.

Project	Isotope(s)	Detector technology, main features, and references
CANDLES[†]	^{48}Ca	Array of scintillator crystals suspended in a volume of liquid scintillator. Possible operation as cryogenic calorimeters. Ajimura *et al.* (2021) and Yoshida *et al.* (2009)
COBRA[†]	^{70}Zn ^{114,116}Cd ^{128,130}Te	CdZnTe semiconductor detector array. Room temperature; multi-isotope; high granularity. Arling *et al.* (2021); Ebert *et al.* (2016a,b); and Zuber (2001)
Selena	^{82}Se	Amorphous ^{enr}Se high resolution, high-granularity CMOS detector array. 3D track reconstruction ($O(10\mu m)$ resolution); room temperature; minimal shielding. Chavarria *et al.* (2017)
NνDEx	^{82}Se	High-pressure gaseous ^{82}SeF$_6$ ion-imaging TPC. $\lesssim 1\%$ energy resolution; precise signal topology; possible multi-isotope. Mei *et al.* (2020) and Nygren *et al.* (2018)
R2D2	^{136}Xe	Spherical TPC. Single readout channel; inexpensive infrastructure. Bouet *et al.* (2021)
AXEL	^{136}Xe	High-pressure TPC operated in proportional scintillation mode. High energy resolution; possible positive ion detection. Obara *et al.* (2020)
JUNO	—	Isotope loaded liquid scintillator. 20 ktons of scintillator; multi-isotope; multi-purpose. Abusleme *et al.* (2021) and Zhao *et al.* (2017)
NuDot	—	Liquid scintillator with quantum dots or perovskites as wavelength shifter for Cherenkov light. Discriminate directional backgrounds; multi-isotope. Aberle *et al.* (2013); Gooding *et al.* (2018); Graham *et al.* (2019); and Winslow and Simpson (2012)
ZICOS	^{96}Zr	Zr-loaded liquid scintillator. Topology and particle discrimination via Cherenkov light readout. Fukuda (2016) and Fukuda *et al.* (2020)
THEIA	—	Water-based loaded liquid scintillator with Cherenkov light readout. Topology and particle discrimination; multi-isotope; multi-purpose; 25 ktons of water. Askins *et al.* (2020)
LiquidO	—	Opaque isotope-loaded liquid scintillator with wavelength shifting fibers for event topology. Room temperature; multi-isotope; multi-purpose. Buck *et al.* (2019) and Cabrera *et al.* (2019)

oped to maximize the discovery sensitivity, but capable of measuring properties of the decay kinematics, such as single-β energy spectra and opening angle distributions connected to the Lorentz structure of the mediating mechanism(s).

In the second scenario, the $0\nu\beta\beta$-decay half-life is above the current limits, but still within the reach of upcoming searches (i.e., $T_{1/2} \approx 10^{26}$–10^{28} years). For this case, only tens of events or fewer would be expected. Measurements of the half-life will hence be affected by large statistical uncertainties at the level of 30% for 10 events, or even 100% for a couple of events. If the signal is at the edge of the detection sensitivities, only some of the experiments may observe a signal, while others would set a limit. Such an inconclusive situation would require further discovery-style experimental investigation to confirm the discovery claims.

It is also possible that the $0\nu\beta\beta$-decay half-life is too small to be discovered by next-generation experiments (i.e., $T_{1/2} > 10^{28}$ years), or the process does not exist at all. In this case, the forthcoming searches will push the half-life constraints by two order of magnitudes, excluding a significant part of the parameter space of interest and ruling out specific models. Further technological developments will then be needed to realize affordable next-to-next generation experiments with scaled sensitivity.

2. Nuclear theory

The extraction of beyond-Standard-Model physics information from half-life measurements relies on NME calculations, which currently differ from each other by about a factor of three. NME calculations might also all be affected by systematic offsets. Promising developments in ab-initio methods and chiral EFT will reduce these uncertainties. Calculations may still disagree due to the different approximations made, but systematic effects ("g_A quenching", the short-range NME contribution, etc.) are expected to be under better control.

As the decay rate depends on the NME squared, nuclear theory uncertainties will likely remain larger than experimental statistical or systematic uncertainties on the half-life, representing the main limitation in the interpretation of future results. These uncertainties will be smaller in nuclei with simpler nuclear structure for which calculations are more robust: an ideal example is ^{48}Ca. Among the most interesting isotopes, NMEs would probably be less reliable for nuclei with more complex structure, such as ^{100}Mo and ^{150}Nd.

NMEs for other beyond-Standard-Model mechanisms will likely carry similar uncertainties as for light neutrino exchange. Calculations of these matrix elements do not pose different challenges, as even light neutrino exchange has a short-range component. Nonetheless, a careful treatment of short-range physics is probably more relevant in these scenarios, where $0\nu\beta\beta$ decay is usually mediated by the exchange of heavy particles.

3. Particle theory

At present, we lack reliable theory predictions for the $0\nu\beta\beta$-decay rate, the origin of the matter-antimatter asymmetry, and the neutrino mass values. A large number of beyond-Standard-Model theories have been proposed, but none can be tested with available data, and might not be testable even considering next-decade experiments. We neither have a model for lepton number violation nor a theory of lepton masses, and its establishment does not seem close. From this point of view, $0\nu\beta\beta$-decay searches are among the most promising sectors to guide future theory developments, and, vice versa, the searches could benefit from theory breakthroughs.

Despite the parameter space broadness, we can identify clear milestones for the experimental program. The Holy Grail for next-generation experiments is to reach the bottom of the inverted ordering parameter space, i.e., $m_{\beta\beta} = 18.4 \pm 1.3\,\mathrm{meV}$. This natural goalpost was immediately identified after the discovery of neutrino oscillations, boosting enormously the community's efforts.

We propose $m_{\beta\beta} \approx 8 - 10\,\mathrm{meV}$ as the next target for the field. As discussed in Sec. III.D.4, there is an accumulation of theoretical motivation to explore $m_{\beta\beta}$ values at this mass scale, which corresponds to the mass scale measured in solar neutrino oscillations ($\sqrt{\Delta m_{\mathrm{sol}}^2} = 8.6 \pm 0.1\,\mathrm{meV}$), and which is pointed to by classes of models focusing on the coarse structure of the mass matrix ($m_{\beta\beta} \approx \sqrt{\Delta m_{\mathrm{atm}}^2} \times \theta_{\mathrm{C}} \approx 10\,\mathrm{meV}$). This scale is interesting also from the experimental point of view: it is almost in the middle of the parameter space remaining after reaching the bottom of the inverted ordering, and can constitute a challenging, and yet conceivable goal for the next-to-next generation of $0\nu\beta\beta$-decay experiments. It is also the vicinity of the minimum that would be imposed on $m_{\beta\beta}$ by cosmological observations if Σ is measured to be just below its current upper bounds.

An ultimate goal would be to reach the floor of the normal ordering parameter space for vanishing m_1, $m_{\beta\beta} \sim |U_{e2}^2|\sqrt{\Delta m_{12}^2} - |U_{e3}^2|\sqrt{\Delta m_{32}^2} = 1.5\,\mathrm{meV}$. Barring flavor symmetries or strongly destructive interference with alternative exchange mechanisms that would force $m_{\beta\beta}$ to be vanishingly small, experiments with sensitivity to this normal-ordering floor would be virtually guaranteed to detect $0\nu\beta\beta$ decay if the Standard Model neutrino is a (dominantly) Majorana particle. Quasi-background-free kiloton experiments would be needed for this endeavor.

B. What would we learn from a discovery?

1. Model-independent consequences

Regardless of the mechanism mediating the decay, and of the uncertainties in the NMEs, a $0\nu\beta\beta$-decay observation would constitute the discovery in a laboratory experiment of a process that creates matter without creating antimatter. This "Little Bang" would prove that lepton number is not a conserved quantum number, and that neutrinos can transform into antineutrinos.

The violation of lepton number is directly observable in $0\nu\beta\beta$ decay, as two new leptons are created without the creation of any antiparticles. The possibility for a neutrino to transform into an antineutrino and vice versa would be proven indirectly. The $0\nu\beta\beta$ decay operator, together with quantum fluctuations, provides a non-zero neutrino-antineutrino transformation channel. However, in the absence of precise theory, its size cannot be predicted. From this point of view, an observation of $0\nu\beta\beta$ decay guarantees only that the Majorana mass is not null. Although it is not favored by the best-motivated models, one cannot rule out the possibility that its value is so small that it does not have any practical consequence. In this case, the neutrino would phenomenologically behave as a Dirac particle, and theory inputs would still be needed to connect $0\nu\beta\beta$ decay with the origin of neutrino masses.

2. Model-dependent consequences

Experiments measure the decay half-life, and NMEs are needed to connect it with the underlying beyond-Standard-Model mechanism. Multiple mechanisms can contribute to the $0\nu\beta\beta$-decay rate, which is proportional to the squared sum of amplitudes for all contributions. While both constructive and destructive interference are possible, a complete cancellation between unrelated mechanisms would require fine-tuned models.

Half-life measurements or bounds on different nuclei provide information on the underlying mechanism. For instance, measuring a half-life of 10^{27} years for ^{76}Ge would imply an expected ^{100}Mo half-life of $(1–3)\times10^{26}$ years if the decay is dominated by the exchange of light neutrinos. Likewise, similar half-life ranges will be predicted for the decay of other isotopes, and also for $0\nu\beta\beta$ decays to excited states. Incompatible half-life measurements could hence prove the existence of other mechanisms driving the decay (Deppisch and Pas, 2007; Gehman and Elliott, 2007; Gráf *et al.*, 2022; Simkovic *et al.*, 2010), but we will need precise estimates of uncertainties and correlations among NME values as recently discussed by Lisi and Marrone (2022) and Agostini *et al.* (2022b).

Measurements of the decay kinematics, which provide information on the Lorentz structure of the mediating mechanism, could conclusively rule-out classes of models or corroborate others. However these properties, as well as decays to excited states, are hard to measure. Experimental efforts beyond the next decade might be needed to collect this information if $0\nu\beta\beta$ decay is not discovered in experiments currently underway or starting soon.

3. Assuming light-neutrino exchange

If the decay is dominantly mediated by the exchange of light neutrinos, a comparison of the measured $m_{\beta\beta}$ with other data would provide new insights on neutrino physics. An observation of $m_{\beta\beta}$ below the minimum value allowed for the inverted ordering would imply that neutrino masses follow the normal ordering. Vice versa, should the inverted ordering be established by neutrino oscillation experiments, the non-observation of $0\nu\beta\beta$ decay in next-generation experiments would rule out Majorana neutrino masses.

Galaxy surveys and measurements of the cosmic microwave background will measure the value of the sum of the neutrino masses Σ in the next decade. Such a measurement would not only set an indirect upper bound on $m_{\beta\beta}$, but could also provide a lower bound. In particular, if Σ is measured to be above 70–80 meV, then $m_{\beta\beta}$ must be larger than $\sqrt{\Delta m_{12}^2}$, suggesting exciting discovery prospects for next-generation $0\nu\beta\beta$-decay searches.

In the near term, direct measurements of the effective kinematic neutrino mass m_β will explore a parameter space that is already excluded by $0\nu\beta\beta$ decay and cosmology. Thus a signal in those experiments, as well as other inconsistencies among neutrino data sets, would strongly point towards new physics beyond the 3-flavor neutrino oscillation and ΛCDM paradigm.

A measurement of $m_{\beta\beta}$ is currently the only conceivable way to obtain information on the values of the Majorana phases in the PMNS matrix, through a global analysis with oscillation measurements. However, only one relative phase can be measured. In addition, constraints on this relative phase can be extracted only if the experimental and nuclear theory uncertainties are strongly reduced below their current levels.

C. What are the odds of a discovery?

1. Model-independent considerations

A wide variety of particle theory models predict $0\nu\beta\beta$ decay. In most of them, unconstrained model parameters prevent a precise prediction of the decay rate. At best, these models provide a lower limit on the half-life, which sets a target for the experiments. The master formula in Eq. 19 connects the half-life to effective operators representing classes of models. In general, the half-life is proportional to the energy scale of the physics responsible for the decay, taken to some power which depends on the dimension of the operator. Operators above dimension 5 typically correspond to energy scales close to or beyond those explored by accelerator experiments. Figure 27 shows that accelerator and $0\nu\beta\beta$-decay experiments are complementary, and highlights how the reach of $0\nu\beta\beta$-decay searches can even exceed that of accelera-

tors for mechanisms other than light neutrino exchange. Note that, for reference, Fig. 27 just shows estimates for the most favored dimension-7 and dimension-9 operators. In general there can be order of magnitude differences for other operators suppressed e.g. by ratios of the nuclear-over-electroweak or chiral-over-nuclear scales.

We also indicate in Fig. 27 the energy scale of 100 TeV. This is a round value, suggestive of a possible ambitious target for next-generation colliders, but also a scale at which new flavor- and beyond-the-Standard-Model physics could manifest. Due to the large variety of possible decay mechanisms, one can consider $0\nu\beta\beta$ decay as a generic search for new physics, similar to accelerator ones, where the decay half-life plays the role of the collision energy. Increasing the half-life sensitivity implies exploring uncharted parameter space, where a discovery can happen at any time.

2. Assuming light-neutrino exchange

The $0\nu\beta\beta$-decay mechanism requiring the least new physics is light neutrino exchange, which only needs the Standard Model neutrino to be a massive Majorana particle. From a general point of view this is a particularly important mechanism, as it is the only one driven by a dimension-5 operator, i.e., the Weinberg operator. Further, it is uniquely connected to neutrino masses and is the dominant decay contribution in many models. In this scenario, the decay rate depends on the effective Majorana mass $m_{\beta\beta}$, which is a function of the neutrino oscillation parameters, Majorana phases, the lightest neutrino mass eigenstate, and the neutrino mass ordering.

The oscillation parameters have been measured precisely, nonetheless we have no information on the Majorana phases, and the mass ordering has not been determined. Although global fits show a preference for normal-ordered masses, we need to wait for the next decade experiments — i.e., JUNO, DUNE, and HyperKamiokande — with the requisite sensitivity to establish the neutrino mass ordering. These unknowns lead to uncertainties on the $m_{\beta\beta}$ value.

Assuming that neutrino masses follow the normal-ordering, any half-life value beyond the current upper limits is allowed. However, for the inverted-ordering case, the half-life has a lower bound corresponding to $m_{\beta\beta} = 18.4 \pm 1.3$ meV. Figure 28 shows the $m_{\beta\beta}$ sensitivity of future $0\nu\beta\beta$-decay experiments. The proposed experimental endeavor will fully test the inverted ordering parameter space, guaranteeing a discovery if this is the true scenario, and offering exciting discovery opportunities also assuming the normal ordering. In fact, since the current best bounds on $m_{\beta\beta}$ are $\sim$160–180 meV — assuming the least favorable NMEs — reaching 18.4 meV means probing 80%–90% of the currently allowed range for the normal ordering.
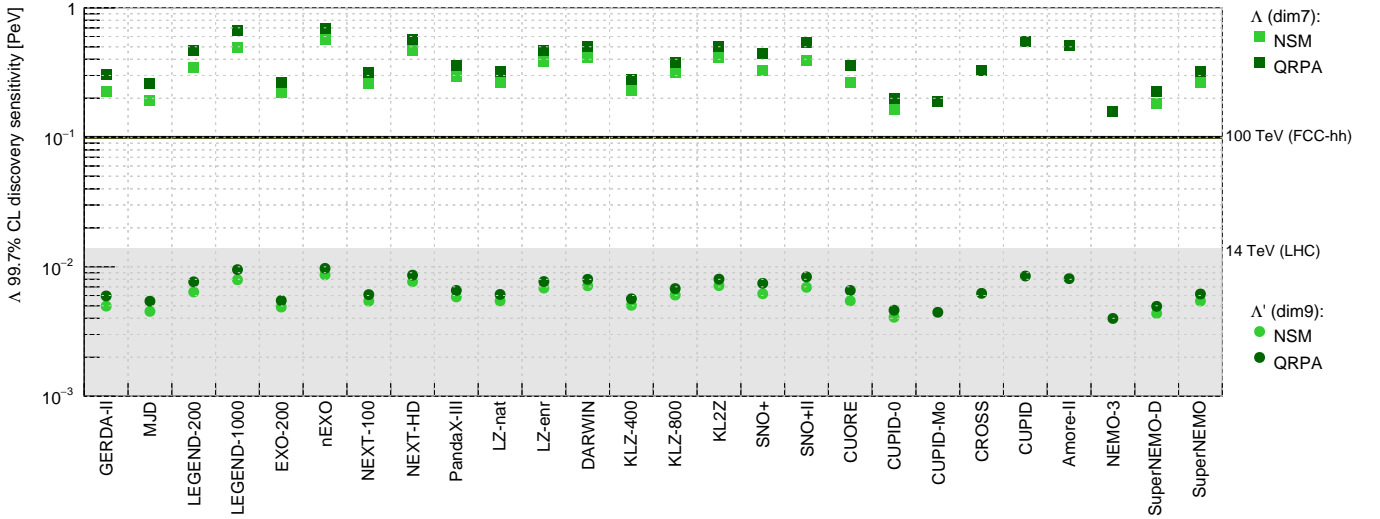
FIG. 27 Discovery sensitivities of current- and next-generation $0\nu\beta\beta$-decay experiments for exchange mechanisms dominated by effective operators of dimension 7 and 9. Values of Λ smaller than the marked values are tested at higher CL. The grey band corresponds roughly to the reach of modern accelerator experiments. The black line indicates an ambitious goal for future circular colliders such as the FCC-hh (Golling *et al.*, 2016).
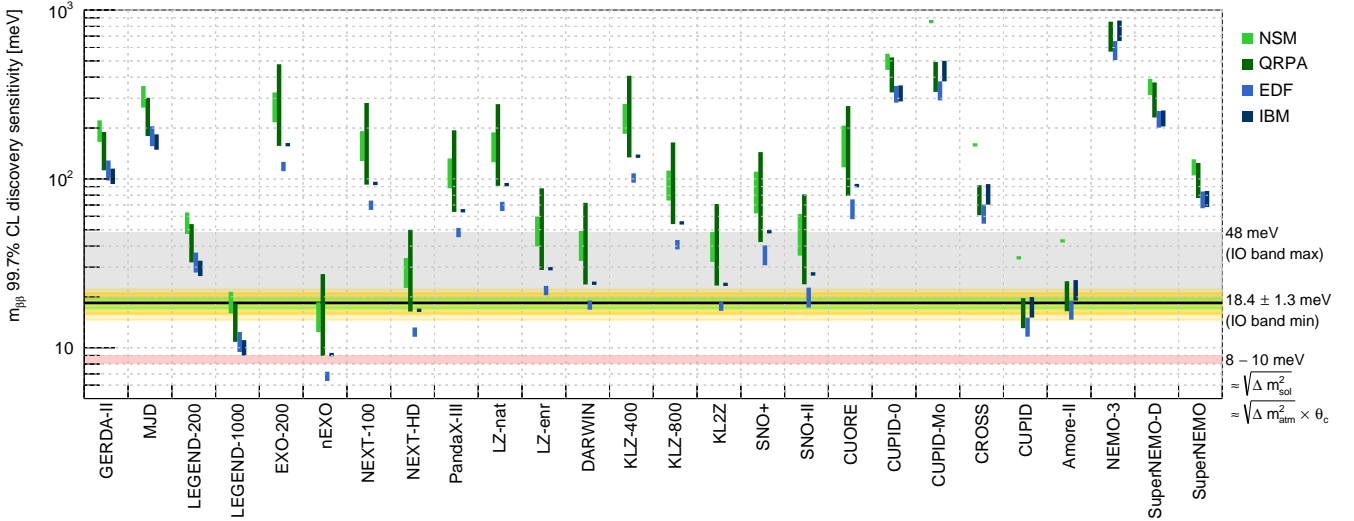

FIG. 28 Discovery sensitivities of current- and next-generation $0\nu\beta\beta$-decay experiments for exchange dominated by effective operators of dimension 5, i.e., the light neutrino exchange. Values of $m_{\beta\beta}$ larger than the marked values are tested at higher CL. The grey band indicates the range of $m_{\beta\beta}$ values for inverted-ordered neutrino masses and vanishing values of the lightest neutrino mass. The minimum value of $m_{\beta\beta}$ for the IO and its 1σ, 2σ, and 3σ uncertainty bands are indicated by the black, green, orange, and yellow bands, respectively. The red band between 8-10 meV indicates a future goal for $0\nu\beta\beta$decay experiments motivated by theoretical and experimental considerations (see discussion in Sec. III.D.4).

It should be mentioned that the parameter space for $m_{\beta\beta}$ might not be equiprobable. A theoretical prejudice for normal-ordered masses and vanishing m_1 would prefer smaller values of $m_{\beta\beta}$, for example. New symmetries predicting specific values for the Majorana phases or the existence of new particles such as sterile neutrinos could favor other corners of the parameter space, or even reduce or open it. In addition, Bayesian analyses assuming flat priors on the Majorana phases and a log-flat prior on Σ favor $m_{\beta\beta}$ values close to the current constraints, providing exciting prospects for the field regardless of the mass ordering.

3. Impact of nuclear physics

How likely a discovery is in the next decade strongly depends on systematic uncertainties on NME calculations. A broad effort to reduce uncertainties is ongoing within the nuclear theory community.

Ab initio approaches offer a promising avenue: by incorporating wider nuclear correlations and currents, measured β-decay rates can now be reproduced without the "quenching" required by previous studies — an ad hoc reduction of calculated matrix elements. The first ab initio matrix elements for $0\nu\beta\beta$-decay nuclei, supported by studies in lighter systems, indicate a mild suppression by tens of percent with respect to the lower values in Tab. I. This suggests that current $0\nu\beta\beta$-decay rate predictions may have to be reduced, but only moderately. Efforts are underway to improve the quality of the results, to include missing momentum-dependent operators — a key difference between β and $0\nu\beta\beta$ decay — and to extend them to heavier nuclei.

The recently recognized short-range term can contribute significantly to the NME. A first ab-initio study in ^{48}Ca suggests that including this physics increases the NME by about 40% percent. A similar enhancement has been found in heavier $0\nu\beta\beta$-decay nuclei with the NSM and with QRPA. Lattice QCD studies are underway to test whether this claimed enhancement is robust. If so, the impact of the new term may balance the longer half-life values anticipated due to the inclusion of the "quenching" physics.

Even if these systematic contributions to NMEs were fully resolved, discrepancies remain between results obtained with different many-body methods. Tests against nuclear structure data can gauge the quality of each calculation. In addition, novel measurements of nuclear observables correlated with $0\nu\beta\beta$-decay NMEs such as second-order Gamow-Teller or electromagnetic transitions can provide insights on each method's strengths and weaknesses.

D. What else can be discovered by $0\nu\beta\beta$-decay experiments?

The unprecedented combination of ultra-low background, high-exposure, high energy resolution, and multivariate analysis capabilities in modern $0\nu\beta\beta$-decay experiments offers exciting discovery opportunities beyond the primary target of observing $0\nu\beta\beta$ decay. This includes searches not only for other L-violating processes, such as neutrinoless electron capture (Blaum et al., 2020) or neutrinoless quadruple-beta decay (Guzowski, 2018), but also for completely decoupled physics.

The existence of new particles and fields, the violation of fundamental principles, and non-standard interactions can each affect, in a characteristic way, the distribution of the summed energy of the electrons emitted in $\beta\beta$ decays. Historically, searches for new particles focused on massive and massless bosons called Majorons, the Goldstone bosons that arise from the spontaneous breakdown of the global $B - L$ symmetry. Searches for the violation of fundamental principles have focused on Lorentz invariance, the Pauli Exclusion Principle, and CPT symmetry. We refer to Bossio and Agostini (2023) for a comprehensive review of this topic. Future searches will have high-sensitivity to additional physics, for instance exotic currents (Deppisch et al., 2020b), and light exotic fermions such as sterile neutrinos or Z_2-odd fermions (Agostini et al., 2021c; Bolton et al., 2021).

In addition to distortions on the energy distribution, next-generation $0\nu\beta\beta$-decay experiments will be highly sensitive to numerous beyond-Standard-Model processes which could generate events with well defined energy depositions and/or time correlations. These searches include B-violating tri-nucleon decay (Albert et al., 2018; Alvis et al., 2019b) and charge-violating electron decay (Abgrall et al., 2017). Dark matter candidates such as WIMPS (Abgrall et al., 2017; Agostini et al., 2020d; Arnold et al., 2020; Liu et al., 2019) and axions (Abgrall et al., 2017; Xu and Elliott, 2017) can also be identified through an excess of events with a well-defined energy distribution or time-modulation. New searches have been proposed for inelastic boosted dark matter (Ha et al., 2019) and fermionic dark matter (Dror et al., 2020), and constraints have already been placed fractional-charge lightly ionizing particles (Alvis et al., 2018).

E. What will be the next paradigm shift?

For half a century, the Standard Model of particle physics has been the field's paradigm. The discovery of the Higgs boson, immediately recognized by the 2013 Nobel Prize in physics, was its crowning achievement. At the same time, we have known for almost two decades that this model is incomplete and needs to be extended, at least to incorporate massive neutrinos.

Extensions inspired by the very same symmetry principles that underlie the Standard Model have been explored in the framework of gauge theories, which include the so-called "Grand Unification" models. These theories have however not been confirmed in spite of the extensive experimental efforts to observe proton decay in the 1980s and 1990s. Some intrinsic features of the Standard Model, such as CP-symmetry in strong interactions, or the nature of radiative corrections in the Higgs sector, have in turn suggested the possible existence of new particles, e.g., axions or supersymmetric particles. Searches for these new particles have also been unsuccessful so far.

In the mean time, cosmological observations have led to the development of a Standard Model of cosmology, ΛCDM. Its very name invokes the existence of two forms of matter that cannot be found in the Standard Model of particle physics: dark matter and dark energy. Furthermore, theoretical cosmology has proved unable to account for the cosmic baryon excess.

Finally, several experimental anomalies have emerged, the most recent of which is the measurement of the

anomalous magnetic moment of the muon (Abi *et al.*, 2021). These anomalies could also point to some missing piece of the Standard Model.

Nonetheless, the only unequivocal manifestation of physics beyond the Standard Model supported by laboratory experiments is the evidence of neutrino oscillation, recognized by the 2015 Nobel Prize in physics as a proof that neutrinos are massive. This suggests that the importance of further studies on the neutrino mass should not be underestimated. The most promising theoretical option is that the mass type is exactly the one proposed by Majorana. Its experimental demonstration is a concrete and well-defined goal to strive for in the exploration of physics beyond the Standard Model.

The best way to probe the Majorana nature of neutrinos is to measure the rate of neutrinoless double beta decay — i.e., the rate at which electron pairs are created in certain nuclear decays — an observation which would lead to a profound change in our understanding of matter. Although we do not have an established theory that can guide us safely in the next steps, we are just starting a pioneering exploration of the next two, uncharted orders of magnitude, an exciting journey that will bring us a step closer to unlock the secrets of the universe.

ACKNOWLEDGMENTS

REFERENCES

Aalbers, J, *et al.* (DARWIN) (2016), "DARWIN: towards the ultimate dark matter detector," JCAP **11**, 017, arXiv:1606.07001 [astro-ph.IM].

Aalseth, C E (2005), "[aip topical workshop on low radioactivity techniques: Lrt 2004 - sudbury, ontario (canada) (12-14 december 2004)] aip conference proceedings - ultra-low-background copper production and clean fabrication,".

Aalseth, C E, *et al.* (2002), "Comment on 'Evidence for neutrinoless double beta decay'," Mod. Phys. Lett. A **17**, 1475–1478, arXiv:hep-ex/0202018.

Aaltonen, T, *et al.* (CDF) (2022), "High-precision measurement of the W boson mass with the CDF II detector," Science **376** (6589), 170–176.

Abe, K, *et al.* (2012a), "Radon removal from gaseous xenon with activated charcoal," Nuclear Instruments and Methods in Physics Research Section A: Accelerators, Spectrometers, Detectors and Associated Equipment **661**, 10.1016/j.nima.2011.09.051.

Abe, K, *et al.* (T2K) (2014), "Observation of Electron Neutrino Appearance in a Muon Neutrino Beam," Phys. Rev. Lett. **112**, 061802, arXiv:1311.4750 [hep-ex].

Abe, S, *et al.* (KamLAND-Zen) (2022), "First Search for the Majorana Nature of Neutrinos in the Inverted Mass Ordering Region with KamLAND-Zen," arXiv:2203.02139 [hep-ex].

Abe, T, P. Maris, T. Otsuka, N. Shimizu, Y. Utsuno, and J. P. Vary (2012b), "Benchmarks of the full configuration interaction, Monte Carlo shell model, and no-core full configuration methods," Phys. Rev. C **86**, 054301.

Aberle, C, A. Elagin, H.J. Frisch, M. Wetstein, and L. Winslow (2014), "Measuring Directionality in Double-Beta Decay and Neutrino Interactions with Kiloton-Scale Scintillation Detectors," JINST **9**, P06012, arXiv:1307.5813 [physics.ins-det].

Aberle, C, J. J. Li, S. Weiss, and L. Winslow (2013), "Optical Properties of Quantum-Dot-Doped Liquid Scintillators," JINST **8**, P10015, arXiv:1307.4742 [physics.ins-det].

Abgrall, N, *et al.* (Majorana) (2014), "The Majorana Demonstrator Neutrinoless Double-Beta Decay Experiment," Adv. High Energy Phys. **2014**, 365432, arXiv:1308.1633 [physics.ins-det].

Abgrall, N, *et al.* (Majorana) (2015), "The Majorana Parts Tracking Database," Nucl. Instrum. Meth. A **779**, 52–62, arXiv:1502.01748 [physics.ins-det].

Abgrall, N, *et al.* (Majorana) (2017), "New limits on Bosonic Dark Matter, Solar Axions, Pauli Exclusion Principle Violation, and Electron Decay from the Majorana Demonstrator," Phys. Rev. Lett. **118** (16), 161801, arXiv:1612.00886 [nucl-ex].

Abgrall, N, *et al.* (LEGEND) (2021), "The Large Enriched Germanium Experiment for Neutrinoless $\beta\beta$ Decay: LEGEND-1000 Preconceptual Design Report," arXiv:2107.11462 [physics.ins-det].

Abi, B, *et al.* (Muon g-2) (2021), "Measurement of the Positive Muon Anomalous Magnetic Moment to 0.46 ppm," Phys. Rev. Lett. **126** (14), 141801, arXiv:2104.03281 [hep-ex].

Abusleme, A, *et al.* (JUNO) (2021), "JUNO Physics and Detector," arXiv:2104.02565 [hep-ex].

Ackermann, K H, *et al.* (GERDA) (2013), "The GERDA experiment for the search of $0\nu\beta\beta$ decay in ^{76}Ge," Eur. Phys.

J. **C73** (3), 2330, arXiv:1212.4067 [physics.ins-det].

Adams, C, *et al.* (NEXT) (2021a), "Sensitivity of a tonne-scale NEXT detector for neutrinoless double beta decay searches," JHEP **2021** (08), 164, arXiv:2005.06467 [physics.ins-det].

Adams, D Q, *et al.* (CUORE) (2021b), "Measurement of the $2\nu\beta\beta$ Decay Half-Life of ^{130}Te with CUORE," Phys. Rev. Lett. **126** (17), 171801, arXiv:2012.11749 [nucl-ex].

Adams, D Q, *et al.* (CUORE) (2022), "Search for Majorana neutrinos exploiting millikelvin cryogenics with CUORE," Nature **604** (7904), 53–58, arXiv:2104.06906 [nucl-ex].

Adhikari, G, *et al.* (nEXO) (2022), "nEXO: neutrinoless double beta decay search beyond 10^{28} year half-life sensitivity," J. Phys. G **49** (1), 015104, arXiv:2106.16243 [nucl-ex].

Adler, S L (1969), "Axial vector vertex in spinor electrodynamics," Phys.Rev. **177**, 2426–2438.

Agafonova, N, *et al.* (OPERA) (2018), "Final results of the opera experiment on $\nu_-\tau$ appearance in the cngs neutrino beam," Phys.Rev.Lett. **120** (21), 211801, [Erratum: Phys.Rev.Lett. 121, 139901 (2018)], arXiv:1804.04912 [hep-ex].

Aghanim, N, *et al.* (Planck) (2018), "Planck 2018 results. VI. Cosmological parameters," arXiv:1807.06209 [astro-ph.CO].

Aghanim, N, *et al.* (Planck) (2020), "Planck 2018 results. VI. Cosmological parameters," Astron. Astrophys. **641**, A6, arXiv:1807.06209 [astro-ph.CO].

Agostini, F, *et al.* (DARWIN) (2020a), "Sensitivity of the DARWIN observatory to the neutrinoless double beta decay of ^{136}Xe," Eur. Phys. J. C **80** (9), 808, arXiv:2003.13407 [physics.ins-det].

Agostini, M, G. Benato, S. Dell'Oro, S. Pirro, and F. Vissani (2021a), "Discovery probabilities of Majorana neutrinos based on cosmological data," Phys. Rev. D **103** (3), 033008, arXiv:2012.13938 [hep-ph].

Agostini, M, G. Benato, and J. Detwiler (2017), "Discovery probability of next-generation neutrinoless double-β decay experiments," Phys.Rev.D **96** (5), 053001, arXiv:1705.02996 [hep-ex].

Agostini, M, G. Benato, J. A. Detwiler, J. Menéndez, and F. Vissani (2021b), "Testing the inverted neutrino mass ordering with neutrinoless double-β decay," Phys. Rev. C **104** (4), L042501, arXiv:2107.09104 [hep-ph].

Agostini, M, E. Bossio, A. Ibarra, and X. Marcano (2021c), "Search for Light Exotic Fermions in Double-Beta Decays," Phys. Lett. B **815**, 136127, arXiv:2012.09281 [hep-ph].

Agostini, M, A. Merle, and K. Zuber (2016), "Probing flavor models with^{76} Ge-based experiments on neutrinoless double-β decay," Eur. Phys. J. C **76** (4), 176, arXiv:1506.06133 [hep-ex].

Agostini, M, *et al.* (GERDA) (2013), "Results on Neutrinoless Double-β Decay of ^{76}Ge from Phase I of the GERDA Experiment," Phys. Rev. Lett. **111** (12), 122503, arXiv:1307.4720 [nucl-ex].

Agostini, M, *et al.* (GERDA) (2015), "Results on $\beta\beta$ decay with emission of two neutrinos or Majorons in^{76} Ge from GERDA Phase I," Eur. Phys. J. **C75** (9), 416, arXiv:1501.02345 [nucl-ex].

Agostini, M, *et al.* (BOREXINO) (2018a), "Comprehensive measurement of *pp*-chain solar neutrinos," Nature **562** (7728), 505–510.

Agostini, M, *et al.* (GERDA) (2018b), "Upgrade for Phase II of the Gerda experiment," Eur. Phys. J. **C78** (5), 388, arXiv:1711.01452 [physics.ins-det].

Agostini, M, *et al.* (GERDA) (2020b), "Final Results of GERDA on the Search for Neutrinoless Double-β Decay," Phys. Rev. Lett. **125** (25), 252502, arXiv:2009.06079 [nucl-ex].

Agostini, M, *et al.* (GERDA) (2020c), "Modeling of GERDA Phase II data," JHEP **03**, 139, arXiv:1909.02522 [nucl-ex].

Agostini, M, *et al.* (GERDA) (2020d), "The first search for bosonic super-WIMPs with masses up to 1 MeV/c^2 with GERDA," Phys. Rev. Lett. **125** (1), 011801, arXiv:2005.14184 [hep-ex].

Agostini, M, *et al.* (BOREXINO) (2022a), "First Directional Measurement of Sub-MeV Solar Neutrinos with Borexino," Phys. Rev. Lett. **128** (9), 091803, arXiv:2112.11816 [hep-ex].

Agostini, Matteo, Frank F. Deppisch, and Graham Van Goffrier (2022b), "Probing the Mechanism of Neutrinoless Double-Beta Decay in Multiple Isotopes," arXiv:2212.00045 [hep-ph].

Agrawal, Prateek, *et al.* (2021), "Feebly-interacting particles: FIPs 2020 workshop report," Eur. Phys. J. C **81** (11), 1015, arXiv:2102.12143 [hep-ph].

Ahmad, Q R, *et al.* (SNO) (2001), "Measurement of the rate of $\nu_e + d \rightarrow p + p + e^-$ interactions produced by ^{8}B solar neutrinos at the Sudbury Neutrino Observatory," Phys. Rev. Lett. **87**, 071301, arXiv:nucl-ex/0106015.

Ahmed, F, and M. Horoi (2020), "Interference Effects for $0\nu\beta\beta$ Decay in the Left-Right Symmetric Model," Phys. Rev. C **101**, 035504.

Ahmed, F, A. Neacsu, and M. Horoi (2017), "Interference between light and heavy neutrinos for $0\nu\beta\beta$ decay in the left–right symmetric model," Phys. Lett. B **769**, 299–304.

Ajimura, S, *et al.* (CANDLES) (2021), "Low background measurement in CANDLES-III for studying the neutrino-less double beta decay of ^{48}Ca," Phys. Rev. D **103** (9), 092008, arXiv:2008.09288 [hep-ex].

Aker, M, *et al.* (KATRIN) (2019), "An improved upper limit on the neutrino mass from a direct kinematic method by katrin," Phys.Rev.Lett. **123** (22), 221802, arXiv:1909.06048 [hep-ex].

Aker, M, *et al.* (KATRIN) (2022), "Direct neutrino-mass measurement with sub-electronvolt sensitivity," Nature Phys. **18** (2), 160–166, arXiv:2105.08533 [hep-ex].

Akerib, D S, *et al.* (LZ) (2015), "LUX-ZEPLIN (LZ) Conceptual Design Report," arXiv:1509.02910 [physics.ins-det].

Akerib, D S, *et al.* (LZ) (2020), "Projected sensitivity of the LUX-ZEPLIN experiment to the $0\nu\beta\beta$ decay of ^{136}Xe," Phys. Rev. C **102** (1), 014602, arXiv:1912.04248 [nucl-ex].

Akhmedov, E, A. Kartavtsev, M. Lindner, L. Michaels, and J. Smirnov (2013), "Improving Electro-Weak Fits with TeV-scale Sterile Neutrinos," JHEP **05**, 081, arXiv:1302.1872 [hep-ph].

Akhmedov, Evgeny K, V. A. Rubakov, and A. Yu. Smirnov (1998), "Baryogenesis via neutrino oscillations," Phys. Rev. Lett. **81**, 1359–1362, arXiv:hep-ph/9803255.

Al Kharusi, S, *et al.* (nEXO) (2018), "nEXO Pre-Conceptual Design Report," arXiv:1805.11142 [physics.ins-det].

Al Kharusi, S, *et al.* (EXO-200) (2020), "Measurement of the Spectral Shape of the β-Decay of ^{137}Xe to the Ground State of ^{137}Cs in EXO-200 and Comparison with Theory," Phys. Rev. Lett. **124**, 232502, 2002.00108.

Alanssari, M, *et al.* (2016), "Single and Double Beta-Decay Q Values among the Triplet Zr96 , Nb96 , and Mo96," Phys. Rev. Lett. **116** (7), 072501.

Albanese, V, *et al.* (SNO+) (2021), "The SNO+ Experiment,"

arXiv:2104.11687 [physics.ins-det].

Albert, J B, *et al.* (EXO-200) (2014), "Improved measurement of the $2\nu\beta\beta$ half-life of ^{136}Xe with the EXO-200 detector," Phys. Rev. **C89** (1), 015502, arXiv:1306.6106 [nucl-ex].

Albert, J B, *et al.* (EXO-200) (2018), "Search for nucleon decays with EXO-200," Phys. Rev. D **97** (7), 072007, arXiv:1710.07670 [hep-ex].

Alduino, C, *et al.* (CUORE) (2017a), "CUORE sensitivity to $0\nu\beta\beta$ decay," Eur. Phys. J. C **77** (8), 532, arXiv:1705.10816 [physics.ins-det].

Alduino, C, *et al.* (CUORE) (2017b), "Measurement of the two-neutrino double-beta decay half-life of ^{130}Te with the CUORE-0 experiment," Eur. Phys. J. **C77** (1), 13, arXiv:1609.01666 [nucl-ex].

Alduino, C, *et al.* (CUORE) (2017c), "The projected background for the CUORE experiment," Eur. Phys. J. C **77** (8), 543, arXiv:1704.08970 [physics.ins-det].

Alduino, C, *et al.* (CUORE) (2018), "First Results from CUORE: A Search for Lepton Number Violation via $0\nu\beta\beta$ Decay of ^{130}Te," Phys. Rev. Lett. **120** (13), 132501, arXiv:1710.07988 [nucl-ex].

Alduino, C, *et al.* (2019), "The CUORE cryostat: An infrastructure for rare event searches at millikelvin temperatures," Cryogenics **102**, 9–21, arXiv:1904.05745 [physics.ins-det].

Alekhin, Sergey, *et al.* (2016), "A facility to Search for Hidden Particles at the CERN SPS: the SHiP physics case," Rept. Prog. Phys. **79** (12), 124201, arXiv:1504.04855 [hep-ph].

Algeri, S, J. Aalbers, K. Dundas Morå, and J. Conrad (2019), "Searching for new physics with profile likelihoods: Wilks and beyond," arXiv:1911.10237 [physics.data-an].

Ali, A, A. V. Borisov, and D. V. Zhuridov (2007), "Probing new physics in the neutrinoless double beta decay using electron angular correlation," Phys. Rev. D **76**, 093009.

Allen, J S (1942), "Experimental evidence for the existence of a neutrino," Phys. Rev. **61**, 692–697.

Altarelli, G, and D. Meloni (2013), "A non supersymmetric SO(10) grand unified model for all the physics below M_{GUT}," JHEP **08**, 021, arXiv:1305.1001 [hep-ph].

Alvarez, V, *et al.* (NEXT) (2012), "NEXT-100 Technical Design Report (TDR): Executive Summary," JINST **7**, T06001, arXiv:1202.0721 [physics.ins-det].

Alvis, S I, *et al.* (Majorana) (2018), "First Limit on the Direct Detection of Lightly Ionizing Particles for Electric Charge as Low as e/1000 with the Majorana Demonstrator," Phys. Rev. Lett. **120** (21), 211804, arXiv:1801.10145 [hep-ex].

Alvis, S I, *et al.* (Majorana) (2019a), "A Search for Neutrinoless Double-Beta Decay in ^{76}Ge with 26 kg-yr of Exposure from the MAJORANA DEMONSTRATOR," Phys. Rev. C **100** (2), 025501, arXiv:1902.02299 [nucl-ex].

Alvis, S I, *et al.* (Majorana) (2019b), "Search for trinucleon decay in the Majorana Demonstrator," Phys. Rev. D **99** (7), 072004, arXiv:1812.01090 [hep-ex].

Ambrosio, M, *et al.* (MACRO) (1995), "Vertical muon intensity measured with MACRO at the Gran Sasso Laboratory," Phys. Rev. D **52**, 3793–3802.

Anderson, E R, S. K. Bogner, R. J. Furnstahl, and R. J. Perry (2010), "Operator Evolution via the Similarity Renormalization Group I: The Deuteron," Phys. Rev. C **82**, 054001.

Andringa, S, *et al.* (SNO+) (2016), "Current Status and Future Prospects of the SNO+ Experiment," Adv. High Energy Phys. **2016**, 6194250, arXiv:1508.05759 [physics.ins-det].

Anton, G, *et al.* (EXO-200) (2019), "Search for Neutrinoless Double-β Decay with the Complete EXO-200 Dataset," Phys. Rev. Lett. **123** (16), 161802, arXiv:1906.02723 [hep-ex].

Anton, G, *et al.* (EXO-200) (2020), "Measurement of the scintillation and ionization response of liquid xenon at MeV energies in the EXO-200 experiment," Phys. Rev. C **101** (6), 065501, arXiv:1908.04128 [physics.ins-det].

Aprahamian, Ani, *et al.* (2015), "Reaching for the horizon: The 2015 long range plan for nuclear science," .

Aprile, E, *et al.* (XENON100) (2017), "Online^{222} Rn removal by cryogenic distillation in the XENON100 experiment," Eur. Phys. J. C **77** (6), 358, arXiv:1702.06942 [physics.ins-det].

Aprile, E, *et al.* (XENON) (2019), "Observation of two-neutrino double electron capture in ^{124}Xe with XENON1T," Nature **568**, 532–535.

Archidiacono, M, T. Brinckmann, J. Lesgourgues, and V. Poulin (2017), "Physical effects involved in the measurements of neutrino masses with future cosmological data," JCAP **02**, 052, arXiv:1610.09852 [astro-ph.CO].

Argyriades, J, *et al.* (NEMO-3) (2010), "Measurement of the two neutrino double beta decay half-life of Zr-96 with the NEMO-3 detector," Nucl. Phys. A **847**, 168–179, arXiv:0906.2694 [nucl-ex].

Arima, A, and F. Iachello (1976), "Interacting boson model of collective states. 1. The Vibrational limit," Annals Phys. **99**, 253–317.

Arima, A, and F. Iachello (1978), "Interacting boson model of collective nuclear states. II. The rotational limit," Annals Phys. **111**, 201–238.

Arima, A, K. Shimizu, W. Bentz, and H. Hyuga (1987), "Nuclear Magnetic Properties and Gamow-teller Transitions," Adv. Nucl. Phys. **18**, 1–106.

Arling, J H, *et al.* (2021), "Commissioning of the COBRA extended demonstrator at the LNGS," Nucl. Instrum. Meth. A **1010**, 165524.

Armatol, A, *et al.* (CUPID) (2020), "A novel technique for the study of pile-up events in cryogenic bolometers," arXiv:2011.11726 [physics.ins-det].

Armengaud, E, *et al.* (2020a), "Precise measurement of $2\nu\beta\beta$ decay of ^{100}Mo with the CUPID-Mo detection technology," Eur. Phys. J. C **80** (7), 674, arXiv:1912.07272 [nucl-ex].

Armengaud, E, *et al.* (2020b), "The CUPID-Mo experiment for neutrinoless double-beta decay: performance and prospects," Eur. Phys. J. C **80** (1), 44, arXiv:1909.02994 [physics.ins-det].

Armengaud, E, *et al.* (CUPID) (2021), "New Limit for Neutrinoless Double-Beta Decay of ^{100}Mo from the CUPID-Mo Experiment," Phys. Rev. Lett. **126** (18), 181802, arXiv:2011.13243 [nucl-ex].

Armstrong, W R, *et al.* (CUPID) (2019), "CUPID pre-CDR," arXiv:1907.09376 [physics.ins-det].

Arnold, R, *et al.* (NEMO) (1995), "Observation of two neutrino double beta decay of Cd-116 with the tracking detector NEMO-2," JETP Lett. **61**, 170–174.

Arnold, R, *et al.* (NEMO) (1996), "Double-beta decay of Cd-116," Z. Phys. C **72**, 239–247.

Arnold, R, *et al.* (NEMO) (1998), "Double beta decay of Se-82," Nucl. Phys. A **636**, 209–223.

Arnold, R, *et al.* (1999), "Double beta decay of Zr-96," Nucl. Phys. A **658**, 299–312.

Arnold, R, *et al.* (SuperNEMO) (2010), "Probing New Physics Models of Neutrinoless Double Beta Decay with SuperNEMO," Eur. Phys. J. C **70**, 927.

Arnold, R, *et al.* (NEMO-3) (2015), "Results of the search for neutrinoless double-β decay in ^{100}Mo with the NEMO-3 experiment," Phys. Rev. D **92** (7), 072011, arXiv:1506.05825 [hep-ex].

Arnold, R, *et al.* (NEMO-3) (2016a), "Measurement of the $2\nu\beta\beta$ decay half-life of ^{150}Nd and a search for $0\nu\beta\beta$ decay processes with the full exposure from the NEMO-3 detector," Phys. Rev. D **94** (7), 072003, arXiv:1606.08494 [hep-ex].

Arnold, R, *et al.* (NEMO-3) (2016b), "Measurement of the double-beta decay half-life and search for the neutrinoless double-beta decay of ^{48}Ca with the NEMO-3 detector," Phys. Rev. **D93** (11), 112008, arXiv:1604.01710 [hep-ex].

Arnold, R, *et al.* (NEMO-3) (2019), "Detailed studies of ^{100}Mo two-neutrino double beta decay in NEMO-3," Eur. Phys. J. C **79**, 440.

Arnold, R, *et al.* (NEMO-3) (2020), "Search for Periodic Modulations of the Rate of Double-Beta Decay of ^{100}Mo in the NEMO-3 Detector," arXiv:2011.07657 [nucl-ex].

Arnquist, I J, *et al.* (2022), "Final Result of the MAJORANA DEMONSTRATOR's Search for Neutrinoless Double-β Decay in ^{76}Ge," arXiv:2207.07638 [nucl-ex].

Artusa, D R, *et al.* (2017), "Enriched TeO$_2$ bolometers with active particle discrimination: towards the CUPID experiment," Phys. Lett. **B767**, 321–329, arXiv:1610.03513 [physics.ins-det].

Asaka, Takehiko, Steve Blanchet, and Mikhail Shaposhnikov (2005), "The nuMSM, dark matter and neutrino masses," Phys. Lett. B **631**, 151–156, arXiv:hep-ph/0503065.

Askins, M, *et al.* (Theia) (2020), "THEIA: an advanced optical neutrino detector," Eur. Phys. J. C **80** (5), 416, arXiv:1911.03501 [physics.ins-det].

Atre, A, T. Han, S. Pascoli, and B. Zhang (2009), "The search for heavy majorana neutrinos," JHEP **05**, 030, arXiv:0901.3589 [hep-ph].

Auerbach, N, and Bui Minh Loc (2018), "Nuclear structure studies of double-charge-exchange Gamow-Teller strength," Phys. Rev. C **98**, 064301.

Auerbach, N, L. Zamick, and D. C. Zheng (1989), Annals Phys. **192**, 77.

Auger, M, *et al.* (2012), "The EXO-200 detector, part I: Detector design and construction," JINST **7**, P05010, arXiv:1202.2192 [physics.ins-det].

Avignone, F T, and S. R. Elliott (2019), "The Search for Double Beta Decay With Germanium Detectors: Past, Present, and Future," Front.in Phys. **7**, 6, arXiv:1901.02805 [nucl-ex].

Avignone, F T, H. S. Miley, R. L. Brodzinski, J. C. Evans, W. K. Hensley, and J. H. Reeves (1986), "Search for the Double Beta Decay of ^{76}Ge," Phys. Rev. C **34**, 666–677.

Avignone, III, F T, S. R. Elliott, and J. Engel (2008), "Double Beta Decay, Majorana Neutrinos, and Neutrino Mass," Rev. Mod. Phys. **80**, 481–516, arXiv:0708.1033 [nucl-ex].

Awasthi, Ram Lal, M. K. Parida, and Sudhanwa Patra (2013), "Neutrino masses, dominant neutrinoless double beta decay, and observable lepton flavor violation in left-right models and SO(10) grand unification with low mass W_R, Z_R bosons," JHEP **08**, 122, arXiv:1302.0672 [hep-ph].

Ayangeakaa, A D, *et al.* (2019), "Evidence for Rigid Triaxial Deformation in ^{76}Ge from a Model-Independent Analysis," Phys. Rev. Lett. **123**, 102501, 1909.03270.

Azzolini, O, *et al.* (CUPID) (2019a), "Background Model of the CUPID-0 Experiment," Eur. Phys. J. **C79** (7), 583, arXiv:1904.10397 [nucl-ex].

Azzolini, O, *et al.* (2019b), "Evidence of Single State Dominance in the Two-Neutrino Double-β Decay of ^{82}Se with CUPID-0," Phys. Rev. Lett. **123** (26), 262501, arXiv:1909.03397 [nucl-ex].

Azzolini, O, *et al.* (CUPID) (2019c), "Final result of CUPID-0 phase-I in the search for the ^{82}Se Neutrinoless Double-β Decay," Phys. Rev. Lett. **123** (3), 032501, arXiv:1906.05001 [nucl-ex].

Babu, K S, and C. N. Leung (2001), "Classification of effective neutrino mass operators," Nucl.Phys.B **619**, 667–689, arXiv:hep-ph/0106054.

Baertsch, R D, and R. N. Hall (1970), "Gamma ray detectors made from high purity germanium," IEEE Transactions on Nuclear Science **17** (3), 235–240.

Bahcall, J, H. Murayama, and C. Peña-Garay (2004), Phys. Rev. D **70**, 033012.

Bahcall, J N (1994), "The Be-7 solar neutrino line: A Reflection of the central temperature distribution of the sun," Phys. Rev. D **49**, 3923–3945, arXiv:astro-ph/9401024.

Bahcall, J N, E. Lisi, D. E. Alburger, L. De Braeckeleer, S. J. Freedman, and J. Napolitano (1996), "Standard neutrino spectrum from B-8 decay," Phys. Rev. C **54**, 411–422, arXiv:nucl-th/9601044.

Bahcall, J N, and R. K. Ulrich (1988), "Solar Models, Neutrino Experiments and Helioseismology," Rev. Mod. Phys. **60**, 297–372.

Bajc, B, A. Melfo, G. Senjanovic, and F. Vissani (2006), "Yukawa sector in non-supersymmetric renormalizable SO(10)," Phys. Rev. D **73**, 055001, arXiv:hep-ph/0510139.

Bally, B, B. Avez, M. Bender, and P. H. Heenen (2014), "Beyond Mean-Field Calculations for Odd-Mass Nuclei," Phys. Rev. Lett. **113**, 162501.

Bally, B, A. Sánchez-Fernández, and T. R. Rodríguez (2021), "Symmetry-projected variational calculations with the numerical suite TAURUS: I. Variation after particle-number projection," Eur. Phys. J. A **57** (2), 69, [Erratum: Eur.Phys.J.A 57, 124 (2021)], arXiv:2010.14169 [nucl-th].

Balysh, A, A. S. De Silva, V. I. Lebedev, K. Lou, M. K. Moe, M. A. Nelson, A. Piepke, A. Pronsky, M. A. Vient, and P. Vogel (1996), "Double beta decay of ^{48}Ca," Phys. Rev. Lett. **77**, 5186–5189, arXiv:nucl-ex/9608001.

Bandac, I, S. Borjabad, A. Ianni, R. Nuñez Lagos, C. Pérez, S. Rodríguez, and J. A. Villar (2017), "Ultra-low background and environmental measurements at Laboratorio Subterráneo de Canfranc (LSC)," Appl. Radiat. Isot. **126**, 127–129.

Bandac, I C, *et al.* (CROSS) (2020), "The $0\nu2\beta$-decay CROSS experiment: preliminary results and prospects," JHEP **01**, 018, [JHEP20,018(2020)], arXiv:1906.10233 [nucl-ex].

Barabash, A (2020), "Precise Half-Life Values for Two-Neutrino Double-β Decay: 2020 Review," Universe **6**, 159, 2009.14451.

Barabash, A S (2011), "Double Beta Decay: Historical Review of 75 Years of Research," Phys. Atom. Nucl. **74**, 603–613, arXiv:1104.2714 [nucl-ex].

Barabash, A S, *et al.* (1995), "Two neutrino double beta decay of Mo-100 to the first excited 0+ state in Ru-100," Phys. Lett. B **345**, 408–413.

Barabash, A S, *et al.* (2014), "Enriched Zn^{100}MoO$_4$ scintillating bolometers to search for $0\nu2\beta$ decay of ^{100}Mo with the LUMINEU experiment," Eur. Phys. J. **C74** (10), 3133, arXiv:1405.6937 [physics.ins-det].

Barabash, AS, *et al.* (2011), "Low background detector with enriched $^{116}CdWO_4$ crystal scintillators to search for dou-

ble β decay of ^{116}Cd," JINST **6**, P08011, arXiv:1108.2771 [physics.ins-det].

Barabash, AS, *et al.* (2018), "Final results of the Aurora experiment to study 2β decay of ^{116}Cd with enriched ^{116}CdWO$_4$ crystal scintillators," Phys. Rev. D **98** (9), 092007, arXiv:1811.06398 [nucl-ex].

Barbieri, R, and G.F. Giudice (1988), "Upper Bounds on Supersymmetric Particle Masses," Nucl. Phys. B **306**, 63–76.

Bardeen, W A (1969), "Anomalous ward identities in spinor field theories," Phys.Rev. **184**, 1848–1857.

Bardin, R K, P. J. Gollon, J. D. Ullman, and C. S. Wu (1967), "Double beta decay in ^{48}Ca and the conservation of leptons," Phys. Lett. B **26**, 112–116.

Bardin, R K, P. J. Gollon, J. D. Ullman, and C. S. Wu (1970), "A search for the double beta decay of 48 Ca and lepton conservation," Nucl. Phys. A **158**, 337–363.

Barea, J, and F. Iachello (2009), "Neutrinoless double-beta decay in the microscopic interacting boson model," Phys. Rev. C **79**, 044301.

Barea, J, J. Kotila, and F. Iachello (2015a), "$0\nu\beta\beta$ and $2\nu\beta\beta$ nuclear matrix elements in the interacting boson model with isospin restoration," Phys. Rev. C **91**, 034304.

Barea, J, J. Kotila, and F. Iachello (2015b), "Limits on sterile neutrino contributions to neutrinoless double beta decay," Phys. Rev. D **92**, 093001.

Baroni, A, L. Girlanda, S. Pastore, R. Schiavilla, and M. Viviani (2016), "Nuclear Axial Currents in Chiral Effective Field Theory," Phys. Rev. C **93** (1), 015501, [Erratum: Phys. Rev.C95,no.5,059901(2017)].

Barrett, B R, P. Navrátil, and J. P. Vary (2013), "Ab initio no core shell model," Prog. Part. Nucl. Phys. **69**, 131–181.

de Barros, N F, and K. Zuber (2011), "Solar neutrino-electron scattering as background limitation for double beta decay," J. Phys. G **38**, 105201, arXiv:1103.5757 [hep-ph].

Basak, S, S. S. Alam, D. Kumar, A. Saha, and T. Bhattacharjee (2021), "Shape coexistence scenario in Sm150 from a γ-γ fast-timing measurement," Phys. Rev. C **104**, 024320.

Basili, R A M, J. M. Yao, J. Engel, H. Hergert, M. Lockner, P. Maris, and J. P. Vary (2019), "Benchmark neutrinoless double-beta decay matrix elements in a light nucleus," arXiv:1909.06501.

Baudis, L, G. Benato, P. Carconi, C. M. Cattadori, P. De Felice, K. Eberhardt, R. Eichler, A. Petrucci, M. Tarka, and M. Walter (2015), "Production and characterization of ^{228}Th calibration sources with low neutron emission for GERDA," JINST **10** (12), P12005, arXiv:1508.05731 [physics.ins-det].

Baudis, L, *et al.* (2011), "Gator: a low-background counting facility at the Gran Sasso Underground Laboratory," JINST **6**, P08010, arXiv:1103.2125 [astro-ph.IM].

Behrens, H, and W. Bühring (1971), "Nuclear beta decay," Nucl. Phys. **A162**, 111–144.

Beller, J, *et al.* (2013), "Constraint on $0\nu\beta\beta$ Matrix Elements from a Novel Decay Channel of the Scissors Mode: The Case of ^{154}Gd," Phys. Rev. Lett. **111**, 172501.

Belley, A, C. G. Payne, S. R. Stroberg, T. Miyagi, and J. D. Holt (2021), "*AbInitio* Neutrinoless Double-Beta Decay Matrix Elements for ^{48}Ca , ^{76}Ge , and ^{82}Se," Phys. Rev. Lett. **126**, 042502, arXiv:2008.06588.

Belli, P, R. Bernabei, F. Cappella, V. Caracciolo, R. Cerulli, A. Incicchitti, and V. Merlo (2020), "Double Beta Decay to Excited States of Daughter Nuclei," Universe **6** (12), 239.

Bellone, J I, S. Burrello, M. Colonna, J.-A. Lay, and H. Lenske (2019), "Sequential Heavy Ion Double Charge Exchange Reactions and the Link to Double β-decay," arXiv:1912.03043.

Benato, G (2015), "Effective majorana mass and neutrinoless double beta decay," Eur.Phys.J.C **75** (11), 563, arXiv:1510.01089 [hep-ph].

Benato, G, *et al.* (2018), "Radon mitigation during the installation of the CUORE $0\nu\beta\beta$ decay detector," JINST **13** (01), P01010, arXiv:1711.07936 [physics.ins-det].

Bender, M, P.-H. Heenen, and P.-G. Reinhard (2003), "Self-consistent mean-field models for nuclear structure," Rev. Mod. Phys. **75**, 121–180.

Benhar, Omar, Riccardo Biondi, and Enrico Speranza (2014), "Short-range correlation effects on the nuclear matrix element of neutrinoless double-β decay," Phys. Rev. C **90** (6), 065504, arXiv:1401.2030 [nucl-th].

Bergstrom, J, M. C. Gonzalez-Garcia, M. Maltoni, C. Pena-Garay, A. M. Serenelli, and N. Song (2016), "Updated determination of the solar neutrino fluxes from solar neutrino data," JHEP **03**, 132, arXiv:1601.00972 [hep-ph].

Bernard, V, N. Kaiser, and U.-G. Meissner (1997), "Aspects of chiral pion - nucleon physics," Nucl. Phys. A **615**, 483–500.

Bertolini, S, L. Di Luzio, and M. Malinsky (2012), "Seesaw Scale in the Minimal Renormalizable SO(10) Grand Unification," Phys. Rev. D **85**, 095014, arXiv:1202.0807 [hep-ph].

Bertsch, G F, and I. Hamamoto (1982), "Gamow-Teller strength at high excitations," Phys. Rev. C **26**, 1323–1326.

Bezrukov, F L (2005), "nu MSM-predictions for neutrinoless double beta decay," Phys. Rev. D **72**, 071303, arXiv:hep-ph/0505247.

Bhattiprolu, P N, S. P. Martin, and J. D. Wells (2021), "Criteria for projected discovery and exclusion sensitivities of counting experiments," Eur. Phys. J. C **81** (2), 123, arXiv:2009.07249 [physics.data-an].

Bhupal Dev, P S, Srubabati Goswami, Manimala Mitra, and Werner Rodejohann (2013), "Constraining Neutrino Mass from Neutrinoless Double Beta Decay," Phys. Rev. D **88**, 091301, arXiv:1305.0056 [hep-ph].

Bilenky, S M, and C. Giunti (2015), "Neutrinoless Double-Beta Decay: a Probe of Physics Beyond the Standard Model," Int. J. Mod. Phys. A **30** (04n05), 1530001, arXiv:1411.4791 [hep-ph].

Bilenky, S M, J. Hosek, and S.T. Petcov (1980), "On oscillations of neutrinos with dirac and majorana masses," Phys.Lett.B **94**, 495–498.

Blaum, K, S. Eliseev, F. A. Danevich, V. I. Tretyak, S. Kovalenko, M. I. Krivoruchenko, Yu. N. Novikov, and J. Suhonen (2020), "Neutrinoless Double-Electron Capture," Rev. Mod. Phys. **92**, 045007, arXiv:2007.14908 [hep-ph].

Blennow, M, E. Fernandez-Martinez, J. Lopez-Pavon, and J. Menéndez (2010), "Neutrinoless double beta decay in seesaw models," JHEP **07**, 096.

Bochkarev, AI, and M.E. Shaposhnikov (1987), "Electroweak Production of Baryon Asymmetry and Upper Bounds on the Higgs and Top Masses," Mod. Phys. Lett. A **2**, 417.

Bodenstein-Dresler, L, *et al.* (COBRA) (2020), "Quenching of g_A deduced from the β-spectrum shape of ^{113}Cd measured with the COBRA experiment," Phys. Lett. B **800**, 135092.

Boger, J, *et al.* (SNO) (2000), "The Sudbury neutrino observatory," Nucl. Instrum. Meth. A **449**, 172–207, arXiv:nucl-ex/9910016.

Bogner, S K, H. Hergert, J. D. Holt, A. Schwenk, S. Binder, A. Calci, J. Langhammer, and R. Roth (2014), "Non-perturbative shell-model interactions from the in-medium similarity renormalization group," Phys. Rev. Lett. **113**, 142501.

Bogner, S K, and D. Roscher (2012), "High-momentum tails from low-momentum effective theories," Phys. Rev. C **86**, 064304.

Bohr, A, and B. R. Mottelson (1953), K. Dan. Vidensk. Selsk. Mat. Fys. Medd **27**, 16.

Bohr, N (1913), "On the Constitution of Atoms and Molecules," Phil. Mag. Ser. 6 **26**, 1–24.

Bolotnikov, A, and B. Ramsey (1997), "The spectroscopic properties of high-pressure xenon," Nuclear Instruments and Methods in Physics Research A **396** (3), 360–370.

Bolton, P D, F. F. Deppisch, Lukáš G., and F. Šimkovic (2021), "Two-Neutrino Double Beta Decay with Sterile Neutrinos," Phys. Rev. D **103** (5), 055019, arXiv:2011.13387 [hep-ph].

Bolton, Patrick D, Frank F. Deppisch, and P. S. Bhupal Dev (2020), "Neutrinoless double beta decay versus other probes of heavy sterile neutrinos," JHEP **03**, 170, arXiv:1912.03058 [hep-ph].

Bolton, Patrick D, Frank F. Deppisch, and P. S. Bhupal Dev (2022), "Neutrinoless double beta decay via light neutralinos in R-parity violating supersymmetry," JHEP **03**, 152, arXiv:2112.12658 [hep-ph].

Bonnet, F, M. Hirsch, T. Ota, and W. Winter (2013), "Systematic decomposition of the neutrinoless double beta decay operator," JHEP **03**, 055, [Erratum: JHEP 04, 090 (2014)], arXiv:1212.3045 [hep-ph].

Bossio, E, and M. Agostini (2023), "A review of exotic physics searches with double-beta decay," .

Bouet, R, et al. (2021), "R2D2 spherical TPC: first energy resolution results," JINST **16** (03), P03012, arXiv:2007.02570 [physics.ins-det].

Brase, Catharina, Javier Menéndez, Eduardo Antonio Coello Pérez, and Achim Schwenk (2021), "Neutrinoless double-beta decay from an effective field theory for heavy nuclei," arXiv:2108.11805 [nucl-th].

Brodzinski, R L, H. S. Miley, J. H. Reeves, and F. T. Avignone (1990), "Further reduction of radioactive backgrounds in ultrasensitive germanium spectrometers," Nucl. Instrum. Meth. A **292**, 337–342.

Brofferio, C, and S. Dell'Oro (2018), "Contributed Review: The saga of neutrinoless double beta decay search with TeO_2 thermal detectors," Rev. Sci. Instrum. **89** (12), 121502, arXiv:1801.03580 [hep-ex].

Brofferio, Chiara, Oliviero Cremonesi, and Stefano Dell'Oro (2019), "Neutrinoless Double Beta Decay Experiments With TeO_2 Low-Temperature Detectors," Front. in Phys. **7**, 86.

Brown, B A (2001), "The nuclear shell model towards the drip lines," Prog. Part. Nucl. Phys. **47**, 517–599.

Brown, B A, M. Horoi, and R. A. Sen'kov (2014), "Nuclear Structure Aspects of Neutrinoless Double-β Decay," Phys. Rev. Lett. **113**, 262501.

Brown, B A, and B. H. Wildenthal (1987), "Empirically optimum M1 operator for sd-shell nuclei," Nucl. Phys. A **474**, 290–306.

Brunner, T, et al. (2015), "An RF-only ion-funnel for extraction from high-pressure gases," Int. J. Mass Spectrometry **379**, 110–120, arXiv:1412.1144 [physics.ins-det].

Buccella, F, D. Falcone, C. S. Fong, E. Nardi, and G. Ric-
ciardi (2012), "Squeezing out predictions with leptogenesis from SO(10)," Phys. Rev. D **86**, 035012, arXiv:1203.0829 [hep-ph].

Buck, C, B. Gramlich, and S. Schoppmann (2019), "Novel Opaque Scintillator for Neutrino Detection," JINST **14** (11), P11007, arXiv:1908.03334 [physics.ins-det].

Butler, M, J.-W. Chen, and X. Kong (2001), "Neutrino deuteron scattering in effective field theory at next-to-next-to-leading order," Phys. Rev. C **63**, 035501.

Cabibbo, N (1963), "Unitary Symmetry and Leptonic Decays," Meeting of the Italian School of Physics and Weak Interactions Bologna, Italy, April 26-28, 1984, Phys. Rev. Lett. **10**, 531–533, [,648(1963)].

Cabrera, A, et al. (2019), "Neutrino Physics with an Opaque Detector," arXiv:1908.02859 [physics.ins-det].

Cacciapaglia, Giacomo, and Francesco Sannino (2022), "The W boson mass weighs in on the non-standard Higgs," Phys. Lett. B **832**, 137232, arXiv:2204.04514 [hep-ph].

Caldwell, A, and K. Kroninger (2006), "Signal discovery in sparse spectra: A Bayesian analysis," Phys. Rev. D **74**, 092003, arXiv:physics/0608249.

Caldwell, A, A. Merle, O. Schulz, and M. Totzauer (2017), "Global Bayesian analysis of neutrino mass data," Phys. Rev. D **96** (7), 073001, arXiv:1705.01945 [hep-ph].

Calvez, S (2017), Development of reconstruction tools and sensitivity of the SuperNEMO demonstrator, Ph.D. thesis (Université Paris Saclay).

Capozzi, F, E. Di Valentino, E. Lisi, A. Marrone, A. Melchiorri, and A. Palazzo (2021), "Unfinished fabric of the three neutrino paradigm," Phys. Rev. D **104** (8), 083031, arXiv:2107.00532 [hep-ph].

Cappuzzello, F, et al. (2018), "The NUMEN project: NUclear Matrix Elements for Neutrinoless double beta decay," Eur. Phys. J. A **54**, 72.

Caravaca, J, F.B. Descamps, B.J. Land, M. Yeh, and G. D. Orebi Gann (2017), "Cherenkov and Scintillation Light Separation in Organic Liquid Scintillators," Eur. Phys. J. C **77** (12), 811, arXiv:1610.02011 [physics.ins-det].

Caravaca, J, B.J. Land, M. Yeh, and G.D. Orebi Gann (2020), "Characterization of water-based liquid scintillator for Cherenkov and scintillation separation," Eur. Phys. J. C **80** (9), 867, arXiv:2006.00173 [physics.ins-det].

Carlson, J, S. Gandolfi, F. Pederiva, S. C. Pieper, R. Schiavilla, K. E. Schmidt, and R. B. Wiringa (2015), "Quantum monte carlo methods for nuclear physics," Rev. Mod. Phys. **87**, 1067–1118.

Case, K M (1957), "Reformulation of the Majorana Theory of the Neutrino," Phys. Rev. **107**, 307–316.

Caurier, E, G. Martinez-Pinedo, F. Nowacki, A. Poves, and A. P. Zuker (2005), "The Shell model as unified view of nuclear structure," Rev. Mod. Phys. **77**, 427–488.

Caurier, E, F. Nowacki, and A. Poves (2008), "Nuclear Structure Aspects of the Neutrinoless Double Beta Decay," Eur. Phys. J. A **36**, 195–200.

Caurier, E, F. Nowacki, and A. Poves (2012), "Shell Model description of the beta beta decay of 136Xe," Phys. Lett. B **711**, 62–64.

Caurier, E, A. P. Zuker, and A. Poves (1990), "A Full $0\hbar\omega$ description of the $2\nu\beta\beta$ decay of ^{48}Ca," Phys. Lett. B **252**, 13–17.

Chadwick, J (1932), "Possible Existence of a Neutron," Nature **129**, 312.

Chadwick, J (1933), "Bakerian lecture. the neutron," Proceedings Mathematical Physical and Engineering Sciences

142, 1–25.

Chakrabortty, Joydeep, H. Zeen Devi, Srubabati Goswami, and Sudhanwa Patra (2012), "Neutrinoless double-β decay in TeV scale Left-Right symmetric models," JHEP **08**, 008, arXiv:1204.2527 [hep-ph].

Chambers, C, *et al.* (nEXO) (2019), "Imaging individual barium atoms in solid xenon for barium tagging in nEXO," Nature **569** (7755), 203–207, arXiv:1806.10694 [physics.ins-det].

Chavarria, A E, C. Galbiati, X. Li, and J. A. Rowlands (2017), "A high-resolution CMOS imaging detector for the search of neutrinoless double β decay in ^{82}Se," JINST **12**, P03022, arXiv:1609.03887 [physics.ins-det].

Chen, X, *et al.* (2017), "PandaX-III: Searching for neutrinoless double beta decay with high pressure^{136}Xe gas time projection chambers," Sci. China Phys. Mech. Astron. **60** (6), 061011, arXiv:1610.08883 [physics.ins-det].

Chikovani, GE, V.A. Mikhailov, and V.N. Roinishvili (1963), "A track spark chamber," Physics Letters **6** (3), 254–255.

Choi, K, K. S. Jeong, and W. Y. Song (2002), "Operator analysis of neutrinoless double beta decay," Phys.Rev.D **66**, 093007, arXiv:hep-ph/0207180.

Chou, W T, E. K. Warburton, and B. Alex Brown (1993), "Gamow-Teller beta-decay rates for A $<=$ 18 nuclei," Phys. Rev. C **47**, 163–177.

Cirigliano, V, W. Dekens, J. De Vries, M. L. Graesser, E. Mereghetti, S. Pastore, M. Piarulli, U. Van Kolck, and R. B. Wiringa (2019), "A renormalized approach to neutrinoless double-beta decay," Phys. Rev. C **100**, 055504.

Cirigliano, V, W. Dekens, J. De Vries, M. L. Graesser, E. Mereghetti, Saori Pastore, and Ubirajara Van Kolck (2018a), "New Leading Contribution to Neutrinoless Double-β Decay," Phys. Rev. Lett. **120**, 202001.

Cirigliano, V, W. Dekens, E. Mereghetti, and A. Walker-Loud (2018b), "Neutrinoless double-β decay in effective field theory: The light-Majorana neutrino-exchange mechanism," Phys. Rev. C **97**, 065501.

Cirigliano, V, W. Dekens, J. de Vries, M. L. Graesser, and E. Mereghetti (2017), "Neutrinoless double beta decay in chiral effective field theory: lepton number violation at dimension seven," JHEP **12**, 082.

Cirigliano, V, W. Dekens, J. de Vries, M. L. Graesser, and E. Mereghetti (2018c), "A neutrinoless double beta decay master formula from effective field theory," JHEP **12**, 097.

Cirigliano, V, W. Dekens, J. de Vries, M. Hoferichter, and E. Mereghetti (2021a), "Determining the leading-order contact term in neutrinoless double β decay," JHEP **05**, 289, 2102.03371.

Cirigliano, V, W. Dekens, J. de Vries, M. Hoferichter, and E. Mereghetti (2021b), "Toward Complete Leading-Order Predictions for Neutrinoless Double β Decay," Phys. Rev. Lett. **126**, 172002, 2012.11602.

Cirigliano, V, *et al.* (2022), "Towards Precise and Accurate Calculations of Neutrinoless Double-Beta Decay: Project Scoping Workshop Report," arXiv:2207.01085 [nucl-th].

Clemenza, M (2018), "Low background neutron activation: a high sensitivity technique for long-lived radionuclides determination in rare events physics experiments," Journal of Radioanalytical and Nuclear Chemistry 10.1007/s10967-018-6333-z.

Cleveland, B T, Timothy Daily, Raymond Davis, Jr., James R. Distel, Kenneth Lande, C. K. Lee, Paul S. Wildenhain, and Jack Ullman (1998), "Measurement of the solar electron neutrino flux with the Homestake chlorine detector," Astrophys. J. **496**, 505–526.

Cleveland, B T, W. R. Leo, C. S. Wu, L. R. Kasday, A. M. Rushton, P. J. Gollon, and J. D. Ullman (1975), "Lepton Conservation in the Double beta Decay of Se-82," Phys. Rev. Lett. **35**, 757–760.

Coello Pérez, E A, J. Menéndez, and A. Schwenk (2018), "Gamow-Teller and double-β decays of heavy nuclei within an effective theory," Phys. Rev. C **98**, 045501.

Coello Pérez, E A, J. Menéndez, and A. Schwenk (2019), "Two-neutrino double electron capture on ^{124}Xe based on an effective theory and the nuclear shell model," Phys. Lett. B **797**, 134885.

Conti, E, *et al.* (EXO-200) (2003), "Correlated fluctuations between luminescence and ionization in liquid xenon," Phys. Rev. B **68**, 054201, arXiv:hep-ex/0303008.

Coraggio, L, L. De Angelis, T. Fukui, A. Gargano, N. Itaco, and F. Nowacki (2019), "Renormalization of the Gamow-Teller operator within the realistic shell model," Phys. Rev. C **100**, 014316.

Coraggio, L, A. Gargano, N. Itaco, R. Mancino, and F. Nowacki (2020), "The calculation of the neutrinoless double-beta decay matrix element within the realistic shell model," Phys. Rev. C **101**, 044315, 2001.00890.

Coraggio, L, N. Itaco, G. De Gregorio, A. Gargano, R. Mancino, and F. Nowacki (2022), "Shell-model calculation of ^{100}Mo double-β decay," Phys. Rev. C **105**, 034312.

Cousins, R D (1995), "Why isn't every physicist a Bayesian?" Am. J. Phys. **63**, 398.

Cowan, C L, F. Reines, F. B. Harrison, H. W. Kruse, and A. D. McGuire (1956), "Detection of the free neutrino: A Confirmation," Science **124**, 103–104.

Cowan, G, K. Cranmer, E. Gross, and O. Vitells (2011), "Asymptotic formulae for likelihood-based tests of new physics," Eur. Phys. J. C **71**, 1554, [Erratum: Eur.Phys.J.C 73, 2501 (2013)], arXiv:1007.1727 [physics.data-an].

Crane, H R, and J. Halpern (1938), "New experimental evidence for the existence of a neutrino," Phys. Rev. **53**, 789–794.

Crane, H R, and J. Halpern (1939), "Further experiments on the recoil of the nucleus in beta-decay," Phys. Rev. **56**, 232–237.

Cremonesi, O, and M. Pavan (2014), "Challenges in Double Beta Decay," Adv. High Energy Phys. **2014**, 951432, arXiv:1310.4692 [physics.ins-det].

Cruz-Torres, R, A. Schmidt, G. A. Miller, L. B. Weinstein, N. Barnea, R. Weiss, E. Piasetzky, and O. Hen (2018), "Short range correlations and the isospin dependence of nuclear correlation functions," Phys. Lett. B **785**, 304–308.

Cruz-Torres, R, *et al.* (2021), "Many-body factorization and position–momentum equivalence of nuclear short-range correlations," Nature Phys. **17**, 306–310.

Dafinei, I, *et al.* (2017), "Production of 82Se enriched Zinc Selenide (ZnSe) crystals for the study of neutrinoless double beta decay," J. Cryst. Growth **475**, 158–170, arXiv:1702.05877 [physics.ins-det].

D'Alise, Alessandra, *et al.* (2022), "Standard model anomalies: Lepton flavour non-universality, g-2 and W-mass," arXiv:2204.03686 [hep-ph].

Danevich, F A, A. Sh. Georgadze, V. V. Kobychev, B. N. Kropivyansky, V. N. Kuts, A. S. Nikolaiko, V. I. Tretyak, and Yu. Zdesenko (1995), "The Research of double beta decay of Cd-116 with enriched Cd-116WO-4 crystal scintillators," Phys. Lett. B **344**, 72–78.

Dassie, D, *et al.* (NEMO) (1995), "Two neutrino double beta

decay measurement of Mo-100," Phys. Rev. D **51**, 2090–2100.

Davis, R (1952), "Nuclear recoil following neutrino emission from beryllium 7," Phys. Rev. **86**, 976–985.

Davis, Jr, R (1955), "Attempt to detect the antineutrinos from a nuclear reactor by the Cl37(anti-nu,e-) A37 reaction," Phys. Rev. **97**, 766–769.

Davoudi, Z, and S. V. Kadam (2021), "Path from Lattice QCD to the Short-Distance Contribution to $0\nu\beta\beta$ Decay with a Light Majorana Neutrino," Phys. Rev. Lett. **126**, 152003, 2012.02083.

Davoudi, Zohreh, William Detmold, Kostas Orginos, Assumpta Parreño, Martin J. Savage, Phiala Shanahan, and Michael L. Wagman (2021), "Nuclear matrix elements from lattice QCD for electroweak and beyond-Standard-Model processes," Phys. Rept. **900**, 1–74, arXiv:2008.11160 [hep-lat].

Davoudi, Zohreh, and Saurabh V. Kadam (2022), "Extraction of low-energy constants of single- and double-β decays from lattice QCD: A sensitivity analysis," Phys. Rev. D **105**, 094502.

Day, P, H. Leduc, B. Mazin, A. Vayonakis, and J. Zmuidzinas (2003), "A broadband superconducting detector suitable for use in large arrays," Nature **425**, 817–21.

De Bianchi, S (2018), "Rethinking antiparticles. Hermann Weyl's contribution to neutrino physics," Stud. Hist. Phil. Sci. B **61**, 68–79.

De Silva, A S, M. K. Moe, M. A. Nelson, and M. A. Vient (1997), "Double beta decays of Mo-100 and Nd-150," Phys. Rev. C **56**, 2451–2467, arXiv:nucl-ex/9706005.

Decamp, D, et al. (ALEPH) (1990), "A precise determination of the number of families with light neutrinos and of the z boson partial widths," Phys.Lett.B **235**, 399–411.

Dekens, Wouter, Jordy de Vries, Kaori Fuyuto, Emanuele Mereghetti, and Guanghui Zhou (2020), "Sterile neutrinos and neutrinoless double beta decay in effective field theory," JHEP **06**, 097.

Delaquis, S, et al. (EXO) (2018), "Deep Neural Networks for Energy and Position Reconstruction in EXO-200," JINST **13** (08), P08023, arXiv:1804.09641 [physics.ins-det].

Dell'Oro, S, S. Marcocci, M. Viel, and F. Vissani (2015), "The contribution of light Majorana neutrinos to neutrinoless double beta decay and cosmology," JCAP **12**, 023, arXiv:1505.02722 [hep-ph].

Dell'Oro, S, S. Marcocci, M. Viel, and F. Vissani (2016), "Neutrinoless double beta decay: 2015 review," Adv. High Energy Phys. **2016**, 2162659, arXiv:1601.07512 [hep-ph].

Dell'Oro, S, S. Marcocci, and F. Vissani (2018a), "Search for creation of electrons in lab," in *Search for creation of electrons in lab*, Vol. 1056, p. 012059.

Dell'Oro, S, S. Marcocci, and F. Vissani (2018b), "Testing creation of matter with neutrinoless double beta decay," in *Testing creation of matter with neutrinoless double beta decay*, Vol. NEUTEL2017 (SISSA) p. 030, arXiv:1710.06732 [hep-ph].

Dentler, M, A. Hernandez-Cabezudo, J. Kopp, P. A.N. Machado, M. Maltoni, I. Martinez-Soler, and T. Schwetz (2018), "Updated global analysis of neutrino oscillations in the presence of ev-scale sterile neutrinos," JHEP **08**, 010, arXiv:1803.10661 [hep-ph].

Deppisch, F, and H. Pas (2007), "Pinning down the mechanism of neutrinoless double beta decay with measurements in different nuclei," Phys. Rev. Lett. **98**, 232501, arXiv:hep-ph/0612165.

Deppisch, F F, L. Graf, J. Harz, and W.-C. Huang (2018), "Neutrinoless Double Beta Decay and the Baryon Asymmetry of the Universe," Phys. Rev. D **98**, 055029.

Deppisch, F F, L. Graf, F. Iachello, and J. Kotila (2020a), "Analysis of light neutrino exchange and short-range mechanisms in $0\nu\beta\beta$ decay," Phys. Rev. D **102** (9), 095016, arXiv:2009.10119 [hep-ph].

Deppisch, F F, Lukas Graf, and F. Šimkovic (2020b), "Searching for New Physics in Two-Neutrino Double Beta Decay," Phys. Rev. Lett. **125** (17), 171801, arXiv:2003.11836 [hep-ph].

Deppisch, F F, M. Hirsch, and H. Pas (2012), "Neutrinoless Double Beta Decay and Physics Beyond the Standard Model," J. Phys. G **39**, 124007, arXiv:1208.0727 [hep-ph].

Deppisch, Frank F, P. S. Bhupal Dev, and Apostolos Pilaftsis (2015a), "Neutrinos and Collider Physics," New J. Phys. **17** (7), 075019, arXiv:1502.06541 [hep-ph].

Deppisch, Frank F, Julia Harz, Martin Hirsch, Wei-Chih Huang, and Heinrich Päs (2015b), "Falsifying High-Scale Baryogenesis with Neutrinoless Double Beta Decay and Lepton Flavor Violation," Phys. Rev. D **92** (3), 036005, arXiv:1503.04825 [hep-ph].

Depuydt, B, A. Theuwis, and I. Romandic (2006), "Germanium: From the first application of czochralski crystal growth to large diameter dislocation-free wafers," Materials Science in Semiconductor Processing **9** (4), 437 – 443, proceedings of Symposium T E-MRS 2006 Spring Meeting on Germanium based semiconductors from materials to devices.

Di Valentino, E, S. Gariazzo, and O. Mena (2021), "Most constraining cosmological neutrino mass bounds," Phys. Rev. D **104** (8), 083504, arXiv:2106.15267 [astro-ph.CO].

Dikmen, E, A. F. Lisetski, B. R. Barrett, P. Maris, A. M. Shirokov, and J. P. Vary (2015), "Ab initio effective interactions for sd-shell valence nucleons," Phys. Rev. C **91** (6), 064301.

Dirac, P A M (1928), "The quantum theory of the electron," Proceedings of the Royal Society of London Series A Containing Papers of a Mathematical and Physical Character (1905-1934) **117**, 610–624.

Doi, M, T. Kotani, and E. Takasugi (1985), "Double beta Decay and Majorana Neutrino," Prog. Theor. Phys. Suppl. **83**, 1.

Dolgoshein, BA, B.U. Rodionov, and B.I. Luchkov (1964), "Streamer chamber," Nuclear Instruments and Methods **29** (2), 270–276.

Dolgov, A D (2002), "Neutrinos in cosmology," Phys. Rept. **370**, 333–535, arXiv:hep-ph/0202122.

Dolinski, Michelle J, Alan W. P. Poon, and Werner Rodejohann (2019), "Neutrinoless Double-Beta Decay: Status and Prospects," Ann. Rev. Nucl. Part. Sci. **69**, 219–251, arXiv:1902.04097 [nucl-ex].

Drewes, Marco (2013), "The Phenomenology of Right Handed Neutrinos," Int. J. Mod. Phys. E **22**, 1330019, arXiv:1303.6912 [hep-ph].

Drewes, Marco, and Shintaro Eijima (2016), "Neutrinoless double β decay and low scale leptogenesis," Phys. Lett. B **763**, 72–79, arXiv:1606.06221 [hep-ph].

Drewes, Marco, Bjorn Garbrecht, Dario Gueter, and Juraj Klaric (2017), "Testing the low scale seesaw and leptogenesis," JHEP **08**, 018, arXiv:1609.09069 [hep-ph].

Drewes, Marco, Yannis Georis, Claudia Hagedorn, and Juraj Klarić (2022a), "Low-scale leptogenesis with flavour and CP symmetries," arXiv:2203.08538 [hep-ph].

Drewes, Marco, Yannis Georis, and Juraj Klarić (2022b), "Mapping the Viable Parameter Space for Testable Leptogenesis," Phys. Rev. Lett. **128** (5), 051801, arXiv:2106.16226 [hep-ph].

Dror, J A, G. Elor, and R. Mcgehee (2020), "Absorption of Fermionic Dark Matter by Nuclear Targets," JHEP **02**, 134, arXiv:1908.10861 [hep-ph].

Dueck, A, and W. Rodejohann (2013), "Fits to SO(10) Grand Unified Models," JHEP **09**, 024, arXiv:1306.4468 [hep-ph].

Duerr, M, M. Lindner, and A. Merle (2011), "On the quantitative impact of the schechter-valle theorem," JHEP **06**, 091, arXiv:1105.0901 [hep-ph].

Ebert, J, *et al.* (2016a), "Results of a search for neutrinoless double-β decay using the COBRA demonstrator," Phys. Rev. C **94** (2), 024603, arXiv:1509.04113 [nucl-ex].

Ebert, J, *et al.* (COBRA) (2016b), "The COBRA demonstrator at the LNGS underground laboratory," Nucl. Instrum. Meth. A **807**, 114–120, arXiv:1507.08177 [physics.ins-det].

Egido, J L (2016), "State-of-the-art of beyond mean field theories with nuclear density functionals," Phys. Scripta **91**, 073003.

Eguchi, K, *et al.* (KamLAND) (2003), "First results from KamLAND: Evidence for reactor anti-neutrino disappearance," Phys. Rev. Lett. **90**, 021802, arXiv:hep-ex/0212021.

Ejiri, H, and S. R. Elliott (2014), "Charged current neutrino cross section for solar neutrinos, and background to $\beta\beta(0\nu)$ experiments," Phys. Rev. C **89** (5), 055501, arXiv:1309.7957 [nucl-ex].

Ejiri, H, and S. R. Elliott (2017), "Solar neutrino interactions with the double beta decay nuclei of ^{82}Se, ^{100}Mo and ^{150}Nd," Phys. Rev. C **95** (5), 055501, arXiv:1703.06915 [nucl-ex].

Ejiri, H, J. Suhonen, and K. Zuber (2019), "Neutrino–nuclear responses for astro-neutrinos, single beta decays and double beta decays," Phys. Rept. **797**, 1–102.

Ejiri, H, *et al.* (1991), "Double beta decays of Mo-100," Phys. Lett. B **258**, 17–23.

Ejiri, H, *et al.* (1995), "Double beta decays of Cd-116," J. Phys. Soc. Jap. **64**, 339–343.

Ekström, A, G. R. Jansen, K. A. Wendt, G. Hagen, T. Papenbrock, S. Bacca, B. Carlsson, and D. Gazit (2014), "Effects of three-nucleon forces and two-body currents on Gamow-Teller strengths," Phys. Rev. Lett. **113** (26), 262504.

Elliott, S R (2012), "Recent Progress in Double Beta Decay," Mod. Phys. Lett. A **27**, 1230009, arXiv:1203.1070 [nucl-ex].

Elliott, S R, and J. Engel (2004), "Double beta decay," J. Phys. G **30**, R183–R215, arXiv:hep-ph/0405078.

Elliott, S R, and M. Franz (2015), "Colloquium: Majorana Fermions in nuclear, particle and solid-state physics," Rev. Mod. Phys. **87**, 137, arXiv:1403.4976 [cond-mat.supr-con].

Elliott, S R, A. A. Hahn, and M. K. Moe (1987), "Direct Evidence for Two Neutrino Double Beta Decay in ^{82}Se," Phys. Rev. Lett. **59**, 2020–2023.

Elliott, S R, A. A. Hahn, M. K. Moe, M. A. Nelson, and M. A. Vient (1992), "Double beta decay of Se-82," Phys. Rev. C **46**, 1535–1537.

Elliott, S R, M. K. Moe, M. A. Nelson, and M. A. Vient (1991), "The Double beta decay spectrum of Mo-100 as measured with a TPC," J. Phys. G **17**, S145–S153.

Ellis, C D, and W. A Wooster (1927), "The average energy of disintegration of radium E," Proc. Roy. Soc. Lond. A **117** (776), 109–123.

Engel, J, and J. Menéndez (2017), "Status and future of nuclear matrix elements for neutrinoless double-beta decay:

a review," Rep. Prog. Phys. **80**, 046301.

Engel, J, F. Šimkovic, and P. Vogel (2014), "Chiral Two-Body Currents and Neutrinoless Double-Beta Decay in the QRPA," Phys. Rev. C **89**, 064308.

Engel, J, P. Vogel, and M. R. Zirnbauer (1988), "Nuclear Structure Effects in Double beta Decay," Phys. Rev. C **37**, 731–746.

Engel, Jonathan, and Gaute Hagen (2009), "Corrections to the Neutrinoless Double-Beta-Decay Operator in the Shell Model," Phys. Rev. C **79**, 064317, arXiv:0904.1709 [nucl-th].

ENSDF, (2021), http://www.nndc.bnl.gov/ensdf.

Entwisle, J P, *et al.* (2016), "Change of nuclear configurations in the neutrinoless double-beta decay of 130Te 130Xe and 136Xe 136Ba," Phys. Rev. C **93**, 064312.

Epelbaum, E, H. Krebs, and U.-G. Meissner (2008), "Delta-excitations and the three-nucleon force," Nucl. Phys. **A806**, 65–78.

Esteban, I, M. C. Gonzalez-Garcia, M. Maltoni, T. Schwetz, and Albert Zhou (2020), "The fate of hints: updated global analysis of three-flavor neutrino oscillations," JHEP **09**, 178, arXiv:2007.14792 [hep-ph].

Ettengruber, Manuel, Matteo Agostini, Allen Caldwell, Philipp Eller, and Oliver Schulz (2022), "Discovering neutrinoless double-beta decay in the era of precision neutrino cosmology," arXiv:2208.09954 [hep-ph].

Faessler, A, M. González, S. Kovalenko, and F. Šimkovic (2014), "Arbitrary mass Majorana neutrinos in neutrinoless double beta decay," Phys. Rev. D **90** (9), 096010.

Faessler, Amand, Thomas Gutsche, Sergey Kovalenko, and Fedor Simkovic (2008), "Pion dominance in RPV SUSY induced neutrinoless double beta decay," Phys. Rev. D **77**, 113012, arXiv:0710.3199 [hep-ph].

Fang, D-L, A. Faessler, and F. Šimkovic (2018), "0$\nu\beta\beta$-decay nuclear matrix element for light and heavy neutrino mass mechanisms from deformed quasiparticle random-phase approximation calculations for ^{76}Ge, ^{82}Se, ^{130}Te, ^{136}Xe, and ^{150}Nd with isospin restoration," Phys. Rev. C **97**, 045503.

Fano, U (1947), "Ionization Yield of Radiations. 2. The Fluctuations of the Number of Ions," Phys. Rev. **72**, 26–29.

Feinberg, G, and M. Goldhaber (1959), "Microscopic tests of symmetry principles," Proceedings of the National Academy of Sciences **45**, 1301–1312.

Fermi, E (1934), "Versuch einer theorie der β-strahlen. i," Zeitschrift für Physik A Hadrons and Nuclei **88**, 161–177.

Fernandes, R R Greenberg; P Bode; Elisabete A De Nadai (2011), "Neutron activation analysis: A primary method of measurement," Spectrochimica Acta Part B: Atomic Spectroscopy **66**, 193–241.

Feruglio, F, A. Strumia, and F. Vissani (2002), "Neutrino oscillations and signals in beta and 0nu2beta experiments," Nucl. Phys. B **637**, 345–377, [Addendum: Nucl.Phys.B 659, 359–362 (2003)], hep-ph/0201291.

Feynman, R P, and M. Gell-Mann (1958), "Theory of Fermi interaction," Phys. Rev. **109**, 193–198.

Finch, S W (2015), *Double-Beta Decay of ^{96}Zr and Double-Electron Capture of ^{156}Dy to Excited Final States*, Ph.D. thesis (Duke University).

Fink, D, *et al.* (2012), "Q-Value and Half-Lives for the Double-Beta-Decay Nuclide 110Pd," Phys. Rev. Lett. **108**, 062502, arXiv:1112.5786 [nucl-ex].

Fiorini, E, A. Pullia, G. Bertolini, F. Cappellani, and G. Restelli (1967), "A Search for Lepton Nonconservation in Double Beta Decay With a Germanium Detector," *Meet-*

ing of the Italian School of Physics and Weak Interactions Bologna, Italy, April 26-28, 1984, Phys. Lett. **25B**, 602–603, [,662(1967)].

Fiorini, E, A. Pullia, G. Bertolini, F. Cappellani, and G. Restelli (1973), "Neutrinoless double-beta decay of76Ge," Nuovo Cimento A Serie **13** (3), 747–763.

Fireman, E L (1948), "Double Beta Decay," Phys. Rev. **74**, 1238.

Fireman, E L (1949), "A measurement of the half-life of double beta-decay from (50)Sn-124," Phys. Rev. **75**, 323–324.

Fireman, E L, and D. Schwarzer (1952), "A re-investigation of the double beta-decay from Sn-124," Phys. Rev. **86**, 451–453.

Fleischmann, A, C. Enss, and G.M. Seidel (2005), "Metallic magnetic calorimeters," in *Cryogenic Particle Detection*, edited by C. Enss (Springer Berlin Heidelberg, Berlin, Heidelberg) pp. 151–216.

Fogli, GL, E. Lisi, A. Marrone, A. Melchiorri, A. Palazzo, P. Serra, and J. Silk (2004), "Observables sensitive to absolute neutrino masses: Constraints and correlations from world neutrino data," Phys.Rev.D **70**, 113003, arXiv:hep-ph/0408045.

Font-Ribera, A, P. McDonald, N. Mostek, B. A. Reid, H.-J. Seo, and A. Slosar (2014), "DESI and other dark energy experiments in the era of neutrino mass measurements," JCAP **05**, 023, arXiv:1308.4164 [astro-ph.CO].

Formaggio, J A, and G. P. Zeller (2012), "From eV to EeV: Neutrino Cross Sections Across Energy Scales," Rev. Mod. Phys. **84**, 1307–1341, arXiv:1305.7513 [hep-ex].

Fox, J M R, and C. W. Johnson (2019), "Uncertainty quantification of an empirical shell-model interaction using principal component analysis," arXiv:1911.05208.

Freck, D V, and J. Wakefield (1962), "Gamma-Ray Spectrum obtained with a Lithium-drifted p-i-n Junction in Germanium," Nature (London) **193** (4816), 669.

Freeman, S J, and J. P. Schiffer (2012), "Constraining the $0\nu2\beta$ matrix elements by nuclear structure observables," J. Phys. G **39**, 124004.

Freeman, S J, et al. (2017), "Experimental study of the rearrangements of valence protons and neutrons amongst single-particle orbits during double-β decay in 100Mo," Phys. Rev. C **96**, 054325.

Freer, M, H. Horiuchi, Y. Kanada-En'yo, D. Lee, and U.-G. Meißner (2018), "Microscopic Clustering in Light Nuclei," Rev. Mod. Phys. **90**, 035004.

Frekers, D, and M. Alanssari (2018), "Charge-exchange reactions and the quest for resolution," Eur. Phys. J. A **54**, 177.

Fremlin, J H, and M C Walters (1952), "An experimental investigation of the stability of nuclei against double beta-disintegration," Proceedings of the Physical Society. Section A **65** (11), 911–915.

Freund, K, et al. (2016), "The Performance of the Muon Veto of the GERDA Experiment," Eur. Phys. J. C **76** (5), 298, arXiv:1601.05935 [physics.ins-det].

Fritzsch, H, and P. Minkowski (1975), "Unified interactions of leptons and hadrons," Annals Phys. **93**, 193–266.

Fujita, Y, B. Rubio, and W. Gelletly (2011), "Spin-isospin excitations probed by strong, weak and electro-magnetic interactions," Prog. Part. Nucl. Phys. **66**, 549–606.

Fukuda, Y (2016), "ZICOS - New project for neutrinoless double beta decay experiment using zirconium complex in liquid scintillator," J. Phys. Conf. Ser. **718** (6), 062019.

Fukuda, Y, S. Moriyama, K. Hiraide, I. Ogawa, T. Gunji,
R. Hayami, S. Tsukadaw, and S. Kurosawa (2020), "ZICOS - Neutrinoless Double Beta Decay experiment using Zr-96 with an organic liquid scintillator -," J. Phys. Conf. Ser. **1468** (1), 012139.

Fukugita, M, and T. Yanagida (1986), "Baryogenesis Without Grand Unification," Phys. Lett. B **174**, 45–47.

Furry, W H (1938), "Note on the Theory of the Neutral Particle," Phys. Rev. **54**, 56–67.

Furry, W H (1939), "On transition probabilities in double beta-disintegration," Phys. Rev. **56**, 1184–1193.

Galan, J, et al. (2020), "Topological background discrimination in the PandaX-III neutrinoless double beta decay experiment," J. Phys. G **47** (4), 045108, arXiv:1903.03979 [physics.ins-det].

Gando, A, et al. (KamLAND-Zen) (2012), "Measurement of the double-β decay half-life of ^{136}Xe with the KamLAND-Zen experiment," Phys. Rev. **C85**, 045504, arXiv:1201.4664 [hep-ex].

Gando, A, et al. (KamLAND-Zen) (2013), "Limit on Neutrinoless $\beta\beta$ Decay of ^{136}Xe from the First Phase of KamLAND-Zen and Comparison with the Positive Claim in ^{76}Ge," Phys. Rev. Lett. **110** (6), 062502, arXiv:1211.3863 [hep-ex].

Gando, A, et al. (KamLAND-Zen) (2016), "Search for Majorana Neutrinos near the Inverted Mass Hierarchy Region with KamLAND-Zen," Phys. Rev. Lett. **117** (8), 082503, [Addendum: Phys.Rev.Lett. 117, 109903 (2016)], arXiv:1605.02889 [hep-ex].

Gando, A, et al. (KamLAND-Zen) (2019), "Precision measurement of the ^{136}Xe two-neutrino $\beta\beta$ spectrum in KamLAND-Zen and its impact on the quenching of nuclear matrix elements," Phys. Rev. Lett. **122**, 192501.

Gando, Y (KamLAND-Zen) (2020), "First results of KamLAND-Zen 800," J. Phys. Conf. Ser. **1468** (1), 012142.

Gazit, D, S. Quaglioni, and P. Navratil (2009), "Three-Nucleon Low-Energy Constants from the Consistency of Interactions and Currents in Chiral Effective Field Theory," Phys. Rev. Lett. **103**, 102502, [Erratum: Phys. Rev. Lett.122,no.2,029901(2019)].

Gehman, V M, and S. R. Elliott (2007), "Multiple-Isotope Comparison for Determining 0 nu beta beta Mechanisms," J. Phys. G **34**, 667–678, [Erratum: J.Phys.G 35, 029701 (2008)], arXiv:hep-ph/0701099.

Gell-Mann, M, and A. Pais (1955), "Behavior of neutral particles under charge conjugation," Phys. Rev. **97**, 1387–1389.

Gell-Mann, M, P. Ramond, and R. Slansky (1979), "Complex spinors and unified theories," in *Complex Spinors and Unified Theories*, Vol. 790927, pp. 315–321, arXiv:1306.4669 [hep-th].

Georgi, H, and S.L. Glashow (1974), "Unity of all elementary particle forces," Phys.Rev.Lett. **32**, 438–441.

Giuliani, A, J. J. Gomez Cadenas, S. Pascoli, E. Previtali, R. Saakyan, K. Schäffner, and S. Schönert (APPEC Committee) (2019), "Double Beta Decay APPEC Committee Report," arXiv:1910.04688 [hep-ex].

Giuliani, A, and A. Poves (2012), "Neutrinoless Double-Beta Decay," Adv. High Energy Phys. **2012**, 857016.

Giunti, C, and T. Lasserre (2019), "eV-scale Sterile Neutrinos," Ann. Rev. Nucl. Part. Sci. **69**, 163–190, arXiv:1901.08330 [hep-ph].

Goeppert-Mayer, M (1935), "Double beta-disintegration," Phys. Rev. **48**, 512–516.

Goeppert-Mayer, M (1949), "On closed shells in nuclei. 2,"

Phys. Rev. **75**, 1969–1970.

Goldhaber, M, L. Grodzins, and A. W. Sunyar (1958), "Helicity of Neutrinos," Phys. Rev. **109**, 1015–1017.

Golling, T, *et al.* (2016), "Physics at a 100 TeV pp collider: beyond the Standard Model phenomena," 10.23731/CYRM-2017-003.441, arXiv:1606.00947 [hep-ph].

Gomez-Cadenas, J J, J. Martin-Albo, M. Mezzetto, F. Monrabal, and M. Sorel (2012), "The Search for neutrinoless double beta decay," Riv. Nuovo Cim. **35** (2), 29–98, arXiv:1109.5515 [hep-ex].

Gomez-Cadenas, Juan J, Francesc Monrabal Capilla, and Paola Ferrario (2019), "High Pressure Gas Xenon TPCs for Double Beta Decay Searches," Front. in Phys. **7**, 51, arXiv:1903.02435 [physics.ins-det].

Gonokami, M (2018), "Statement from the president of the university of tokyo concerning the start of hyper-kamiokande," https://www.hyperk.org/?p=365, accessed 2021 December.

Gonzalez, D, *et al.* (2000), "Current IGEX results for neutrinoless double-beta decay of Ge-76," Nucl. Phys. B Proc. Suppl. **87**, 278–280.

Gooding, D, J. Gruszko, C. Grant, B. Naranjo, and L. Winslow (2018), "Light Yield of Perovskite Nanocrystal-Doped Liquid Scintillator," arXiv:1807.06634 [physics.ins-det].

de Gouvea, A, and J. Jenkins (2008), "A survey of lepton number violation via effective operators," Phys.Rev.D **77**, 013008, arXiv:0708.1344 [hep-ph].

de Gouvea, Andre (2005), "See-saw energy scale and the LSND anomaly," Phys. Rev. D **72**, 033005, arXiv:hep-ph/0501039.

de Gouvea, Andre (2007), "GeV seesaw, accidentally small neutrino masses, and Higgs decays to neutrinos," arXiv:0706.1732 [hep-ph].

de Gouvea, Andre (2022), "Model dependence in neutrinoless double-beta decay probes," Seattle Snowmass Summer Meeting.

de Gouvea, Andre, and Petr Vogel (2013), "Lepton Flavor and Number Conservation, and Physics Beyond the Standard Model," Prog. Part. Nucl. Phys. **71**, 75–92, arXiv:1303.4097 [hep-ph].

de Graaff, A, Y.-C. Cai, C. Heymans, and J. A. Peacock (2019), "Probing the missing baryons with the Sunyaev-Zel'dovich effect from filaments," Astron. Astrophys. **624**, A48, arXiv:1709.10378 [astro-ph.CO].

Graesser, M L (2017), "An electroweak basis for neutrinoless double β decay," JHEP **08**, 099.

Graesser, Michael L, Gang Li, Michael J. Ramsey-Musolf, Tianyang Shen, and Sebastián Urrutia-Quiroga (2022), "Uncovering a chirally suppressed mechanism of $0\nu\beta\beta$ decay with LHC searches," arXiv:2202.01237 [hep-ph].

Graf, L, F. F. Deppisch, F. Iachello, and J. Kotila (2018), "Short-Range Neutrinoless Double Beta Decay Mechanisms," Phys. Rev. D **98**, 095023.

Gráf, Lukáš, Manfred Lindner, and Oliver Scholer (2022), "Unraveling the $0\nu\beta\beta$ decay mechanisms," Phys. Rev. D **106** (3), 035022, arXiv:2204.10845 [hep-ph].

Graham, E, D. Gooding, J. Gruszko, C. Grant, B. Naranjo, and L. Winslow (2019), "Light Yield of Perovskite Nanocrystal-Doped Liquid Scintillator," 10.1088/1748-0221/14/11/P11024, arXiv:1908.03564 [physics.ins-det].

Granena, F, *et al.* (NEXT) (2009), "NEXT, a HPGXe TPC for neutrinoless double beta decay searches," arXiv:0907.4054 [hep-ex].

Grant, C (2020), "Results from kamland-zen and sno+," .

Greuling, E, and R. C. Whitten (1960), "Lepton conservation and double beta-decay," Annals of Physics **11**, 510–533.

Gribov, VN, and B. Pontecorvo (1969), "Neutrino astronomy and lepton charge," Phys.Lett.B **28**, 493.

Gruszko, J, B. Naranjo, B. Daniel, A. Elagin, D. Gooding, C. Grant, J. Ouellet, and L. Winslow (2019), "Detecting Cherenkov light from 1–2 MeV electrons in linear alkylbenzene," JINST **14** (02), P02005, arXiv:1811.11144 [physics.ins-det].

Guiseppe, V E, C. D. Christofferson, K. R. Hair, and F. M. Adams (2018), "A Review and Outlook for the Removal of Radon-Generated Po-210 Surface Contamination," AIP Conf. Proc. **1921** (1), 070003, arXiv:1712.08167 [physics.ins-det].

Guzowski, P (NEMO-3) (2018), "The first ever search for neutrinoless quadruple beta decay," in *Prospects in Neutrino Physics*, pp. 154–158, arXiv:1804.00280 [hep-ex].

Gysbers, P, *et al.* (2019), "Discrepancy between experimental and theoretical β-decay rates resolved from first principles," Nature Phys. **15**, 428–431.

Ha, C, *et al.* (COSINE-100) (2019), "First Direct Search for Inelastic Boosted Dark Matter with COSINE-100," Phys. Rev. Lett. **122** (13), 131802, arXiv:1811.09344 [astro-ph.IM].

Haaranen, M, J. Kotila, and J. Suhonen (2017), "Spectrum-shape method and the next-to-leading-order terms of the β-decay shape factor," Phys. Rev. C **95**, 024327.

Haaranen, M, P. C. Srivastava, and J. Suhonen (2016), "Forbidden nonunique β decays and effective values of weak coupling constants," Phys. Rev. C **93**, 034308.

Hagen, G, G. R. Jansen, and T. Papenbrock (2016), "Structure of ^{78}Ni from first principles computations," Phys. Rev. Lett. **117**, 172501.

Hagen, G, S. J. Novario, Z. H. Sun, T. Papenbrock, G. R. Jansen, J. G. Lietz, T. Duguet, and A. Tichai (2022), "Angular-momentum projection in coupled-cluster theory: structure of ^{34}Mg," arXiv:2201.07298 [nucl-th].

Hagen, G, T. Papenbrock, M. Hjorth-Jensen, and D. J. Dean (2014), "Coupled-cluster computations of atomic nuclei," Rept. Prog. Phys. **77**, 096302.

Hall, L J, and M. Suzuki (1984), "Explicit r-parity breaking in supersymmetric models," Nucl.Phys.B **231**, 419–444.

Haller, E E, N. P. Palaio, M. Rodder, W. L. Hansen, and E. Kreysa (1984), "Ntd germanium: A novel material for low temperature bolometers," in *Neutron Transmutation Doping of Semiconductor Materials*, edited by R. D. Larrabee (Springer US, Boston, MA) pp. 21–36.

Hanna, G C, and B. Pontecorvo (1949), "The β Spectrum of H^3," Phys. Rev. **75**, 983–984.

Harkins, W D, and E. D. Wilson (1915a), "The structure of complex atoms and the changes of mass and weight involved in their formation," Proc. Nat. Acad. Sci. USA **1**, 276–283.

Harkins, W D, and E. D. Wilson (1915b), "The structure of complex atoms. the hydrogen-helium system. [second paper on atomic structure.]," Journal of the American Chemical Society **37**, 1383–1396.

Harvey, J A, and M. S. Turner (1990), "Cosmological baryon and lepton number in the presence of electroweak fermion number violation," Phys. Rev. D **42**, 3344–3349.

Haxel, O, J. H. D. Jensen, and H. E. Suess (1949), "On the "Magic Numbers" in Nuclear Structure," Phys. Rev. **75** (11), 1766–1766.

Haxton, W C, and G. J. Stephenson (1984), "Double beta Decay," Prog. Part. Nucl. Phys. 12, 409–479.

Hayes, A C, P. Navrátil, and J. P. Vary (2003), "Neutrino C-12 scattering in the ab initio shell model with a realistic three body interaction," Phys. Rev. Lett. 91, 012502.

Hayes, A C, and I. S. Towner (2000), "Shell model calculations of neutrino scattering from C-12," Phys. Rev. C 61, 044603.

Hebeler, K, J. D. Holt, J. Menendez, and A. Schwenk (2015), "Nuclear forces and their impact on neutron-rich nuclei and neutron-rich matter," Ann. Rev. Nucl. Part. Sci. 65, 457–484.

Heisenberg, W (1932a), "Über den bau der atomkerne. i," Zeitschrift für Physik A Hadrons and Nuclei 77, 1–11.

Heisenberg, W (1932b), "Über den bau der atomkerne. ii," Zeitschrift für Physik A Hadrons and Nuclei 78, 156–164.

Heisenberg, W (1933), "Über den bau der atomkerne. iii," Zeitschrift für Physik A Hadrons and Nuclei 80, 587–596.

Helset, A, and A. Kobach (2020), "Baryon number, lepton number, and operator dimension in the smeft with flavor symmetries," Phys.Lett.B 800, 135132, arXiv:1909.05853 [hep-ph].

Henderson, J, et al. (2019), "Triaxiality in selenium-76," Phys. Rev. C 99, 054313.

Hergert, H, S. K. Bogner, T. D. Morris, A. Schwenk, and K. Tsukiyama (2016), "The In-Medium Similarity Renormalization Group: A Novel Ab Initio Method for Nuclei," Phys. Rept. 621, 165–222.

Hernández, P, M. Kekic, J. López-Pavón, J. Racker, and J. Salvado (2016), "Testable Baryogenesis in Seesaw Models," JHEP 08, 157, arXiv:1606.06719 [hep-ph].

Hicks, S F, et al. (2022), "Nuclear structure of Te130 from inelastic neutron scattering and shell model analysis," Phys. Rev. C 105, 024329.

Higashiyama, K, K. Yanase, N. Yoshinaga, A. Umeya, and E. Uehara, A. Teruya (2020), J. Phys G.

Hinohara, N, and J. Engel (2014), "Proton-Neutron Pairing Amplitude as a Generator Coordinate for Double-Beta Decay," Phys. Rev. C 90, 031301.

Hinohara, Nobuo, and Jonathan Engel (2022), "Global calculation of two-neutrino double-β decay within the finite amplitude method in nuclear density functional theory," Phys. Rev. C 105, 044314.

Hirsch, M, M.A. Diaz, W. Porod, J.C. Romao, and J.W.F. Valle (2000a), "Neutrino masses and mixings from supersymmetry with bilinear r parity violation: A theory for solar and atmospheric neutrino oscillations," Phys.Rev.D 62, 113008, [Erratum: Phys.Rev.D 65, 119901 (2002)], arXiv:hep-ph/0004115.

Hirsch, M, J. C. Romao, and J. W. F. Valle (2000b), "Bilinear R-parity violating SUSY: Neutrinoless double beta decay in the light of solar and atmospheric neutrino data," Phys. Lett. B 486, 255–262, arXiv:hep-ph/0002264.

Hoferichter, M, Philipp Klos, J. Menéndez, and A. Schwenk (2019), "Nuclear structure factors for general spin-independent WIMP-nucleus scattering," Phys. Rev. D 99, 055031.

Hoferichter, M, J. Menéndez, and A. Schwenk (2020), "Coherent elastic neutrino-nucleus scattering: EFT analysis and nuclear responses," Phys. Rev. D 102, 074018, 2007.08529.

Holt, J D, and J. Engel (2013), "Effective double-β-decay operator for ^{76}Ge and ^{82}Se," Phys. Rev. C 87, 064315.

't Hooft, G (1976), "Symmetry breaking through bell-jackiw anomalies," Phys.Rev.Lett. 37, 8–11.

Hoppe, E W, C. E. Aalseth, O. T. Farmer, T. W. Hossbach, M. Liezers, H. S. Miley, N. R. Overman, and J. H. Reeves (2014), "Reduction of radioactive backgrounds in electroformed copper for ultra-sensitive radiation detectors," Nucl. Instrum. Meth. A 764, 116–121.

Horoi, M, and B.A. Brown (2013), "Shell-model analysis of the ^{136}Xe double beta decay nuclear matrix elements," Phys. Rev. Lett. 110, 222502.

Horoi, M, and A. Neacsu (2016a), "Analysis of mechanisms that could contribute to neutrinoless double-beta decay," Phys. Rev. D 93, 113014.

Horoi, M, and A. Neacsu (2016b), "Shell model predictions for ^{124}Sn double-β decay," Phys. Rev. C 93, 024308.

Horoi, M, and A. Neacsu (2018), "Shell model study of using an effective field theory for disentangling several contributions to neutrinoless double-β decay," Phys. Rev. C 98, 035502.

Horoi, M, A. Neacsu, and S. Stoica (2022), "A Statistical Analysis for the Neutrinoless Double-Beta Decay Matrix element of ^{48}Ca," arXiv:2203.10577 [nucl-th].

Hyvarinen, J, and J. Suhonen (2015), "Nuclear matrix elements for $0\nu\beta\beta$ decays with light or heavy Majorana-neutrino exchange," Phys. Rev. C 91, 024613.

IAEA, (2015), The Fukushima Daiichi Accident, Non-serial Publications (INTERNATIONAL ATOMIC ENERGY AGENCY, Vienna).

Ianni, Aldo (2020), "Considerations on Underground Laboratories," J. Phys. Conf. Ser. 1342 (1), 012003.

Ichikawa, Y, et al. (2019), "Interplay between nuclear shell evolution and shape deformation revealed by the magnetic moment of ^{75}Cu," Nature Phys. 15, 321–325.

Ichimura, M, H. Sakai, and T. Wakasa (2006), "Spin-isospin responses via (p,n) and (n,p) reactions," Prog. Part. Nucl. Phys. 56, 446–531.

Inghram, M G, and J. H. Reynolds (1949), "On the double beta-process," Phys. Rev. 76, 1265–1266.

Inghram, M G, and J. H. Reynolds (1950), "Double beta-decay of Te-130," Phys. Rev. 78, 822–823.

Irwin, KD (1995), "An application of electrothermal feedback for high resolution cryogenic particle detection," Applied Physics Letters 66 (15), 10.1063/1.113674.

Irwin, KD, and G.C. Hilton (2005), "Transition-edge sensors," in Cryogenic Particle Detection, edited by C. Enss (Springer Berlin Heidelberg, Berlin, Heidelberg) pp. 63–150.

Iwata, Y, N. Shimizu, T. Otsuka, Y. Utsuno, J. Menéndez, M. Honma, and T. Abe (2016), "Large-scale shell-model analysis of the neutrinoless $\beta\beta$ decay of ^{48}Ca," Phys. Rev. Lett. 116 (11), 112502.

Iwata, Y, N. Shimizu, Y. Utsuno, M. Honma, T. Abe, and T. Otsuka (2015), "Ingredients of nuclear matrix element for two-neutrino double-beta decay of 48Ca," JPS Conf. Proc. 6, 030057, 1409.4003.

Jansen, G R, J. Engel, G. Hagen, P. Navrátil, and A. Signoracci (2014), "Ab-initio coupled-cluster effective interactions for the shell model: Application to neutron-rich oxygen and carbon isotopes," Phys. Rev. Lett. 113, 142502.

Jiao, C, and C. W. Johnson (2019), "The marriage of rotational and vibrational modes in generator-coordinate-type calculations, with application to neutrinoless double-beta decay," Phys. Rev. C 100, 031303.

Jiao, C F, J. Engel, and J. D. Holt (2017), "Neutrinoless double-beta decay matrix elements in large shell-model

spaces with the generator-coordinate method," Phys. Rev. C **96**, 054310.

Jiao, C F, M. Horoi, and A. Neacsu (2018), "Neutrino-less double-β decay of 124Sn, 130Te, and 136Xe in the Hamiltonian-based generator-coordinate method," Phys. Rev. C **98**, 064324.

Jokiniemi, L, T. Miyagi, S. R. Stroberg, J. D. Holt, J. Kotila, and J. Suhonen (2021a), "Ab initio calculation of muon capture on ^{24}Mg," arXiv:2111.12992 [nucl-th].

Jokiniemi, L, P. Soriano, and J. Menéndez (2021b), "Impact of the leading-order short-range nuclear matrix element on the neutrinoless double-beta decay of heavy nuclei," 2107.13354.

Jokiniemi, L, and J. Suhonen (2019), "Muon-capture strength functions in intermediate nuclei of $0\nu\beta\beta$ decays," Phys. Rev. C **100**, 014619.

Jokiniemi, L, J. Suhonen, H. Ejiri, and I. H. Hashim (2019), "Pinning down the strength function for ordinary muon capture on 100 Mo," Phys. Lett. B **794**, 143–147.

Jokiniemi, Lotta, Beatriz Romeo, Pablo Soriano, and Javier Menéndez (2022), "Neutrinoless $\beta\beta$-decay nuclear matrix elements from two-neutrino $\beta\beta$-decay data," arXiv:2207.05108 [nucl-th].

Jones, B J P, et al. (NEXT) (2021), "The Dynamics of Ions on Phased Radio-frequency Carpets in High Pressure Gases and Application for Barium Tagging in Xenon Gas Time Projection Chambers," arXiv:2109.05902 [physics.ins-det].

Joshipura, A S, and K. M. Patel (2011), "Fermion Masses in SO(10) Models," Phys. Rev. D **83**, 095002, arXiv:1102.5148 [hep-ph].

JSC Isotope, (last accessed: Sep. 2020a), http://www.isotop.ru/en/view/1653/.

JSC Isotope, (last accessed: Sep. 2020b), http://www.isotop.ru/en/view/1658/.

JSC Isotope, (last accessed: Sep. 2020c), http://www.isotop.ru/en/view/1667/.

JSC Isotope, (last accessed: Sep. 2020d), http://www.isotop.ru/en/view/1308/.

Kajantie, K, M. Laine, K. Rummukainen, and M. E. Shaposhnikov (1996), "The Electroweak phase transition: A Nonperturbative analysis," Nucl. Phys. B **466**, 189–258, arXiv:hep-lat/9510020.

Kajita, Takaaki (2016), "Nobel Lecture: Discovery of atmospheric neutrino oscillations," Rev. Mod. Phys. **88** (3), 030501.

Kalkstein, M I, and W. F. Libby (1952), "An Investigation of the Double Beta-Decay of Sn-12450," Phys. Rev. **85**, 368–369.

Kaptanoglu, T, M. Luo, and J. Klein (2019), "Cherenkov and Scintillation Light Separation Using Wavelength in LAB Based Liquid Scintillator," JINST **14** (05), T05001, arXiv:1811.11587 [physics.ins-det].

Katayama, Y, K. Matumoto, S. Tanaka, and E. Yamada (1962), "Possible unified models of elementary particles with two neutrinos," Prog. Theor. Phys. **28**, 675.

Keefer, G, et al. (KamLAND) (2015), "Laboratory studies on the removal of radon-born lead from KamLAND's organic liquid scintillator," Nucl. Instrum. Meth. A **769**, 79–87, arXiv:1312.0977 [physics.ins-det].

Kishimoto, T (CANDLES) (2018), "CANDLES for the study of ^{48}Ca double beta decay and its future prospect," DBD18 workshop, Waikoloa HI, US.

Kishimoto, T, K. Matsuoka, T. Fukumoto, and S. Umehara (2015), "Calcium isotope enrichment by means of multi-channel counter-current electrophoresis for the study of particle and nuclear physics," PTEP **2015** (3), 033D03.

Kitching, T D, A. F. Heavens, and S. Das (2015), "3D Weak Gravitational Lensing of the CMB and Galaxies," Mon. Not. Roy. Astron. Soc. **449** (2), 2205–2214, arXiv:1408.7052 [astro-ph.CO].

Klapdor-Kleingrothaus, H V, A. Dietz, H. L. Harney, and I. V. Krivosheina (2001a), "Evidence for neutrinoless double beta decay," Mod. Phys. Lett. A **16**, 2409–2420, arXiv:hep-ph/0201231.

Klapdor-Kleingrothaus, H V, and I. V. Krivosheina (2006), "The evidence for the observation of 0nu beta beta decay: The identification of 0nu beta beta events from the full spectra," Mod. Phys. Lett. A **21**, 1547–1566.

Klapdor-Kleingrothaus, H V, I. V. Krivosheina, A. Dietz, and O. Chkvorets (2004), "Search for neutrinoless double beta decay with enriched Ge-76 in Gran Sasso 1990-2003," Phys. Lett. B **586**, 198–212, arXiv:hep-ph/0404088.

Klapdor-Kleingrothaus, H V, et al. (2001b), "Latest results from the Heidelberg-Moscow double beta decay experiment," Eur. Phys. J. A **12**, 147–154, arXiv:hep-ph/0103062.

Kleemann, J, et al. (2021), "Majorana parameters of the interacting boson model of nuclear structure and their implication for $0\nu\beta\beta$ decay," Phys. Rev. C **104** (6), L061302.

Klein, J (2017), personal communication.

van Kolck, U (1994), "Few nucleon forces from chiral Lagrangians," Phys. Rev. C **49**, 2932–2941.

Kolhinen, VS, et al. (2010), "Double-beta decay Q value of Nd-150," Phys. Rev. C **82**, 022501.

Kortelainen, M, O. Civitarese, J. Suhonen, and J. Toivanen (2007), "Short-range correlations and neutrinoless double beta decay," Phys. Lett. B **647**, 128–132.

Kostensalo, J, M. Haaranen, and J. Suhonen (2017), "Electron spectra in forbidden β decays and the quenching of the weak axial-vector coupling constant gA," Phys. Rev. C **95**, 044313.

Kostensalo, J, and J. Suhonen (2017), "gA -driven shapes of electron spectra of forbidden β decays in the nuclear shell model," Phys. Rev. C **96**, 024317.

Kostensalo, J, and J. Suhonen (2020), "Consistent large-scale shell-model analysis of the two-neutrino $\beta\beta$ and single β branchings in ^{48}Ca and ^{96}Zr," Phys. Lett. B **802**, 135192.

Kotila, J, and J. Barea (2016), "Occupation probabilities of single particle levels using the microscopic interacting boson model: Application to some nuclei of interest in neutrinoless double-β decay," Phys. Rev. C **94**, 034320.

Kotila, J, and F. Iachello (2012), "Phase space factors for double-β decay," Phys. Rev. C **85**, 034316, arXiv:1209.5722 [nucl-th].

Kotila, Jenni, Jacopo Ferretti, and Francesco Iachello (2021), "Long-range neutrinoless double beta decay mechanisms," arXiv:2110.09141 [hep-ph].

Krebs, H, E. Epelbaum, and U. G. Meißner (2017), "Nuclear axial current operators to fourth order in chiral effective field theory," Annals Phys. **378**, 317–395.

Kumar, A, P. C. Srivastava, J. Kostensalo, and J. Suhonen (2020), "Second-forbidden nonunique $\beta-$ decays of Na24 and Cl36 assessed by the nuclear shell model," Phys. Rev. C **101**, 064304, 2007.08122.

Kumar, A, P. C. Srivastava, and J. Suhonen (2021), "Second-forbidden nonunique β^- decays of ^{59,60}Fe: possible candidates for g_A sensitive electron spectral-shape measurements," Eur. Phys. J. A **57**, 225, 2101.03046.

Kuzmin, VA, V.A. Rubakov, and M.E. Shaposhnikov (1985), "On the Anomalous Electroweak Baryon Number Nonconservation in the Early Universe," Phys. Lett. B **155**, 36.

Kwiatkowski, A A, *et al.* (2014), "New determination of double-β-decay properties in 48Ca : High-precision Q$\beta\beta$-value measurement and improved nuclear matrix element calculations," Phys. Rev. **C89** (4), 045502, arXiv:1308.3815 [nucl-ex].

LaFerriere, B D, T. C. Maiti, I. J. Arnquist, and E. W. Hoppe (2015), "A novel assay method for the trace determination of Th and U in copper and lead using inductively coupled plasma mass spectrometry," Nucl. Instrum. Meth. A **775**, 93–98.

Land, B J, Z. Bagdasarian, J. Caravaca, M. Smiley, M. Yeh, and G. D. Orebi Gann (2021), "MeV-scale performance of water-based and pure liquid scintillator detectors," Phys. Rev. D **103** (5), 052004, arXiv:2007.14999 [physics.ins-det].

Landau, L D (1957), "On the conservation laws for weak interactions," Nucl. Phys. **3**, 127–131.

Lattanzi, M, and M. Gerbino (2018), "Status of neutrino properties and future prospects - Cosmological and astrophysical constraints," Front. in Phys. **5**, 70, arXiv:1712.07109 [astro-ph.CO].

Laubenstein, M (2017), "Screening of materials with high purity germanium detectors at the laboratori nazionali del gran sasso," International Journal of Modern Physics A **32**, 1743002.

Lawson, J S (1951), "A lower limit on the half-life of Sn-124," Phys. Rev. **81**, 299.

Lee, M H (AMoRE) (2020), "AMoRE: A search for neutrinoless double-beta decay of 100Mo using low-temperature molybdenum-containing crystal detectors," JINST **15** (08), C08010, arXiv:2005.05567 [physics.ins-det].

Lee, T D, and C.-N. Yang (1956), "Question of Parity Conservation in Weak Interactions," Phys. Rev. **104**, 254–258.

Lee, T D, and C. N. Yang (1957), "Parity nonconservation and a two-component theory of the neutrino," Physical Review (Series I) **105**, 1671–1675.

Lehman, Landon (2014), "Extending the Standard Model Effective Field Theory with the Complete Set of Dimension-7 Operators," Phys. Rev. D **90** (12), 125023, arXiv:1410.4193 [hep-ph].

Lehnert, B, E. Andreotti, D. Degering, M. Hult, M. Laubenstein, T. Wester, and K. Zuber (2016), "Double beta decays into excited states in ^{110}Pd and ^{102}Pd," J. Phys. G **43** (11), 115201, arXiv:1606.06616 [nucl-ex].

Leipunski, A I; Rutherford, Lord (1936), "Determination of the energy distribution of recoil atoms during β decay and the existence of the neutrino," Mathematical Proceedings of the Cambridge Philosophical Society **32**, 301.

Lenske, H, F. Cappuzzello, M. Cavallaro, and M. Colonna (2019), "Heavy ion charge exchange reactions as probes for nuclear β-decay," Prog. Part. Nucl. Phys. **109**, 103716.

Leonard, D S, *et al.* (2008), "Systematic study of trace radioactive impurities in candidate construction materials for EXO-200," Nucl. Instrum. Meth. A **591**, 490–509, arXiv:0709.4524 [physics.ins-det].

Leonard, D S, *et al.* (2017), "Trace radioactive impurities in final construction materials for EXO-200," Nucl. Instrum. Meth. A **871**, 169–179, arXiv:1703.10799 [physics.ins-det].

Levine, C A, A. Ghiorso, and G. T. Seaborg (1950), "Half-life of double beta-decay," Phys. Rev. **77**, 296.

Li, Gang, Michael Ramsey-Musolf, and Juan Carlos Vasquez (2021a), "Left-Right Symmetry and Leading Contributions to Neutrinoless Double Beta Decay," Phys. Rev. Lett. **126** (15), 151801, arXiv:2009.01257 [hep-ph].

Li, Hao-Lin, Zhe Ren, Ming-Lei Xiao, Jiang-Hao Yu, and Yu-Hui Zheng (2021b), "Complete set of dimension-nine operators in the standard model effective field theory," Phys. Rev. D **104** (1), 015025, arXiv:2007.07899 [hep-ph].

Liao, Yi, and Xiao-Dong Ma (2020), "An explicit construction of the dimension-9 operator basis in the standard model effective field theory," JHEP **11**, 152, arXiv:2007.08125 [hep-ph].

Lincoln, D L, J. D. Holt, G. Bollen, M. Brodeur, S. Bustabad, J. Engel, S. J. Novario, M. Redshaw, R. Ringle, and S. Schwarz (2013), "First direct double-β decay Q-Value measurement of^{82} Se in support of understanding the nature of the Neutrino," Phys. Rev. Lett. **110** (1), 012501, arXiv:1211.5659 [nucl-ex].

Lindner, Manfred, Farinaldo S. Queiroz, and Werner Rodejohann (2016), "Dilepton bounds on left–right symmetry at the LHC run II and neutrinoless double beta decay," Phys. Lett. B **762**, 190–195, arXiv:1604.07419 [hep-ph].

Lisi, Eligio, and Antonio Marrone (2022), "Majorana neutrino mass constraints in the landscape of nuclear matrix elements," Phys. Rev. D **106** (1), 013009, arXiv:2204.09569 [hep-ph].

Liu, Z Z, *et al.* (CDEX) (2019), "Constraints on Spin-Independent Nucleus Scattering with sub-GeV Weakly Interacting Massive Particle Dark Matter from the CDEX-1B Experiment at the China Jinping Underground Laboratory," Phys. Rev. Lett. **123** (16), 161301, arXiv:1905.00354 [hep-ex].

Lonardoni, D, J. Carlson, S. Gandolfi, J. E. Lynn, K. E. Schmidt, A. Schwenk, and X. Wang (2018), "Properties of nuclei up to $A = 16$ using local chiral interactions," Phys. Rev. Lett. **120**, 122502.

López Vaquero, N, T. R. Rodríguez, and J. L. Egido (2013), "Shape and pairing fluctuations effects on neutrinoless double beta decay nuclear matrix elements," Phys. Rev. Lett. **111**, 142501.

Maalampi, J, and J. Suhonen (2013), "Neutrinoless Double β^+/ EC Decays," Adv. High Energy Phys. **2013**, 505874.

Maiezza, A, M. Nemevsek, F. Nesti, and G. Senjanovic (2010), "Left-right symmetry at lhc," Phys.Rev.D **82**, 055022, arXiv:1005.5160 [hep-ph].

Majorana, E (1933), "Über die kerntheorie," Zeitschrift für Physik A Hadrons and Nuclei **82**, 137–145.

Majorana, E (1937), "Teoria simmetrica dell'elettrone e del positrone," Nuovo Cim. **14**, 171–184.

Maki, Z, M. Nakagawa, and S. Sakata (1962), "Remarks on the unified model of elementary particles," Prog. Theor. Phys. **28**, 870–880, [,34(1962)].

Mangano, G, G. Miele, S. Pastor, O. Pisanti, and S. Sarikas (2012), "Updated BBN bounds on the cosmological lepton asymmetry for non-zero θ_{13}," Phys. Lett. B **708**, 1–5, arXiv:1110.4335 [hep-ph].

Marsh, B A, *et al.* (2018), "Characterization of the shape-staggering effect in mercury nuclei," Nature Phys. **14**, 1163–1167.

Martín-Albo, J, *et al.* (NEXT) (2016), "Sensitivity of NEXT-100 to Neutrinoless Double Beta Decay," JHEP **05**, 159, arXiv:1511.09246 [physics.ins-det].

Martínez-Pinedo, G, A. Poves, E. Caurier, and A. P. Zuker (1996), "Effective g_A in the pf shell," Phys. Rev. C **53**, R2602, arXiv:nucl-th/9603039 [nucl-th].

Marx, G (1953), "Die wechselwirkung der elementar-teilchen und die erhaltungssätze," Acta Physica Academiae Scientiarum Hungaricae **3**, 55–58.

der Mateosian, E, and M. Goldhaber (1966), "Limits for lepton-conserving and lepton-nonconserving double beta decay in Ca-48," Phys. Rev. **146**, 810–815.

Matsuda, K, Y. Koide, T. Fukuyama, and H. Nishiura (2002), "How far can the SO(10) two Higgs model describe the observed neutrino masses and mixings?" Phys. Rev. D **65**, 033008, [Erratum: Phys.Rev.D 65, 079904 (2002)], arXiv:hep-ph/0108202.

McCarthy, J A (1953), "Search for double beta-decay in sn^{124} and zr^{96}," Phys. Rev. **90**, 853–857.

McCarthy, J A (1955), "Search for double beta decay in ca^{48}," Phys. Rev. **97**, 1234–1236.

McDonald, A D, et al. (2018), "Demonstration of Single Barium Ion Sensitivity for Neutrinoless Double Beta Decay using Single Molecule Fluorescence Imaging," Phys. Rev. Lett. **120** (13), 132504, arXiv:1711.04782 [physics.ins-det].

McDonald, Arthur B (2016), "Nobel Lecture: The Sudbury Neutrino Observatory: Observation of flavor change for solar neutrinos," Rev. Mod. Phys. **88** (3), 030502.

Mei, D, and A. Hime (2006), "Muon-induced background study for underground laboratories," Phys. Rev. D **73**, 053004, arXiv:astro-ph/0512125.

Mei, Y, X. Sun, and N. Xu (2020), "Topmetal CMOS direct charge sensing plane for neutrinoless double-beta decay search in high-pressure gaseous TPC," arXiv:2010.09226 [physics.ins-det].

Meija, Juris, Tyler B. Coplen, Michael Berglund, Willi A. Brand, Paul De Bièvre, Manfred Gröning, Norman E. Holden, Johanna Irrgeher, Robert D. Loss, Thomas Walczyk, and Thomas Prohaska (2016), "Isotopic compositions of the elements 2013 (iupac technical report)," Pure and Applied Chemistry **88** (3), 293–306.

Meitner, L, and W. Orthmann (1930), "Über eine absolute bestimmung der energie der primären β-strahlen von radium e," Zeitschrift für Physik A Hadrons and Nuclei **60**, 143–155.

Menéndez, J (2018), "Neutrinoless $\beta\beta$ decay mediated by the exchange of light and heavy neutrinos: The role of nuclear structure correlations," J. Phys. G **45**, 014003.

Menéndez, J, D. Gazit, and A. Schwenk (2011), "Chiral two-body currents in nuclei: Gamow-teller transitions and neutrinoless double-beta decay," Phys. Rev. Lett. **107**, 062501.

Menéndez, J, N. Hinohara, J. Engel, G. Martínez-Pinedo, and T. R. Rodréguez (2016), "Testing the importance of collective correlations in neutrinoless $\beta\beta$ decay," Phys. Rev. C **93**, 014305.

Menéndez, J, A. Poves, E. Caurier, and F. Nowacki (2009a), "Deformation and the nuclear matrix elements of the neutrinoless $\beta\beta$ decay," Proceedings, International School of Physics "Enrico Fermi", 170th Course, "Measurements of Neutrino Mass": Varenna, Italy, June 17-27, 2008, Proc. Int. Sch. Phys. Fermi **170**, 163–174.

Menéndez, J, A. Poves, E. Caurier, and F. Nowacki (2009b), "Disassembling the Nuclear Matrix Elements of the Neutrinoless beta beta Decay," Nucl. Phys. **A818**, 139–151.

Menéndez, J, A. Poves, E. Caurier, and F. Nowacki (2009), "Occupancies of individual orbits, and the nuclear matrix element of the ^{76}Ge neutrinoless $\beta\beta$ decay," Phys. Rev. C **80**, 048501.

Menéndez, J, A. Poves, E. Caurier, and F. Nowacki (2011), "Novel Nuclear Structure Aspects of the $0\nu\beta\beta$ - Decay," New quests in nuclear structure. Proceedings, 10th International Spring Seminar on Nuclear Physics, Vietri sul Mare, Italy, May 21-25, 2010, J. Phys. Conf. Ser. **267**, 012058.

Menéndez, J, T. R. Rodríguez, G. Martínez-Pinedo, and A. Poves (2014), "Correlations and neutrinoless $\beta\beta$ decay nuclear matrix elements of pf-shell nuclei," Phys. Rev. C **90**, 024311.

Minkowski, P (1977), "$\mu \to e\gamma$ at a rate of one out of 10^9 muon decays?" Phys.Lett.B **67**, 421–428.

Mitra, M, G. Senjanovic, and F. Vissani (2012), "Neutrinoless double beta decay and heavy sterile neutrinos," Nucl.Phys.B **856**, 26–73, arXiv:1108.0004 [hep-ph].

Moe, M K (1991), "New approach to the detection of neutrinoless double beta decay," Phys. Rev. C **44**, 931–934.

Mohapatra, R N, and G. Senjanovic (1980), "Neutrino mass and spontaneous parity nonconservation," Phys.Rev.Lett. **44**, 912.

Monrabal, F, et al. (NEXT) (2018), "The Next White (NEW) Detector," JINST **13** (12), P12010, arXiv:1804.02409 [physics.ins-det].

Moore, D C, S. R. Golwala, B. Bumble, B. Cornell, P. K. Day, H. G. LeDuc, and J. Zmuidzinas (2012), "Position and energy-resolved particle detection using phonon-mediated microwave kinetic inductance detectors," Appl. Phys. Lett. **100**, 232601, arXiv:1203.4549 [astro-ph.IM].

Morris, T D, J. Simonis, S. R. Stroberg, C. Stumpf, G. Hagen, J. D. Holt, G. R. Jansen, T. Papenbrock, R. Roth, and A. Schwenk (2018), "Structure of the lightest tin isotopes," Phys. Rev. Lett. **120**, 152503.

Morrison, L, et al. (2020), "Quadrupole deformation of ^{130}Xe measured in a Coulomb-excitation experiment," Phys. Rev. C **102**, 054304.

Mount, B J, M. Redshaw, and E. G. Myers (2010), "Double-beta-decay Q values of Se-74 and Ge-76," Phys. Rev. **C81**, 032501.

Mustonen, M T, and J. Engel (2013), "Large-scale calculations of the double-β decay of $^{76}Ge, ^{130}Te, ^{136}Xe$, and ^{150}Nd in the deformed self-consistent Skyrme quasiparticle random-phase approximation," Phys. Rev. C **87**, 064302.

Muto, K (1994), "Neutrinoless double beta decay beyond closure approximation," Nucl. Phys. A **577**, 415C–420C.

Nakamura, S, T. Sato, Vladimir P. Gudkov, and K. Kubodera (2001), "Neutrino reactions on the deuteron," Phys. Rev. C **63**, 034617.

Navrátil, P, S. Quaglioni, G. Hupin, C. Romero-Redondo, and A. Calci (2016), "Unified ab initio approaches to nuclear structure and reactions," Phys. Scripta **91**, 053002.

Neacsu, A, and M. Horoi (2015), "Shell model studies of the ^{130}Te neutrinoless double-beta decay," Phys. Rev. C **91**, 024309.

Nemevsek, Miha, Goran Senjanovic, and Vladimir Tello (2013), "Connecting Dirac and Majorana Neutrino Mass Matrices in the Minimal Left-Right Symmetric Model," Phys. Rev. Lett. **110** (15), 151802, arXiv:1211.2837 [hep-ph].

Neufcourt, L, Y. Cao, W. Nazarewicz, E. Olsen, and F. Viens (2019), "Neutron drip line in the Ca region from Bayesian model averaging," Phys. Rev. Lett. **122**, 062502.

Neuhauser, W, M. Hohenstatt, P. E. Toschek, and H. Dehmelt (1980), "Localized visible Ba$^+$ mono-ion oscillator," Phys. Rev. A **22** (3), 1137–1140.

von Neumann-Cosel, P, A. Poves, J. Retamosa, and A. Richter (1998), "Magnetic dipole response in nuclei at

the N =28 shell closure: a new look," Phys. Lett. B **443**, 1–6.

Ney, E M, J. Engel, and N. Schunck (2022), "Two-body weak currents in heavy nuclei," Phys. Rev. C **105**, 034349.

Nilles, H-P, and N. Polonsky (1997), "Supersymmetric neutrino masses, r symmetries, and the generalized μ problem," Nucl.Phys.B **484**, 33–62, arXiv:hep-ph/9606388.

Nisi, S, L. Copia, I. Dafinei, and M. L. Di Vacri (2017), "ICP-MS measurement of natural radioactivity at LNGS," Int. J. Mod. Phys. A **32** (30), 1743003.

Nomura, Kosuke (2022), "Two-neutrino double-β decay in the mapped interacting boson model," Phys. Rev. C **105**, 044301.

Nones, C (2021), "Bingo," Presentation at TAUP 2021.

Novario, S, P. Gysbers, J. Engel, G. Hagen, G. R. Jansen, T. D. Morris, P. Navrátil, T. Papenbrock, and S. Quaglioni (2021), "Coupled-Cluster Calculations of Neutrinoless Double-β Decay in ^{48}Ca," Phys. Rev. Lett. **126**, 182502, arXiv:2008.09696.

NSAC NLDBD Subcommittee, (2014), "Report to the nuclear science advisory committee," https://science.osti.gov/-/media/np/nsac/pdf/docs/2014/NLDBD_Report_2014_Final.pdf.

NSAC NLDBD Subcommittee, (2015), "Report to the nuclear science advisory committee," https://science.osti.gov/-/media/np/nsac/pdf/docs/2016/NLDBD_Report_2015_Final_Nov18.pdf.

Nygren, D (2009), "High-pressure xenon gas electroluminescent TPC for 0nu beta beta-decay search," Nucl. Instrum. Meth. A **603**, 337–348.

Nygren, D R (1974), "The Time Projection Chamber: A New 4 pi Detector for Charged Particles," eConf **C740805**, 58.

Nygren, D R, B. J. P. Jones, N. López-March, Y. Mei, F. Psihas, and J. Renner (2018), "Neutrinoless Double Beta Decay with ^{82}SeF$_6$ and Direct Ion Imaging," JINST **13** (03), P03015, arXiv:1801.04513 [physics.ins-det].

Nzobadila Ondze, J C, *et al.* (2021), "Investigation of pair-correlated 0^+ states in ^{134}Ba via the ^{136}Ba(p,t) reaction," Phys. Rev. C **103**, 034329.

Obara, S, *et al.* (2020), "AXEL: High-pressure Xe gas TPC for BG-free $0\nu2\beta$ decay search," Nucl. Instrum. Meth. A **958**, 162803, arXiv:1909.09343 [physics.ins-det].

Ohlsson, T, and M. Pernow (2021), "Flavor symmetries in the Yukawa sector of non-supersymmetric SO(10): numerical fits using renormalization group running," JHEP **09**, 111, arXiv:2107.08771 [hep-ph].

Otsuka, T, A. Arima, and F. Iachello (1978), "Nuclear shell model and interacting bosons," Nucl. Phys. A **309**, 1–33.

Otsuka, T, and Y. Tsunoda (2016), "The role of shell evolution in shape coexistence," J. Phys. G **43**, 024009.

Otsuka, Takaharu, Alexandra Gade, Olivier Sorlin, Toshio Suzuki, and Yutaka Utsuno (2020), "Evolution of shell structure in exotic nuclei," Rev. Mod. Phys. **92**, 015002.

Palaio, N P, M. Rodder, E. E. Haller, and E. Kreysa (1983), "Neutron-transmutation-doped germanium bolometers," Int. J. Infrared Milli. Waves **4** (6), 933–943.

Palanque-Delabrouille, N, C. Yèche, N. Schöneberg, J. Lesgourgues, M. Walther, S. Chabanier, and E. Armengaud (2020), "Hints, neutrino bounds and WDM constraints from SDSS DR14 Lyman-α and Planck full-survey data," JCAP **04**, 038, arXiv:1911.09073 [astro-ph.CO].

Park, T S, L. E. Marcucci, R. Schiavilla, M. Viviani, A. Kievsky, S. Rosati, K. Kubodera, D. P. Min, and M. Rho (2003), "Parameter free effective field theory calcu-

lation for the solar proton fusion and hep processes," Phys. Rev. C **67**, 055206.

Pas, H, M. Hirsch, H. V. Klapdor-Kleingrothaus, and S. G. Kovalenko (1999), "Towards a superformula for neutrinoless double beta decay," Phys. Lett. B **453**, 194–198.

Pas, H, M. Hirsch, H. V. Klapdor-Kleingrothaus, and S. G. Kovalenko (2001), "A Superformula for neutrinoless double beta decay. 2. The Short range part," Phys. Lett. B **498**, 35–39.

Päs, H, and W. Rodejohann (2015), "Neutrinoless Double Beta Decay," New J. Phys. **17** (11), 115010, arXiv:1507.00170 [hep-ph].

Pastore, S, A. Baroni, J. Carlson, S. Gandolfi, S. C. Pieper, R. Schiavilla, and R. B. Wiringa (2018a), "Quantum Monte Carlo calculations of weak transitions in $A = 6$–10 nuclei," Phys. Rev. C **97** (2), 022501.

Pastore, S, J. Carlson, V. Cirigliano, W. Dekens, E. Mereghetti, and R. B. Wiringa (2018b), "Neutrinoless double-β decay matrix elements in light nuclei," Phys. Rev. C **97**, 014606.

Pati, J C, and A. Salam (1974), "Lepton number as the fourth color," Phys.Rev.D **10**, 275–289, [Erratum: Phys.Rev.D 11, 703–703 (1975)].

Patterson, R B (2015), "Prospects for Measurement of the Neutrino Mass Hierarchy," Ann. Rev. Nucl. Part. Sci. **65**, 177–192, arXiv:1506.07917 [hep-ex].

Pauli, W (1930), "Dear radioactive ladies and gentlemen," published in Phys. Today 31N9, 27 (1978), letter to L. Meitner.

Pearce, R M, and E. K. Darby (1952), "Double beta-decay of sn^{124}," Phys. Rev. **86**, 1049–1050.

Petcov, S T (2013), "The Nature of Massive Neutrinos," Adv. High Energy Phys. **2013**, 852987, arXiv:1303.5819 [hep-ph].

Piquemal, F (NEMO) (2006), "The SuperNEMO project," Phys. Atom. Nucl. **69**, 2096–2100.

Pirinen, P, and J. Suhonen (2015), "Systematic approach to β and $2\nu\beta\beta$ decays of mass $A =100$–136 nuclei," Phys. Rev. C **91**, 054309.

Pisanti, O (2020), "Improved nuclear reaction network for a reliable estimate of primordial Deuterium yield," J. Phys. Conf. Ser. **1468** (1), 012010.

Poda, Denys, and Andrea Giuliani (2017), "Low background techniques in bolometers for double-beta decay search," Int. J. Mod. Phys. A **32** (30), 1743012, arXiv:1711.01075 [physics.ins-det].

Pontecorvo, B (1947), "Nuclear capture of mesons and the meson decay," Phys. Rev. **72**, 246.

Pontecorvo, B (1957a), "Inverse beta processes and nonconservation of lepton charge," Zh. Eksp. Teor. Fiz. **34**, 247.

Pontecorvo, B (1957b), "Mesonium and anti-mesonium," Sov. Phys. JETP **6**, 429, [Zh. Eksp. Teor. Fiz.33,549(1957)].

Pontecorvo, B (1967), "Neutrino Experiments and the Problem of Conservation of Leptonic Charge," Zh. Eksp. Teor. Fiz. **53**, 1717–1725.

Pontecorvo, B (1968), "Superweak interactions and double beta decay," Physics Letters B **26**, 630–632.

Poves, A (2017), "Shell model spectroscopy far from stability," J. Phys. G **44**, 084002.

Poves, A, R. P. Bahukutumbi, K. Langanke, and P. Vogel (1995), "Double beta decay of ^{48}Ca revisited," Phys. Lett. B **361**, 1–4.

Povinec, P P (SuperNEMO) (2017), "Background constrains of the SuperNEMO experiment for neutrinoless double

beta-decay searches," Nucl. Instrum. Meth. A **845**, 398–403.

Prezeau, G, M. Ramsey-Musolf, and P. Vogel (2003), "Neutrinoless double beta decay and effective field theory," Phys. Rev. D **68**, 034016.

Primakoff, H, and S. P. Rosen (1959), "Double beta decay," Rept. Prog. Phys. **22** (1), 121–166.

Primakoff, H, and S. P. Rosen (1969), "Nuclear double-beta decay and a new limit on lepton nonconservation," Phys. Rev. **184**, 1925–1933.

Prout, W (1816), "Correction of a mistake in the essay on the relation between the specific gravities of bodies in their gaseous state and the weights of their atoms," Annals of philosophy **7** (1816), 111–113.

Puppi, G (1948), "On Mesons in Cosmic Radiation. (In Italian)," *Meeting of the Italian School of Physics and Weak Interactions Bologna, Italy, April 26-28, 1984*, Nuovo Cim. **5**, 587–588, [,590(1948)].

Racah, G (1937), "On the symmetry of particle and antiparticle," Nuovo Cim. **14**, 322–328.

Rahaman, S, *et al.* (2008), "Q value of the Mo-100 Double-Beta Decay," Phys. Lett. **B662**, 111–116, arXiv:0712.3337 [nucl-ex].

Rahaman, S. and Elomaa, V. V. and Eronen, T. and Hakala, J. and Jokinen, A. and Kankainen, A. and Rissanen, J. and Suhonen, J. and Weber, C. and Äystö, J., (2011), "Double-beta decay Q values of ^{116}Cd and ^{130}Te," Phys. Lett. **B703**, 412–416.

Rebeiro, B M, *et al.* (2020), "Benchmarking ^{136}Xe Neutrinoless $\beta\beta$ Decay Matrix Element Calculations with the ^{138}Ba(p,t) Reaction," arXiv:2002.02987.

Rebeiro, B M, *et al.* (2021), "Spectroscopy of states in ^{136}Ba using the $^{138}Ba(p,t)$ reaction," Phys. Rev. C **104**, 034309.

Redshaw, M, B. J. Mount, E. G. Myers, and F. T. Avignone, III (2009), "Masses of Te-130 and Xe-130 and Double-beta-Decay Q Value of Te-130," Phys. Rev. Lett. **102**, 212502, arXiv:0902.2139 [nucl-ex].

Redshaw, M, E. Wingfield, J. McDaniel, and E. G. Myers (2007), "Mass and double-beta-decay Q value of Xe-136," Phys. Rev. Lett. **98**, 053003.

Reines, F, and C. L. Cowan (1953), "Detection of the free neutrino," Phys. Rev. **92**, 830–831.

Renner, J, *et al.* (NEXT) (2019), "Energy calibration of the NEXT-White detector with 1% resolution near Q$_{\beta\beta}$ of^{136}Xe," JHEP **10**, 230, arXiv:1905.13110 [physics.ins-det].

Richardson, Thomas R, Matthias R. Schindler, Saori Pastore, and Roxanne P. Springer (2021), "Large-N_c analysis of two-nucleon neutrinoless double-β decay and charge-independence-breaking contact terms," Phys. Rev. C **103**, 055501.

Ritz, S, *et al.* (HEPAP Subcommittee) (2014), "Building for Discovery: Strategic Plan for U.S. Particle Physics in the Global Context," .

Rivilla, I, *et al.* (2020), "Fluorescent bicolour sensor for low-background neutrinoless double β decay experiments," Nature **583** (7814), 48–54.

Roberts, A, *et al.* (2013), "Proton pair correlations and the neutrinoless double-β decay of ^{76}Ge," Phys. Rev. C **87**, 051305.

Robledo, L M, T. R. Rodríguez, and R. R. Rodríguez-Guzmán (2019), "Mean field and beyond description of nuclear structure with the Gogny force: A review," J. Phys. G **46**, 013001.

Roca-Maza, X, H. Sagawa, and G. Colo' (2019), "Double charge-exchange phonon states," arXiv:1907.06368.

Rodejohann, W (2011), "Neutrino-less Double Beta Decay and Particle Physics," Int. J. Mod. Phys. E **20**, 1833–1930, arXiv:1106.1334 [hep-ph].

Rodejohann, W (2012), "Neutrinoless double beta decay and neutrino physics," J. Phys. G **39**, 124008, arXiv:1206.2560 [hep-ph].

Rodin, V A, A. Faessler, F. Šimkovic, and P. Vogel (2003), "On the uncertainty in the 0 nu beta beta decay nuclear matrix elements," Phys. Rev. C **68**, 044302.

Rodin, V A, A. Faessler, F. Šimkovic, and P. Vogel (2006), "Assessment of uncertainties in QRPA $0\nu\beta\beta$-decay nuclear matrix elements," Nucl. Phys. A **766**, 107–131.

Rodriguez, T R, and G. Martinez-Pinedo (2010), "Energy density functional study of nuclear matrix elements for neutrinoless $\beta\beta$ decay," Phys. Rev. Lett. **105**, 252503.

Rodriguez, T R, and G. Martinez-Pinedo (2013), "Neutrinoless $\beta\beta$ decay nuclear matrix elements in an isotopic chain," Phys. Lett. B **719**, 174–178.

Romeo, B, J. Menéndez, and C. Peña (2021), "$\gamma\gamma$ decay as a probe of neutrinoless $\beta\beta$ decay nuclear matrix elements," arXiv:2102.11101.

Romero, A M, J. M. Yao, B. Bally, T. R. Rodríguez, and J. Engel (2021), "Application of an efficient generator-coordinate subspace-selection algorithm to neutrinoless double-β decay," Phys. Rev. C **104** (5), 054317, arXiv:2105.03471 [nucl-th].

Ross, G G, and J.W.F. Valle (1985), "Supersymmetric models without r-parity," Phys.Lett.B **151**, 375–381.

Roth, R (2009), "Importance Truncation for Large-Scale Configuration Interaction Approaches," Phys. Rev. C **79**, 064324.

Rutherford, E (1920a), "Bakerian lecture. nuclear constitution of atoms," Proceedings Mathematical Physical and Engineering Sciences **97**, 374–400.

Rutherford, E (1920b), "Nuclear constitution of atoms." Nature **105**, 500–501.

Sagawa, H, and T. Uesaka (2016), "Sum rule study for Double Gamow-Teller states," Phys. Rev. C **94**, 064325.

Sakharov, A D (1967), "Violation of CP Invariance, C asymmetry, and baryon asymmetry of the universe," Pisma Zh. Eksp. Teor. Fiz. **5**, 32–35.

Salam, A (1957), "On parity conservation and neutrino mass," Nuovo Cim. **5**, 299–301.

Santopinto, E, H. García-Tecocoatzi, R. I. Magaña Vsevolodovna, and J. Ferretti (2018), "Heavy-ion double-charge-exchange and its relation to neutrinoless double-β decay," Phys. Rev. C **98**, 061601.

Sarkar, S, Y. Iwata, and P. K. Raina (2020), "Nuclear matrix elements for λ mechanism of $0\nu\beta\beta$ of ^{48}Ca in nuclear shell-model: Closure versus nonclosure approach," Phys. Rev. C **102**, 034317, 2003.04002.

Schechter, J, and J.W.F. Valle (1982), "Neutrinoless double beta decay in su(2) x u(1) theories," Phys.Rev.D **25**, 2951.

Schwingenheuer, B (2013), "Status and prospects of searches for neutrinoless double beta decay," Annalen Phys. **525**, 269–280, arXiv:1210.7432 [hep-ex].

Senjanovic, Goran, and Vladimir Tello (2019), "Disentangling the seesaw mechanism in the minimal left-right symmetric model," Phys. Rev. D **100** (11), 115031, arXiv:1812.03790 [hep-ph].

Sen'kov, R A, and M. Horoi (2013), "Neutrinoless double-β decay of ^{48}Ca in the shell model: Closure versus nonclosure

approximation," Phys. Rev. C **88**, 064312.

Sen'kov, R A, and M. Horoi (2016), "Shell-model calculation of neutrinoless double-β decay of ^{76}Ge," Phys. Rev. C **93** (4), 044334.

Sen'kov, R A, M. Horoi, and B. A. Brown (2014), "Neutrinoless double-β decay of ^{82}Se in the shell model: beyond closure approximation," Phys. Rev. C **89**, 054304.

Shaposhnikov, M (2009), "Baryogenesis," J. Phys. Conf. Ser. **171**, 012005.

Sharp, D K, S. J. Freeman, B. D. Cropper, P. J. Davies, T. Faestermann, T. M. Hatfield, R. Hertenberger, S. J. F. Hughes, P. T. Macgregor, and H. F Wirth (2019), "Pairing properties of the double-β emitter ^{116}Cd," Phys. Rev. C **100**, 024329, 1910.12093.

Shimizu, N, T. Abe, M. Honma, T. Otsuka, T. Togashi, Y. Tsunoda, Y. Utsuno, and T. Yoshida (2017), "Monte Carlo shell model studies with massively parallel supercomputers," Phys. Scripta **92**, 063001.

Shimizu, N, J. Menéndez, and Kentaro Yako (2018), "Double Gamow-Teller Transitions and its Relation to Neutrinoless $\beta\beta$ Decay," Phys. Rev. Lett. **120**, 142502.

Shimizu, N, Y. Tsunoda, Y. Utsuno, and T. Otsuka (2021), "Variational approach with the superposition of the symmetry-restored quasiparticle vacua for nuclear shell-model calculations," Phys. Rev. C **103**, 014312, 2011.03157.

Shirai, J (KamLAND-Zen) (2017), "Results and future plans for the KamLAND-Zen experiment," J. Phys. Conf. Ser. **888** (1), 012031.

Simkovic, Fedor, Rastislav Hodak, Amand Faessler, and Petr Vogel (2011), "Relation between the $0\nu\beta\beta$ and $2\nu\beta\beta$ nuclear matrix elements revisited," Phys. Rev. C **83**, 015502.

Simkovic, Fedor, John Vergados, and Amand Faessler (2010), "Few active mechanisms of the neutrinoless double beta-decay and effective mass of Majorana neutrinos," Phys. Rev. D **82**, 113015, arXiv:1006.0571 [hep-ph].

Simón, A, et al. (NEXT) (2020), "Boosting background suppression in the NEXT experiment through Richardson-Lucy deconvolution," JHEP **21**, 146, arXiv:2102.11931 [physics.ins-det].

Söderström, P A, et al. (2020), "Electromagnetic character of the competitive $\gamma\gamma/\gamma$-decay from ^{137m}Ba," Nature Commun. **11**, 3242, 2001.00554.

Song, L S, J. M. Yao, P. Ring, and J. Meng (2014), "Relativistic description of nuclear matrix elements in neutrinoless double-β decay," Phys. Rev. C **90** (5), 054309.

Song, L S, J. M. Yao, P. Ring, and J. Meng (2017), "Nuclear matrix element of neutrinoless double-β decay: Relativity and short-range correlations," Phys. Rev. C **95**, 024305.

Stefanik, D, R. Dvornicky, F. Šimkovic, and P. Vogel (2015), "Reexamining the light neutrino exchange mechanism of the $0\nu\beta\beta$ decay with left- and right-handed leptonic and hadronic currents," Phys. Rev. C **92**, 055502.

Steinberger, J (1949), "On the use of subtraction fields and the lifetimes of some types of meson decay," Phys.Rev. **76**, 1180–1186.

Stroberg, S R, S. K. Bogner, H. Hergert, and J. D. Holt (2019), "Non-Empirical Interactions for the Nuclear Shell Model: An Update," Ann. Rev. Nucl. Part. Sci. **69**, 307–362.

Stroberg, S R, A. Calci, H. Hergert, J. D. Holt, S. K. Bogner, R. Roth, and A. Schwenk (2017), "A nucleus-dependent valence-space approach to nuclear structure," Phys. Rev. Lett. **118**, 032502.

Sudarshan, E C G, and R. e. Marshak (1958), "Chirality invariance and the universal Fermi interaction," Phys. Rev. **109**, 1860–1860.

Suhonen, J (2013), "Double beta decays of ^{124}Xe investigated in the QRPA framework," J. Phys. G **40**, 075102.

Suhonen, J, and O. Civitarese (1998), Phys. Rep. **300**, 124.

Suhonen, J, and O. Civitarese (2008), "Effects of orbital occupancies on the neutrinoless beta beta matrix element of Ge-76," Phys. Lett. B **668**, 277–281.

Suhonen, J, and O. Civitarese (2010), "Effects of orbital occupancies and spin-orbit partners on 0 nu beta beta-decay rates," Nucl. Phys. A **847**, 207–232.

Suhonen, J T (2017), "Value of the Axial-Vector Coupling Strength in β and $\beta\beta$ Decays: A Review," Front.in Phys. **5**, 55.

Suzuki, T, Satoshi Chiba, T. Yoshida, Toshitaka Kajino, and T. Otsuka (2006), "Neutrino nucleus reactions based on new shell model Hamiltonians," Phys. Rev. C **74**, 034307.

Swenson, L J, A. Cruciani, A. Benoit, M. Roesch, C. S. Yung, A. Bideaud, and A. Monfardini (2010), "High-speed phonon imaging using frequency-multiplexed kinetic inductance detectors," Appl. Phys. Lett. **96**, 263511, arXiv:1004.5066 [physics.ins-det].

Szwec, S V, et al. (2016), "Rearrangement of valence neutrons in the neutrinoless double-β decay of ^{136}Xe," Phys. Rev. C **94**, 054314.

Takahisa, K, H. Ejiri, H. Akimune, H. Fujita, R. Matumiya, T. Ohta, T. Shima, M. Tanaka, and M. Yosoi (2017), "Double charge exchange (^{11}B,^{11}Li) reaction for double beta decay response," arXiv:1703.08264.

Takaki, M, et al. (2015), "Heavy-Ion Double-Charge Exchange Study via a 12C(18O,18Ne)12Be Reaction," Proceedings, 2nd Conference on Advances in Radioactive Isotope Science (ARIS2014): Tokyo, Japan, June 1-6, 2014, JPS Conf. Proc. **6**, 020038.

Tanimura, H, G. Hinshaw, I. G. McCarthy, L. Van Waerbeke, N. Aghanim, Y.-Z. Ma, A. Mead, A. Hojjati, and T. Tröster (2019), "A Search for Warm/Hot Gas Filaments Between Pairs of SDSS Luminous Red Galaxies," Mon. Not. Roy. Astron. Soc. **483** (1), 223–234, arXiv:1709.05024 [astro-ph.CO].

Taniuchi, R, et al. (2019), "78Ni revealed as a doubly magic stronghold against nuclear deformation," Nature **568**, 53.

Tello, Vladimir, Miha Nemevsek, Fabrizio Nesti, Goran Senjanovic, and Francesco Vissani (2011), "Left-Right Symmetry: from LHC to Neutrinoless Double Beta Decay," Phys. Rev. Lett. **106**, 151801, arXiv:1011.3522 [hep-ph].

Terasaki, J (2015), "Many-body correlations of quasiparticle random-phase approximation in nuclear matrix elements of neutrinoless double-β decay," Phys. Rev. C **91**, 034318.

Terasaki, J (2020), "Strength of the isoscalar pairing interaction determined by a relation between double-charge change and double-pair transfer for double- β decay," Phys. Rev. C **102** (4), 044303, arXiv:2003.03542 [nucl-th].

Terasaki, J, and Y. Iwata (2019), "Effective axial-vector current coupling and isoscalar pairing interaction for quasiparticle random-phase approximation approach to double-β and β decays," Phys. Rev. C **100**, 034325.

Theodórsson, M Laubenstein; M Hult; J Gasparro; D Arnold; S Neumaier; G Heusser; M Köhler; P Povinec; J-L Reyss; M Schwaiger; P (2004), "Underground measurements of radioactivity," Applied Radiation and Isotopes **61**, 10.1016/j.apradiso.2004.03.039.

Thies, J H, et al. (2012), "High-resolution Zr-96 (He-3, t)

experiment and the matrix element for double-beta decay," Phys. Rev. C **86**, 054323.

Toh, Y, *et al.* (2013), "Evidence for rigid triaxial deformation at low energy in ^{76}Ge," Phys. Rev. C **87**, 041304.

Tomoda, T (1991), "Double beta decay," Rept. Prog. Phys. **54**, 53–126.

Touschek, B (1948), "Zur theorie des doppelten β-zerfalls," Zeitschrift für Physik A Hadrons and Nuclei **125**, 108–132.

Touschek, L A Radicati; B (1957), "On the equivalence theorem for the massless neutrino," Il Nuovo Cimento Series 10 **5**, 1693–1699.

Towner, IS (1997), "Quenching of spin matrix elements in nuclei," Phys. Rep. **155**, 263.

Tretyak, V I (2011), "False starts in history of searches for 2β decay, or Discoverless double beta decay," AIP Conf. Proc. **1417** (1), 129–133, arXiv:1112.4183 [nucl-ex].

Tretyak, VI, and Yuri G. Zdesenko (2002), "Tables of double beta decay data: An update," Atom. Data Nucl. Data Tabl. **80**, 83–116.

Twelker, K, *et al.* (2014), "An apparatus to manipulate and identify individual Ba ions from bulk liquid Xe," Rev. Sci. Instrum. **85**, 095114, arXiv:1407.0618 [physics.ins-det].

Uesaka, T, *et al.* (2015), RIKEN RIBF NP-PAC , NP1512–RIBF141.

Umehara, S, *et al.* (2008), "Neutrino-less double-beta decay of Ca-48 studied by Ca F(2)(Eu) scintillators," Phys. Rev. C **78**, 058501, arXiv:0810.4746 [nucl-ex].

Van Isacker, P, J. Engel, and K. Nomura (2017), "Neutron-proton pairing and double-β decay in the interacting boson model," Phys. Rev. C **96**, 064305.

Vasenko, A A, I. V. Kirpichnikov, V. A. Kuznetsov, A. S. Starostin, A. G. Dzhanian, G. E. Markosian, V. M. Oganesian, V. S. Pogosov, A. G. Tamanian, and S. R. Shakhazizian (1990), "New Results in the Itep / Yepi Double Beta Decay Experiment With Enriched Germanium Detector," Mod. Phys. Lett. A **5**, 1299–1306.

Vergados, J D, H. Ejiri, and F. Simkovic (2012), "Theory of Neutrinoless Double Beta Decay," Rept. Prog. Phys. **75**, 106301, arXiv:1205.0649 [hep-ph].

Vietze, L, P. Klos, J. Menéndez, W. C. Haxton, and A. Schwenk (2015), "Nuclear structure aspects of spin-independent WIMP scattering off xenon," Phys. Rev. **91**, 043520.

Vissani, F (1998a), "Do experiments suggest a hierarchy problem?" Phys. Rev. D **57**, 7027–7030, arXiv:hep-ph/9709409.

Vissani, F (1998b), "Large mixing, family structure, and dominant block in the neutrino mass matrix," JHEP **11**, 025, arXiv:hep-ph/9810435.

Vissani, F (1999), "Signal of neutrinoless double beta decay, neutrino spectrum and oscillation scenarios," JHEP **06**, 022, arXiv:hep-ph/9906525.

Vissani, F (2001), "Expected properties of massive neutrinos for mass matrices with a dominant block and random coefficients order unity," Phys. Lett. B **508**, 79–84, arXiv:hep-ph/0102236.

Vissani, F (2021), "What Is Matter According to Particle Physics, and Why Try to Observe Its Creation in a Lab?" Universe **7** (3), 61, arXiv:2103.02642 [hep-ph].

Vogel, P (2012), "Nuclear structure and double beta decay," J. Phys. G **39**, 124002, arXiv:1208.1992 [nucl-th].

Vogel, P, M. Ericson, and J. D. Vergados (1988), "Sum Rules for Two Particle Operators and Double Beta Decay," Phys. Lett. B **212**, 259–263.

Vogel, P, and M. R. Zirnbauer (1986), "Suppression of the

Two Neutrino Double beta Decay by Nuclear Structure Effects," Phys. Rev. Lett. **57**, 3148–3151.

Volpe, C, N. Auerbach, G. Colo, T. Suzuki, and N. Van Giai (2000), "Microscopic theories of neutrino C-12 reactions," Phys. Rev. C **62**, 015501.

Šimkovic, F, P. Domin, and S. V. Semenov (2001), "The Single state dominance hypothesis and the two neutrino double beta decay of Mo-100," J. Phys. G **27**, 2233–2240.

Šimkovic, F, R. Dvornický, Dušaň Stefánik, and A. Faessler (2018a), "Improved description of the $2\nu\beta\beta$ -decay and a possibility to determine the effective axial-vector coupling constant," Phys. Rev. C **97**, 034315.

Šimkovic, F, A. Faessler, H. Muther, V. Rodin, and M. Stauf (2009), "The $0\nu\beta\beta$-decay nuclear matrix elements with self-consistent short-range correlations," Phys. Rev. C **79**, 055501.

Šimkovic, F, V. Rodin, A. Faessler, and P. Vogel (2013), "$0\nu\beta\beta$ and $2\nu\beta\beta$ nuclear matrix elements, quasiparticle random-phase approximation, and isospin symmetry restoration," Phys. Rev. C **87**, 045501.

Šimkovic, F, A. Smetana, and P. Vogel (2018b), "$0\nu\beta\beta$ nuclear matrix elements, neutrino potentials and SU(4) symmetry," Phys. Rev. C **98**, 064325.

Walz, C, *et al.* (2015), "Observation of the competitive double-gamma nuclear decay," Nature **526**, 406.

Wang, K C (1942), "A suggestion on the detection of the neutrino," Phys. Rev. **61**, 97–97.

Wang, L-J, J. Engel, and J. M. Yao (2018), "Quenching of nuclear matrix elements for $0\nu\beta\beta$ decay by chiral two-body currents," Phys. Rev. C **98** (3), 031301.

Wang, Li, *et al.* (CDEX) (2017), "First results on ^{76}Ge neutrinoless double beta decay from CDEX-1 experiment," Sci. China Phys. Mech. Astron. **60** (7), 071011, arXiv:1703.01877 [hep-ex].

Wang, X B, A. C. Hayes, J. Carlson, G. X. Dong, E. Mereghetti, S. Pastore, and R. B. Wiringa (2019), "Comparison between Variational Monte Carlo and Shell Model Calculations of Neutrinoless Double Beta Decay Matrix Elements in Light Nuclei," Phys. Lett. B **798**, 134974.

Warburton, E K, J. A. Becker, B. A. Brown, and D. J. Millener (1988), "First-forbidden beta decay near a = 40," Ann. Phys. **187**, 471.

Warburton, W K, B. Dwyer-McNally, M. Momayezi, and J. E. Wahl (2004), "Ultra-low background alpha particle counter using pulse shape analysis," in *IEEE Symposium Conference Record Nuclear Science 2004.*, Vol. 1, pp. 577–581 Vol. 1.

Weinberg, S (1979), "Baryon and lepton nonconserving processes," Phys.Rev.Lett. **43**, 1566–1570.

Weinberg, S (1980), "Varieties of baryon and lepton nonconservation," Phys.Rev.D **22**, 1694.

Weiss, Ronen, Pablo Soriano, Alessandro Lovato, Jaview Menendez, and R. B. Wiringa (2021), "Neutrinoless double-beta decay: combining quantum Monte Carlo and the nuclear shell model with the generalized contact formalism," arXiv:2112.08146 [nucl-th].

Welliver, B (2021), Talk at APS-DNP 2021 Conference.

Wick, G C (1934), "Sugli elementi radioattivi di F. Joliot e I. Curie," Rendiconti dell'Accademia dei Lincei **19**, 69–72.

Wigner, E P (1949), "Invariance in physical theory," Proceedings of the American Philosophical Society **93** (7), 521–526.

Wilczek, F, and A. Zee (1979), "Operator analysis of nucleon decay," Phys.Rev.Lett. **43**, 1571–1573.

Wildenthal, B H, M. S. Curtin, and B. A. Brown (1983),

"Predicted features of the beta decay of neutron-rich sd-shell nuclei," Phys. Rev. C **28**, 1343–1366.

Winslow, L, and R. Simpson (2012), "Characterizing Quantum-Dot-Doped Liquid Scintillator for Applications to Neutrino Detectors," JINST **7**, P07010, arXiv:1202.4733 [physics.ins-det].

Wirth, R, J. M. Yao, and H. Hergert (2021), "Ab initio calculation of the contact operator contribution in the standard mechanism for neutrinoless double beta decay," arXiv:2105.05415.

Wojcik, M, G. Zuzel, and H. Simgen (2017), "Review of high-sensitivity Radon studies," Int. J. Mod. Phys. A **32** (30), 1743004.

Wu, C S, E. Ambler, R. W. Hayward, D. D. Hoppes, and R. P. Hudson (1957), "Experimental Test of Parity Conservation in β Decay," Phys. Rev. **105**, 1413–1414.

Wulandari, H, J. Jochum, W. Rau, and F. von Feilitzsch (2004), "Neutron flux underground revisited," Astropart. Phys. **22**, 313–322, arXiv:hep-ex/0312050.

Xu, W, and S. R. Elliott (2017), "Solar Axion Search Technique with Correlated Signals from Multiple Detectors," Astropart. Phys. **89**, 39–50, arXiv:1610.03886 [hep-ex].

XUNDL, (2021), http://www.nndc.bnl.gov/ensdf/ensdf/xundl.jsp.

Yanagida, Y (1979), "Horizontal gauge symmetry and masses of neutrinos," in *Horizontal gauge symmetry and masses of neutrinos*, Vol. 7902131, pp. 95–99.

Yao, J M, B. Bally, J. Engel, R. Wirth, T. R. Rodríguez, and H. Hergert (2020), "*AbInitio* Treatment of Collective Correlations and the Neutrinoless Double Beta Decay of ^{48}Ca," Phys. Rev. Lett. **124**, 232501, arXiv:1908.05424.

Yao, J M, A. Belley, R. Wirth, T. Miyagi, C. G. Payne, S. R. Stroberg, H. Hergert, and J. D. Holt (2021), "*Abinitio* benchmarks of neutrinoless double-β decay in light nuclei with a chiral Hamiltonian," Phys. Rev. C **103**, 014315, 2010.08609.

Yao, J M, J. Engel, L. J. Wang, C. F. Jiao, and H. Hergert (2018), "Generator-coordinate reference states for spectra and $0\nu\beta\beta$ decay in the in-medium similarity renormalization group," Phys. Rev. C **98**, 054311.

Yao, J M, I. Ginnett, A. Belley, T. Miyagi, R. Wirth, S. Bogner, J. Engel, H. Hergert, J. D. Holt, and S. R. Stroberg (2022a), "Ab initio studies of double Gamow-Teller transition and its correlation with neutrinoless double beta decay," arXiv:2204.12971 [nucl-th].

Yao, J M, J. Meng, Y. F. Niu, and P. Ring (2022b), "Beyond-mean-field approaches for nuclear neutrinoless double beta decay in the standard mechanism," Prog. Part. Nucl. Phys. **126**, 103965.

Yao, J M, L. S. Song, K. Hagino, P. Ring, and J. Meng (2015), "Systematic study of nuclear matrix elements in neutrinoless double-β decay with a beyond-mean-field covariant density functional theory," Phys. Rev. C **91**, 024316.

Yoshida, S, T. Kishimoto, I. Ogawa, R. Hazama, S. Umehara, K. Matsuoka, D. Yokoyama, K. Ichihara, and Y. Tatewaki (2009), "Ultra-violet wavelength shift for undoped CaF_2 scintillation detector by two phase of liquid scintillator system in CANDLES," Nucl. Instrum. Meth. A **601**, 282–293.

Yoshida, S, N. Shimizu, T. Togashi, and T. Otsuka (2018a), "Uncertainty quantification in the nuclear shell model," Phys. Rev. C **98**, 061301.

Yoshida, S, Y. Utsuno, N. Shimizu, and T. Otsuka (2018b), "Systematic shell-model study of β-decay properties and Gamow-Teller strength distributions in A~40 neutron-rich nuclei," Phys. Rev. C **97**, 054321.

Yoshinaga, N, K. Yanase, K. Higashiyama, E. Teruya, and D. Taguchi (2018), "Structure of nuclei with masses 76 and 82 and nuclear matrix elements of neutrinoless double beta decay," Prog. Theor. Exp. Phys. **2018**, 023D02.

Yue, Qian (2021), "Cdex-300ν: neutrinoless double beta decay experiment based on ^{76}ge," TAUP.

Zeldovich, Y B, E. Jackson, and A. Granik (1993), "On the theory of elementary particles.: Conservation of the nuclear charge and a possible new type of v-particles," in *Selected Works of Yakov Borisovich Zeldovich, Volume II: Particles, Nuclei, and the Universe* (Princeton University Press) pp. 56–61.

Zhao, J, L.-J. Wen, Y.-F. Wang, and J. Cao (2017), "Physics potential of searching for $0\nu\beta\beta$ decays in JUNO," Chin. Phys. C **41** (5), 053001, arXiv:1610.07143 [hep-ex].

Zhi, Q, E. Caurier, J. J. Cuenca-Garcia, K. Langanke, G. Martinez-Pinedo, and K. Sieja (2013), "Shell-model half-lives including first-forbidden contributions for r-process waiting-point nuclei," Phys. Rev. C **87**, 025803.

Zinner, N T, K. Langanke, and P. Vogel (2006), "Muon capture on nuclei: Random phase approximation evaluation versus data for $6 \leq Z \leq 94$ nuclei," Phys. Rev. C **74**, 024326.

Zuber, K (2001), "COBRA: Double beta decay searches using CdTe detectors," Phys. Lett. B **519**, 1–7, arXiv:nucl-ex/0105018.

Zyla, P A, *et al.* (Particle Data Group) (2020), "Review of Particle Physics," PTEP **2020** (8), 083C01, and 2021 update.